MINISTRY OF EDUCATION AND SCIENCE OF UKRAINE

NATIONAL TECHNICAL UNIVERSITY OF UKRAINE
“IGOR SIKORSKY KYIV POLYTECHNIC INSTITUTE”

K.Ivanko, N.Ivanushkina

Advances in Digital Processing of Low-Amplitude Components of Electrocardiosignals

Kyiv, 2017

UDC 621.391:004.93:616.12-073.97(075.8)621.38:61(0.75.8)

Reviewers:
O.Kovalenko, Doctor of Medical Sciences,
Professor of International Research and Training Center for Information Technologies and Systems of NASU

O.Sharpan, Doctor of Technical Sciences,
Professor of Igor Sikorsky Kyiv Polytechnic Institute

Responsible Editor:
V. Timofeev, Doctor of Technical Sciences,
Professor of Igor Sikorsky Kyiv Polytechnic Institute

Advances in Digital Processing of Low-Amplitude Components of Electrocardiosignals: Teaching book/K.Ivanko, N.Ivanushkina.— Kyiv, 2017.—198 p.
ISBN _____

The teaching book is devoted to development and research of methods and tools for non-invasive detection of subtle manifistations of heart electrical activity. Particular attention is paid to the improvement of information and algorithmic support of high resolution electrocardiography for early diagnosis of myocardial electrical instability, as well as for the evaluation of the functional state of the fetus during pregnancy examination.

The theoretical basis accompanied by the examples of implementation of the discussed algorithms with the help of MATLAB. The teaching book is intended for students, graduate students, as well as specialists in the field of biomedical electronics and medical professionals.

ISBN _____

This manual has been published within the framework of the BME-ENA project under the responsibility of National Technical University of Ukraine.
The BME-ENA “Biomedical Engineering Education Tempus Initiative in Eastern Neighbouring Area”, Project Number: 543904-TEMPUS-1-2013-1-GR-TEMPUS-JPCR is a Joint Project within the TEMPUS IV program. This project has been funded with support from the European Commission. This publication reflects the views only of the author, and the Commission cannot be held responsible for any use which may be made of the information contained therein.

Co-funded by the
Tempus Programme
of the European Union

CONTENT

INTRODUCTION

The development of digital processing of biomedical signals and implementation of information technology in medical practice create conditions for improvement of diagnostic methods in cardiology. The use of special equipment for electrocardiogram registration and digital signal processing techniques provide information that can not be obtained by analysis of standard electrocardiogram.

The classic use of high resolution electrocardiography is non-invasive detection of markers of myocardial electrical instability to predict cardiac arrhythmias. It is believed that the first signs of electrical instability of the heart reflect the exhaustion of regulatory systems at the level of individual cells of the myocardium. Changes in energy and metabolic processes that occur in the deterioration of electrical stability of the myocardium at the cellular and subcellular levels and microstructural violations can not be detected by conventional clinical and physiological methods of functional diagnostics. These changes in the first stage of the disease often does not manifest clinically.

The first part of the teaching book focuses on simulation of action potential and membrane ionic currents in cardiomyocytes and nerve fibers. It presents a mathematical model based on 6 ordinary differential equations that describe the ionic currents at the level of cardiomyocyte, transmembrane potential with action potential generation, as well as activation and inactivation functions for potassium, sodium and calcium channels of cardiomyocytes.

The second part of the teaching book is devoted to development of diagnostic ECG systems of new generation, which are characterized by the use of complex mathematical transformations for estimation of

parameters of electrical potentials considering biophysics and electrophysiology of myocardium. The systems of high resolution electrocardiography (HR ECG) allow investigation of subtle manifestations of cardiac electrical activity. Early diagnosis of cardiovascular system state, which developed on the basis of HR ECG methods, has essentially new opportunities and begins to be widely applied in clinical practice. To the tasks of investigation of subtle structure of ECG belongs detection of electrical violations of myocardial homogeneity based on registration and analysis of atrial and ventricular late potentials by the systems of high resolution electrocardiography. The presence of late potentials is associated with an increased probability of dangerous cardiac arrhythmias. Particularly difficult is the study of atrial late potentials, which occur as high frequency microbursts in terminal part of P wave and have nearly the same amplitude as noise components of cardiosignal. The amplitude of atrial late potentials is much lower than the amplitude of ventricular late potentials. Atrial late potentials reflect the presence of fragmented delayed depolarization of the atria and are markers of myocardial electrophysiological disorders that lead to supraventricular arrhythmias such as atrial fibrillation and paroxysmal atrial tachycardia. Detection of late potentials may be based on the use of a broad class of algorithms from the conventional analysis in the time and frequency domains to the complex procedures of pattern recognition.

Combined method of analysis of low-amplitude components of electrocardiosignals is developed. It is intended for detection of late potentials representing pathological cardiac electrical activity and based on the creation of eigensubspaces of signals and noise at different

combinations of wavelet decomposition and decomposition in eigenvectors basis.

The third part of the teaching book is dedicated to detection and evaluation of beat-to-beat T wave alternans in electrocardiogram. The task of developing of theoretically justified methods and algorithms for early prediction of potentially dangerous atrial arrhythmias is very important because of the wide spread of cardiovascular diseases and their significant contribution to the structure of mortality and disability of socially active groups. To reveal diagnostic features related to T wave alternans, variations in amplitude and shape of T waves from synthetic and clinical recordings were explored by means of time-domain analysis, Poincare plots, and principal component analysis together with clustering analysis. The proposed methods make it possible to eliminate noises and interferences in recorded electrocardiograms, and also to detect the morphology changes of T waves.

The fourth part of the teaching book is focused on noninvasive research of atrial electrical activity by its extraction from the surface electrocardiogram recordings. Spectral and time-frequency analysis is performed for fibrillatory frequency detection and tracking. It is shown that atrial electrical activity and ventricular activity can be separated from real multichannel recordings with symptoms of atrial fibrillation by means of independent component analysis. To identify the source that corresponds to atrial electrical activity, the frequency spectrums and coefficients of skewness and kurtosis are determined. Also atrial activity extraction is performed by average beat subtraction method. The comparison of obtained results is carried out. Spectral analysis by Fast Fourier Transform and Multiple Signal Classification methods as well as

time-frequency analysis are used to find and track dominant atrial fibrillation frequency.

The fifth part of the teaching book demonstrates another example of the investigation of subtle structure of ECG, which consists in separation of fetal and maternal electrocardiosignals obtained by the abdominal recording. Despite significant advances in clinical electrocardiography, this direction is still in early stage of development. It is caused by lack of necessary databases of fetal ECG in norm and with the presence of defects, low amplitude of fetal ECG compared to the high-amplitude maternal signal, as well as the presence of abdominal noise components in the abdominal ECG signal. The proposed method of fetal ECG separation from the abdominal maternal electrocardiosignals makes it possible to separate from the noisy mixture of signals the low-amplitude component of fetal ECG that is the independent source of cardiac electrical activity. This allows determination of fetal heart rate variability and morphological parameters of fetal cardiac cycles for assessment of fetal condition during pregnancy.

The teaching book presents the research of simulated and real electrocardiosignals. It can be useful for students, graduate students, as well as for developers of new methods and means of high resolution electrocardiography.

SECTION 1
BIOELECTRIC PROCESSES OF CELL MEMBRANE

1.1. Structure and functions of cell membrane

Vital activity of any organism is accompanied by bioelectric processes. The appearance of electrical potentials in living cells is associated with the physicochemical properties of cell membranes. All living organisms consist of cells, which surrounded by biological membranes with thickness about 6-10 nm.

Biological membranes are the limited supramolecular structures, which form the cells and their intracellular environment and provide all functions of organism. The most important function of biological membranes is regulation of ions and substances transport [1]. The structure of the membrane composed of lipids, carbohydrates and protein components (Fig. 1.1).

One of the first membrane models is bilayer model of lipid membrane ("double sandwich"). In this model lipid molecules are arranged in two layers in such a way that the polar heads, which have hydrophilic properties, are directed outward, and nonpolar tails, which have hydrophobic properties, are directed into the membrane. Protein components penetrate the bilayer of the membrane. Lipid layer effectively prevents the process of free passage of ions through the membrane.

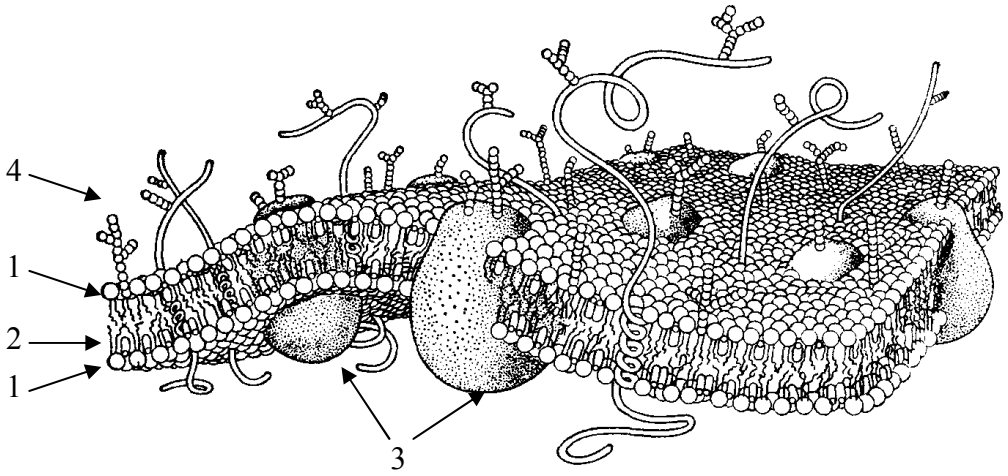

Fig. 1.1. Structure of the cell membrane:

1 ─ hydrophilic lipid head, 2 ─ of hydrophobic lipid molecules,

3 ─ protein molecule, 4 ─ carbohydrate molecules

Hydrophobic tails form the internal structure of the membrane, which behaves like a dielectric with a relative dielectric constant and thickness d = 30Å. The capacity C_m of following structure is about 1μF/cm^2 [1].

The functions of membrane proteins include formation of the channels, which enable exchange of ions between intra- and extracellular environments. Functional model of membrane channels (Fig.1.2) consists of the aqueous pores, through which ions have the ability to penetrate the membrane, selectivity filter, which displays property of selective permeability channels for different ions and sensor with control gates.

On the base of functional model ion channels can be classified by selectivity according to the ions that pass through the channels: sodium, potassium, calcium, chloride.

Also, functional model allows classification of ion channels depending on the control facilities:

- independent channels;
- potential-dependent channels;

- ligand-dependent channels;

- jointly-controlled channels (activated by ligands and membrane potential);

- stimulus-driven channels (mehano-sensitive, temperature-sensitive).

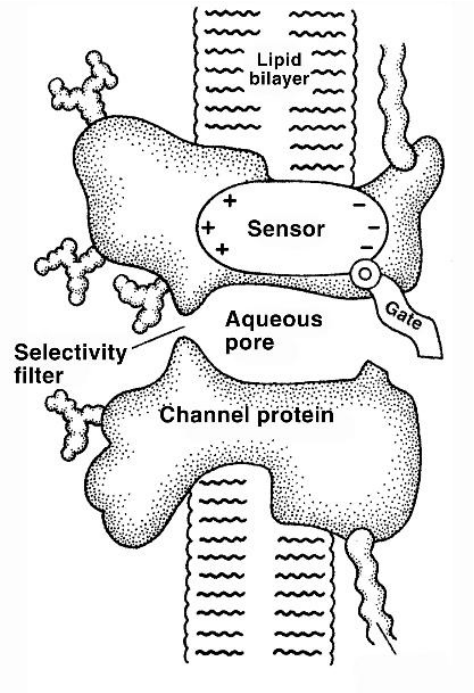

Fig. 1.2. Functional model of membrane channels [1]

1.2. Nature and modeling of membrane resting potential

One of the most characteristic features of living cells at rest is a potential difference between the inside part of cell and environment, which is known as resting potential. Registration of the resting potential is carried out by inserting the electrode into the cell (registered voltage is approximately -70 mV).

1.2.1. Nernst-Planck equation and Nernst potential

In all excitable cells intracellular potassium concentration is much higher than the potassium concentration outside cell and extracellular concentrations of sodium and chlorine are much higher comparing to their intracellular concentrations [1].

Inequality of ions concentration in the intra- and extracellular space cause the diffusion of ions from the region with their high concentration to the region with low concentration. Due to the fact that ions have electric charges, membrane has a certain electric capacity. The charges are collected on the membrane, leading to the emergence of a potential difference. This potential difference creates in the thickness of the membrane the electric field, which generates forces acting on all the charged particles inside the membrane. Thus, the total current of ions through the membrane has diffusive and drift components:

$$\vec{J} = \vec{J}_{dif} + \vec{J}_{dr} = -ZD\vec{\nabla}N - ZN\mu\vec{\nabla}\varphi,$$

where Z is ion charge, D is diffusion coefficient, N is ion concentration as a function of coordinates, μ is mobility; φ is potential of electric field inside the membrane.

Then, the full density of the ion current across the membrane can be found using *Nernst-Planck equation:*

$$\vec{J} = -ZD\left(\vec{\nabla}N + \frac{Z}{q}\frac{N}{\varphi_T}\vec{\nabla}\varphi\right),$$

where φ_T is thermal potential, q is electron charge.

Nernst-Planck equation is used to obtain quantitative estimation of the membrane potential. Under the equilibrium conditions the force of the

electric field exactly compensates diffusion force, and full density of the ion current across the membrane equals zero:

$$\vec{J} = -D_c Z\left(\vec{\nabla} N_c + \frac{Z}{q}\frac{N_c}{\varphi_T}\vec{\nabla}\varphi\right) = 0,$$

where D_c is diffusion coefficient of cations, N_c is concentration of cations.

From this equation we can find potential difference with regard to assumption of integration on the membrane thickness from the intracellular space *i* to the extracellular space *e.*

For biological cell membrane potential is determined as the difference between internal and external potentials. Thus, the potential difference on the membrane is V_m:

$$V_m = \varphi_i - \varphi_e = \varphi_T \frac{q}{Z} \ln \frac{N_{Ce}}{N_{Ci}}$$

The resulting value of the membrane potential is called the *Nernst potential.* It can be regarded as an electrical measure, which counterbalances the diffusion force that arises from the difference in concentrations on opposite sides of the permeable membrane.

Nernst potential for cations can be defined as:

$$V_C = \varphi_T \frac{q}{|Z|} \ln \frac{N_{Ce}}{N_{Ci}}$$

where N_{Ce} is extracellular concentration of cations, N_{Ci} is intracellular concentration of cations.

Nernst potential for anions can be found as:

$$U_A = \varphi_T \frac{q}{|Z|} \ln \frac{N_{Ai}}{N_{Ae}},$$

where N_{Ae} is extracellular concentration of anions, N_{Ai} is intracellular concentration of anions.

1.2.2. Goldman equation

Membrane potential is a weighted sum of the Nernst potentials for different ions. The weights in this amount depend on on the ability of membrane to pass through itself a variety of presented ions. To take into account for the influence of membrane permeability for different ions on the membrane potential, we have to solve Nernst-Planck equation, based on membrane processes. In general, biological membrane can not be in the state of equilibrium for all ions.

Nernst potentials for K^+, Na^+, Cl^- ions under their usual concentrations have different values. Thus, none of the membrane Nernst potentials can simultaneously balance all ions. Resting potential can be found from the condition of equilibrium $J = 0$.

$$p_K[K]_e + p_{Na}[Na]_e + p_{Cl}[Cl]_i - \left(p_K[K]_i + p_{Na}[K]_i + p_{Cl}[Cl]_e\right) \cdot e^{\frac{V_m}{\varphi_T}} = 0$$

where $[K]_i$ and $[K]_e$ are intra- and extracellular concentrations of potassium ions, $[Na]_i$ and $[Na]_e$ are intra- and extracellular concentrations of sodium ions, $[Cl]_l$ and $[Cl]_e$ are intra- and extracellular concentrations of chlorine ions, p_K is permeability of potassium ions, p_{Na} is permeability of sodium ions, p_{Cl} is permeability of chlorine ions.

From this formula we can obtain the resting potential:

$$V_m = \varphi_T \ln\left[\frac{p_K[K]_e + p_{Na}[Na]_e + p_{Cl}[Cl]_i}{p_K[K]_i + p_{Na}[Na]_i + p_{Cl}[Cl]_e}\right].$$

This equation is called the *equation of Goldman*. Goldman equation shows that the membrane potential is independent from the absolute values of membrane permeability for different ions and depends only on their relationship $p_K : p_{Na} : p_{Cl}$. If the membrane is permeable only to one type of ions (for example, $p_K >> p_{Na}$ and $p_K >> p_{Cl}$), then the membrane potential equals Nernst potential of that type of ions, for which membrane is permeable (such as K^+ ions).

The impact of chlorine ions to creation of resting potential in comparison with the impact of potassium ions is secondary. This is due to the fact that the intracellular concentration of chlorine ions is very small and under a small influx or outflow of ions is subjected to large relative changes. Consequently, the movement of chloride ions will lead its concentration on both sides of the membrane to practically fixed ratio of the concentrations of potassium ions. Therefore, in many practical problems, it can be assumed, that the chlorine ions are in equilibrium or absent. In this case the resting potential is defined as:

$$V_m \approx \varphi_T \ln\frac{[K]_e + \alpha[Na]_e}{[K]_i + \alpha[Na]_i},$$

where $\alpha = \frac{p_{Na}}{p_K}$.

1.2.3. Parallel-conductance model

The assumption of the presence of independent conducting ion channels allows construction of a circuitry model of membrane, known as the parallel-conductance model [1]. Each of the branches of the electrical circuit reflects the contribution of certain type of ions to the total membrane current (Fig. 1.3).

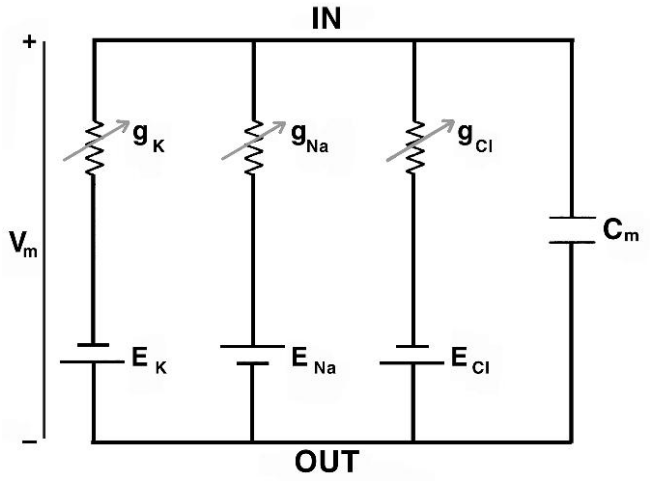

Fig. 1.3. The parallel-conductance model of membrane (IN = intracellular space, OUT = extracellular space) [1]

Independent conductance channels are presented for K^+, Na^+ and Cl^- ions. The voltage sources in the equivalent circuit simulate Nernst potentials for each type of ions:

$$E_K = -\varphi_T \ln \frac{[K]_e}{[K]_i};$$

$$E_{Na} = \varphi_T \ln \frac{[Na]_e}{[Na]_i};$$

$$E_{Cl} = -\varphi_T \ln \frac{[Cl]_i}{[Cl]_e}.$$

Complete membrane current can be defined as:

$$J = g_K \left(V_m + E_K\right) + g_{Na} \left(V_m - E_{Na}\right) + g_{Cl} \left(V_m + E_{Cl}\right) + C_m \frac{dV_m}{dt}.$$

At equilibrium $J = 0$ and $\frac{dV_m}{dt} = 0$. Then

$$V_m = \frac{g_{Na}E_{Na} - g_K E_K - g_{Cl}E_{Cl}}{g_{Na} + g_K + g_{Cl}}.$$

This equation is known as the equation of parallel conductances. According to it, V_m is a weighted average of values E_K, E_{Na}, E_{Cl}, depending on the relative conductivities.

1.3. Nature and modeling of action potential

1.3.1. Simulation of conductivity of ion channels

A typical current through a single channel consists of discrete random jumps. According to experimental data, current fluctuations can be explained by opening and closing of the channel, which has a fixed conductance. The current switches between two discrete levels and durations of open and closed positions are described by random variables. The current, which is created by a large number of channels, corresponds to the average current of the whole cell. Let's consider relationships that describe macroscopic properties of the membrane by a total effect of a large number (N_Σ) of individual channels, among which N_O channels are open and N_C channels are closed ($N_\Sigma = N_O + N_C$). It is believed that over time some channels randomly switch from the closed position to the open and vice versa [1-3].

$$N_O \underset{\beta}{\overset{\alpha}{\rightleftarrows}} Nc$$

If α is the speed of channels switching from closed position to open and β is speed of switching from open position into closed, then the full speed of changing the open channels is determined as:

$$\frac{dN_O}{dt} = \alpha N_C - \beta N_O = \alpha\left(N_\Sigma - N_O\right) - \beta N_O$$

Suppose that $p = \frac{N_o}{N_\Sigma}$ is the probability that the channel is open, then

$$\frac{dp}{dt} = \alpha(1-p) + \beta p$$

The last equation can be rewritten as

$$\frac{dp}{dt} = \frac{p_\infty - p}{\tau}$$

where $\tau = \frac{1}{\alpha + \beta}$ is relaxation period, $p_\infty = \alpha\tau$ is the steady-state value. The decision of the equation is an expression

$$p = p_\infty - (p_\infty - p_0)e^{-\frac{t}{\tau}},$$

where p_0 is the probability that the channel is in the open position at the moment t=0. Character of the solution depends on the ratio between the values of p_0 and p_∞ (Fig. 1.4).

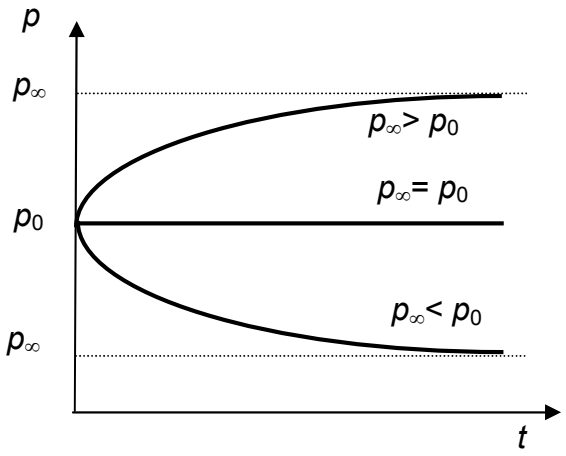

Fig. 1.4. Probability function $p(t)$ depending on the ratio between the values of p_0 and p_∞

If $p_\infty = p_0$, then the probability that the channel is in the open state is independent from time and corresponds to the steady state. When $p_\infty > p_0$, function $p(t)$ increases due to the opening of the channels over time. This process is called activation of the channels, and the function $p(t)$ is known as *activation function*. When $p_\infty < p_0$, the inactivation of the channels occurs and the channels change their state to the closed position. In this case, the function $p(t)$ is called inactivation function.

Described dependences are fair for so-called individual channels. The real ion channels are composed of several subunits, each of which can be described as a single channel. The channel is considered to be open, if all the subunits are also open. If p_i is the probability that i subunit is in the open state, then for the channel, which consists of k subunits, function $p(t)$, is defined as

$$p(t) = \prod_{i=1}^{k} p_i(t).$$

Biological membranes contain a large number of several types of ion channels. With stimulation such electrically active tissues can generate an electrical impulse - action potential (AP). Action potential depends on the voltage applied to the stimulating electrodes and its polarity. If the stimulus amplitude is small, then stimulus artifact can be registered, which coincides in time with the stimulus and occurs through direct capacitive connection of the stimulator and recording tool. Increasing the amplitude of the stimulus we can reach a level at which an answer, potential of the cell occurs, indicating the threshold nature of the phenomenon. With increasing of the stimulus amplitude above the threshold, amplitude of action potential remains unchanged.

By placing a microelectrode inside the cell, a change in intracellular potential relative to extracellular potential can be measured. At rest state, the membrane has a negative potential of 60-100 mV. The cycle of the action potential consists of fast depolarization (1) that implies increasing of the transmembrane potential, then follows the slow repolarization (2) of the membrane and return to the resting state of the membrane (3) (Fig. 1.5).

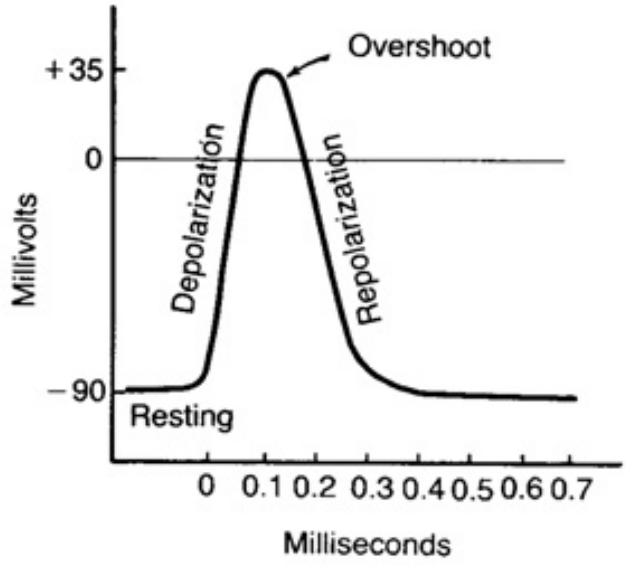

Fig.1.5. The main phases of action potential [4]

The answer of the excitable membranes does not occur until the stimulus reaches a certain level, called the threshold potential. For all stimuli, which applied to the cell with amplitude higher than the threshold, action potentials have the same amplitude.

To understand the origin of the action potential we must turn to the Goldman equation. In deriving the Goldman equation a key assumption implies the existence of a steady state, in which the full density of ion flow is equal to zero J=0. At the top of the action potential $\frac{dV_m}{dt} = 0$, and therefore total current density through the membrane must also be zero (quasi-stationary state). However, at the peak value of action potential membrane permeability is different from the permeability at rest. Experimentally determined, that the peak of action potential is approaching the Nernst potential for sodium, but never exceeds it. This result is consistent with a possible increase in sodium permeability.

It has been shown that good match between theory and experiment is achieved if accept $p_K : p_{Na} : p_{Cl}$ = 1.0 : 0.01 : 0.45 at rest and $p_K : p_{Na} : p_{Cl}$ = 1.0 : 10.0 : 0.45 at the peak of action potential. The influence of chlorine on behavior of membrane at rest is negligible. As a result, given the difference of permeabilities p_K and p_{Na}, as a first approximation we can assume that

at rest $V_m \approx E_K = \varphi_T \ln \frac{[K]_e}{[K]_i}$;

at the peak of action potential $V_m \approx E_{Na} = \varphi_T \ln \left[\frac{[Na]_e}{[Na]_i} \right]$.

1.3.2. Simulation of action potential in cardiomyocytes

Classification of models of heart electrical activity is based on the description of bioelectric processes, which take place at different levels of organization: cell, tissue and organ. Cellular level models reflect the occurrence of action potential in cardiomyocytes. Simulation at the tissue level describes AP distribution processes in myocardium, and organ-level models allow investigation of dynamics of cardiac conduction system.

Cellular-level models are based on a fundamental approach, which was proposed by Hodgkin and Huxley in the simulation of ionic currents and membrane AP for nerve fiber [2]. For simulation of action potential in cardiomyocyte, it is necessary to take into account that AP of cardiomyocyte differs from the AP of nerve fiber due to the presence of weighty contribution of calcium current. Duration of AP in axon is 1 ms, whereas duration of AP in myocardial contractile cells is 250-300 ms, that allows implementation of synchronous excitation and contraction of the heart structures for blood ejection. There are important physiological differences between nodal cells and atrial or ventricular cells of heart due to the specific differences in ion channels and mechanisms of repolarization. Therefore, action potentials in cardiomyocytes of various heart structures (sinus and atrioventricular node, atrial and ventricular cardiomyocytes) are different in shape and duration.

One of the first modern models of myocardium is a model by McAllister R.E., Noble D., and Tsien R.W. [5], which includes all membrane currents that were confirmed experimentally, as well as intracellular calcium currents, which are closely linked to muscle contraction. One of the latest models is the model of the myocardium by

Luo and Rudy [6, 7]. Model of Luo and Rudy is a modern model of heart membrane, which extends the previous models by using single-channel parameter measurements. The fundamental approach of modeling, which was proposed more than fifty years ago by Hodgkin and Huxley in [2], remains unchanged.

Improvement of the model was performed taking into account experimental data accumulated by many authors by introducing new features and functions for membrane currents due to the complexity of cardiac membrane and bioelectric processes in cardiomyocytes.

Arrhythmias, being the most common heart diseases, are caused by violations in the formation and/or propagation of the action potential. To investigate such violations of the heart electrical activity, experimental methods and methods of mathematical simulation are performed, complementing each other. Different researchers have created a wide variety of models that simulate the appearance of the action potential in cardiomyocytes [3]. There are complex detailed models for the simulation of action potential with using a large number of gate variables. For example, the Luo–Rudy model consists of 14 ODEs [6], the Courtemanche et al. model consists of 21 ODEs [8], the Winslow et al. model uses 32 ODEs [9], the Puglisi–Bersmode model contains 17 ODEs [10]. However, the use of the relatively simple model allows us to reproduce a variety of forms of action potentials in cardiomyocytes without unnecessary complications.

For simulation of action potential in cardiomyocytes, modification of the generalized model of Hodgkin-Huxley was performed by adding a branch corresponding to the calcium ion channel [11].

Model of cell membrane at occurrence of action potential in cardiomyocyte is described by the parallel-conductance model (Fig. 1.6),

based on the assumption of the presence of independent ion channels for K^+, Na^+ and Ca^{2+} ions, as well as leakage through the membrane. Each branch of the electrical circuit reflects the contribution of one type of ions to total membrane current. The membrane of cardiomyocytes has selective permeability to ions of various types. The voltage sources in the equivalent circuit simulate Nernst potentials for each type of ion.

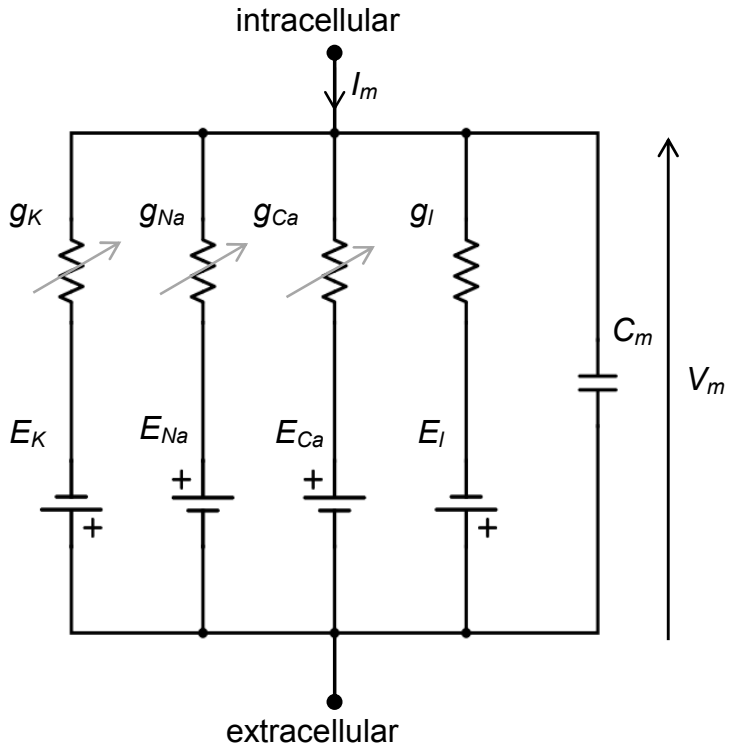

Fig. 1.6. The parallel-conductance model of cardimyocyte's cell membrane. Independent conductance channels are presented for K^+, Na^+, Ca^{2+} and leakage together with other factors. The battery polarity is chosen to show, that usually Nernst potentials of E_K and E_l are negative (inside potential is more negative than outside), whereas E_{Na} and E_{Ca} are positive (inside potential is more positive than outside)

Transmembrane potential at any moment of time can be represented as

$$V_m(t) = V_{m0} + v_m(t) \qquad (1.1)$$

where $v_m(t)$ is the alternating component of membrane potential, V_{m0} is resting potential determined from the parallel-conductance model of membrane as

$$V_{m0} = \frac{-g_{K0}E_K + g_{Na0}E_{Na} + g_{Ca0}E_{Ca} - g_lE_l}{g_{K0} + g_{Na0} + g_{Ca0} + g_l}, \qquad (1.2)$$

where g_{K0}, g_{Na0} and g_{Ca0} are the conductances of potassium, sodium and calcium ions at rest; E_K, E_{Na}, and E_{Ca} are electromotive forces of sources, which simulate Nernst potential of potassium, sodium and calcium respectively; g_l is the leakage conductivity through the membrane; E_l is electromotive force of source, which simulates Nernst potential for chlorine ions, leakage and other factors that affect the membrane potential in rest. Value of E_l in practice is selected so, that for a given conductivity g_l resting potential is equal to a predetermined value V_{m0}.

As follows from the parallel-conductance model, the variable component of the membrane potential during the flow of the depolarizing current I_d through the membrane must satisfy the differential equation

$$\frac{dv_m}{dt} = \frac{1}{C_m}\left(-I_K(v_m,t) - I_{Na}(v_m,t) - I_{Ca}(v_m,t) - I_l + I_d\right), \qquad (1.3)$$

where

$$I_K(v_m,t) = g_K(v_m,t)(V_{m0} + v_m + E_K),$$

$$I_{Na}(v_m,t) = g_{Na}(v_m,t)(V_{m0} + v_m - E_{Na}),$$

$$I_{Ca}(v_m,t) = g_{Ca}(v_m,t)(V_{m0} + v_m - E_{Ca})$$

are time dependences of potassium, sodium and calcium currents respectively;

$I_l = g_l(V_{m0} + v_m + E_l)$ is the leakage current through the membrane;

$I_d = \begin{cases} I_{d0}, & 0 < t < T_d \\ 0, & t \geq T_d \end{cases}$ is depolarizing current; I_{d0} is the amplitude of depolarizing current;

T_d is duration of depolarizing pulse.

During the membrane polarization conductance of potassium, sodium and calcium channels can be described by the equations:

$$g_K(v_m,t) = g_{K\max} n^4(v_m,t), \tag{1.4}$$

$$g_{Na}(v_m,t) = g_{Na\max} m^3(v_m,t) h(v_m,t), \tag{1.5}$$

$$g_{Ca}(v_m,t) = g_{Ca\max} d(v_m,t) f(v_m,t), \tag{1.6}$$

where $g_{K\max}, g_{Na\max}$ and $g_{Ca\max}$ are the membrane conductances for potassium, sodium and calcium ions respectively in the case all the channels of the membrane for this type of ions are in the open state; *n* is activation function of potassium channels; *m* is activation function of sodium channels; *h* is inactivation function for sodium channels; *d* is activation function of calcium channels and *f* is inactivation function for calcium channels.

Activation and inactivation functions have the meaning of probability, that activation or inactivation ion channel subunit is in the open state at the moment. These gating variables change from zero to one and they are the solutions of the set of nonlinear ordinary differential equations (ODE). The proposed model contains ionic currents, which are determined by five gating variables *n*, *m*, *h*, *d*, and *f*.

$$\frac{dn}{dt} = \frac{n_\infty - n}{\tau_n}, \qquad \frac{dm}{dt} = \frac{m_\infty - m}{\tau_m}, \tag{1.7}$$

$$\frac{dh}{dt} = \frac{h_\infty - h}{\tau_h}, \qquad \frac{dd}{dt} = \frac{d_\infty - d}{\tau_d}, \qquad \frac{df}{dt} = \frac{f_\infty - f}{\tau_f},$$

where

$$n_\infty = \frac{1}{1 + \exp\left(\frac{V_{hn} - v_m}{V_{Sn}}\right)},$$

$$m_\infty = \frac{1}{1 + \exp\left(\frac{V_{hm} - v_m}{V_{Sm}}\right)}, \qquad h_\infty = \frac{1 - h_{\min}}{\left(1 + \exp\left(\frac{v_m - V_{hh}}{V_{Sh}}\right)\right)^{P_h}} + h_{\min},$$

$$d_\infty = \frac{1}{1 + \exp\left(\frac{V_{hd} - v_m}{V_{Sd}}\right)}, \qquad f_\infty = \frac{1 - f_{\min}}{\left(1 + \exp\left(\frac{v_m - V_{hf}}{V_{Sf}}\right)\right)^{P_f}} + f_{\min},$$

$n_\infty, m_\infty,$ and d_∞ are the steady-state values of activation function for potassium, sodium and calcium channels respectively; h_∞ and f_∞ are the steady-state values of inactivation function for sodium and calcium channels; $h_{\min}$ and $f_{\min}$ are minimum values of inactivation for sodium and

calcium channels; V_{hn}, V_{hm} and V_{hd} are voltages of semi-activation for potassium, sodium and calcium channels; V_{Sn}, V_{Sm} and V_{Sd} are voltages of activation shape for potassium, sodium and calcium channels; V_{hh} and V_{hf} are voltages of semi-inactivation for sodium and calcium channels; V_{Sh} and V_{Sf} are voltages of inactivation shape for sodium and calcium channels; P_h and P_f are degrees of relaxation of inactivation for sodium and calcium channels.

Relaxation periods of activation $\tau_n, \tau_m,$ and τ_d for potassium, sodium and calcium channels were determined as follows

$$\tau_n = \tau_{n\max}\left(\frac{1-r_n}{\left(1+\exp\left(\frac{v_m - V_{h\tau n}}{V_{s\tau n}}\right)\right)^{P_{\tau n}}} + r_n\right),$$

$$\tau_m = \tau_{m\max}\left(\frac{1-r_m}{\left(1+\exp\left(\frac{v_m - V_{h\tau m}}{V_{s\tau m}}\right)\right)^{P_{\tau m}}} + r_m\right),$$

$$\tau_d = \tau_{d\max}\left(\frac{1-r_d}{\left(1+\exp\left(\frac{v_m - V_{h\tau d}}{V_{s\tau d}}\right)\right)^{P_{\tau d}}} + r_d\right),$$

where $\tau_{n\max}, \tau_{m\max},$ and $\tau_{d\max}$ are maximum relaxation periods of activation for potassium, sodium and calcium channels; $r_n, r_m,$ and r_d are ratios of minimum relaxation period to maximum relaxation period of

activation for potassium, sodium and calcium channels; $V_{h\tau n}$, $V_{h\tau m}$, and $V_{h\tau d}$ are voltages of semi-relaxation of activation; $V_{S\tau n}$, $V_{S\tau m}$, and $V_{S\tau d}$ are voltages of relaxation shape of activation; $P_{\tau n}$, $P_{\tau m}$, and $P_{\tau d}$ are degrees of relaxation of activation for potassium, sodium and calcium channels, respectively.

Relaxation periods of inactivation τ_h and τ_f for sodium and calcium channels were determined as follows

$$\tau_h = \tau_{h\max}\left(\frac{1-r_h}{\left(1+\exp\left(\frac{v_m - V_{h\tau h}}{V_{S\tau h}}\right)\right)^{P_{\tau h}}} + r_h\right),$$

$$\tau_f = \tau_{f\max}\left(\frac{1-r_f}{\left(1+\exp\left(\frac{v_m - V_{h\tau f}}{V_{S\tau f}}\right)\right)^{P_{\tau f}}} + r_f\right),$$

$\tau_{h\max}$ and $\tau_{f\max}$ are maximum relaxation periods of inactivation for sodium and calcium channels; r_h and r_f are ratios of minimum relaxation period to maximum relaxation period of inactivation for sodium and calcium channels; $V_{h\tau h}$ and $V_{h\tau f}$ are voltages of semi-relaxation of inactivation; $V_{S\tau h}$ and $V_{S\tau f}$ are voltages of relaxation shape of inactivation; $P_{\tau h}$ and $P_{\tau f}$ are degrees of relaxation of inactivation for sodium and calcium channels, respectively.

The initial conditions are

$$
\begin{aligned}
v_m(0) &= 0, \\
n(0) &= n_0, \\
m(0) &= m_0, \\
d(0) &= d_0, \\
h(0) &= h_0, \\
f(0) &= f_0,
\end{aligned}
\tag{1.8}
$$

where n_0, m_0, d_0, h_0 and f_0 can be found as $n_\infty, m_\infty, d_\infty, h_\infty$ and f_∞ for $v_m = 0$.

Maximal conductances of the membrane for K^+, Na^+ and Ca^{2+} channels are defined as

$$g_{K\max} = \frac{g_{K0}}{n_0^4}; \tag{1.9}$$

$$g_{Na\max} = \frac{g_{Na0}}{m_0^3 h_0}; \tag{1.10}$$

$$g_{Ca\max} = \frac{g_{Na0}}{d_0 f_0}. \tag{1.11}$$

Equation (1.3), the set of equations for all gating variables (1.7), as well as initial conditions (1.8) make Cauchy problem relatively functions v_m, n, m, d, h and f, which is a set of stiff differential equations. Therefore, to solve it, the implicit methods of integration should be used [12]. Using the predictor-corrector method, in order to avoid overflow of the computer grid, step Δt in the initial segment of integration should not be too large. The initial value should be selected as $\Delta t < T_d$, where T_d is duration of the depolarizing pulse.

As a simplified, but a rough solution of the Cauchy problem, the following method can be used. Suppose that speed of transitions of

activation and inactivation subunits of ion channels from closed state into open and backwards changes slightly within the integration step. Then relaxation periods $\tau_n, \tau_m, \tau_h, \tau_d, \tau_f$ and values $n_\infty, m_\infty, d_\infty, h_\infty, f_\infty$ can be considered as slightly changing. Accepting that these values are the constants depending only on voltage and not on time, differential equations can be solved explicitly. Then

$$
\begin{aligned}
n(v_m,t) &= n_\infty - (n_\infty - n_0)\exp(-t/\tau_n);\\
m(v_m,t) &= m_\infty - (m_\infty - m_0)\exp(-t/\tau_m);\\
h(v_m,t) &= h_\infty - (h_\infty - h_0)\exp(-t/\tau_h);\\
d(v_m,t) &= d_\infty - (d_\infty - d_0)\exp(-t/\tau_d);\\
f(v_m,t) &= f_\infty - (f_\infty - f_0)\exp(-t/\tau_f).
\end{aligned}
$$

Such approach makes it possible to analyze the parameters of the model and find their primary approximation in accordance with action potential shape.

The value of E_l is determined from (1.2). Values $g_{K\max}$, $g_{Na\max}$, and $g_{Ca\max}$ are found from the equations (1.9-1.11) given the fact, that n_0, m_0, d_0, h_0 and f_0 are the values of activation and inactivation functions $n_\infty, m_\infty, d_\infty, h_\infty$ and f_∞ for the steady state, when $v_m(0) = 0$.

Together with transmembrane potential dependence on the time for action potential generation, changes of membrane currents for potassium ions, sodium, calcium and influence of leakage, chlorine ions, and other factors that affect the membrane potential are considered in the model using the Hodgkin-Huxley formalism. The model of electrical activity in cardiomyocyte simulates action potential dynamics and

dynamics of transmembrane currents.

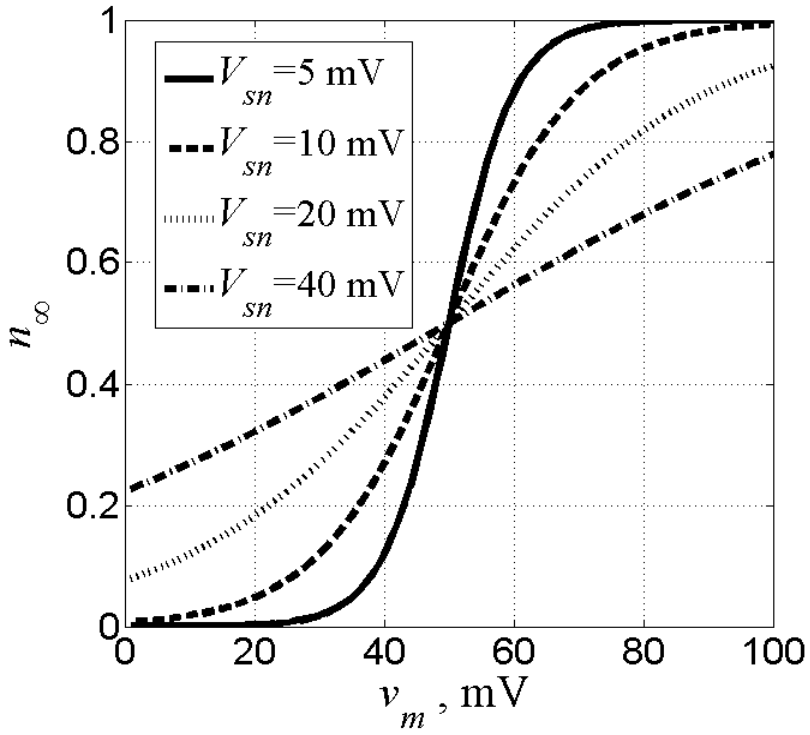

Fig. 1.7. Activation function for potassium channel versus alternating component of membrane potential for the voltages of semi-activation V_{hn} = 50 mV and various voltages of activation shape V_{sn}

To obtain the correct results with the considered model, it is necessary to identify the model parameters and the relationships between their values. For the occurrence of action potential, the condition $|I_{Na}| > |I_K|$ is necessary. In this condition the overall flow of cations into the cell causes an increase in potential V_m and starts the process, which characterizes the growth phase of action potential. Growth of V_m causes growth of g_{Na}, as channel conductivity is a function that depends continuously on the transmembrane potential, which in turn leads to a further increase of V_m, etc. The relaxation period of activation of sodium channels τ_m is very small. The action potential can arise, when

$\tau_m << \tau_n$ and τ_h, in case of a state with a low value of *n*, normal value of *m* and increased value of *h*. This combination of three parameters leads

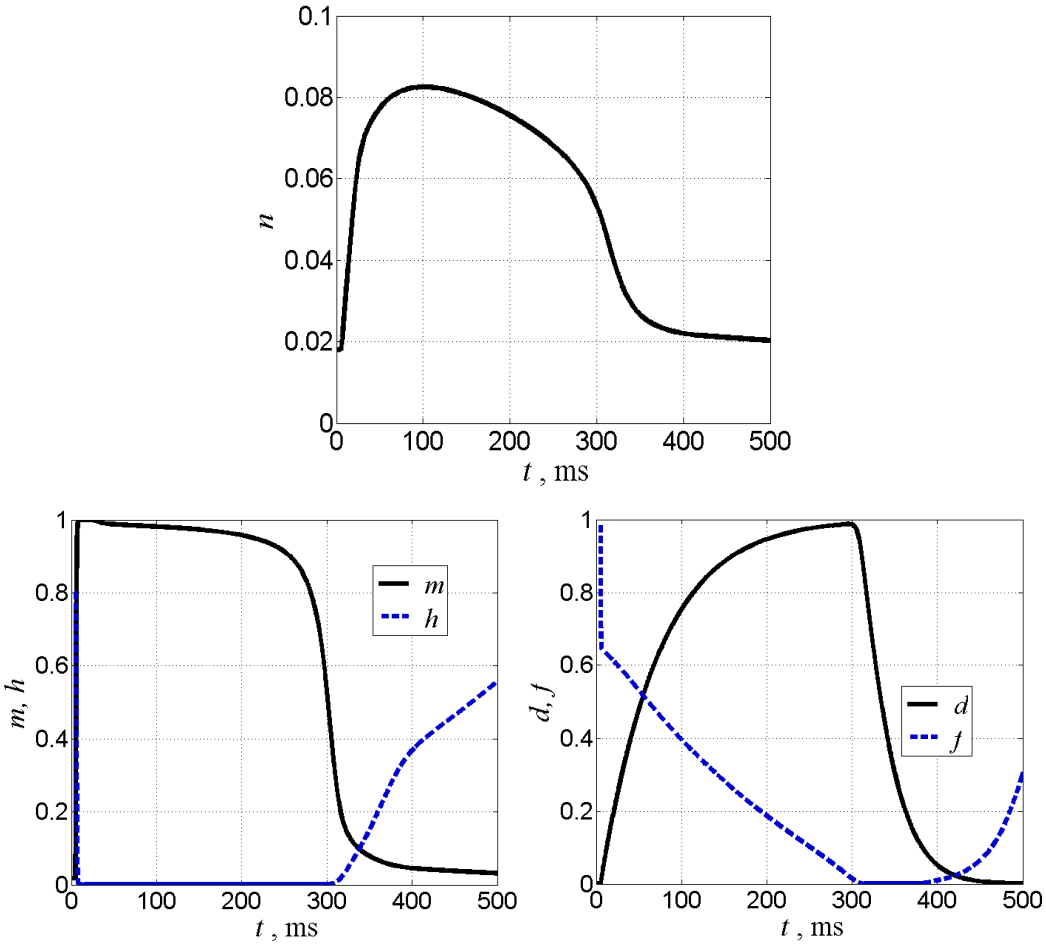

Fig.1.8. Gating variables, which determine ionic currents in the model: a) activation function (*n*) of potassium channels; b) activation (*m*) and inactivation (*h*) functions of sodium channels; c) activation (*d*) and inactivation (*f*) functions of calcium channels

to the fulfillment of the condition $|I_{Na}| > |I_K|$ and excitation may occur in a cell.

Resting membrane potential is mostly determined by high potassium permeability (conductance) and its value is close to the Nernst potential of potassium E_K. Taking this into account, it can be seen from the

equation (1.2), that conductance of calcium ions at rest g_{Ca0} should be small and should not practically affect the resting potential value.

Meanwhile, in order to make calcium current to contribute to the stage of cardiomyocyte membrane repolarization, especially in the plateau phase of the action potential, the maximum conductance of the membrane for calcium channels $g_{Ca\max}$ should be quite large and comparable to $g_{K\max}$. This can be achieved by a very small value of the parameter d_0, which in its turn is provided by large value of V_{hd} and small value of V_{sd}. Maximum relaxation period of inactivation of calcium channels $\tau_{f\max}$ defines the duration of repolarization, which is long enough in cardiomyocytes. Therefore, it is necessary to specify $\tau_{d\max} < \tau_{f\max}$. The equations, listed above, were solved for simulation of action potential in ventricular cardiomyocytes using parameter values presented in TABLE I. Gating variables for potassium, sodium and calcium channels, obtained by solving the set of differential equations, are presented in Fig.1.8, a-c.

Obtained simulated action potentials for atrial and ventricular cardiomyocytes (Fig. 1.9) in accordance with the theoretical information [1-4] have three characteristic phases: depolarization, plateau and repolarization. Depolarization phase is determined by a sharp increase of AP amplitude due to the growth of membrane permeability for sodium ions. Plateau phase describes the slow decline of action potential, which is explained by the simultaneous work of two types of channels - slow calcium channels and potassium channels. Repolarization phase is determined by the faster decline in AP amplitude, which is caused by closing of calcium channels and strengthening of the outward potassium current.

TABLE I. PARAMETERS OF THE MODEL

Para-meter	Value	Parameter	Value	Parameter	Value
C_m	1 μF/cm^2	V_{hm}	40 mV	$\tau_{d\,max}$	70 ms
V_{m0}	-85 mV	V_{hh}	7 mV	$\tau_{f\,max}$	260 ms
E_K	80 mV	V_{hd}	34 mV	$V_{h\tau n}$	40 mV
E_{Na}	50 mV	V_{hf}	5 mV	$V_{h\tau m}$	40 mV
E_{Ca}	120 mV	V_{sn}	50 mV	$V_{h\tau h}$	50 mV
g_{K0}	$7\cdot10^{-7}$ S/cm^2	V_{sm}	10 mV	$V_{h\tau d}$	20 mV
g_{Na0}	$5\cdot10^{-8}$ S/cm^2	V_{sh}	-5 mV	$V_{h\tau f}$	75 mV
g_{Ca0}	$8\cdot10^{-10}$ S/cm^2	V_{sd}	2.5 mV	$V_{s\tau n}$	20 mV
g_l	$15\cdot10^{-6}$ S/cm^2	V_{sf}	-1 mV	$V_{s\tau m}$	10 mV
I_{d0}	$7\cdot10^{-5}$ A/cm^2	$\tau_{n\,max}$	50 ms	$V_{s\tau h}$	-50 mV
T_d	0.5 ms	$\tau_{m\,max}$	0.5 ms	$V_{s\tau d}$	20 mV
V_{hn}	200 mV	$\tau_{h\,max}$	2 ms	$V_{s\tau f}$	10 mV

The model, based on the formalism of Hodgkin-Huxley, should be considered as a model describing the average values of membrane currents. It assumes, that membrane contains a large number of channels, which simultaneously operate in a cardiomyocyte, so the description of membrane currents results in averaging over the ensemble of channels.

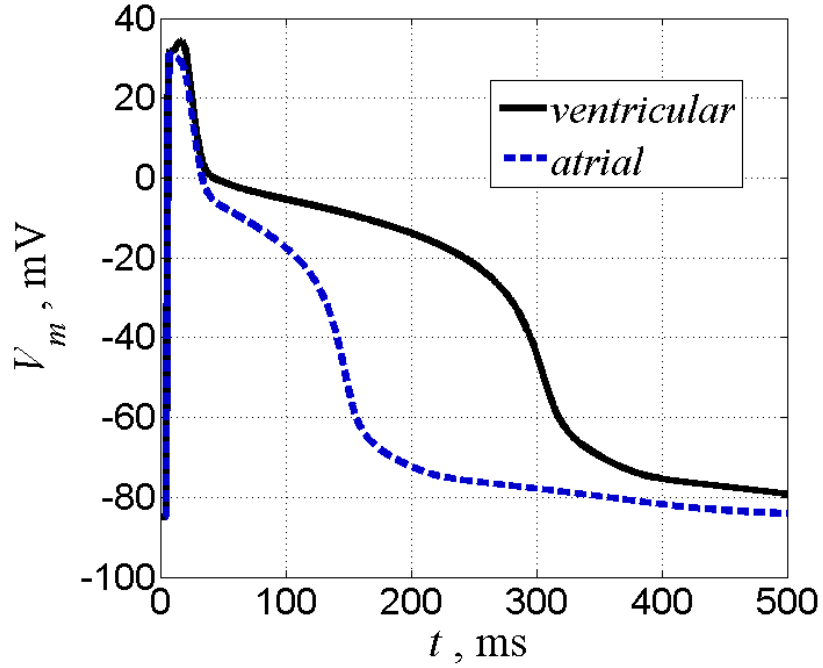

Fig. 1.9. Simulated action potentials for atrial and ventricular cardiomyocytes

Pacemaker signals arise in specialized cardiomyocytes, which able to generate periodical oscillations of their membrane potential [1, 13]. Pacemaker cells are located in the sinoatrial node (SAN). The pacemaker impulses propagate from the SAN through cardiac conduction system: the atrioventricular node (AVN), Bundle of His and Purkinje fibers network, and cause the contraction of the myocardium. The cycle generation of SAN action potential determines the heart rate.

The spontaneous depolarization (Fig. 1.10) is unique property of SAN cells that necessary for SAN pacemaker activity. There is important physiological difference between nodal cells and ventricular cells due to the specific mechanisms in ion channels. The potential for cardiomyocyte action of the working myocardium (atria and ventricles) does not normally develop spontaneously. Generation of the action potential is caused by a wave of depolarization of neighboring cells of the

cardiomyocyte, and its membrane potential becomes less negative.

Pacemaker heart cells (or rhythm drivers) do not need external stimuls to generate action potential, since they have their own automatism, that is, the ability to spontaneously depolarize and to develop the action potential.

The properties of rhythm drivers are possessed by cells of the sinoatrial, atrioventricular nodes and Purkinje fibers (natural pacemakers). The cells of the ventricular myocardium do not normally have automaticity, but they can acquire this ability in myocardial ischemia [13].

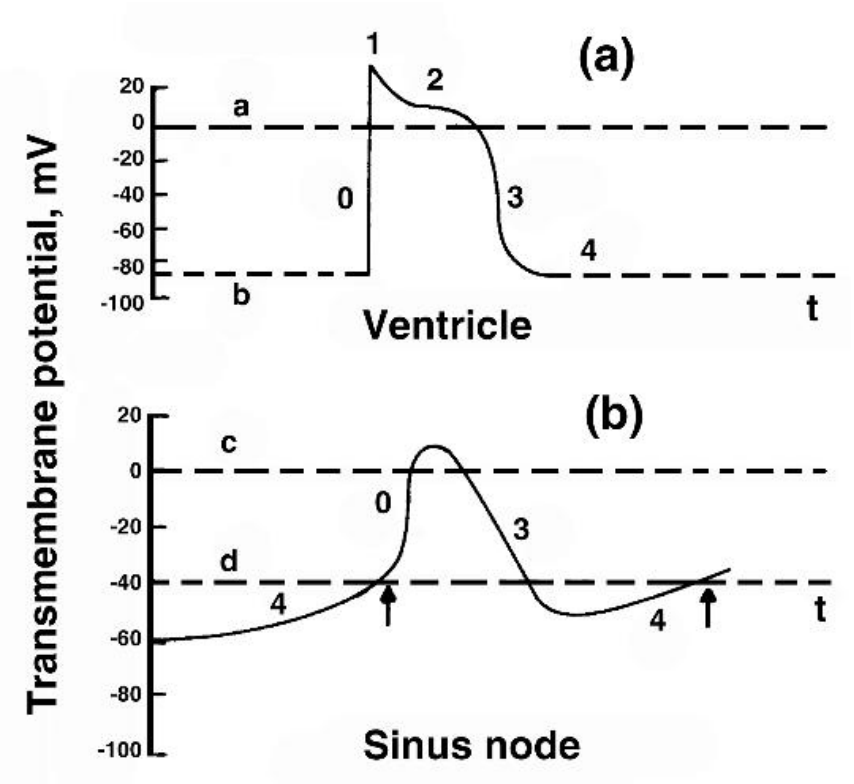

Fig. 1.10. Membrane potential V_m for ventricular cells (a) and SAN cells (b) [1].

The action potential of pacemaker cells (in contrast to atrial and ventricular myocardium cells) has three features:

1. The negative potential in pacemaker cells reaches a value of -60 mV, which is much less than the resting potential of ventricular myocardial cells (-90 mV). The fast sodium channels of pacemaker cells remain inactive with such a potential.

2. The phase 4 of the action potential for pacemaker cells is not horizontal (Fig. 1.10, b), but has an upward character, which reflects a gradual, spontaneous depolarization due to pacemaker current, which is carried by Na^+ ions. The ion channels, through which the pacemaker flow passes, differ from the fast sodium channels responsible for the depolarization phase of myocardial cells. Penetration of positively charged Na^+ ions through the pacemaker channels helps the membrane potential during phase 4 to become less negative until it reaches the threshold potential. In this case, a slow inactivation of the pacemaker channels occurs.

3. The phase 0 of the action potential for pacemaker cells has a longer duration and a smaller amplitude than in myocardial cells. This can be explained by the fact that the fast sodium channels of pacemaker cells are inactive, and the excitation of the action potential is due to the flow of Ca^{2+} currents into the cell through slow calcium channels.

The repolarization of pacemaker cells occurs in the same way as in ventricular myocardial cells. It is due to the inactivation of calcium channels, as well as the activation of potassium channels and the release of K^+ ions from the cell.

Different currents of the SAN ion channels contribute to the generation of action potential, but their functional roles and interactions are still not understood [13-15].

In the recent papers three hypotheses were proposed to explain the mechanism underling the cardiac automaticity. Authors [14] discribed the

"membrane clock" model of pacemaking, which includes the "funny" current (I_f), an inward Na^+/K^+ current, activated by membrane hyperpolarization at negative voltages. In the "calcium clock" model and "coupled-clock" model of pacemaking [15] the key mechanism in the diastolic depolarization was a spontaneous rhythmic phenomenon of Ca^{2+} release from the sarcoplasmic reticulum (SR). And authors [13] focused on functional role of voltage gated Ca^{2+} channels of two families: *L*-type and *T*-type .

Ca^{2+} currents of *L*- and *T*-type were recorded in cells of SAN, AVN, and Purkinje Fibers. The current of *L*-type ($I_{Ca,L}$) was defined as a "high"-threshold Ca^{2+} current, activated from about -30 mV and the Ca^{2+} current of *T*-type ($I_{Ca,T}$) was defined as a "low" threshold Ca^{2+} current, activated at −50 mV, moreover both currents participated at the latter half of the slow diastolic depolarization.

1.3.3. Simulation of action potential in nerve fibers

Simulation of action potential in the membrane of nerve fiber is based on parallel-conductance model (Fig. 1.11), in which independent conductance channels are presented for K^+, Na^+, and Cl^- ions (channel for Cl^- can be replaced on channel for leakage through the membrane). Total membrane current is the sum of currents for each branch of the electrical circuit.

To solve the Cauchy problem a system of differential equations is constructed. This system contains four equations, that describe membrane potential v_m, activation function for potassium *n*, activation function for sodium *m*, inactivation function for sodium *h*.

$$\frac{dv_m}{dt} = \frac{1}{C_m}\left(-I_K(v_m,t) - I_{Na}(v_m,t) - I_l + I_d\right), \tag{1.12}$$

$$\frac{dn}{dt} = \frac{n_\infty - n}{\tau_n}, \tag{1.13}$$

$$\frac{dm}{dt} = \frac{m_\infty - m}{\tau_m}, \tag{1.14}$$

$$\frac{dh}{dt} = \frac{h_\infty - h}{\tau_h}, \tag{1.15}$$

where $I_K(v_m, t)$ is dependent on time potassium current,

$I_{Na}(v_m, t)$ is dependent on time sodium current,

I_l is leakage current through the membrane,

$\tau_n = \frac{1}{\alpha_n + \beta_n}$ is the relaxation period of activation for potassium channels,

$\alpha_n = \frac{10(0.01 - v_m)}{\exp\left(\frac{0.01 - v_m}{0.01}\right) - 1}$ is rate for switching of activation subunits for potassium channels from closed state to open,

$\beta_n = 125\exp\left(-\frac{v_m}{0.08}\right)$ is rate for switching of activation subunits for potassium channels from open position to closed,

$n_\infty = \alpha_n \tau_n$ is the steady-state value of activation function for potassium

$\tau_m = \frac{1}{\alpha_m + \beta_m}$ is the relaxation period of activation for sodium channels,

$\alpha_m = \frac{100(0.025 - v_m)}{\exp\left(\frac{0.025 - v_m}{0.01}\right) - 1}$ is rate for switching of activation subunits for sodium channels from closed position to open,

$\beta_m = 4 \cdot 10^3 \exp\left(-\frac{v_m}{0.018}\right)$ is rate for switching of activation subunits for sodium channels from open position to closed,

$m_\infty = \alpha_m \tau_m$ is the steady-state value of activation function for sodium,

$\tau_h = \frac{1}{\alpha_h + \beta_h}$ is the relaxation period of inactivation for sodium channels,

$\alpha_h = 70 \exp\left(-\frac{v_m}{0.002}\right)$ is rate for switching of inactivation subunits for sodium channels from closed position to open,

$\beta_h = \frac{10^3}{\exp\left(\frac{0.03 - v_m}{0.01}\right) + 1}$ is rate for switching of inactivation subunits for sodium channels from open position to closed,

$h_\infty = \alpha_h \tau_h$ is the steady-state value of inactivation function for sodium.

To simulate of action potential in the membrane of nerve a system of differential equations is solved with initial conditions:

$$v_m(0) = 0, \quad n(0) = n_0, \quad m(0) = m_0, \quad h(0) = h_0. \qquad (1.16)$$

Thus, equations (1.12) - (1.16) are Cauchy problem relatively functions $v_m(t)$, n, m and h. This Cauchy problem can be presented as:

$$\frac{dv_m}{dt} = f_1(v_m, n, m, h, t);$$
$$\frac{dn}{dt} = f_2(v_m, n, m, h, t);$$
$$\frac{dm}{dt} = f_3(v_m, n, m, h, t);$$
$$\frac{dh}{dt} = f_4(v_m, n, m, h, t),$$

where the functions f_1, f_2, f_3, f_4 are determined by the equations (1.12) - (1.15) and the initial conditions are determined by the expressions (1.16).

There is the period after appearance of the action potential, during which the membrane cannot be excited. This period is called refractory period (Fig. 1.11, 1.12).

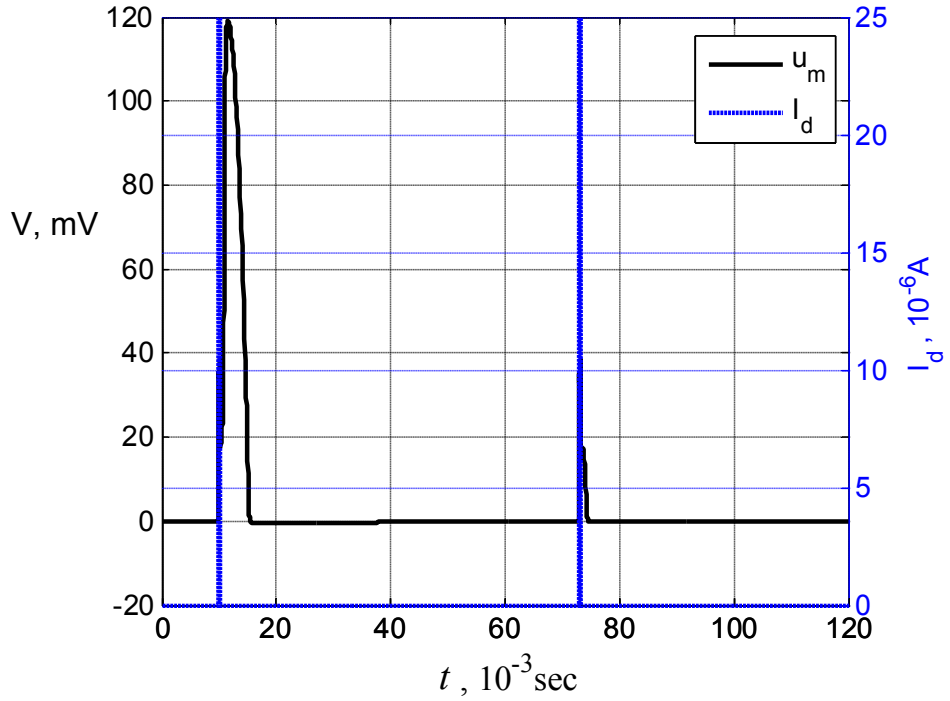

Fig. 1.11. Membrane potential under the excitation by two depolarizing pulses with a period less than the refractory period

The presence of this condition can be explained on the basis of the behavior of the inactivation function for sodium channels *h*. After appearance of action potential the function *h* reduces to a very low value, which prohibits occurrence of excitation. To return to a normal level of function *h* some time should pass. Also the activation function of

potassium channels *n* have to decrease, since the implementation of condition: $|I_{Na}|> |I_K|$ is necessary for appearance of excitation.

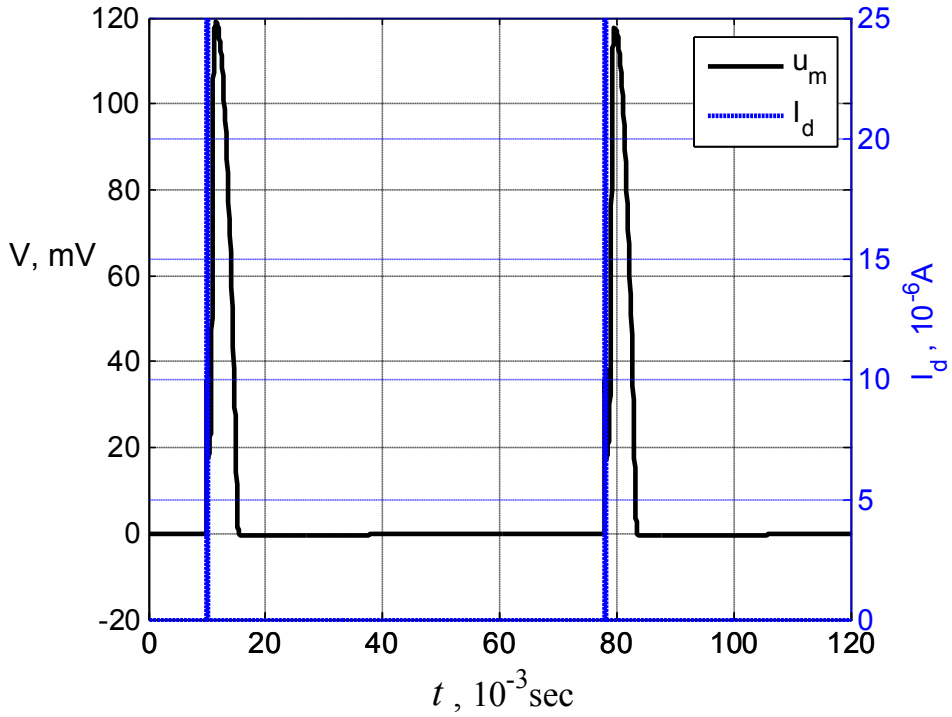

Fig. 1.12. Membrane potential under the excitation by two depolarizing pulses with a period more than the refractory period

Experimental studies have shown, that excitation of the membrane may occur after prolonged hyperpolarization. Since the electrode in the external environment is an anode, this phenomenon is called anode break excitation of the cell. The presence of such effect can be explained as follows. Immediately before the removal of hyperpolarization the level of *h* goes down, while the levels of *m* and *n* rise up. However, after restoring of normal V_m, the activation function of sodium channels *m* quickly restores its value, since the relaxation period of activation for sodium channels τ_m is very small. Consequently, as a result of $\tau_m << \tau_n, \tau_h$, there is a state, which is characterized by reduced value of *n*, normal value of *m* and increased value of *h*. This combination of

three parameters creates a condition $|I_{Na}| > |I_K|$, resulting in a possible excitation occurrence (Fig. 1.13).

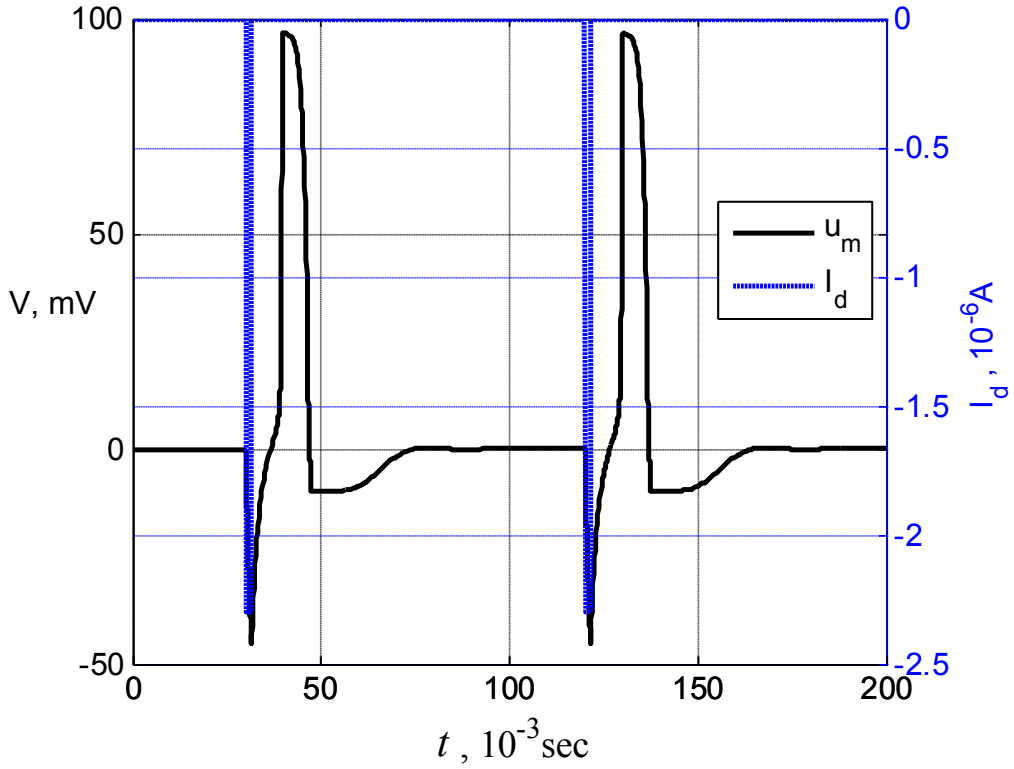

Fig. 1.13. Membrane potential under anode break excitation of the cell

1.3.4. Modeling of the circulation of exciting impulse in the myocardium

The purpose of modeling of excitation wave circulation in the heart structures is the research at the level of myocardial cells of mechanisms that cause arrhythmia. Cardiac arrhythmias are basically produced by one of three mechanisms: enhanced automaticity, triggered activity, or reentry mechanism. Reentry mechanism occurs when a propagating impulse does not fade out after normal activation of the heart and persists to re-excite the heart after the end of refractory period. This electrophysiologic mechanism is responsible for the majority of

arrhythmias.

For one-dimensional modeling of the excitation impulse circulation a closed loop for reentry mechanism simulation in the myocardium is obtained by connecting the ends of the fiber. The membranes of cardiomyocytes have selective permeability for different types of ions. Membrane model (MM) for the case of action potential emergence is presented by parallel-conductance model, based on the assumption of existence of independent channels for K^+, Na^+ and Ca^{2+} ions.

In modeling of excitation impulse circulation by of reentry mechanism a modification of the model with leading core and a generalized model of Hodgkin-Huxley was performed by creating a one-dimensional ring model in the form of a closed chain of N cardiomyocytes (Fig. 1.14) [16-21], N = 100-120.

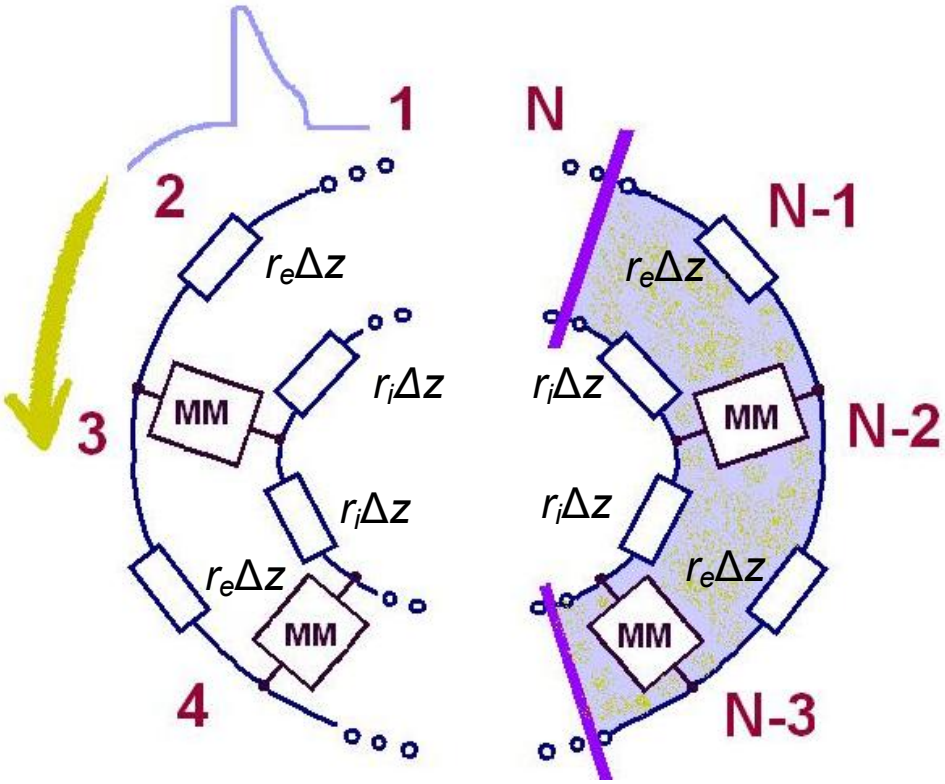

Fig. 1.14. Ring model of reentry circle with inhomogeneity of electrophysiological parameters of myocardial cells

Membrane potential $V_m(z, t)$ is a function of time t and spatial coordinate z taken along the direction of propagation of the action potential. In this case, $V_m(z,t) = V_{m0} + v_m(z,t)$, where V_{m0} is the resting membrane potential, $v_m(z, t)$ is the variable component of the membrane potential, which is a deviation from the membrane potential. Model of the leading core connects the second derivative on the membrane potential with current flowing through the membrane and the external excitation current:

$$\frac{\partial^2 v_m}{\partial z^2} = (r_i + r_e) i_m + i_p r_e,$$

where i_m is membrane current per unit length, measured in A/m;

r_e and r_i are axial resistances of extracellular and intracellular environment per unit length, measured in Ohm/m;

i_p is external stimulus, measured in A/m. Taking into account the fact that

$$r_e = \frac{4\rho_e}{\pi D^2},$$

$$r_i = \frac{4\rho_i}{\pi D^2},$$

$$i_m = J_m \pi D,$$

we can obtain that

$$\frac{\partial^2 v_m}{\partial z^2} = \frac{4(\rho_i + \rho_e)}{D} J_m + \frac{4\rho_e}{\pi D^2} i_p,$$

where ρ_e and ρ_i are resistivities of extracellular and intracellular environment, measured in Ohm · m;

J_m is membrane current density, measured in A/m^2;

D is diameter of the cylindrical cell.

The spread of cardiac action potential along the fiber is represented as a differential equation:

$$\frac{\partial^2 v_m}{\partial z^2} - \frac{4(\rho_i + \rho_e)}{D} C_m \frac{\partial v_m}{\partial t} = \frac{4(\rho_i + \rho_e)}{D}\left(J_K + J_{Na} + J_{Ca} + J_l\right) + \frac{4\rho_e}{\pi D^2} i_p .$$

Pathway in myocardium [0, *L*] is divided by uniform grid with a step $\Delta z = \frac{L}{N}$, where *L* is length of reentry circle, *N* is number of mesh nodes. Cardiomyocytes length ranges from 20 microns for atria to 60-140 microns for ventricles and 150-200 microns for cells of Purkinje fibers. Simulating reentry loop with length in range of 8 – 12 mm, number of mesh nodes z_i must be chosen equal to the number of cells in the investigated area, for instance *N* = 100 – 120.

The second spatial derivative of the membrane potential in the grid of nodes can be approximated by using an interpolation polynomial of Lagrange and calculated explicitly:

$$\frac{\partial^2 v_m(z_i, t)}{\partial z^2} = \frac{v_{i\text{-}1}(t) - 2v_i(t) + v_{i+1}(t)}{\Delta z^2}, \quad i=\overline{2,\ N\text{-}1}.$$

Given the fact, that pathway is the reentry circle, the second spatial derivative of the membrane potential in the endpoints of the fiber is defined as:

$$\frac{\partial^2 v_m(z_1, t)}{\partial z^2} = \frac{v_N(t) - 2v_1(t) + v_2(t)}{\Delta z^2};$$

$$\frac{\partial^2 v_m(z_N, t)}{\partial z^2} = \frac{v_1(t) - 2v_N(t) + v_{N\text{-}1}(t)}{\Delta z^2}.$$

Determination of membrane potential v_m and activation function of potassium channels *n*, activation function of sodium channels *m*, inactivation function for sodium channels *h*, activation function of calcium channels *d* and inactivation function for calcium channels *f* was carried out by solving the system of differential equations. Numerous parameters of the defined functions are vectors that determine the electrophysiological properties of each individual cell in the reentry loop.

The speed of action potential propagation through the cardiac tissue significantly varies in different areas of the heart. This speed directly depends on diameter of muscle fibers involved in the process. Conduction through cells of AV node, which have small diameter, is much slower than conduction through cells of Purkinje fibers with large diameter. The velocity of conduction also depends directly on the intensity of local depolarizing ion current, which in turn directly depends on intensity of action potential increase. Rapid depolarization facilitates rapid conduction. Differences in capacitance and (or) resistance of cell membranes are also the factors, which cause the difference in values of speed of action potential propagation at certain areas of the heart.

The anatomical reentry mechanism is the simplest case for modeling the circular motion of the excitation pulse. When excitation pulse circulates in anatomically isolated enclosed chain, the path length is fixed and determined by perimeter of the anatomical structure, which forms the unexcited central part of the closed path. The reentry loop in this case is usually characterized by a large size of general perimeter of the circle (macro reentry). Modeling this case, we do not need to simulate a region with altered electrophysiological parameters. The same parameters can be used for all cells in the enclosed chain.

The functional reentry mechanism is determined by the

electrophysiological properties of the myocardial tissue. When these properties change, the length of the closed path changes too. The size of reentry circuit is not fixed, and its position is not strictly localized. This mechanism is usually characterized by a small loop and referred as micro reentry (6 - 10 mm in atrial fibrillation).

Considering that differences in refractoriness period and other electrophysiological parameters of neighboring cell groups can cause circulation in the tissues of atria, ventricles and Purkinje fibers, the mathematical model was constructed in such a way, that the enclosed loop was inhomogeneous in its parameters. By varying the range of values of the variables that affect appearance and maintenance of reentry mechanism, and also changing the size of the loop and the ratio of the lengths of sections with different electrophysiological parameters, different patterns of propagation of excitation pulse along the investigated chain were obtained.

The results of the simulation showed, that at different ratios of the parameters of cardiomyocytes in two sections of enclosed path, the existence of such variants is possible:

- a single passage of the excitation pulse along the loop without the occurrence of circulation (Fig. 1.15);
- occurrence of continuous circulation of the excitation pulse, for interruption of which the external intervention is required (Fig. 1.16);
- several turns of the excitation pulse along enclosed chain with following attenuation (Fig. 1.17);
- propagation of the excitation pulse only along the region with normal electrophysiological parameters and instantaneous attenuation in the affected region of the loop without the occurrence of circulation.

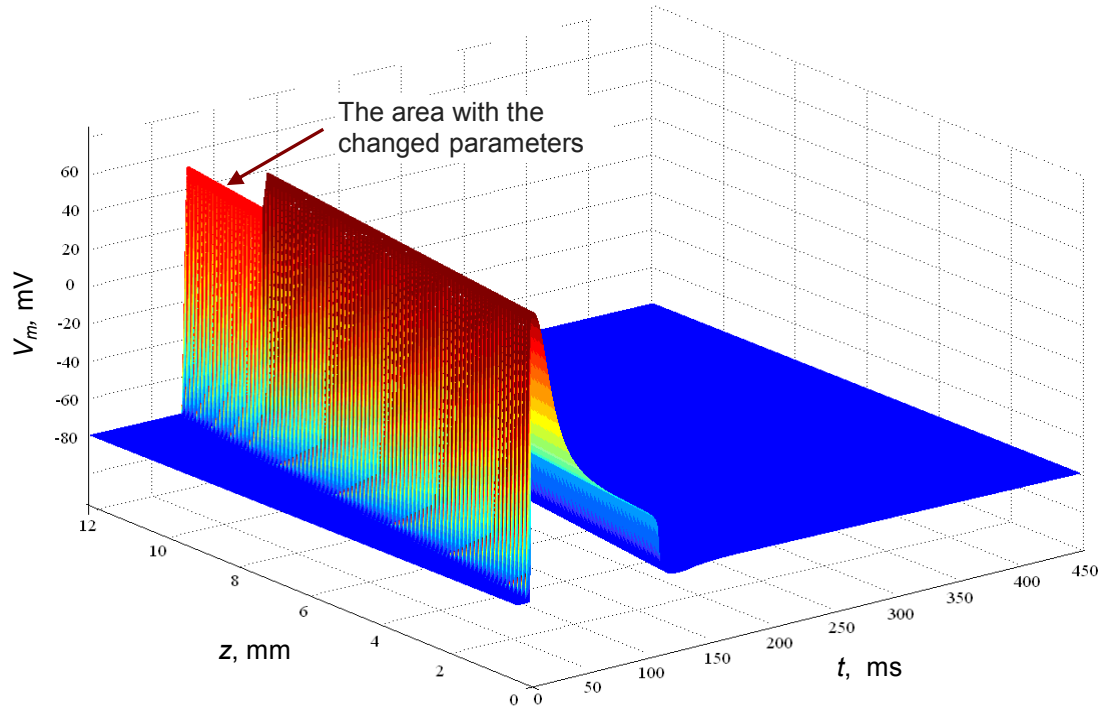

Fig. 1.15. Single passage of the excitation pulse without circulation

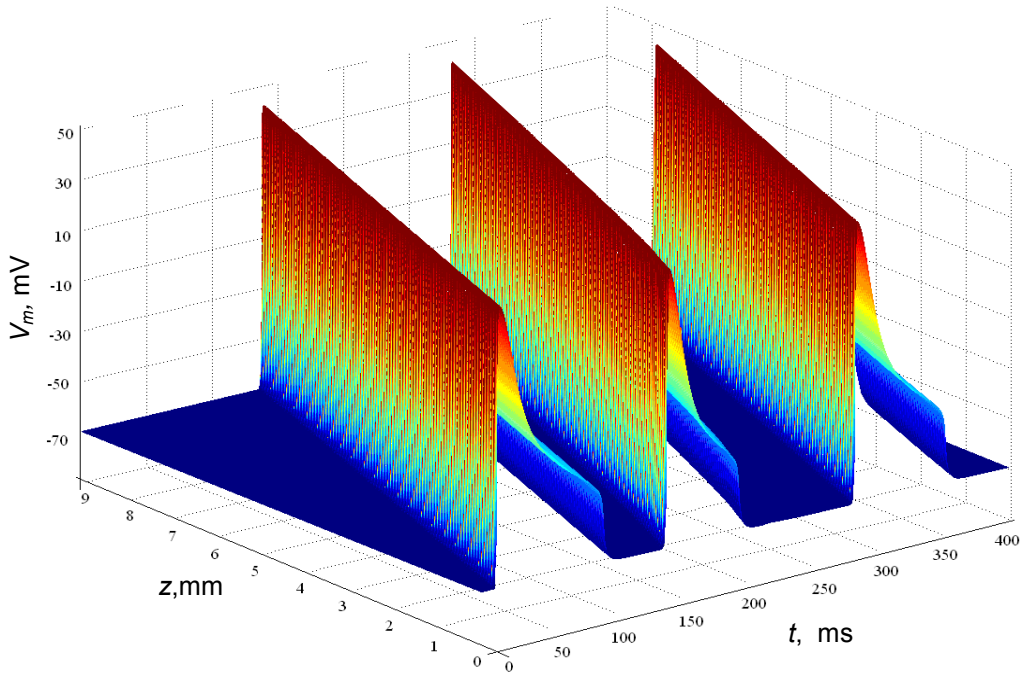

Fig. 1.16. Spatio-temporal representation of the continuous circulation of the excitation pulse along the loop with delayed propagation of action potentials

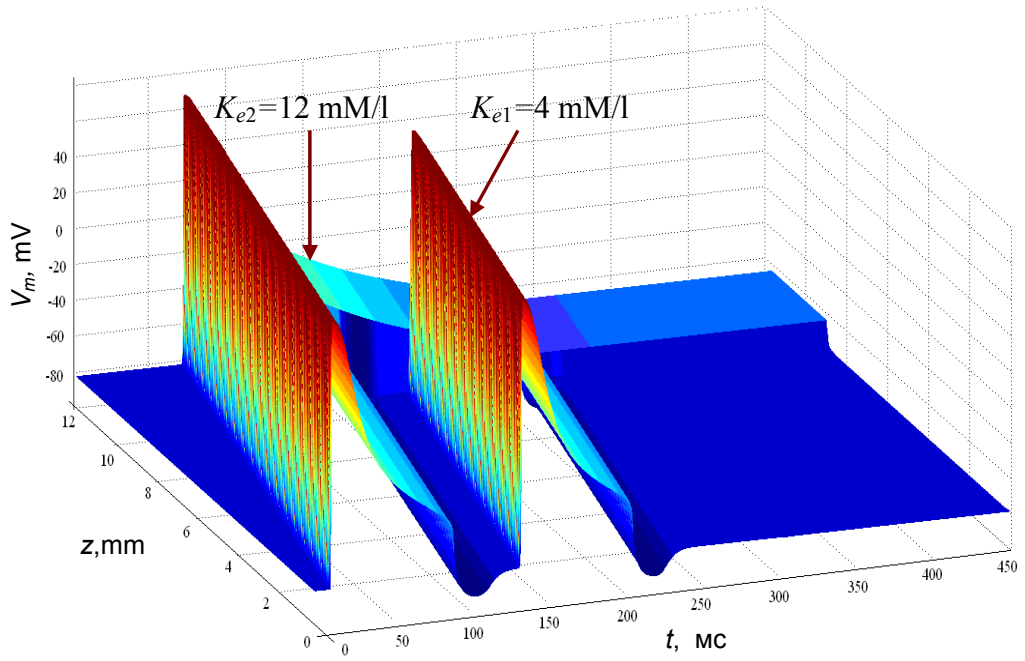

Fig. 1.17. Spatio-temporal propagation of action potential along the loop, which contains a region with an increased extracellular concentration of potassium ions K_{e2}

Action potential conduction, i.e. velocity of excitation propagation in cardiac structures, depends on the anatomical and physiological factors. The anatomical factors are diameter of the muscle fibers (10 – 15 μm for cardiomyocytes) and geometric arrangement of the muscle fibers. The velocity of conduction along the muscle fiber is greater than in the transverse direction. The physiological factors are amplitude of action potential, depolarization speed, as well as value of rest potential.

Normally, the excitation pulse spreads along the tissues of the heart at speed of 0.5 - 5 m/s. One of the reasons leading to the development of continuous circulation of the excitation pulse is the slow propagation of action potentials. Fig. 1.16 shows the simulated results of the excitation pulse circulation by reentry mechanism, obtained by decrease in the conducting speed to 0.068 m/s, caused by a change in the

electrophysiological parameters of cardiomyocytes in the atrial affected region.

The time of the excitation pulse turnover t_t around the loop can be defined as:

$$t_t = \frac{L}{v_c},$$

where L is the length of the circle; v_c is the speed of the excitation pulse conduction. Propagating at velocity of 0.068 m/s along a loop with L=10 mm, the excitation pulse returns to its initial point of motion through 147 ms, i.e. at the end of an effective refractory period of 145 ms. The cells, which recovered their excitability, reactivate and maintain the circulation of the excitation pulse according to reentry mechanism.

The increase in the action potential on the affected areas occurs unevenly. In regions with a notable decrease in the action potential, the slow wave excitation can occur. Decrease in the negative value of the resting potential as a result of partial depolarization also slows down conduction velocity.

At rest state, the intracellular concentration of potassium ions for myocardial cells is approximately 30 times higher than the extracellular concentration. Resting potential becomes less negative, when the extracellular concentration of potassium ions K_e increases. Changes in intracellular potassium concentration K_i are limited and do not significantly affect the value of V_{m0}. Fig. 1.17 depicts the simulation results for K_i = 150 mM/l throughout the entire length of the conductive path, K_{e1} = 4 mM/l in the main region and K_{e2} = 12 mM/l in the anomalous region. The excitation pulse in this case made 1 complete

turnover along the loop with L=12 mm, then again passed through the main loop section, equal in this case to 2/3 of the total circumference. The attenuation of the excitation pulse occurred at the boundary of the region with an increased extracellular concentration of potassium ions.

CONCLUSIONS

The changes of shape, duration, and pathways of action potentials propagation in the heart are manifestations of the mechanisms underlying the development of arrhythmias. In some cases, spontaneous attenuation of the excitation wave and termination of its circulation after several turnovers along a closed path are observed, in other cases a short strong single electric pulse is required to interrupt the circulation, which is used in clinical practice.

The proposed models can be used to determine the boundary conditions, under which the circulation of the excitation pulse leads to a breakdown of heart rhythm.

CONTROL QUESTIONS AND TASKS

1. Explain the phenomenon of selective permeability of biomembranes.
2. What concentration is bigger for potassium ions in muscle and nerve cells: intracellular concentration K_i or extracellular concentration K_e?
3. What concentration is bigger for sodium ions in muscle and nerve cells: intracellular concentration Na_i or extracellular concentration Na_e?

4. Explain the Nernst-Planck equation.

5. Explain how to identify the Nernst potential.

6. Explain the Goldman equation.

7. Explain the nature of the resting potential. Which factors does it depend on?

8. How does change the membrane resting potential, in case if

- intracellular concentration of sodium ions Na_i increases (decreases);
- extracellular concentration of sodium ions Na_e increases (decreases);
- intracellular concentration of potassium ions K_i increases (decreases);
- extracellular concentration of potassium ions K_e increases (decreases);
- permeability of K^+ ions increases (decreases);
- permeability of Na^+ ions increases (decreases)?

9. Draw the parallel-conductance model.

10. Explain the phenomena of action potential genesis.

11. What condition should be fulfilled between sodium and potassium currents (I_{Na} and I_K) for the emergence of membrane action potential?

12. How does the amplitude of action potential of the cell membrane change, if the intracellular concentration of sodium ions Na_i increases?

13. What is the refractory period and what are the mechanisms of this phenomenon?

14. What is the mechanism of anode break excitation of the cell?

15. Explain the system of equations for solving the Cauchy problem for the process of propagation of the action potential along cellular fiber.

REFERENCES

[1] R. Plonsey and R. Barr, *Bioelectricity. A Quantitative Approach*, third ed. New York: Springer Science+Business Media, LLC, 2007.

[2] A.Hodgkin and A. Huxley, "A quantitative description of membrane current and its application to conduction and excitation in nerve" *J. Physiol.*, 117, pp. 500–544, 1952.

[3] R.R. Aliev, "Computer modelling of heart electrical activity," Advances of Physiological Sciences, vol. 41. no. 3, pp. 44-63, 2010.

[4] http://www.all-fizika.com/article/index.php?id_article=1977

[5] McAllister R.E., Noble D., Tsien R.W. "Reconstruction of the electrical activitity of cardiac purkinje fibres," J. Physiol., vol. 251, pp. 1–59, 1975.

[6] C. Luo and Y. Rudy, "A model of ventricular cardiac action potential," Circ. Res., 68, 1501–1526, 1991.

[7] C. Luo and Y. Rudy, “A dynamic model of the cardiac ventricular action potential. i. Simulations of ionic currents and concentration changes,” Circ. Res., vol. 74, no. 6, pp. 1071–1096, 1994.

[8] M. Courtemanche, R. J. Ramirez and S. Nattel, “Ionic mechanisms underlying human atrial action potential properties: Insights from a mathematical model,” Amer. J. Physiol., vol. 275, no. 1, pp. H301–H321, 1998.

[9] R. L. Winslow et al., “Mechanisms of altered excitation-contraction coupling in canine tachycardia induced heart failure, ii model studies,” Circ.Res., vol.84, no.5, pp.571– 586, 1999.

[10] J. L. Puglisi and D. M. Bers, “Labheart: An interactive computer model of rabbit ventricular myocyte ion channels and ca transport,”

Amer. J. Physiol. Cell Physiol., vol. 281, no. 6, pp. C2049–C2060, 2001.

[11] Simulation of action potential in cardiomyocytes / Ivanko K., Ivanushkina N., Prokopenko Y.// Proceedings of 2017 IEEE 37th International Scientific Conference on Electronics and Nanotechnology (ELNANO). – 2017. – pp. 358-362.

[12] R. J. Spiteri, and R. C. Dean, "On the Performance of an Implicit–Explicit Runge–Kutta Method in Models of Cardiac Electrical Activity," IEEE Trans. on Biomed. Eng., vol. 55, no. 5, pp. 1488-1495, 2008.

[13] Pietro Mesirca, Angelo G. Torrente, Matteo E. Mangoni. Functional role of voltage gated Ca^{2+} channels in heart automaticity/ Front Physiol v.6; 2015.

[14] D. Difrancesco. The role of the funny current in pacemaker activity. Circ. Res. 2010, 106, 434–446.

[15] E. G. Lakatta, V. A. Maltsev, T. M. Vinogradova. A coupled SYSTEM of intracellular Ca^{2+} clocks and surface membrane voltage clocks controls the timekeeping mechanism of the heart's pacemaker. Circ. Res. 2010, 106, 659–673

[16] Haas H. Refractoriness of cardiac muscle as affected by intercalated disks: a model study implications for fibrillation and defibrillation / Haas H., Solchenbach K. // General physiology and biophysics. — 2004. — № 23 (2). — P. 133 — 171.

[17] Hund T. J. Dynamics of action potential head-tail interaction during reentry in cardiac tissue ionic mechanisms / T. J. Hund, N. F. Otani, Y. Rudy // American journal of physiology. Heart and circulatory physiology. — 2000. — Vol. 279. — P. 1869 — 1879.

[18] Sinha S. Termination of reentry in an inhomogeneous ring of model cardiac cells / S. Sinha, D. J. Christini // Physical Review. Statistical, Nonlinear and Soft Matter Physics. — 2002. — № 66. — P. 1— 7.

[19] Breuer J. Death, dynamics and disorder: Terminating reentry in excitable media by dynamically-induced inhomogeneities / J. Breuer, S. Sinha // Pramana: journal of physics. — 2005. — № 64 (4). — P. 553 — 562.

[20] Chen W. Dynamics of Sustained Reentry in a Loop Model with Discrete Gap Junction Resistances / W. Chen, M. Potse, A. Vinet // Phys. Rev. E. — 2007. — №76.— P. 1 — 6.

[21] Johnson C.R. Termination of reentrant propagation by a single extracellular stimulus in an atrial ring model / C. R. Johnson, R. C. Barr // Conference Proceedings of the 23rd Annual International Conference of the IEEE Engineering in Medicine and Biology Society. — 2001. — Vol. 1. — P. 398 — 401.

SECTION 2

IDENTIFICATION AND ASSESSMENT OF LATE POTENTIALS AS MARKERS OF CARDIAC ELECTRICAL INSTABILITY

2.1. Electrical conduction system of the heart

It is well-known that vital activity of any organism is accompanied by the bioelectric currents passing inside the organism, which emerge as a result of the electrical activity of cells. Cardiac electrical activity is characterized by an aggregate of electrical phenomena that can be registered using different methods of electrocardiography, providing a picture of temporal changes of the potential difference on the surface of human body. The signal, registered from the surface ECG electrodes, reflects the function or dysfunction of ion channels and represents an integration of electrophysiological processes of millions of cardiomyocytes.

Contraction of cardiac cells occurs, when the electrical impulse excitation extends along their membranes. Coordination of contractile activity of individual cells of cardiac muscle is achieved through the spread of action potentials from one cell to another. Action potentials propagate along the surface of cells and spread in heart from cell to cell through close contact parts of membranes, through which the internal local electric current passes. Active depolarization in any part of the membrane leads to local streams of intracellular and extracellular fluid, resulting in passive membrane depolarization of neighboring areas to their maximum voltage and emergence of depolarization.

Atrial and ventricular myocardium is synchronized in their work by specialized system responsible for the processes of excitation in the

heart (Fig. 2.1). The main components of the conduction system of the heart are the sinoatrial node, atrial interstitial ways, atrioventricular node, His bundle (atrioventricular bundle) and Purkinje fibers [1].

Sinoatrial node normally functions as an intracardiac pacemaker, generating action potentials that spread in cardiac cells, causing contraction of the heart. The velocity of signals conduction in atrial cells is about 1 m/s, and wave of action potential reaches atrioventricular node in about 0.08 s after it occurred. Atrioventricular node is a small cluster of specialized cells located on the surface of the right atrial septum. The bottom part of atrioventricular node consists of parallel-oriented fibers, which normally form only a bridge of adjacent cells through the formation of the heart that creates support for cardiac valves and electrically isolates the atria from the ventricles. Distribution of impulse in this region of atrioventricular node is very slow, with the velocity 0.05 m/s, so the time between excitation of atria and ventricles of the heart is normally about 0.15 seconds.

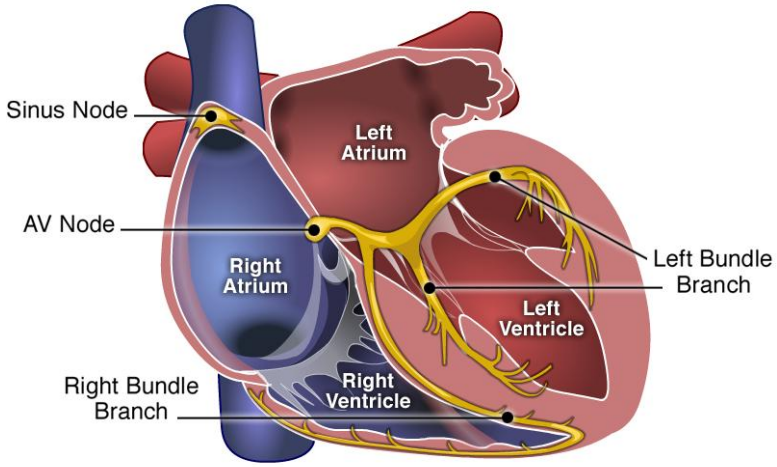

Fig. 2.1. Electrical conduction system of the heart

In the area, where His bundle entries into the tissue of interventricular septum, the bundle splits into left and right branches

consisting of Purkinje fibers of large diameter. These specialized fibers rapidly (at velocity of 3 m/sec) conduct impulses to the muscle tissue of the right and left ventricles. A wave of excitation runs along numerous Purkinje fibers and reaches the muscle cells. This leads to rapid, almost simultaneous excitation of ventricular muscle cells [1].

The electric field, caused by the electrical activity of the heart, can be measured by electrodes placed on the surface of the body. Electrocardiography method allows registration of potentials difference between two points on the body surface, which changes over time as a result of electrical processes that occur during the cardiac cycle.

Due to the fact, that at each moment of time potential at any point of the body is defined by a set of elementary dipoles, in a rough approximation the potential as a whole can be described by vector sum of the individual dipole moments. In this case, the placement of real sources in space is neglected, because all elements of dipole sources are assumed being located in the same point. As a result, only a total dipole is considered, which is called dipole or vector of the heart. It is believed that the heart vector changes in modulus and direction rather smoothly. The idea to consider the heart as an electric generator with a dipole structure is fundamental for ECG simulation and methods of clinical interpretation of electrocardiograms.

The main structural elements of the electrocardiogram are P wave, QRS complex and T wave (Fig. 2.2). P wave reflects the depolarization of the right and left atria. QRST ventricular complex reflects the complex process of propagation (QRS complex) and attenuation (RS-T segment and T wave) of excitation in the myocardium of the ventricles (ventricular depolarization and repolarization).

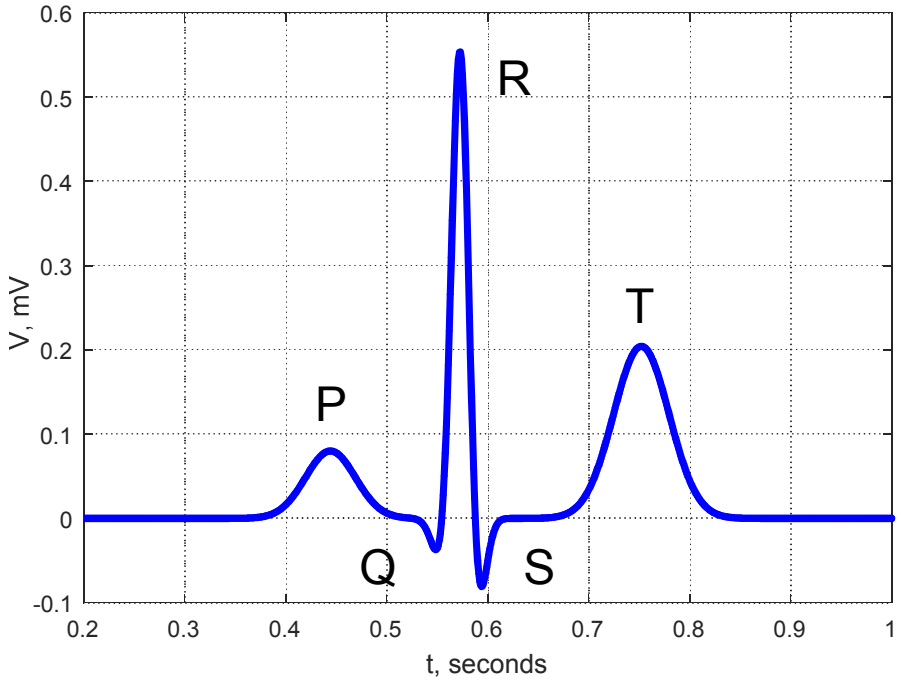

Fig. 2.2. The main structural elements of the electrocardiogram

Sometimes on ECG, particularly in the right chest leads, immediately after the T wave a small positive U wave is registered. It is believed that the U wave corresponds to the period of short-term increase in the excitability of myocardial ventricles. Amplitudes and the ratio of positive (P, R, T) and negative waves (Q and S) in different leads are dependent on how the heart vector turns around its axis.

Modern electrocardiographs allow registration of multi-channel ECG, which makes it possible to obtain more accurate information on the electric field of the heart by simultaneously recording of several different electrocardiographic leads. In clinical practice, the most widely used system is 12 standard ECG leads system, which is mandatory for every electrocardiographic examination of the patient and includes 3 standard leads, 3 unipolar enhanced leads from limbs, and 6 chest leads.

2.2. Atrial arrhythmias and mechanisms of their occurrence

The analysis of the heart rate includes determination of the excitation source, investigation of heart rate regularity and evaluation of conductivity functions [1-2]. Regularity of heart rate is assessed by comparing the length of R-R intervals, measured between the peaks of R waves in consecutively registered cardiac cycles. Regular or proper heart rhythm is diagnosed, when the durations of R-R intervals are approximately the same and variation of the received values does not exceed ±10% of the average duration of R-R intervals. In other cases incorrect (irregular) heart rate is diagnosed. Improper heart rhythm (arrhythmia) may occur in extrasystolia, atrial fibrillation, sinus arrhythmia, etc.

Definition of arrhythmia includes any anomaly of frequency, regularity or place of origin of excitement, as well as violations in impulses propagation and change of the normal sequence of atrial and ventricular activation. Cardiac disorders of rhythm and conduction can be caused by different pathologies. But ultimately, any abnormalities and arrhythmias are the result of the critical changes in the electrical activity of myocardial cells.

The reasons of arrhythmias include the following factors [1]:

1) violation of formation of excitation impulse:

• changes in normal automatism of sinoatrial node;

• occurrence of abnormal automatism of specialized cells of conduction system and cardiomyocytes (ectopic activity);

• trigger activity of heart cells (early or late post depolarization);

2) violation of conduction of excitation impulse:

• abnormal prolongation of refractory period;

• reducing in diastolic resting potential;

• violation of intercellular interaction;

• attenuation of conduction of excitation impulse;

• unidirectional blocking of excitation impulse propagation and development of reentry of excitation wave (the reentry mechanism);

3) combined pathology of formation and conduction of excitation impulse.

2.3. Circulation of excitation wave in the myocardium by the reentry mechanism

The major electrophysiological mechanism, which leads to arrhythmias caused by the violation of excitation impulse conduction, is the reentry mechanism [1-3]. The electric excitation impulse, making movement along a closed path (loop), returns to the place of its origin and repeats the movement. Normally, after the orderly propagation of excitation impulse through the conducting structures of the heart, the surrounding areas are prevented from the excitement by refractory state.

Depending on the factors, which give rise to circulation of excitation wave, there are several types of reentry mechanism: anatomical, functional and combined.

The components of anatomical reentry loop are anatomical structures of myocardium:

- atrioventricular node;
- bundles of fibers of His-Purkinje system;
- additional abnormal conducting way (bundle of Kent);
- mouth of hollow veins;
- tricuspid valve ring;

- scar area (the presence of border zone in the area of postinfarction scarring);

- aneurysm.

The size and shape of functional reentry loop are determined by the changes in electro-physiological parameters of myocardial cells such as:

- heterogeneity of refractoriness;

- shortening of effective refractory period (difference of refractivity periods of myocardial areas);

- dispersion of conductivity;

- increase in extracellular potassium concentration;

- reduction in the speed of impulse conduction;

- decrease in resting potential of cardiomyocytes;

- premature activation;

- anisotropic structure of cardiac muscle.

The reentry mechanism represents a pathological sign of cardiac electrical activity, based on the appearance in a specific myocardial area of unidirectional block and reentry of excitation wave (cardiac impulse). This process is related to the disorder in conduction of cardiac action potentials. The periodic (ordered) “macro-reentry” is typical for paroxysmal tachycardias, atrial and ventricular flutters. Aperiodic (disordered) “micro-reentry” leads to the chaotic process of pulse propagation, which is observed during the atrial and ventricular fibrillations. Localization of reentry circles may change over time due to the presence of spatial gradients of parameters and characteristics of heart tissue.

Violation of excitation in the heart can be caused by many different factors, which lead to changes in excitability and cable properties of the membranes of heart fibers. To large extent electrophysiological

properties of the cells are determined by the nature of metabolism in the myocardium and depend on changes in electrolyte balance, level of the resting potential and threshold potential, steepness of depolarization. In the absence of severe congenital or acquired diseases of specialized heart tissues the most common cause of abnormalities is impulse propagation in fibers with low membrane potential.

Despite the fact that the method of electrocardiography has been known for more than 100 years, the electrocardiographic technologies undergo continuous refinement. The development of methods and techniques of electrocardiography leads to a new direction in ECG diagnostics known as non-invasive electrophysiology. This direction is based on modern advanced methods of registration, digital processing of electrocardiosignals, that make it possible to measure and estimate additional data, which is inaccessible by the standard ECG assessment methods. The development of diagnostic electrocardiologic systems of new generation involves the implementation of mathematical methods of ECG analysis, employing complex transformations for the estimation of parameters of electric potentials of myocardium, based on biophysics and electrophysiology of the heart. Among the systems enabling us to investigate and study the subtle signs of cardiac electrical activity, the systems of high-resolution electrocardiography should be noted (HR ECG) [2-3].

Non-invasive high-resolution technologies in ECG make it possible to register and detect low-amplitude signals invisible in ordinary electrocardiogram by using more sophisticated technical facilities and digital processing of electrocardiosignals. These signals with amplitude up to 40-50 μV can be located at any part of the cardiac cycle.

An important task, aimed at improvement of risk stratification of patients, is the search for additional predictors that can detect the fact of presence of vulnerable myocardium and predict the possibility of malignant arrhythmias. Apart from myocardial imaging techniques (magnetic resonance imaging, computed tomography, tissue Doppler), such electrocardiographic parameters as alternation of T wave and HR ECG with detection of atrial and ventricular late potentials can serve as the prognostic markers for the selection of patients for implantation of cardioverters-defibrillators [1, 2].

The first signs of electrical instability of myocardium reflect changes in the electrophysiological processes occurring at the cellular level, which does not appear in the initial stage of the disease in the form of substantial functional and anatomical changes [1]. The non-invasive methods for detection of heart disease enable diagnosis at the early stage. Development of the methods for identification and assessment of early signs of heart disorders makes it possible to catch the sight of disease at its initial stage. Digital processing of electrocardiographic signals allows us to extract information, which can not be obtained by the visual analysis of the standard electrocardiogram [2, 3]. Therefore, improvement of methods and tools for automated detection of low amplitude components of electrocardiosignals through development of methodological and algorithmic support of high resolution ECG systems is an actual task**.**

2.4. Biophysical bases of genesis of atrial and ventricular late potentials

Pathological changes in the functional state of the myocardium may occur in the structure of ECG even before the manifestation of clinical symptoms. However, low-amplitude ECG components that have important diagnostic information do not appear on the background of high-amplitude waves and noise in the recording of standard electrocardiogram. Non-invasive technology of high-resolution electrocardiography, performed by improving of technical facilities and digital processing of electrocardiosignals, allows registration and identification of low amplitude signals, which are not visible on a conventional electrocardiogram. There are micropotentials of different types: early and late atrial potentials, early and late ventricular potentials. The most extensively studied markers of myocardial electric instability are atrial and ventricular late potentials (ALP and VLP) [2].

Ventricular late potentials are the low-amplitude (20 - 40 μV from the body surface) high-frequency (40 - 250 Hz) electrical signals, which are localized at the end of QRS complex or beginning of ST segment and have duration of several tens of milliseconds (Fig. 2.3).

Bioelectrical signals, recorded from a body surface in the form of localized at the beginning of QRS complex low-amplitude high-frequency fragmented electrical activity, are called early ventricular potentials.

By analogy with ventricular late potentials the slowing of the activation conduction in atria in patients with atrial fibrillation was identified. Atrial late potentials are the low-amplitude high-frequency signals (5-20 μV), which are located at the end of P wave or within the

isoelectric part of cardiac interval PQ. It is thought that atrial late potentials are the markers of atrial tachyarrhythmias and ventricular late potentials are the markers of ventricular tachyarrhythmias, which develop through the “reentry” mechanism.

Atrial fibrillation is characterized by disordered activation with many microwaves, which simultaneously spread in atria [4-9]. Thus one of the main conditions of paroxysmal atrial fibrillation by reentry mechanism is the slowing of conduction that causes atrial activation time extension. The emergence of reentry in atrium depends on the spatial differences in membrane properties and anatomic disorganization of atrial muscle tissue, when individual muscle fibers are separated by connective tissue, leading to heterogeneity of atrial electrophysiological properties. The presence of areas with delayed fragmented conduction of excitation impulse in patients with paroxysmal forms of fibrillation and atrial flutter is confirmed. Also of great importance is forecasting of development of atrial fibrillation in patients after surgery on the heart. Currently there are no completely reliable approaches for prediction of atrial arrhythmias, though atrial fibrillation/flutter are the most widespread forms of cardiac arrhythmias and their prevalence increases with age.

Low-amplitude activity is registered also in the initial part of the P wave as early atrial potentials, but their value remains poorly understood. It is believed that early atrial potentials reflect the presence of areas with fragmented delayed sinoatrial conducting and they are markers of sinus node weakness syndrome.

The presence of atrial or ventricular late (or early) potentials is associated with an increased probability of life-threatening cardiac arrhythmias.

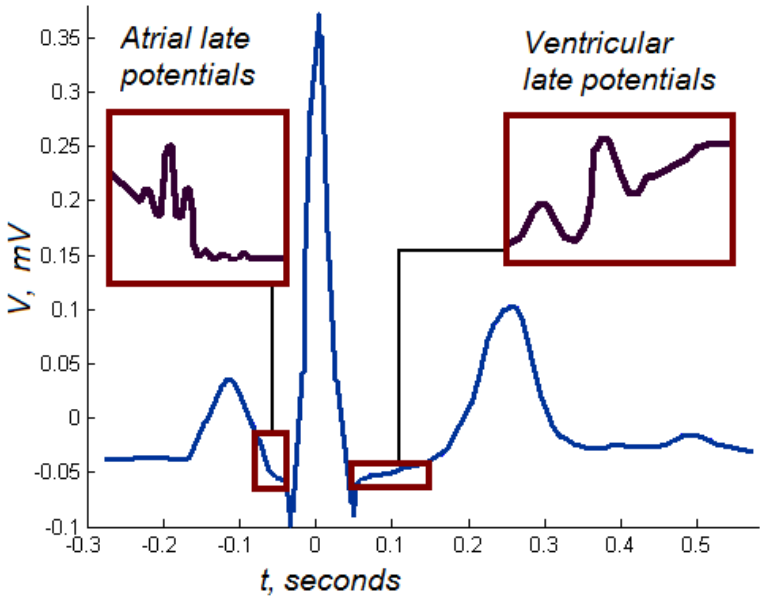

Fig. 2.3. Localization of atrial and ventricular late potentials on ECG

The emergence of late potentials on ECG signal reflects the slow and fragmented depolarization associated with the "reentry" circles. Inhomogeneity of electrophysiological characteristics of myocardial regions results in formation of fragmented electrocardiogram, which can be registered directly during the performance of intracardiac elecfrophysiological investigations. The reentry phenomenon, resulting in the electrical cardiac instability, is characterized by the multifactor nature of origination and covers different areas in terms of size and place of localization.

Developing the approaches to identification of low-amplitude ECG components, it is necessary to consider that micro-potentials may appear on ECG at different time moments. Regular micropotentials are present in all cardiac cycles with a permanent time shift concerning the reference point, such as R wave. Irregular micropotentials occur in a certain part of cardiac cycle in a random moment of time relatively to high-amplitude components of ECG. The presence of micro-potentials, which do not appear in every cardiac cycle, is also possible. Based on

intracardiac studies two cases of non-stationary manifestation of micro-potentials are distinguished:

- micropotentials, which repeat their shape from one cardiac cycle to another, but occur at random moment of time (they are not synchronized with high-amplitude waves of ECG signal);

- micropotentials, which do not repeat their shape from one cardiac cycle to another (realization of a random process).

2.5. Peculiarities of late potentials detection in the systems of high resolution electrography

Establishment of diagnostic and prognostic importance of late potentials requires additional research [10-31]. Design and development of new methods for investigation of subtle structure of ECG will allow revealing of patients at high risk for dangerous arrhythmias and optimization of their treatment.

For the purpose of detection of late potentials, which are the markers of tachyarrythmia development, it is necessary to refine the methods of registration and processing of electrocardiosignals in HR ECG systems. Noninvasive registration from the body surface, identification and analysis of late potentials are the challenging tasks due to the fact that the amplitude of late potentials may be much smaller than the amplitude of noise components of ECG [2, 3, 10-13].

Noise and interferences occurring in the ECG signal have the different nature and include:

- power line interference;
- polarization of the electrodes, resulting in a shift of zero signal level;

- artifacts of electrodes displacement;
- motion artifacts;
- muscular activity;
- baseline drift caused by breathing;
- noise of electronic equipment.

In the process of amplification together with increase of amplitude of diagnostically important electrocardiosignals noise also increases. To eliminate noise and reveal low-amplitude ECG components, computer signal averaging is performed. It is based on the property of the repeatability of ECG signal and implements the principle of pseudo synchronous accumulation (Fig. 2.4). Averaging of multiple cardiocycles (from 100 to 400 ECG complexes) forms the basis of high-resolution electrocardiogram [1-3, 10, 14-19]. The method allows us to separate signal from noise by a significant improvement in signal/noise ratio. Since noise is a random process, it is not synchronized with the investigated electrocardiosignal. Noise superimposes randomly from one complex to another, so averaging leads to the significant reduction of its amplitude. In contrast to the noise, diagnostically useful cardiosignal repeats with a certain frequency (not chaotically), therefore its amplitude stabilizes due to the averaging. As a result of averaging, the signal/noise ratio increases. It is possible to average the cardiac cycles with synchronization on P, Q, R waves in implementation of HR ECG method.

One of the conditions of the correct signal averaging is identity (similarity) of investigated ECG complexes. Highly noisy cardiac cycles must not participate in the averaging. For this purpose a reference cardiac cycle is automatically selected. Each subsequent complex is compared to the reference cardiac cycle and included in the analysis in

case of quite high coefficient of correlation with the reference cardiac cycle (at least 0.95).

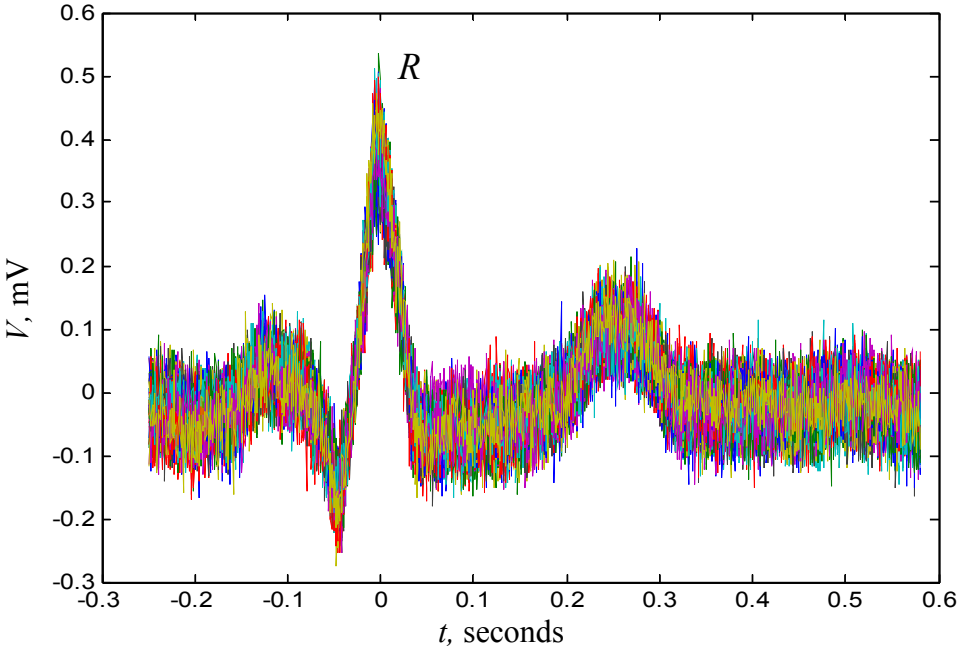

Fig. 2.4. Accumulation of cardiac cycles with the synchronization on R wave

According to the standard requirements for analysis of late potentials adopted by the European Society of Cardiology, American Heart Association, American College of Cardiology [10] in the systems of HR ECG for converting the analog signal to digital ECG data must be sampled at no less than 1000 Hz frequency and analog-to-digital converted with at least 12-bit precision. It is considered that sampling below 1,000 Hz may preclude recovery of potential signals of interest. Notch filters for power line interference should not be used.

One of the first studies of ventricular late potentials detection are the works of M.B. Simson [11-13]. The approach to registration and methods of analysis of HR ECG are considered in them, as well as the connection between the presence of ventricular late potentials with the

possibility of future ventricular tachyarrhythmias are considered in these papers.

Implementation of temporal analysis according to Simson method involves averaging of cardiosignal in three orthogonal Frank leads X, Y, Z, followed by filtration in the frequency range of 40-250 Hz (Fig. 2.5). Analysis of their total vector magnitude $\sqrt{X^2 + Y^2 + Z^2}$ determines the time and amplitude quantitative parameters, based on which conclusion about the presence or absence of late potentials is made (Fig. 2.6).

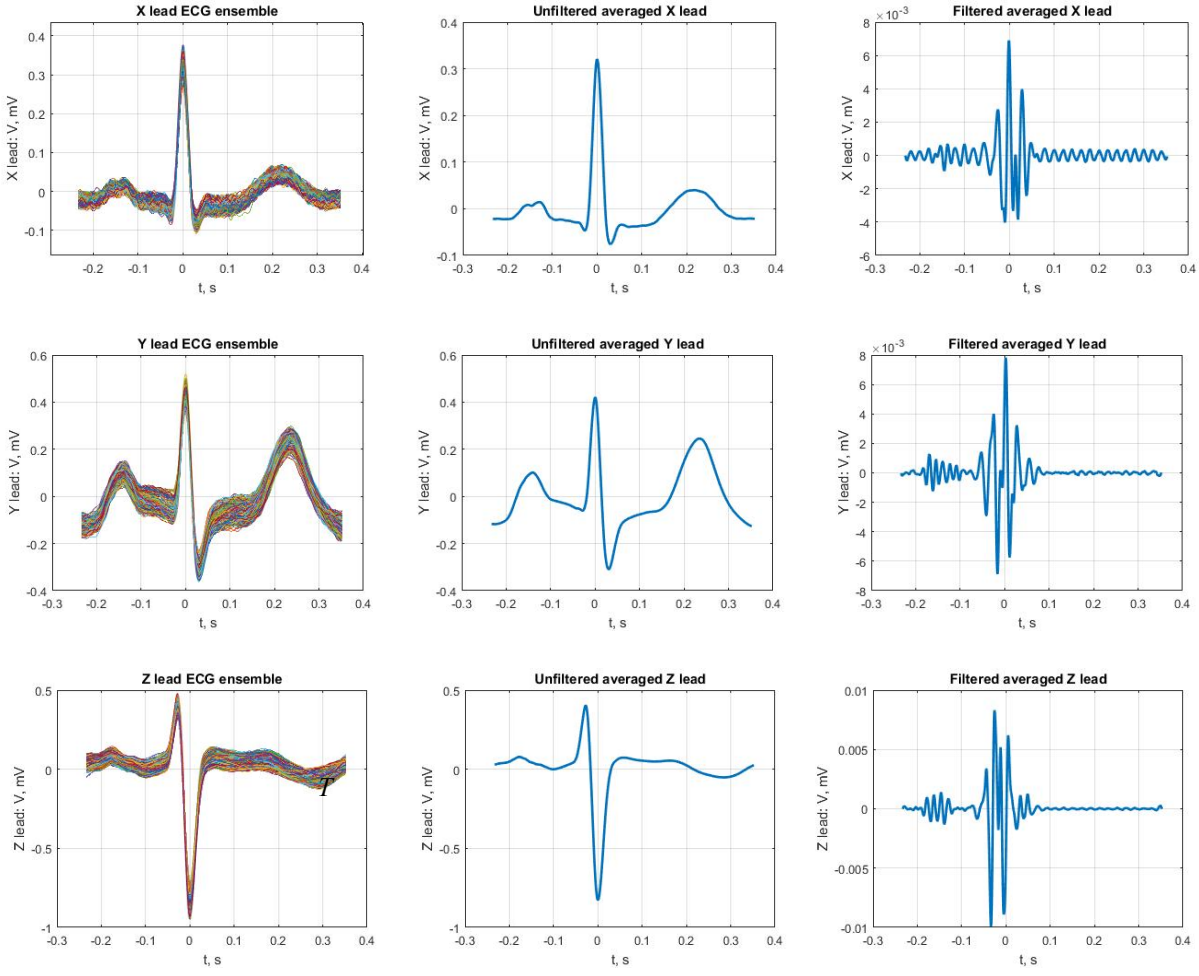

a) b) c)

Fig. 2.5. a) accumulation of cardiocycles with synchronization on R wave in three orthogonal Frank leads X, Y, Z; b) averaging of cardiosignal; c) filtration in the frequency range of 40-250 Hz

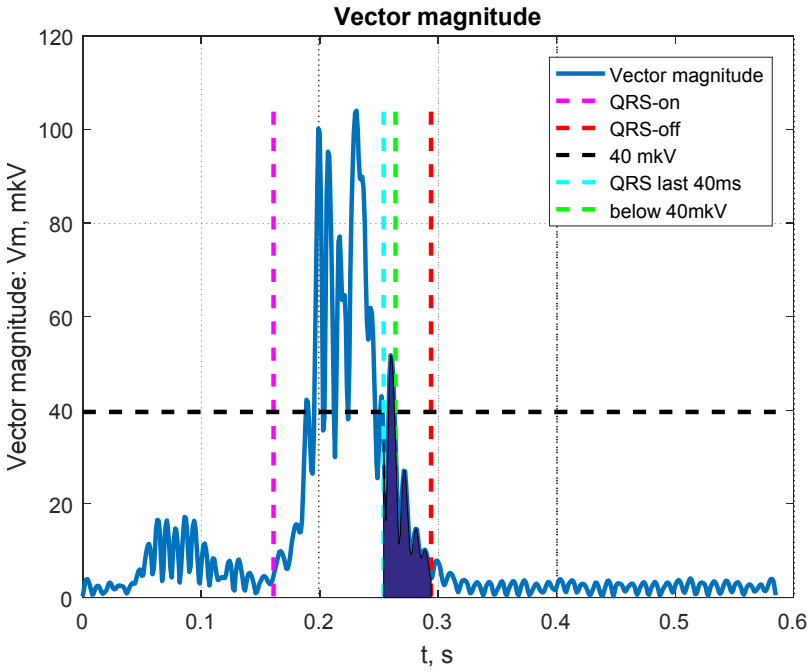

Fig. 2.6. Analysis of total vector magnitude $\sqrt{X^2+Y^2+Z^2}$ for detection of ventricular late potentials

Standard analysis of ventricular late potentials implies determination of the filtered QRS duration, root mean square voltage of the terminal 40 msec of the filtered QRS complex, and amount of time when the filtered QRS complex remains below 40 μV [10].

Representative criteria for the presence of ventricular late potentials:

1) the filtered QRS complex is greater than 114 msec,

2) there is less than 20 μV of signal in the last 40 msec of the vector magnitude complex,

3) the terminal vector magnitude complex remains below 40 μV for more than 38 msec.

The time parameters of the filtered P wave include the following indicators:

1) duration of the filtered P wave (Fi*P*).

2) difference between the durations of the filtered and unfiltered P waves (Fi*P* — UnFi*P*).

3) duration of signals < 5 μV (D5).

The amplitude parameters of the ALP are the root mean square amplitude (RMS) of:

1) total P wave (RMS*P*).

2) last 10-20-30 ms of P wave (Last 10-20-30 or RMS 10-20-30).

RMS 20 is the most commonly used amplitude parameter.

The approach with averaging of cardiac cycles eliminates the possibility of the detection of irregular late potentials and investigation of dynamic changes of their parameters from beat to beat. Variability of frequency content, amplitude and localization of late potentials is possible. The disadvantages of the signal averaging method include likelihood of making errors due to "smoothing" of high frequency signals in case of frequency, duration and shape changes of late potentials from beat to beat. In case of nonstationarity manifestation of micro-potentials signal accumulation is possible in principle, but only with strongly reduced amplitude and increased duration.

In the signal-averaged ECG the non-stationary components are significantly weakened. Subtraction of the signal-averaged ECG from a separate cardiocycle with the presence of irregular micro-potentials allows compensation of high-amplitude stationary ECG waves. The interval of possible occurrence of potentials of atrial delayed depolarization is the terminal part of P wave. Then the difference signal in the terminal part of P wave present the amount of atrial late potentials and noise, and other intervals of the cardiocycle contain only noise (Fig. 2.7).

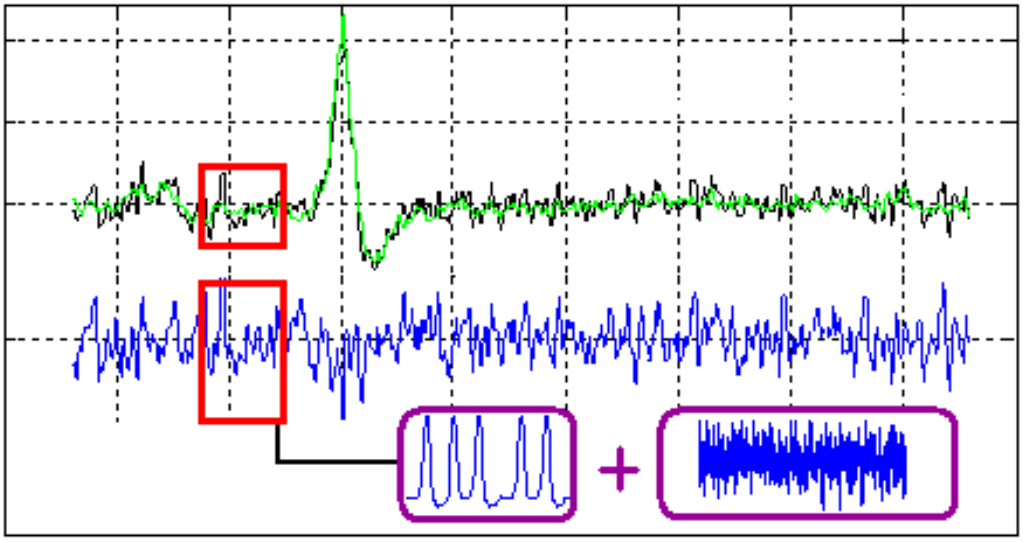

Fig. 2.7. Obtaining of a difference signal between the investigated cardiocycle and the signal-averaged ECG

Frequently, in the systems of HR ECG, a spectral analysis of the electrocardiogram is performed, in which the changes of the amplitude-frequency characteristics of a certain part of the average cardiac cycle are estimated. For this purpose, the Fourier transform method, by which the ECG signal is decomposed into the components of sinusoidal oscillations of the different frequencies and amplitudes, is used. The accuracy of detection of late potentials is determined by the choice of the width of a window function. Choosing a window with small width provides more accurate information about the temporal localization of the late potentials, but it has a bad effect on the spectral resolution.

The main power of the QRS complex is concentrated in the frequency range of 2-30 Hz with the presence of a maximum at a frequency of about 15 Hz. The P and T waves correspond to lower frequency range. The network interference can be usually seen at 50 or 60 Hz (Fig. 2.8, 2.9). The presence of atrial or ventricular late potentials manifests in the form of the high-frequency components in the range of

40 – 250 Hz (according to some sources, up to 1000 Hz). Late potentials appear rather as weak harmonics against the background of the main spectrum, which complicates their detection.

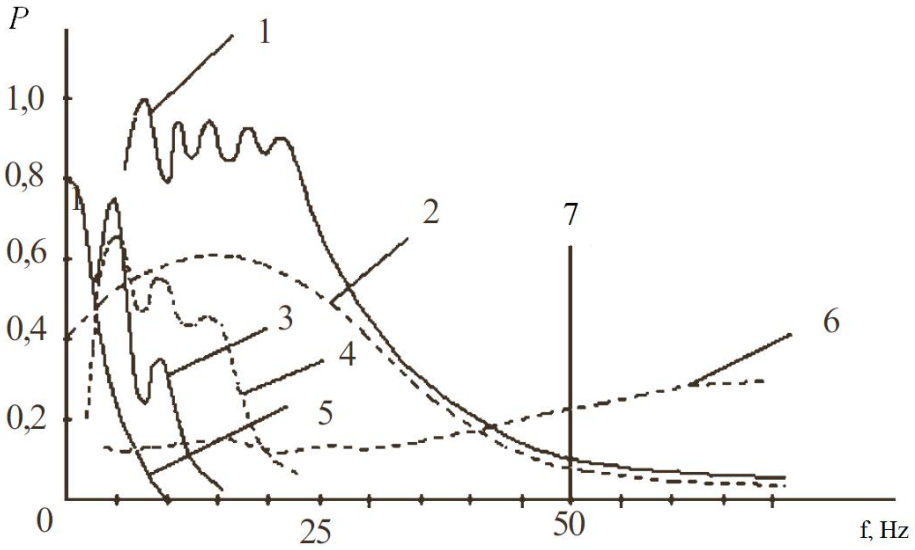

Fig. 2.8. Characteristics of the relative power spectral density of the ECG signal and noise components: 1 - ECG signal, 2 - QRS complex, 3 - movement artifacts, 4 - P, T waves, 5 - polarization voltage, 6 - noise of muscles, 7 - frequency of network interference

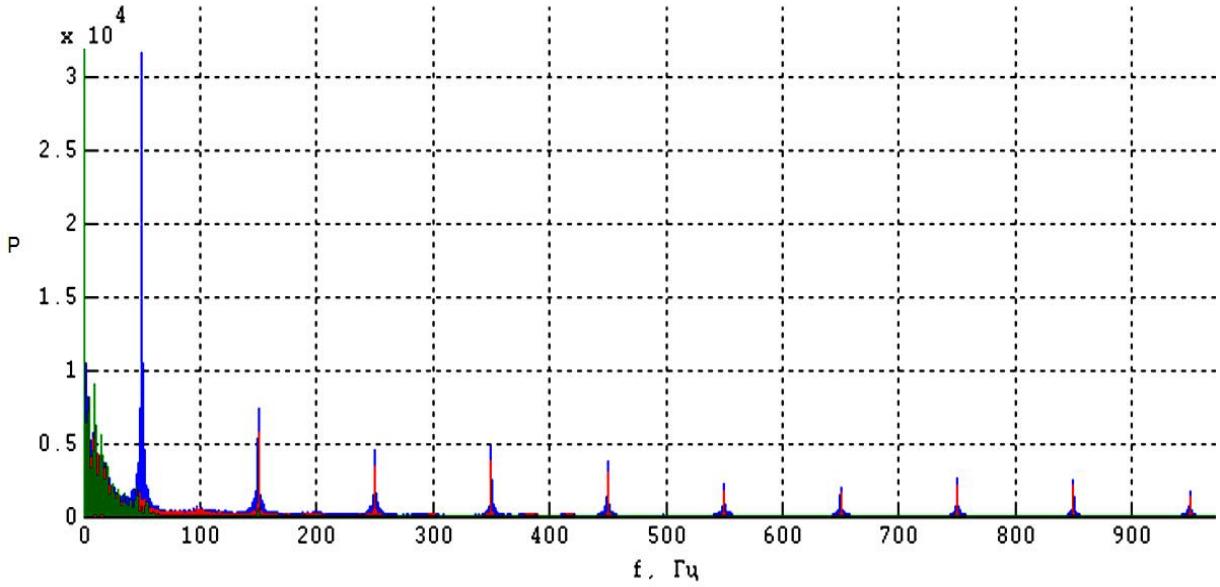

Fig. 2.9. Manifestation of network interference with a base frequency of 50 Hz and its odd harmonics in the spectrum of the electrocardiosignal registered in the system of HR ECG

The principle of the spectral-time mapping method [32-37], which is based on the local Fourier transformation, consists in calculating the spectrum using a "window" moving along a time axis in the terminal part of P wave for ALP detection or in the terminal part of QRS complex and along the ST segment for VLP detection. Such a frequency-time transformation of the cardiac signal allows observing the change in its spectral content in time. The distribution of the power of the spectral components, which reflects the spectrum change in time, is called the spectrogram:

$$P(\omega,\tau)=\left|\int_{-\infty}^{\infty} S(t)g^{*}(t-\tau)e^{-j\omega t}dt\right|^{2}.$$

As a result of the spectral-time analysis, a three-dimensional graph of frequency, time and amplitude or power of the spectral components is constructed.

The spectral power in spectral-time mapping method is calculated by conducting the fast Fourier transform of 25 segments of 80 ms in length, shifted on 3 ms from each other. The degree of correlation between the values of the frequency spectrum of 2-25 segments and the first segment is determined. Next, the normality factor is calculated as the ratio between the mean values of the correlation coefficients of the last five segments and others, expressed in percentage terms. The criterion for the presence of ALP or VLP is the low value of the normality factor (less than 30%). The disadvantage of the method of spectral-time mapping is the influence of the various noises on the results.

Thus, the temporal analysis by the Simson method, spectral analysis and spectral-time mapping, which are the most widely used in

the systems of HR ECG, have a number of shortcomings, which do not provide with high accuracy of late potentials detection. The promising direction of improvement of HR ECG systems is development of new methods for ECG analysis to identify low-amplitude components using alternative coordinate bases.

2.6. Simulation of late potentials in ECG

Late potentials, recorded by invasive way from the epicardium surface of the infarct zone, are asynchronous multiphase fluctuations, reflecting the delayed activation in areas of damaged myocardium. Depending on the nature of electrophysiological pathological changes in myocardium, late potentials can have different duration, amplitude and character of their manifestation on ECG.

For simulation of late potentials in ECG, it was taken into account that late potentials are high-frequency low-amplitude components of electrocardiosignal, which usually do not repeat their shape in different patients. Late potentials models can differ in their appearance, but their parameters should characterize low-amplitude high-frequency activity in the terminal part of P wave for the class "pathology - ALP presence" or in the terminal part of QRS complex and along the ST segment for the class "pathology - VLP presence".

The variety of processes, that are sources of signals of late potentials, allows applying of different ways for ALP models creation. As a model of high-frequency activity in the terminal part of P wave, the sine wave can be used with frequency inherent in late potentials (80 Hz in the experiment [32]). To obtain more complex shape of late potentials, the

test signal of late potentials can be presented as a sum of harmonic components with different frequencies in the range of 40 - 250 Hz:

$$x(t)=A_1 Sin(2\pi f_1 t+\varphi_1)+A_2 Sin(2\pi f_2 t+\varphi_2)+...+A_n Sin(2\pi f_n t+\varphi_n),$$

where $A_1 - A_n$ are amplitudes of harmonic components;

$f_1 - f_n$ and $\varphi_1 - \varphi_n$ are frequencies and phases of harmonic components.

Fig. 2.10 shows simulated ALP signal, which is the sum of three sinusoids with frequencies f_1 = 80 Hz, f_2 = 95 Hz, f_3 = 120 Hz and amplitudes A_1 = 10 μV, A_2 = 5 μV, A_3 = 8 μV.

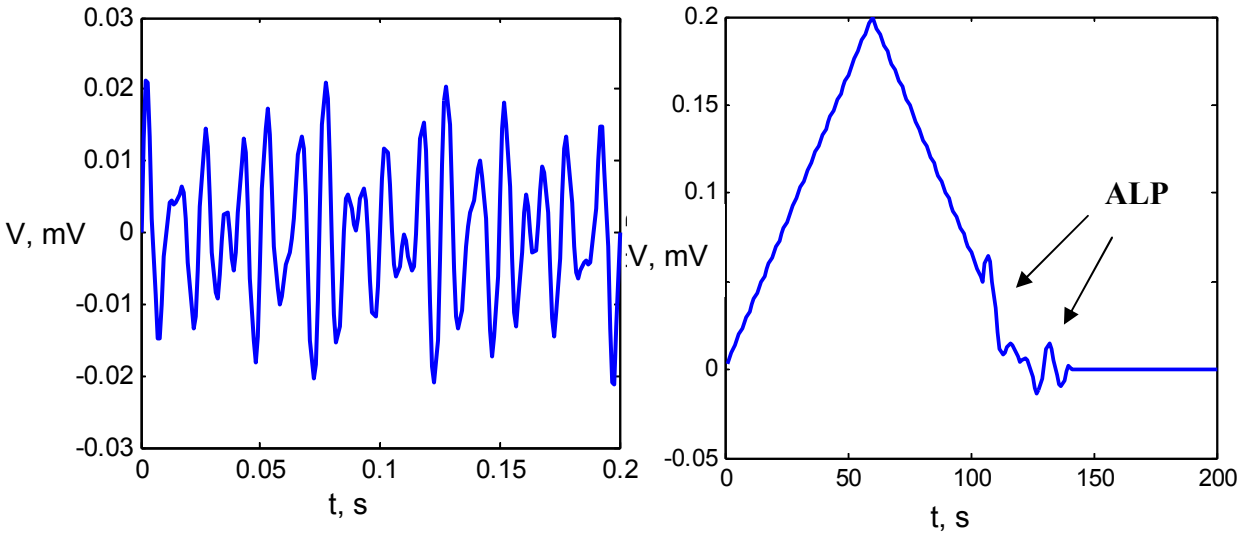

a) b)

Fig. 2.10. ALP simulation: a) test signal of ALP;
b) sum of 3 sinusoids in the terminal part of P wave

Taking into account the changes in amplitude of late potentials, as their model the different segments of amplitude-modulated signal can be added to the terminal of P wave, where carrier signal $x_c(t) = A_c Sin(2\pi f_c t)$ is modulated by periodic signal $x_s(t) = A_s Sin(2\pi f_s t)$:

$$x_{AM}(t) = (A_c + x_s(t))Sin(2\pi f_c t),$$

where A_c and A_s are amplitudes of harmonic components;

f_c and f_s are frequencies of harmonic components, respectively.

Fig. 2.11, a shows the amplitude-modulated signal with parameters A_c = 1 μV, A_s = 10 μV, f_c = 5 Hz, f_s = 120 Hz, and Fig. 2.11, b presents the simulated signal of P wave with ALP which are a segment of amplitude-modulated periodic signal.

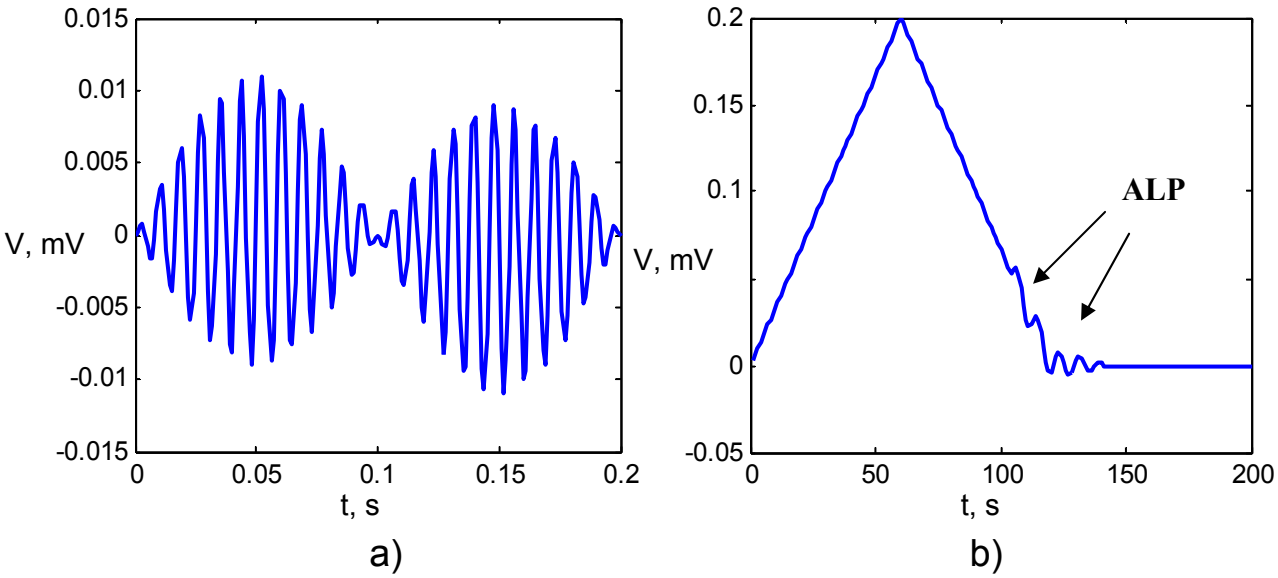

Fig. 2.11. ALP simulation: a) amplitude-modulated test signal;
b) ALP at the terminal part of P wave

Taking into account the characteristics of electrophysiological processes, which underlie the emergence of potential of delayed depolarization, the model of late potentials can also be formed as a sequence of action potentials with varying amplitude (Fig. 2.12), which can be obtained by solving a system of differential equations for parallel-conductance model and generalized model of Hodgkin-Huxley [38].

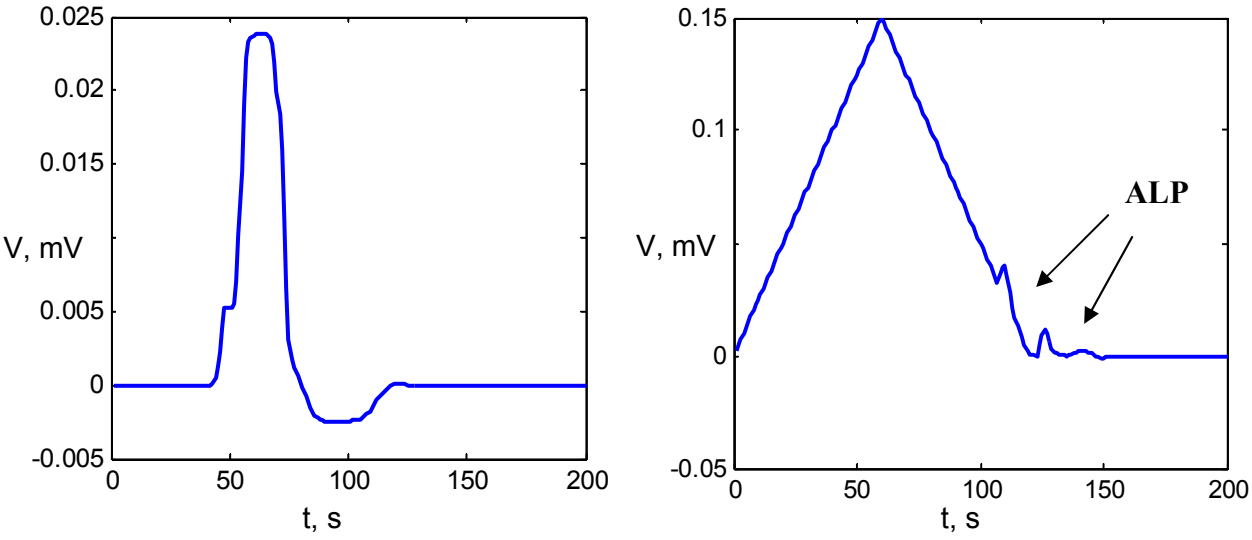

a) b)

Fig. 2.12. ALP simulation: a) transmembrane action potential;
b) ALP in the terminal part of P wave

Changing of the parameters used for the simulation provides a different view of late potentials and allows taking into account the individual manifestation for different patients and checking the possibility of late potentials detection by methods of digital processing of electrocardiosignals.

2.7. Analysis of the subtle structure of the electrocardiogram

To assess the state of heart electrical activity and detect early signs of atrial tachyarrhythmias, features of ALP, found as P wave parameters in time or frequency domain, are used. However, the results of late potentials detection, obtained using standard methods of ECG analysis, have a low predictive value. An increase in the predictive value of the diagnosis can be achieved by identifying additional characteristics of the late potentials in alternative coordinate bases.

2.7.1. Features of wavelet analysis of electrocardiosignals

The limitation of the spectral analysis is the inability to determine the exact localization of a specific frequency component of the cardiosignal in time, which is fundamentally important for the early diagnosis of violations of the electrophysiological properties of the myocardium. In contrast to the Fourier transform, the wavelet transform provides a two-dimensional analysis, in which the scale and coordinate are considered as independent variables, that enables the analysis of signals in two spaces - scale and temporal. The results of ECG wavelet analysis contain not only information on the distribution of cardiac energy along the frequency components, but also information on time coordinates, in which certain frequency components are detected or where rapid changes in the frequency components of the cardiac signal occur.

The wavelet transform is a multi-level analysis, effective for researching signals that simultaneously contain high-frequency components of short duration and long-term low-frequency components. This feature is suitable for the task of detection of low-amplitude high-frequency components of the cardiac signal and their analysis separately from high-amplitude low-frequency ECG waves [39-51].

Continuous wavelet transformation (CWT) is defined as [51]:

$$W_{\psi}(a,b) = \left\langle f(t), \psi_{a,b}(t) \right\rangle = \\ = \int_{-\infty}^{\infty} f(t)\psi_{a,b}^{*}(t)dt = \frac{1}{\sqrt{|a|}} \int_{-\infty}^{\infty} f(t)\psi^{*}\left(\frac{t-b}{a}\right)dt, \qquad a,b \in \mathbf{R}, \quad a \neq 0,$$

where < > is the operator of the scalar product;

* is the operator of complex conjugation;

$\psi_{a,b}$ is two-parameter family of functions:

$$\psi_{a,b}(t) = \frac{1}{\sqrt{|a|}}\psi^*\left(\frac{t-b}{a}\right),$$

where b is the parameter that determines the displacement along the time axis t;

a is the scaling factor responsible for stretching and compressing of the maternal wavelet function $\psi(t)$.

Thus, a set of wavelet functions $\{\psi_{a,b}(t)\}$ is a set of the scalable (stretched or compressed, depending on the value of the parameter a) and displaced (depending on the value of the parameter b) copies of a single prototype — mother wavelet function $\psi(t)$. Mother wavelets are functions, which are limited in time and location on the time axis and have a spectrum localized in some frequency area. Requirements for mother wavelet functions are determined by the possibility of restoration of the investigated signal $f(t)$ by its wavelet spectrum $W_\psi(a,b)$.

Reconstruction of the signal is carried out according to the formula of the inverse wavelet transform [51]:

$$f(t) = \frac{1}{C_\psi}\int_{-\infty}^{+\infty}\int_{-\infty}^{+\infty} W_\psi(a,b)\psi_{a,b}(t)\frac{da\,db}{a^2},$$

where C_ψ is a constant depending on the selected wavelet.

In order to reconstruct the function $f(t)$ from $W_\psi(a, b)$, function $\psi(t)$ must meet certain requirements. Wavelets used for CWT are normalized functions:

$$\int_{-\infty}^{\infty} |\psi(t)|^2\, dt = 1.$$

To obtain an inverse wavelet transform, the finiteness of the integral $C_\psi = \int_{-\infty}^{\infty} \frac{|\psi(\omega)|^2}{|\omega|} d\omega < \infty$ is necessary, where $\psi(\omega)$ is direct Fourier integral transform for a function $\psi(t) \in L^2(\mathbf{R})$: $\psi(\omega) = \int_{-\infty}^{\infty} \psi(t) e^{-i\omega t} dt$.

Also for the function $\psi(t)$ the necessary condition is the fulfillment of the requirement of zero mean [51]:

$$\psi(0) = \int_{-\infty}^{+\infty} \psi(t) dt = 0 \ ,$$

that at satisfaction of a condition $t\psi(t) \in L^1(\mathbf{R})$ becomes a sufficient condition for the wavelet function $\psi(t)$ used for CWT.

Often, for analysis of signals it is necessary that not only zero, but all the first moments are equal to zero:

$$\int_{-\infty}^{\infty} t^m \psi(t) dt = 0 .$$

Such a wavelet is called the wavelet of the *m*-th order. Wavelets with a large number of zero moments allow, ignoring the most regular polynomial components of the signal, analysis of the small-scale fluctuations.

The coefficients of continuous wavelet transforms contain information about the energy of individual components of ECG signal and time of their appearance. It allows simultaneous investigation of the slow and fast dynamics of changes in the cardiac signal in time, as well

as detection of such local features as the presence of late potentials (Fig. 2.13).

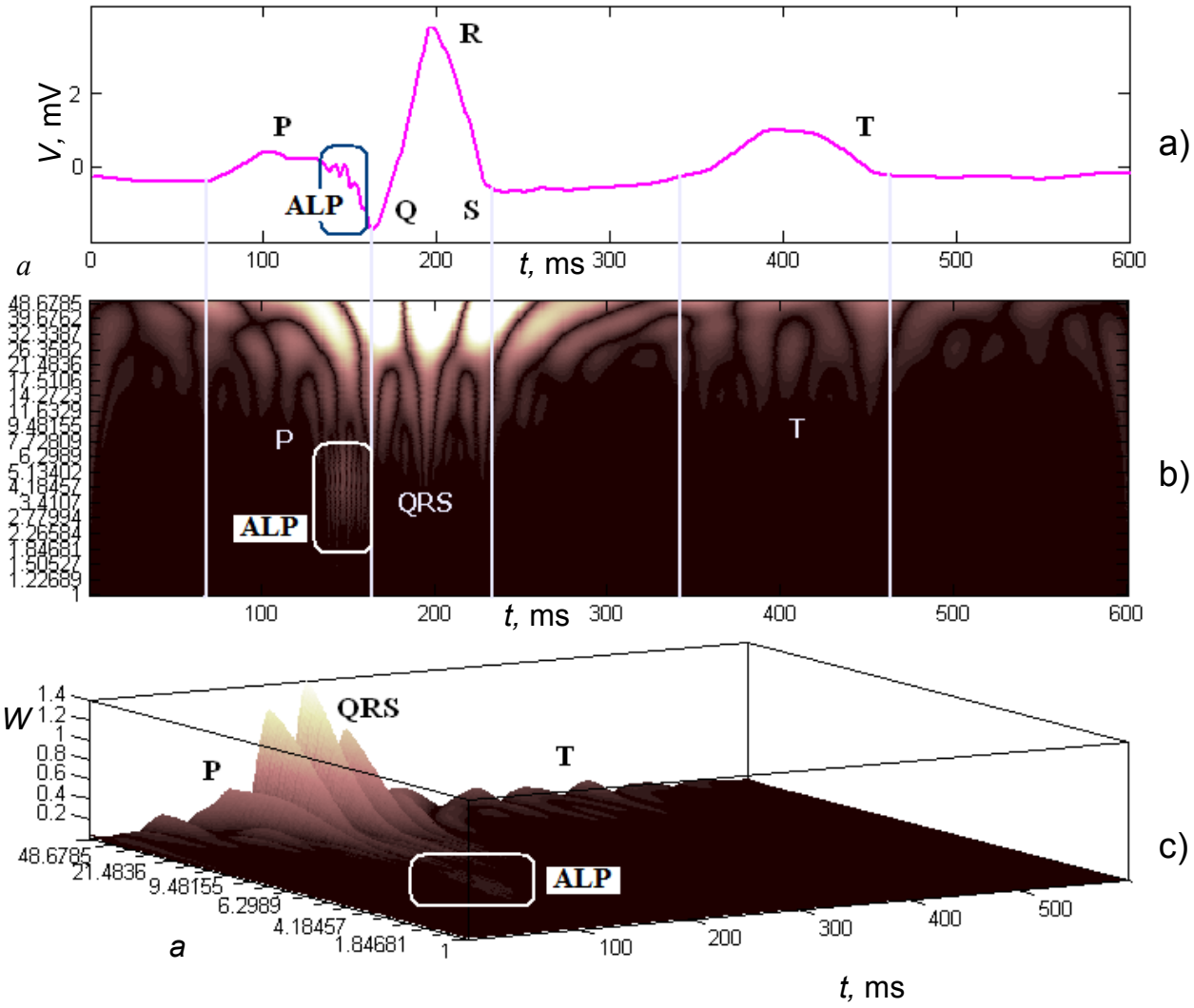

Fig. 2.13. CWT analysis of ECG: a) cardiocycle with the presence of simulated ALP in the terminal part of P wave; b) two-dimensional scalogram; c) three-dimensional scalogram

In the frequency representation, ECG signal has different components: low-frequency and low-amplitude P and T waves, QRS complex of higher frequency and larger amplitude, and late potentials, characterized by the lowest amplitude and high frequency. Detection of late potentials is complicated by noise components of ECG signal.

The possibility of using continuous wavelet analysis for ALP detection can be considered on the example of a model experiment in the MATLAB system. A model of ECG signal with the presence of ALP in the terminal part of P wave was constructed. To the ECG signal 5 potentials were added, which were obtained by solving the system of differential equations for the parallel-conductance model and the generalized Hodgkin-Huxley model.

To detect ALP, it is necessary to choose wavelet function, which is similar in form to ALP, and allows the most accurate determination of their presence in the terminal part of P wave. On wavelet-scalogram of the simulated ECG signal with ALP presence, the best results are obtained using such wavelet functions as the Meyer wavelet, Gauss wavelet of 4^{th} order, Morley wavelet, Coifman wavelet, symmetric wavelet of 4^{th} order.

To estimate the range of scales of continuous wavelet transformation, in which the presence of high-frequency micro-potentials can be detected, it is necessary to take into account the length of the discrete electrocardiosignal being investigated, as well as the central frequency of the wavelet function [51]. For example, the length of the simulated cardiocycle is 1000 samples, and Coifman wavelet of the fifth order has a central frequency of F_c = 0.6897 Hz. Then the central frequency of the wavelet, which will be used for the first level of the wavelet decomposition, is F_1 = 0.6897 * 1000 = 689.7 Hz. For each next level of wavelet decomposition the frequency of the wavelet will be 2 times lower than for the previous one, i.e. F_2 = 344.8 Hz, F_3 = 172.4 Hz.

Such a change in the frequencies, when moving from one scale to another, leads to the fact that the high frequencies, characteristic for ALP, are represented on the scalogram by several levels and practically

invisible. Using the log scale allows stretching the high-frequency range of scalogram.

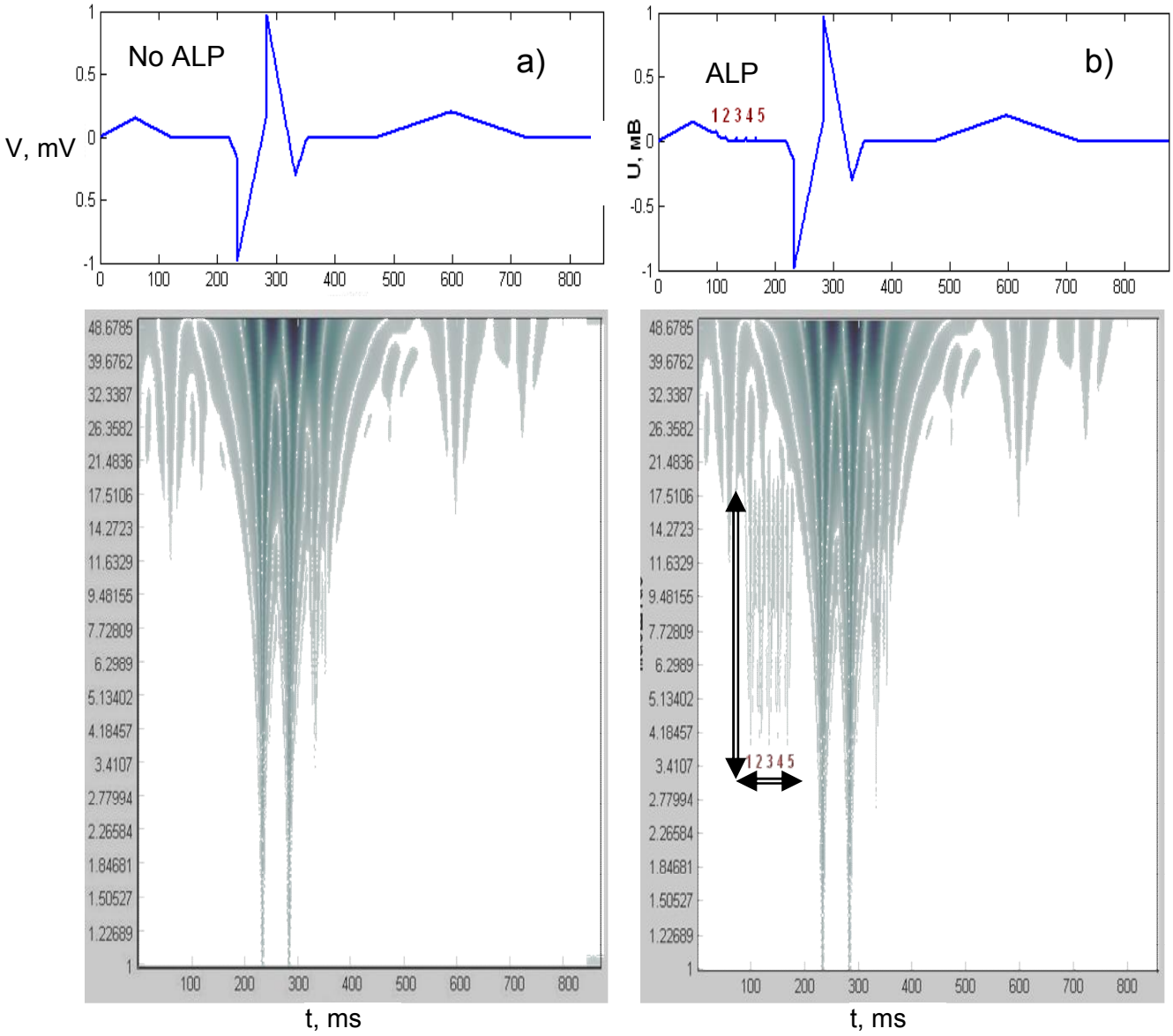

Fig. 2.14. Models of cardiocycle and wavelet scalogram in logarithmic scale: a) absence of micro-potentials:
b) presence of 5 micro-potentials at the end of P wave

Fig. 2.14 shows models of cardiocycle in norm and with ALP presence at the end of P wave, as well as wavelet scalograms of these signals in logarithmic scale. High energy of ECG waves masks the low

energy of low amplitude ALP. In the range of scales *a* = 3.8 - 17.5 in the time interval of 90-180 ms, 5 separate components are observed (Fig. 2.15). This range of scales corresponds to a frequency range of 40 - 180 Hz.

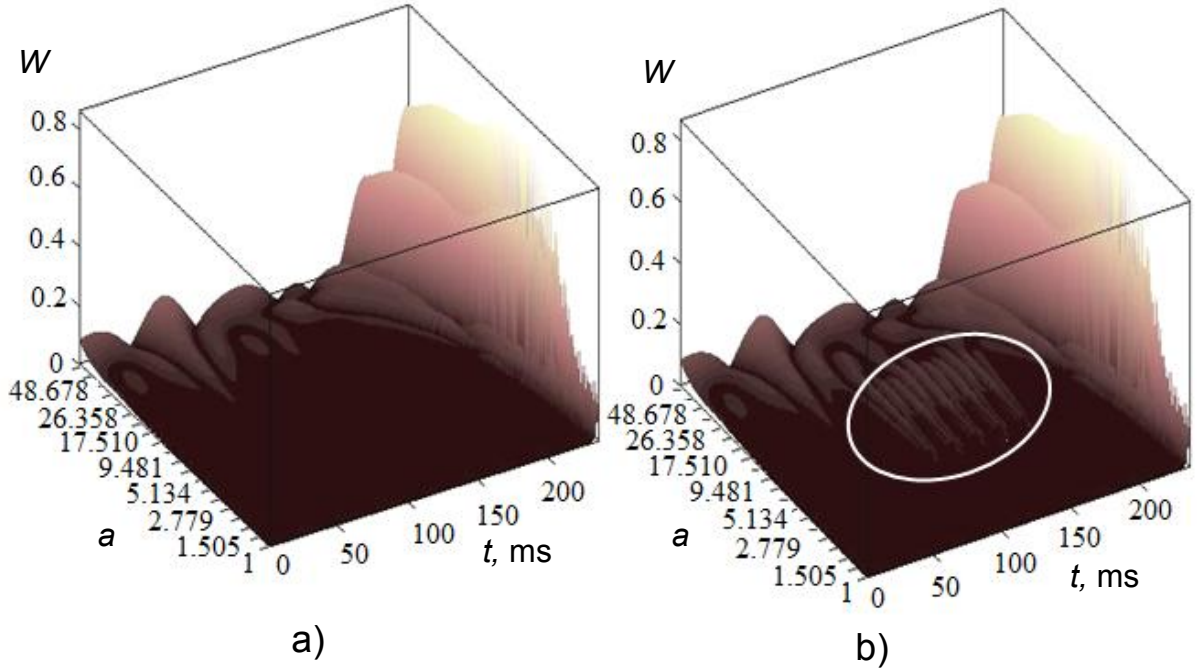

a) b)

Fig. 2.15. Wavelet scalograms:

a) absence of micro-potentials; b) presence of 5 micro-potentials

2.7.2. Combined method for analysis of the subtle structure of electrocardiosignal for late potentials identification

Discrete wavelet transform operates with discrete values of parameters *a* and *b*. These parameters are usually set in the form of power-law functions, avoiding excessive number of operations and calculated coefficients, which is typical for CWT.

In multilevel discrete wavelet decomposition of the electrocardiogram approximation coefficients *cA*, representing the smoothed signal for the contour analysis of ECG, and detail coefficients *cD*, which describe the high frequency fluctuations of ECG, are

determined. For analysis of ECG signal on different scales, filters of low and high frequencies with different cutoff frequencies are used. Vectors of wavelet coefficients are obtained by means of a mathematical operation of convolution for the investigated signal *S* with a low pass filter for determining the approximation coefficients cA_1 and with a high pass filter to determine the detail coefficients cD_1 [51]. In the next step, the coefficients of approximation cA_1 are decomposed in two parts for obtaining cA_2 and cD_2. The procedure can be repeated to the required level of decomposition *N* (Fig. 2.16).

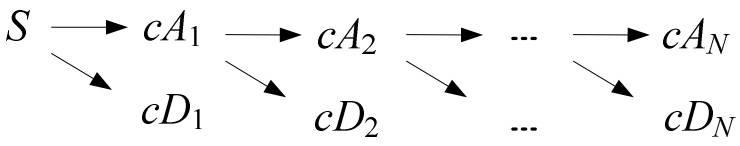

Fig. 2.16. Tree of discrete wavelet decomposition of the signal *S* to the level *N*

Thus, the signal *S* is presented as the sum of the approximating component, which is determined by the approximation coefficients of *N* level of wavelet decomposition (a_N), and all the detailing components, which are determined by the detail coefficients of levels from 1 to *N* (d_N, d_{N-1}, ... d_1) (Fig. 2.17):

$$S = a_N + d_N + d_{N-1} + \ldots + d_1.$$

The method of HR ECG involves the registration and averaging of 100-400 ECG complexes. In the case of insufficient for signal averaging length of ECG recording, the presence of residual noise does not allow

us to analyze the morphology of the terminal part of P wave and to conclude whether or not micro-potentials are present (Fig. 2.18).

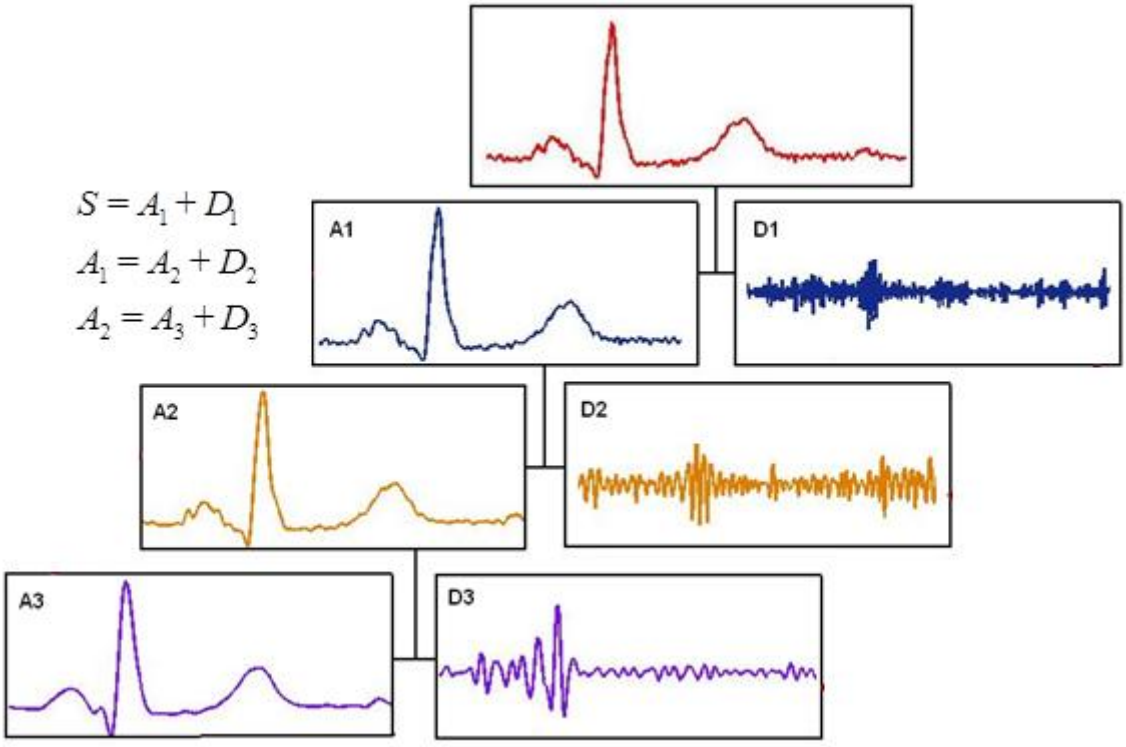

Fig. 2.17. Discrete wavelet decomposition of ECG signal to the 3rd level

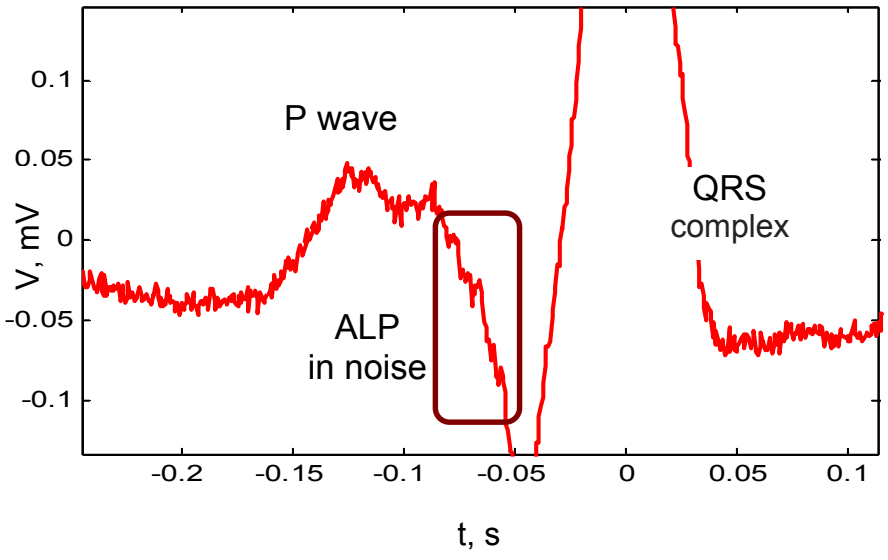

Fig. 2.18. The presence of residual noise after signal averaging

The wavelet decomposition of the ECG signal allows obtaining of approximation coefficients, representing a smoothed signal, and detail coefficients, describing high-frequency oscillations. Fig. 2.19 demonstrates wavelet decomposition of P wave without ALP and with presence of ALP. As a result of discrete wavelet decomposition of P wave up to the 5^{th} level, the approximation coefficients, which represent the smoothed P wave, and detail coefficients, which describe high frequency oscillations, are obtained. Data dimension can be reduced by removing large-scale wavelet-coefficients, responsible for the form of high-amplitude (in comparison with ALP) P wave. Model experiments showed that the signs of ALP can be found at d_1 level of detail representing the high-frequency low-amplitude bursts. The other levels of discrete wavelet decomposition reflect the features of lower frequency components.

The noise component is less than the amplitude of the main signal, and manifests itself mainly in the detail coefficients. The easiest way to remove noise is threshold processing of wavelet coefficients. There are as hard and soft methods of threshold processing of wavelet coefficients. In the case of hard threshold processing, all coefficients larger than the threshold τ or equal to it in absolute value are left unchanged, and coefficients smaller than τ are zeroed. If soft threshold processing with zeroing coefficients smaller in absolute value than τ, the absolute values of the remaining coefficients are reduced on τ. In the systems of HR ECG, the problem of noise removal is complicated by the fact that amplitude of late potentials is close to the amplitude of noise components. In the presence of noise, it is impossible to detect late potentials by means of wavelet decomposition, since noise components

and late potentials appear at the same levels of wavelet decomposition of P wave (Fig. 2.20).

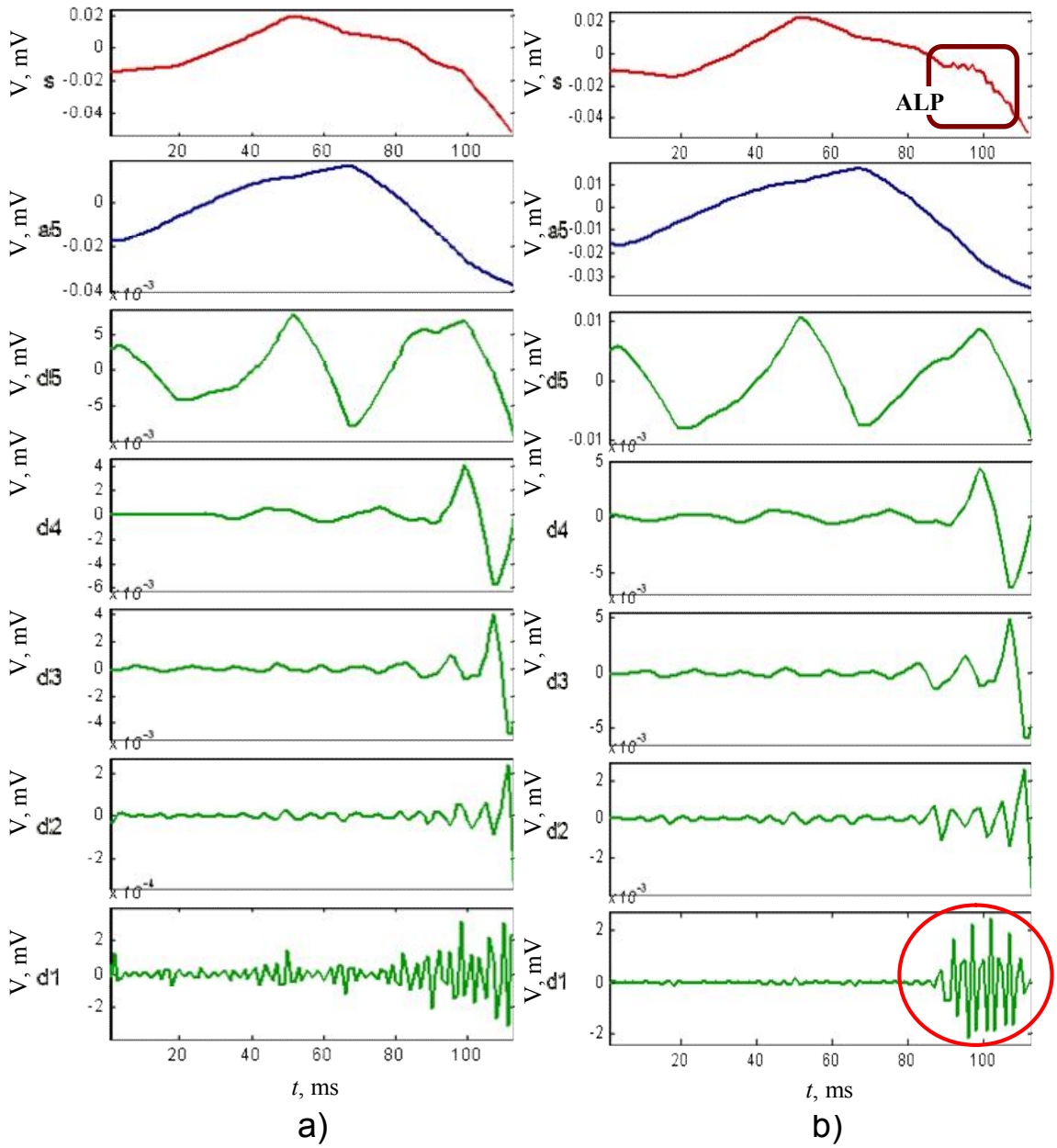

Fig. 2.19. Discrete wavelet decomposition up to the 5th level:
a) P wave without ALP; b) P wave with ALP

Threshold processing of detail coefficients does not yield satisfactory results. The setting of small threshold values preserves the

noise background in the detail coefficients, and the signal-to-noise ratio increases insignificantly. The choice of large threshold values for the processing of the detail coefficients leads to the loss of information about the presence of ALP.

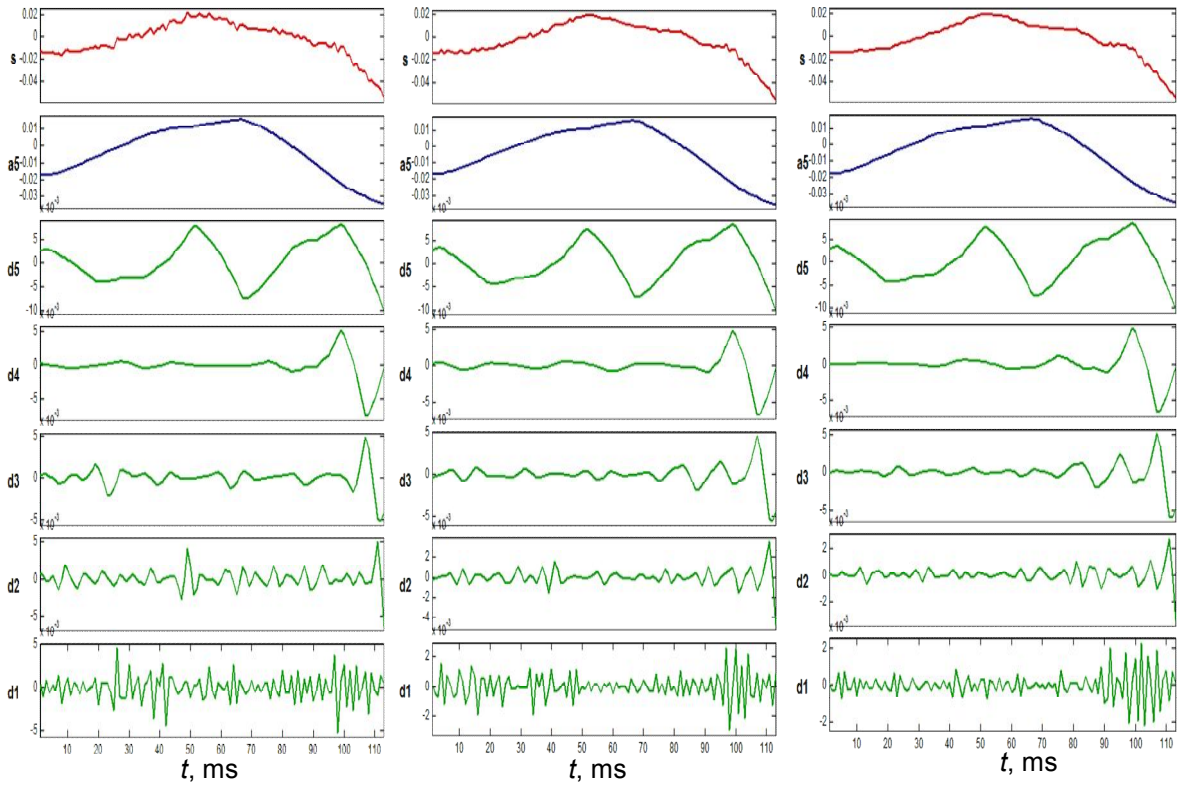

a) b) c)

Fig. 2.20. Discrete wavelet decomposition up to the 5th level of P wave with ALP and different signal-to-noise ratio (SNR): a) SNR =55 dB; b) SNR =60 dB; c) SNR =65 dB

Given the specific features of late potentials, the information about noise components should not be completely removed, thus losing the characteristics of ALP, but separated from the information about electrocardiogram. In this case, the use of the method of eigenvectors, which allows the division of signal and noise subspaces, is justified.

Existing methods of analysis of low-amplitude components of electrocardiosignals can be divided into two classes, depending on the availability of a priori information about the investigated signals. The knowledge of time and/or frequency characteristics of the signals and the use of standard basic functions is typical for the I-st class of methods. For the II-nd class of methods, on the basis of a minimum of a priori information about signal properties, the eigen basic functions derived from the data are applied. For the analysis of low-amplitude components of electrocardiosignals a combined approach, which includes several stages with the use of methods of analysis of the I-st and the II-nd classes, is encouraged to use: wavelet transformation, decomposition in the basis of eigenvectors, principal component analysis. For the tasks of processing of low-amplitude components of ECG the different combinations of these methods can be utilized [52-58].

Let us consider the application of the eigenvectors method for ECG analysis. Each *i*-realization in the ensemble of registered electrocardiosignals corresponds to a set of samples $E_i = [e_{i1}, e_{i2}, ...e_{iN}]$, where *N* is the amount of samples. The ensemble of *M* realizations can be presented as matrix *E*. Then the matrix of the ensemble of observations *E* and the covariance matrix *C* obtained for the ensemble of observations can be written as follows:

$$E = \begin{bmatrix} e_{11} & e_{12} & \dots & e_{1N} \\ e_{21} & e_{22} & \dots & e_{2N} \\ \vdots & \vdots & & \vdots \\ e_{M1} & e_{M2} & \dots & e_{MN} \end{bmatrix}, \quad C = \begin{bmatrix} c_{11} & c_{12} & \dots & c_{1N} \\ c_{21} & c_{22} & \dots & c_{2N} \\ \vdots & \vdots & & \vdots \\ c_{N1} & c_{N2} & \dots & c_{NN} \end{bmatrix},$$

where the elements c_{ij} of the matrix C can be presented as follows

$$c_{ij} = \sum_{k=1}^{M}(e_{ki} - m_k)(e_{kj} - m_k),$$

m_k is the average value calculated for the k-th realization.

With the methods of decomposition in the basis of eigenvectors and principal component analysis, the subspaces of eigen basic functions, which are determined from observations of the ensemble of electrocardiosignals, are constructed.

The method of decomposition in the basis of eigenvectors and principal component analysis decorrelate the ensemble of registered electrocardiosignals by projecting the data on the orthogonal axes of the eigenvectors of the covariance matrix:

$$E = UDV^T,$$

where E is observations matrix (the ensemble of registered electrocardiosignals) with dimension $M \times N$; D is the diagonal matrix with diagonal elements equal to the square root of the eigenvalues λ_i of the covariance matrix C; V is $N \times N$ matrix of eigenvectors of the covariance matrix C; U is $M \times M$ matrix of E projections on the eigenvectors of matrix C.

Performing principal component analysis, the major eigenvectors corresponding to the most significant eigenvalues are retained ($p << M$). According to the set of the major eigenvectors, a new matrix of ECG observations is constructed with filtration from noise components.

$$E_{new} = UD_pV^T,$$

where D_p is the diagonal matrix with diagonal elements equal to the square root of the most significant eigenvalues λ_i of the covariance matrix C.

On the basis of wavelet decomposition, electrocardiosignals preprocessing and postprocessing can be performed, resulting in the formation of the subspace of wavelet coefficients of low amplitude components Y. The approximation coefficients of multiresolution wavelet transform correspond to the low-frequency components of ECG signal and the detail coefficients correspond to high frequency components. Depending on the features of detectable pathology, signs of low amplitude components of electrocardiosignals can be found either at lower levels of detail components (for high-frequency character of identified components), or at the highest levels of detail components (for low-frequency character of identified components).

Extraction and evaluation of late potentials is possible to perform through the creation of eigensubspaces of wavelet patterns of low-amplitude components of ECG (Fig. 2.21). Suggested procedure for atrial late potentials recognition is based on the determination of eigenvalues and eigenvectors of the covariance matrix defined for wavelet coefficients sets, which comprise signs of late potentials and specified for each P wave in the ensemble of ECG realizations.

Eigenvector $\mathbf{V}_1$ of covariance matrix $\mathbf{C}_w$, defined for wavelet coefficients sets with signs of late potentials, corresponds to the largest eigenvalue λ_1. The first principal component determined by eigenvector $\mathbf{V}_1$ can be considered as a filtered set of the detail wavelet coefficients cD_1. The signal reconstructed on this set of wavelet coefficients can be considered as a component of ECG that in the case of atrial delayed depolarization contains the signs of late potentials purified from noise

and high-amplitude part of P wave. The remaining vectors of eigenbasis characterize the noise subspace, concretely, a mixture of the less significant components of the useful signal with physiological interferences and uncorrelated measuring noise.

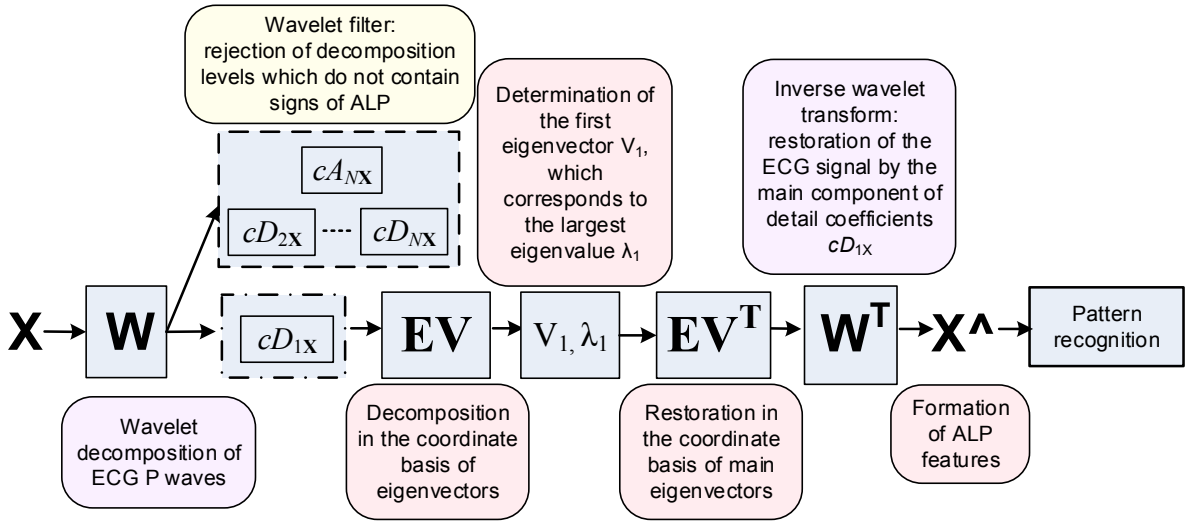

Fig. 2.21.General scheme of complex method of ECG analysis to identify ALP as the combination of the wavelet transform and decomposition in the coordinate basis of eigenvectors

Decomposition of the ensemble of d_1 detail components, corresponding to the ensemble of investigated P waves, in the coordinate basis of eigenvectors, demonstrates that the information about ALP is located in the signal subspace, namely, in the principal component of P wave, which is restored from the first eigenvector in the basis of eigenvectors V_1-V_6 (Fig. 2.22). The subspace of noise corresponding to the other eigenvectors contains the noise components. Therefore, the combined method of analysis makes it possible to combine the effective separation of levels of wavelet transform containing ALP attributes with the separation of diagnostically important

low-amplitude signal and noise.

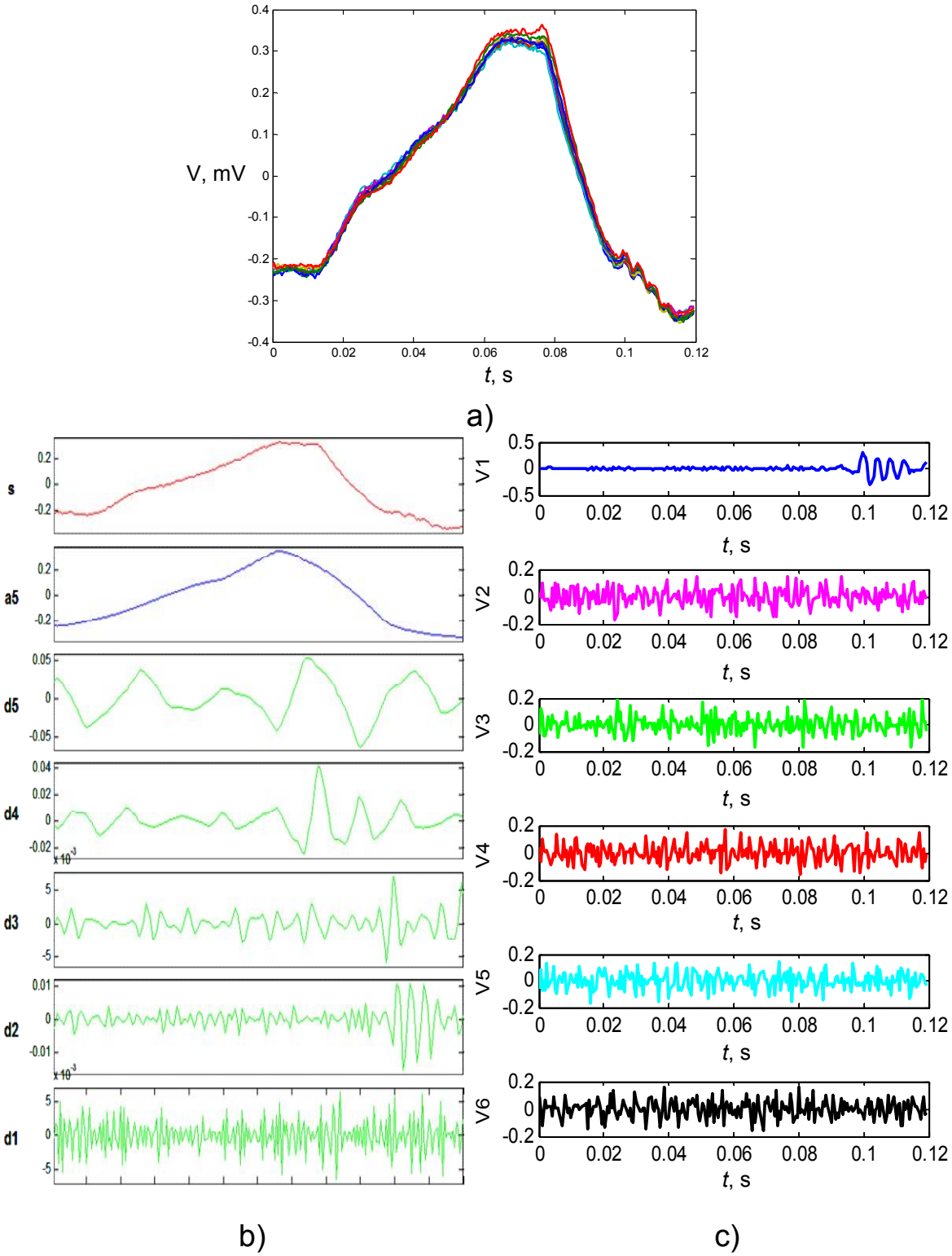

Fig. 2.22. a) ensemble of the investigated P waves; b) wavelet decomposition of P wave; c) decomposition of the ensemble of d_1 detail components in the coordinate basis of eigenvectors

The value of coefficient of correlation *r* between the simulated ALP, added to the P waves together with noise, and the ALP, detected by using the proposed combined method, amounts to 0.92 for the results presented in Fig. 2.23. It should be noted that despite small amplitude of detected signals and the presence of noise, the extracted ALP preserve the information about their shape, amplitude and quantity.

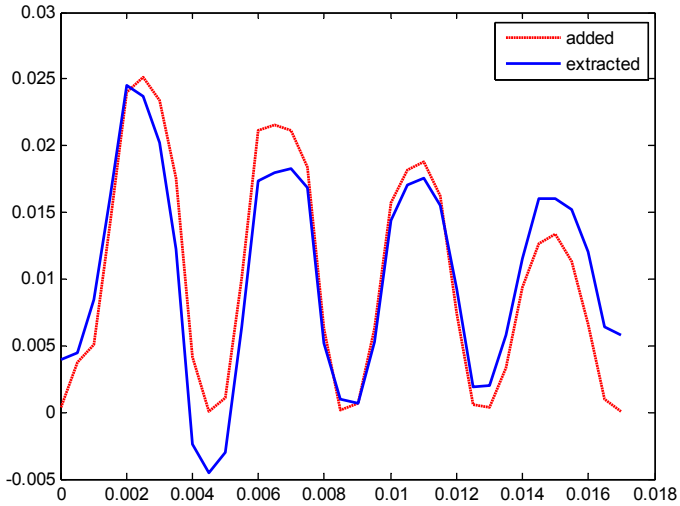

Fig. 2.23. Simulated ALP, added to the P waves together with noise, and ALP, detected by using the proposed combined method

In order to detect signs of atrial late potentials on the background of noise by means of the proposed method, a model experiment was conducted. 340 P waves extracted from ECG signals of several patients were used as data set for classification (Fig. 2.24). The real ECG recordings, preliminary filtered from the high-frequency components, were considered as the norm without ALP. Then, additive white gaussian noise was added to these signals. The noise in HR ECG recordings was simulated by superimposing P waves and a gaussian additive noise signal with signal-to-noise ratio of 65 dB. At the initial assumption about the possibility of the "norm" and "pathology", cardiocycles with such P waves are normal, because they do not contain ALP.

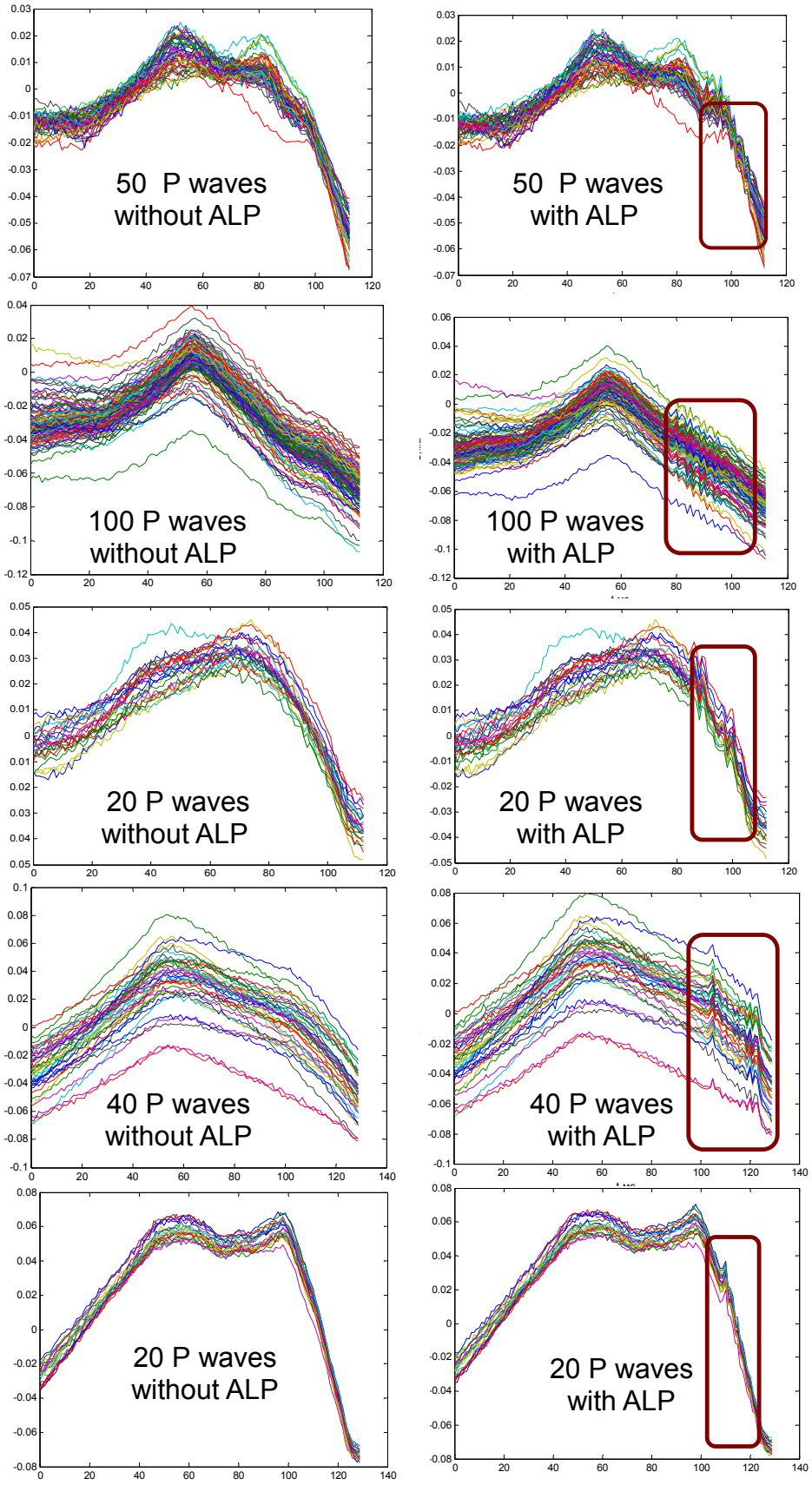

Fig. 2.24. Data used for classification

To the terminal part of each distorted by noise P wave the simulated late potentials were added. These P waves represented the pathology and contained simulated ALP, which were different in their amplitude, shape and duration. To simulate ALP in some cases the Hodgkin-Huxley equations were solved and the action potentials with low amplitude were added to the terminal part (30 ms) of P waves. In another cases ALP activity was simulated as the sum of sinusoids with frequency range from 40 to 250 Hz and amplitudes of 1-10 μV. For each patient ALP were simulated different in their amplitude, shape and quantity.

Analysis of cardiocycles with such P waves involves the detection of late potentials on the background noise. For the initial ensembles of cardiosignals the sets of wavelet coefficients cD_1 were obtained by means of wavelet decomposition up to the 5th level with a "symmetric" wavelet of the 4th order.

Parameter

$$L = \frac{\lambda_i}{\sum_{k=1}^{N} \lambda_k} \cdot 100\%$$

makes sense of the part of the variance in percentage, which is used to estimate the proportion of the information contained in the component determined by the eigenvector $\mathbf{V}_i$.

The obtained sets of eigenvalues explain the use of the component determined by the first eigenvector $\mathbf{V}_1$. For example, decomposition in a basis of eigenvectors performed for wavelet coefficients cD_1 of the ECG signals with ALP presence in background noise obviously shows that the largest proportion of the dispersion L = 63%, i.e. the largest amount of the information about ALP, corresponds to the first principal component

(Fig. 2.25, b). The proportion of the variance is approximately equal for remaining eigenvalues and determined by the noise components. In absence of ALP wavelet coefficients contain only noise and, consequently, the proportion of the variance for the first component is not significantly higher than the corresponding parameter for the other components in the set of 10 eigenvalues (Fig. 2.25, a).

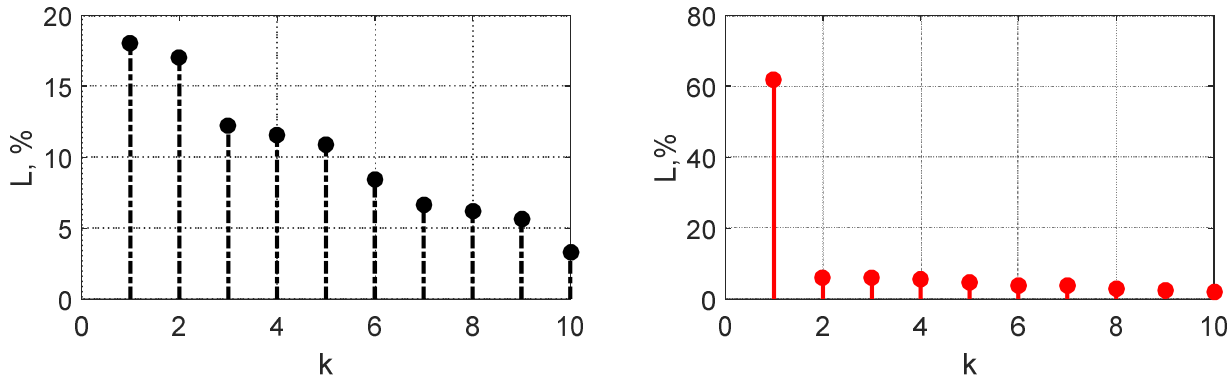

a) b)

Fig. 2.25. Parameter *L* for the first 10 eigenvalues:
a) absence of ALP; b) presence of ALP

Reconstruction in the time-amplitude domain was made by inverse wavelet transform performed using only the main first component of wavelet coefficients cD_1. This component for the case of the late potentials absence on the background noise has a form typical for noise, and in the presence of late potentials, it contains the peaks of late potentials, individual and peculiar to each patient (Fig. 2.26, 2.27).

The use of the proposed complex method made it possible to distinguish ALP bursts from the noise and determine the temporal area of their localization. For P waves corresponding to the absence of ALP reconstructed signal does not contain high-amplitude ALP bursts above the general noise level.

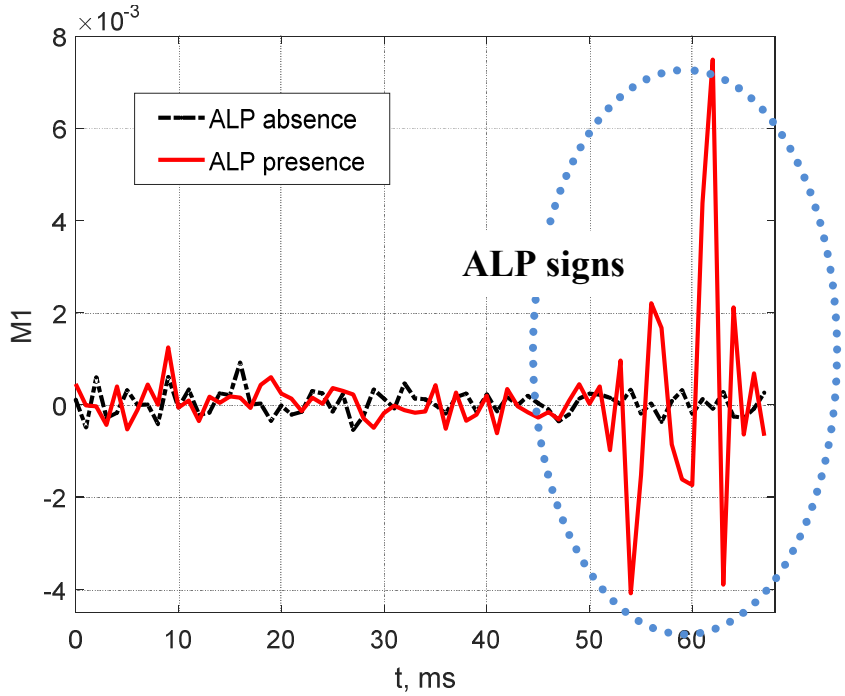

Fig. 2.26. The first main component corresponding to the largest eigenvalue for the cases of absence and presence of ALP in noise

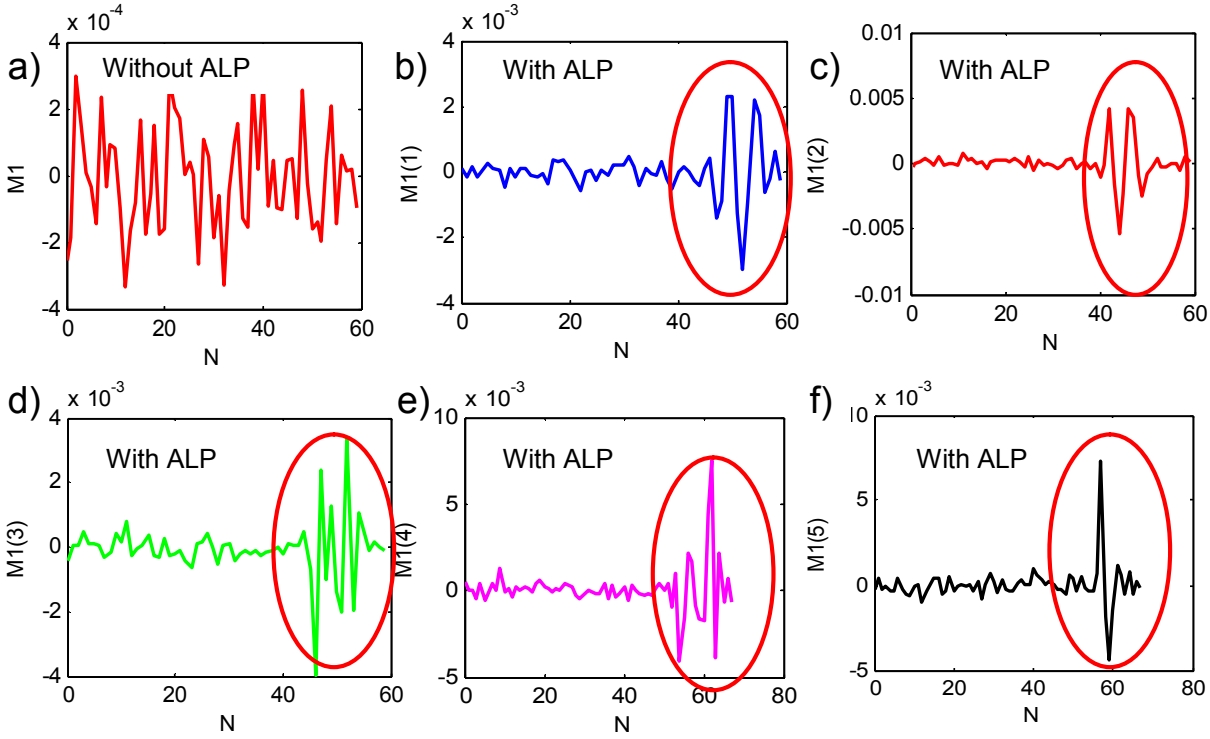

Fig. 2.27. The first main component corresponding to the largest eigenvalue: a) for the case of ALP absence on the background noise; b-f) for cases of ALP existence on the background noise

Visual analysis of raw data before processing can not conclude on the presence or absence of late potentials in the terminal part of ECG P wave. Application of the proposed method makes it possible to distinguish between the noise and late potentials and to determine the region of their localization (Fig. 2.28).

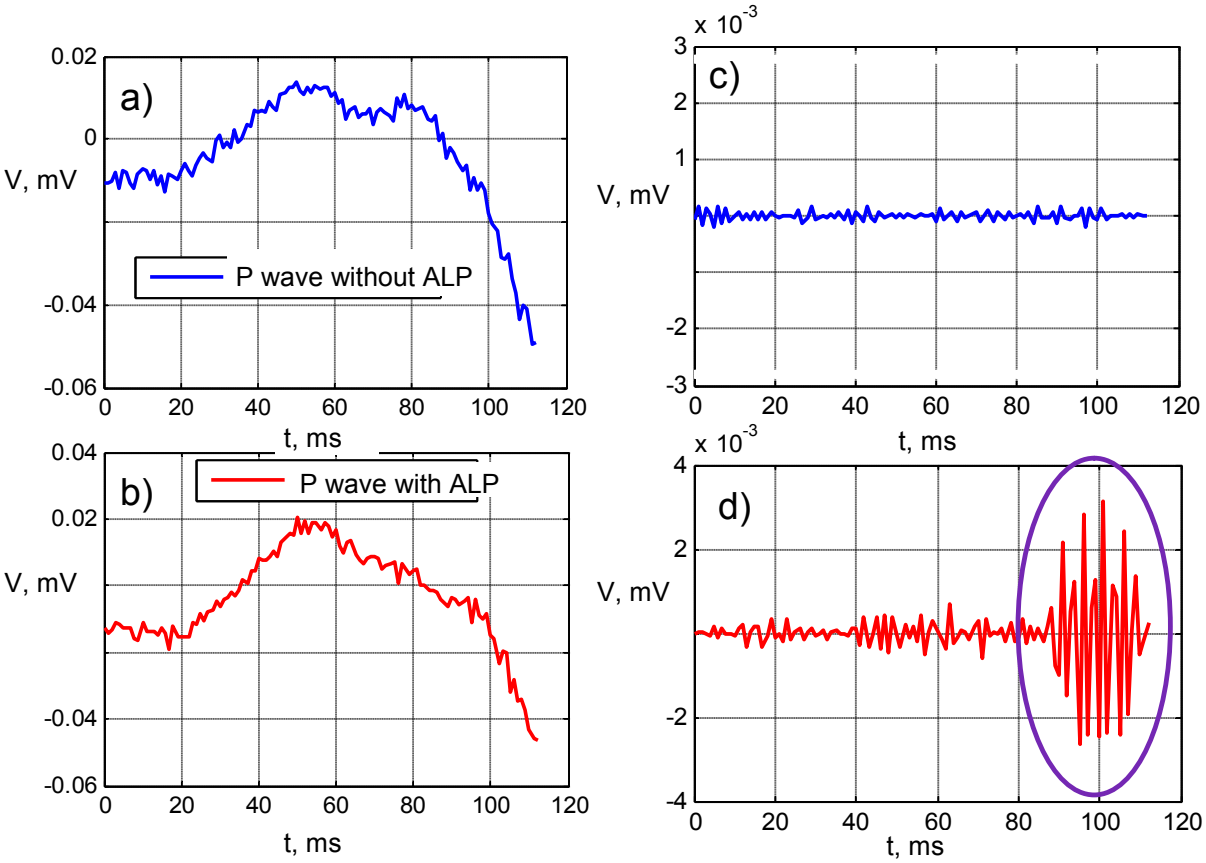

Fig. 2.28. Application of the complex method:
a) P wave without ALP; b) P wave with ALP;
c) ALP are absent in the high-frequency component of P wave after processing; d) ALP are present in the high-frequency component of P wave after processing

To estimate high-frequency P wave components, the following parameters based on the ratio of the eigenvalues can be used [52-58]:

$$R = \lambda_1 \Big/ \sum_{i=1}^{N} \lambda_i \; ;$$

$$K = \sum_{i=2}^{N} \lambda_i \Big/ \sum_{i=1}^{N} \lambda_i \; ;$$

$$S = \sum_{i=1}^{N} \lambda_i \; .$$

Analysis of points groups in three-dimensional feature space indicates the presence of two clouds of data. The cluster with the close packing of points corresponds to data relating to P waves without ALP, representing the class “norm". Large enough, comparing with the first case, the spread of features within the second cluster, representing the class "pathology", is caused by the individual character of late potentials for each patient (Fig. 2.29).

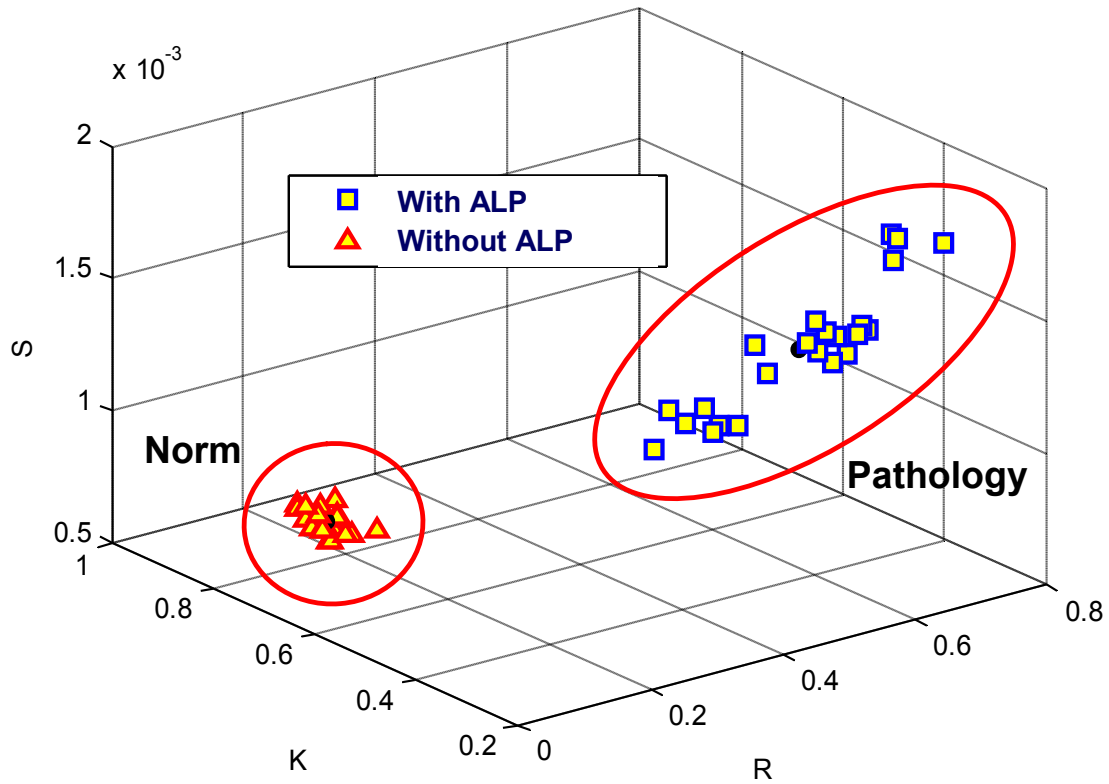

Fig. 2.29. Atrial late potentials pattern recognition

A similar picture of points distribution is observed for another choice of ALP features. Parameter *R* is determined as ratio of the first eigenvalue to the sum of all eigenvalues of the covariance matrix for an ensemble of detail wavelet coefficients cD_1. *M* parameter is determined as maximum of the absolute values of the signal *A*, reconstructed by the main component of the detail coefficients cD_1: $M = \max|A|$. Fig. 2.30 shows 2 non-overlapping clusters for 2 classes in ALP pattern recognition: “norm - ALP absence” and “pathology - ALP presence”. Classification is done the better, the smaller the distance to the center point of the cluster within the cluster and the greater the distance between the centers of the different clusters.

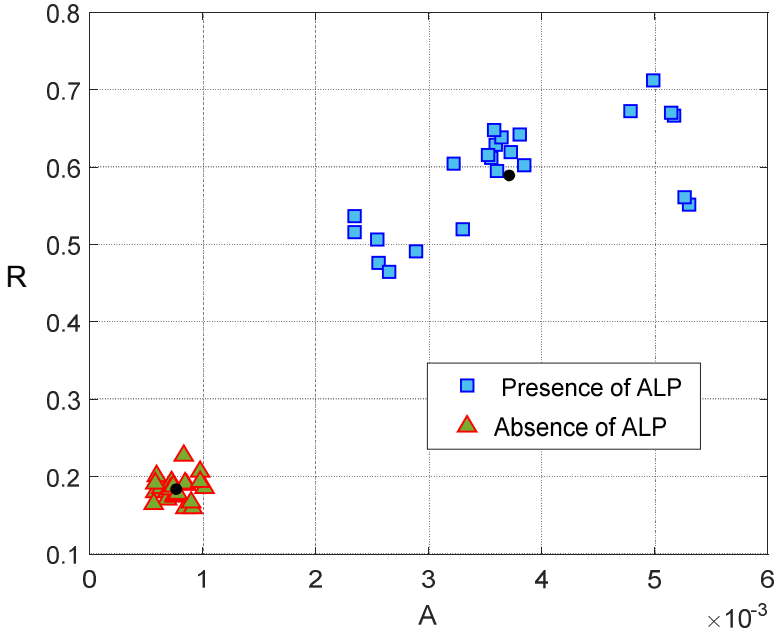

Fig. 2.30. The results of data clustering

Application of the proposed method allowed us to separate initial ECG data into 2 classes: norm and pathology (Fig. 2.31).

In the development of approaches to late potentials detection, cluster analysis can be considered as a preliminary stage of recognition,

which is conducted to select the most significant features of late potentials and to prepare a training set to provide the possibility of automated diagnostic decision on the patient's condition.

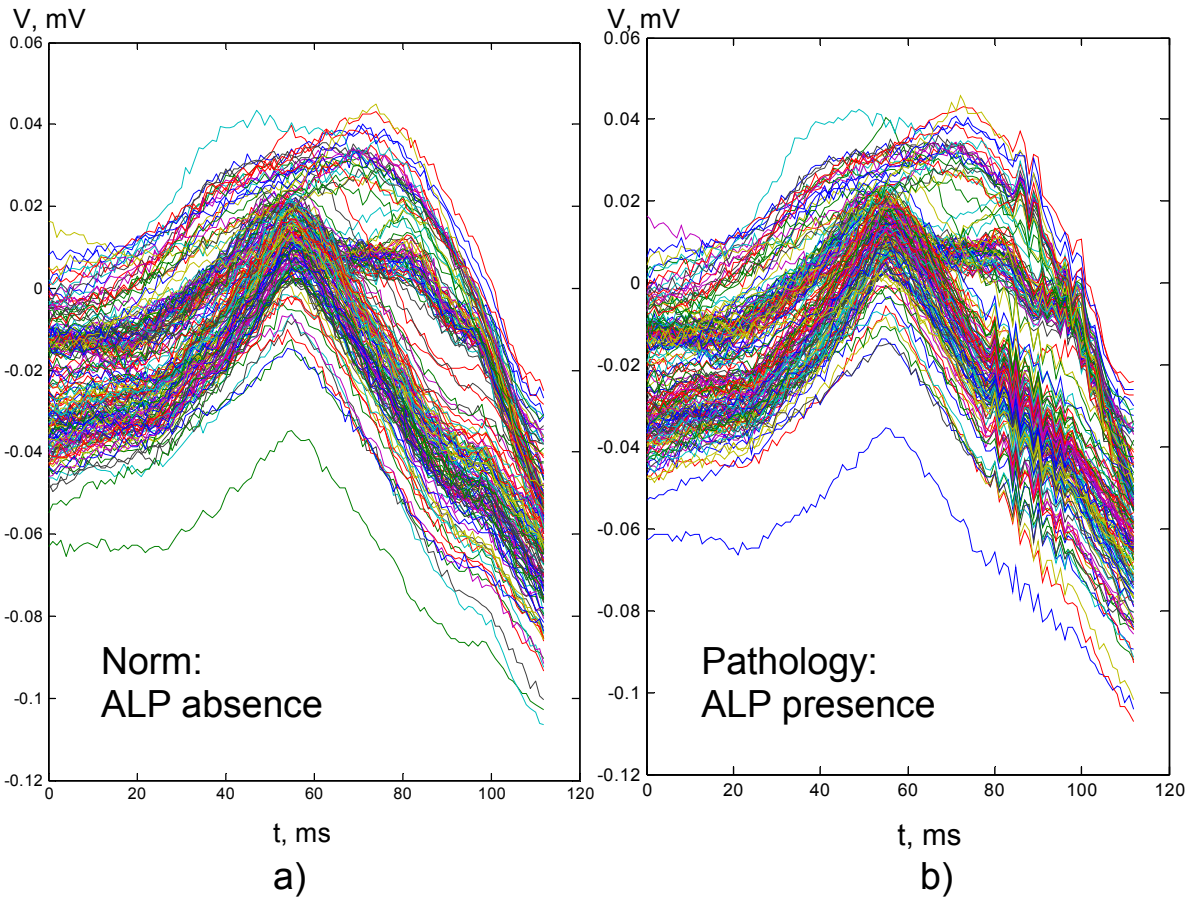

Fig. 2.31. Separation of P waves into 2 Classes: a) norm; b) pathology

CONCLUSIONS

The search for predictors, which can detect the fact of the presence of vulnerable myocardium and predict development of arrhythmia, is an important task aimed at patients risk stratification. Widespread use in clinical practice of many approaches to the analysis of late potentials is still limited through medical ambiguity of the results and requires additional clinical studies and their interpretation. Improvement of methods of processing of low amplitude components of bioelectric

signals allows diagnose of heart malfunction at the stage, when classical methods do not show abnormalities.

The proposed combined method allows the detection of low amplitude components of ECG that are markers of cardiac electrical instability. The use of the combined method makes it possible to distinguish the bursts of late potentials from the noise and to determine the temporal area of their localization.

CONTROL QUESTIONS AND TASKS

1. Draw schematically electrical conduction system of the heart.
2. Explain the principle of ECG registration.
3. How problems in the heart are detected?
4. Explain which waves are distinguished on the standard electrocardiogram.
5. What is happening in the heart during the P, QRS, and T waves?
6. What electrophysiologic event does P wave reflect?
7. What electrophysiologic event does T wave reflect?
8. What do you know about normal heart rate and heart rhythm disturbance?
9. Explain the theoretical and methodological aspects of using the method of high-resolution electrocardiography.
10. Explain the reasons of genesis of atrial and ventriclar late potentials.
11. What are the requirements for high-resolution electrocardiography systems?
12. What are the main advantages of signal averaging in high-resolution electrocardiography systems?

13. Which sources of instrumental and physiological artifacts, presented in ECG recordings, do you know? How do these artifacts manifest themselves on the spectrum of electrocardiograms?

14. What are the ways to eliminate noise components of ECG signal or reduce their impact?

15. Draw a typical ECG signal with its waves and noise components. Explain, how the ECG signal changes during the filtration process using: a) low pass filter with a cutoff frequency of 200 Hz? b) high pass filter with a cutoff frequency of 5 Hz?

16. An electrocardiogram with a sampling frequency of 2000 Hz has been registered in the system of HR ECG. The spectral components of the essential ECG signal appear up to 100 Hz. The signal is distorted by a periodic interference with a base frequency of 50 Hz and a third, fifth and seventh harmonics of this frequency. Draw a schematic spectrum of the ECG and show the components associated with the artifacts.

17. What are the advantages and disadvantages of spectral analysis of ECG?

18. Explain the features of continuous and discrete wavelet transform of ECG signals.

19. What are the advantages and disadvantages of using wavelet transform to ECG analysis?

20. How the appropriate wavelet function for wavelet analysis of biomedical signal can be selected?

21. Explain the features of decomposition in the basis of eigenvectors.

22. Explain the features of the complex method of ECG analysis as the combination of the wavelet transform and decomposition in the coordinate basis of eigenvectors.

REFERENCES

[1] Cardiology Guide / [ed. V. N. Kovalenko]. — K.: Morion, 2008. — 1404 pp.

[2] New methods of electrocardiography / [ed. S.V. Grachev, G.G. Ivanov, A.L. Syrkin].— Moscow: Technosphere, 2007.— 552 p.

[3] Ivanushkina N. G. Technologies of high resolution in electrocardiography: teaching book / N.G. Ivanushkina, V.O. Feschechko. — K .: NTUU "KPI", 2007. — 116 p.

[4] Veenhuyzen G. D. Atrial fibrillation/ G. D. Veenhuyzen, C. S. Simpson, H. Abdollah // Canadian Medical Association Journal. — 2004. — Vol. 7 (171). — P. 760 — 775.

[5] Allessie M. A. Experimental evaluation of Moe's multiple wavelet hypothesis of atrial fibrillation / M. A. Allessie, W. J. Lammers, F. I. Bonke, J. Hollen // Cardiac Arrhythmias; eds. D. P. Zipes, J. Jalife. — N. Y.: Grune & Stratton, 1985. — P. 265 — 276.

[6] Moe G. K. A computer model of atrial fibrillation / G. K. Moe, W. C. Rheinbolt, J. A. Abildskov// Am. Heart J. — 1964. — Vol. 67. — P. 200 — 220.

[7] Moe G. K. On the multiple wavelet hypothesis of atrial fibrillation / G. K. Moe // Arch. Int. Pharmacodyn. Ther. — 1962. — Vol. 140. — P. 183 — 188.

[8] Leir C.V. Prolonged atrial conduction. A major predisposing factor for the development of atrial flutter / C. V. Leir, J. A. Meacham, S. F. Schaal // Circulation. — 1978. — Vol. 2 (57). — P. 213 — 216.

[9] Prolonged and fractionated right atrial electrograms during sinus rhythm in patients with paroxysmal atrial fibrillation and sick sinus

node syndrome / M. Tanigawa, M. Fakatani, A. Konoe [et al.] // J. Am. Coll. Cardiol. — 1991. — Vol. 17. — P. 403 — 408.

[10] Detection of patients at risk for paroxysmal atrial fibrillation during sinus rhythms by P wave-triggered signal-averaged electrocardiogram /M. Fukunami, T. Yamada, M. Ohmoni [et al.] // Circulation. — 1991. — Vol. 83. — P. 162 — 169.

[11] Value of the atrial signal-averaged electrocardiogram in identifying patients with paroxysmal atrial fibrillation / G. Opolski, J. Stanislawska, K. Slomka [et al.] // Int. J. Cardiol. — 1991. — Vol. 30. — P. 315 — 319.

[12] Detection of patients at risk for reccurens of atrial fibrillation after succesful electrical cardioversion by signal-avareged P-wave ECG / G. Opolski, P. Scislo, J. Stanislavska [et al.] / Int. J. Cardiol. — 1997. — Vol. 60 (2). — P. 181 — 185.

[13] Signal averaging P wave analysis in patients with lone atrial fibrillation / P. Marconi, G. Castelli, A. Montereggi [et al.] / Ital. Cardiol. — 1991. — Vol. 21. — P. PPP31075 — 1081.

[14] Reproducibility of the signal averaged P wave: time and frequency domain analysis / P. Stafford, J. Cooper, J. Fothergill [et al.] // Heart. — 1997. — Vol. 77 (5). — P. 412 — 416.

[15] Stafford P. Quantitative analysis of signal-averaged P waves in idiopathic paroxysmal atrial fibrillation / P. Stafford, I. Turner, R. Vincent // Am. J. Cardiol. — 1991. — Vol. 68. — P. 751 — 755.

[16] Guidera S. The signal averaged P wave duration: a rapid and noninvasive marker of risk of atrail fibrillation / S. Guidera, J. S. Steinberg // J. Am. Coll. Cardiol. — 1993. — Vol. 21. — P. 1645 — 1651.

[17] P-wave dispertion index: a marker of patients with paroxysmal atrial fibrillation / G. Q. Villiani, M. Piepoli, A. Rosi [et al.] // Int. J. Cardiol. — 1996. — Vol. 55 (2). — P. 169 — 175.

[18] The best criterion for discrimination between patients with and without paroxysmalatrial fibrillation on signal-averaged electrocardiogram / N. Gondo, K. Kumagai, K. Matsuo [et al.] // Am. J. Cardiol. — 1995. — Vol. 75. — P. 93 — 95.

[19] Analysis of the P-wave in the signal averaged electrocardiogram. Normal value and reproducibility / M. Hofman, L. Goedel-Meinen, A. Bekhoff [et al.] // PACE. — 1996. — Vol. 19. — P. 1928 — 1932.

[20] Dennis A. R. Prognostic significance of ventricular tachycardia and fibrillation induced at programmed stimulation and delayed potentials detected on the signal-averaged electrocardiograms of survivors of acute myocardial infarction / A. R. Dennis, D. A. Richards, D. V. Cogy // Circulation. — 1986. — Vol. 74. — P. 731 — 745.

[21] The prognostic significance of quantitative signal-averaged variables relative to clinical variables, site of myocardial infarction, ejection fraction and ventricular premature beats / J. F. Gomes, S. L. Winters, M. Martinson [et al.] // JACC. — 1989. — Vol. 13. — P. 377 — 384.

[22] Ogawa H. Problems on evaluating signal-averaged P wave as a predictor of atrial fibrillation or flutter the importance of frequency range of the filter and the influence of left atrial overload / H. Ogawa, H. Fukusaki, Y. Ohnishi // Japan. Circulation J. — 1989. — Vol. 21. — P. 534 — 538.

[23] A Prospective Study to Predict the Transition from Paroxysmal Atrial Fibrillation to Chronic Atrial Fibrillation by Signal-averaged Electrocardiography / H. Ogita, M. Fukunami, T. Shimonagata [et al.] // Circulation. — 1991. — Vol. 83. — P. 162 — 169.

[24] Influence of age, lead axis, frequency of arrhyrhmic episodes, and atrial demensions on P wave triggered SAECG in patients with lone paroxysmal atrial fibrillation / A. Michelucci, L. Padeletti, A. Chelucci [et al.] // Pacing-Clin. Electrophysiology. — 1996. — Vol. 19. — № 5. — P. 758 — 767.

[25] Risk for atrial fibrillation in patients with hypertrophic cardiomyopathy assessed by signal averaged P wave duration / F. Cecchi, A. Montereggi, I. Olivotto [et al.] // Heart. — 1997. — Vol. 78 (1). — P. 44 — 49.

[26] High resolution methods for detection of electrophysiological changes in the ischaemic heart / I. Provaznik, J. Bardonova, M. Novakova [et al.] // Scripta medica. — 2002. — № 5 (75). — P. 223 — 230.

[27] Standards for analysis of ventricular late potentials using high-resolution or signal-averaged electrocardiography: a statement by a task force committee of the European Society of Cardiology, the American College of Cardiology / G. Breithardt, M. E. Cain, N. El-Sherif [et al.] // J. Amer. Col. Cardiol. — 1991. — Vol. 17. — P. 999 — 1006.

[28] Simson M. B. Use of signals in the terminal QRS complex to identify patients with ventricular tachycardia after myocardial infarction / M. B. Simson // Circulation. — 1981. — Vol. 64. — P. 235 — 242.

[29] Relation between late potentials on the body surface and directly recorded fragmented electrograms in patients with ventricular tachycardia / M. B. Simson, W. I. Unterrver, S. R. Spielman [et al.] // Am. J. Cardiology. — 1983. — Vol. 51. — P. 105 — 112.

[30] Simson M. B. Detection of delayed ventricular activation on the body surface in dogs / M. B. Simson, D. Euler, E. I. Michelson // American Journal of Physiology. — 1981. — Vol. 241. — P. 363 — 369.

[31] Prediction of atrial fibrillation from surface ECG: review of methods and algorithms/ S. Poli, V. Barbaro, P. Bartolini [et al.] // Ann I-st Super Sanità. — 2003. — № 39 (2). — P. 195 — 203.

[32] Wiley Encyclopedia of Biomedical Engineering/ [ed. M. Akay]. — 2006.— 4152 p.

[33] Single-beat analysis of ventricular late potentials in the surface electrocardiogram using the spectrotemporal pattern recognition algorithm in patients with coronary artery disease/ P. Steinbigler, R. Haberl, G. Jilge [et al.] // European Heart Journal. — 1998. — № 19 (3). — P. 435 — 446.

[34] Time-Frequency and Wavelets in Biomedical Signal Processing / [ed. Metin Akay]. — IEEE Press, 1997. — 652 p.

[35] Lantian Song. The Time-Frequency Analysis of Abnormal ECG Signals/ Lantian Song, Fengqin Yu // Lecture Notes in Computer Science. — 2010. — Vol. 6330. — P. 60 — 66.

[36] Dickhaus H. Time-frequency analysis of ventricular late potentials/ H. Dickhaus, L. Khadra, J. Brachmann // Meth. Inform. Med. — 1994. — Vol. 33.— № 2. — P. 187 — 195.

[37] Addison P. S. Time-frequency analysis of biosignals / P. S. Addison, J. Walker, R. C. Guido // IEEE Engineering in medicine and biology. — 2009. — № 28. — P. 14 — 29.

[38] Plonsey R. Bioelectricity: A Quantitative Approach, 3rd edition/ R. Plonsey, R.C. Barr// Springer. — 2007. — 528 p.

[39] Ishikawa Y. Wavelet Theory-Based Analysis of High-Frequency, High-Resolution Electrocardiograms: A New Concept for Clinical Uses/ Y. Ishikawa // Progress in Biomedical Research. — 2002. — Vol. 7. — № 3. — P. 179 — 184.

[40] Detection of small variations of ECG features using wavelet / A. K. Haque, M. H. Ali, M. A. Kiber, M. T. Hasan // ARPN Journal of Engineering and Applied Sciences. — 2009. — Vol. 4. — № 6. — P. 27 — 30.

[41] Using Supervised Fuzzy Clustering and CWT for Ventricular Late Potentials Detection in HRECG Signal / G. S. Khorshidi, A. Jaafari, A. Pourmorteza [et al.] // Proc. EUSFLAT Conf. — 2007. — P. 63 — 69.

[42] Moga M. Continuous Wavelet Transform in ECG Analysis. A Concept or Clinical Uses / M. Moga, V. D. Moga, Gh. I. Mihalas // Connecting medical informatics and bio-informatics. Proceedings of MIE. — 2005. — P. 1143 — 1148.

[43] Bunluechokchai S. Analysis of the high resolution ECG with the continuous wavelet transform / S. Bunluechokchai, M. J. English // Computers in Cardiology. — 2003.— № 30. — P. 553 — 556.

[44] Comparing Wavelet Transforms for Recognizing Cardiac Patterns/ L. Senhadji, G. Carrault, J. J. Bellanger [et al.] // IEEE Engineering

in Medicine and Biology Magazine. — № 3. — 1995. — P. 167 — 173.

[45] Saritha C. ECG Signal Analysis Using Wavelet Transforms / C. Saritha, V. Sukanya, Y. N. Murthy // Bulg. J. Phys. — № 35. — 2008. — P. 68 — 77.

[46] Mahmoodabadi S. Z. ECG feature extraction using daubechies wavelets / S. Z. Mahmoodabadi, A. Ahmadian, M. D. Abolhasani // Proceedings of the 5th International Conference VIIP. — 2005. — P. 343 — 348.

[47] Mousa A. Neural Network Detection of Ventricular Late Potentials in ECG Signals Using Wavelet Transform Extracted Parameters / A. Mousa, A. Yilmaz // IEEE Proceedings of the 23rd Annual EMBS International Conference. — 2001. — P. 1668 — 1671.

[48] Héctor Mesa. Adapted Wavelets for Pattern Detection / Héctor Mesa // Progress in Pattern Recognition, Image Analysis and Applications. — Proceedings CIARP, 2005. — P. 933 — 944.

[49] Wavelets and their applications / [ed. M. Misiti, Y. Misiti, G. Oppenheim, J.-M. Poggi]. — 2007. — 332 p.

[50] Allen R. L. Signal Analysis: Time, Frequency, Scale, and Structure / R. L. Allen, D. W. Mills. — Wiley, 2004. — 937 p.

[51] N. Smolentsev. Fundamentals of the theory of wavelets. Wavelets in MATLAB / N.K. Smolentsev.— Moscow:DMK Press, 2008. — 448 p.

[52] Estimation of atrial fibrillatory wave from single-lead atrial fibrillation electrocardiograms using principal component analysis concepts/ F. Castells, C. Mora, J. J. Rieta [et al.] // Medical and Biological

Engineering and Computing. — 2005. — Vol. 43. — № 5. — P. 557 — 560.

[53] Moody G. B. QRS morphology representation and noise estimation using the Karhunen-Loève transform / G. B. Moody, R. G. Mark // Computers in Cardiology. — 1989. — P. 269 — 272.

[54] Morphological Descriptors Based on Eigen Value Decomposition for P-Wave Analysis / F. Castells, J. Lorenz, A. M. Climent [et al.] // Computers in Cardiology.—2008.—№ 35. — P. 245 — 248.

[55] N. A. Matveyeva, N. G. Ivanushkina, and K. O. Ivanko, "Combined method for detection of atrial late potentials" in Proceedings of IEEE 33th International Scientific Conference on Electronics and Nanotechnology, Kyiv, 2013, pp. 285–289.

[56] Ivanko K. O. Identification and assessment of electrocardiographic markers of cardiac electrical instability/ K.O. Ivanko, N. G. Ivanushkina, Y.S. Karplyuk // Science news of National Technical University of Ukraine "Kyiv Polytechnic Institute". - 2017. - № 1. - pp. 37-47: http://nbuv.gov.ua/UJRN/NVKPI_2017_1_6

[57] Formation of the diagnostic HR ECG features of post-traumatic myocardial dystrophy/Ivanushkina N., Chesnokova O., Ivanko K., Karplyuk Y., Chaikovskiy I., Sofienko S., Mjasnikov G. // Proceedings of 2016 IEEE 36th International Scientific Conference on Electronics and Nanotechnology (ELNANO).–2016.–pp. 206-209.

[58] Analysis of low-amplitude signals of cardiac electrical activity/ N.G. Ivanushkina, K.O. Ivanko, V.I. Timofeyev//Radioelectronics and Communications Systems (distributed by Springer) – 2014. – Vol.57. – №10 – p.465-473.

SECTION 3

IDENTIFICATION AND ASSESSMENT OF T WAVE ALTERNANS AS A PREDICTOR OF LIFE-THREATENING VENTRICULAR TACHYARRHYTHMIAS

3.1. T wave alternans phenomenon

Another task of extraction of diagnostically important information from the surface electrocardiogram is analysis of the electrical alternans of ventricular repolarization. Identification and evaluation of T wave alternans is a promising direction in electrocardiography. The term "T wave alternans" (TWA) refers to the alternation of amplitude or temporal characteristics of the ST interval and T wave (ST-T complex) and involves measuring of the differences in amplitude, shape, and/or time of the T wave in successive cardiac cycle [1, 2].

The appearance of TWA on the ECG can be explained by the presence of repolarization alternation at the level of ventricular cardiomyocytes. TWA reflects periodic beat-to-beat variation in the electrophysiological characteristics of the myocardial cells in various pathological processes, which lead to violations of repolarization of cardiomyocytes, and serves as a predictor of life-threatening ventricular tachyarrhythmias. Macro and micro alternans can be distinguished on ECG. Macro alternans is apparent on the ECG with the naked eye and represents significant change in the morphology of the T wave (its amplitude, shape, length, polarity). Microvolt level beat-to-beat fluctuations could not be revealed by visual inspection and demand

advanced digital processing techniques and computational algorithms for their detection and assessment.

It is thought that TWA is the result of spatial or temporal dispersion of repolarization [1-3]. Heterogeneity of electrophysiological properties of the myocardium cells (spatial changes in duration, shape or speed of propagation of action potentials) forms a substrate for reentry mechanism (mechanism of excitation wave reentry), which consequently leads to arrhythmia. TWA is closely associated with arrhythmogenic mechanisms and reflects the propensity of the myocardium to the development of ventricular tachyarrhythmias; therefore, it is believed to be a marker of increased risk of sudden cardiac death. Even in healthy subjects the subtle beat-to-beat fluctuations in T-wave amplitude could be observed. Changes in electrophysiological characteristics of myocardial cells under various pathological processes lead to variation of the amplitude of these beat-to-beat fluctuations. Characteristics of low amplitude but clinically significant beat-to-beat fluctuations can be used as a noninvasive diagnostic tool.

ABAB pattern is typical for T wave alternans, wherein one type of T wave is observed in the odd cardiocycles (type A, the waves with a lower amplitude in Fig. 3.1), and the different type of T wave can be seen in the even cardiocycles (type B, the waves with a larger amplitude). However, the other types of alternans are believed to be possible, when at some point of time a change of phase of alternans occurs, such as in ABBABA pattern.

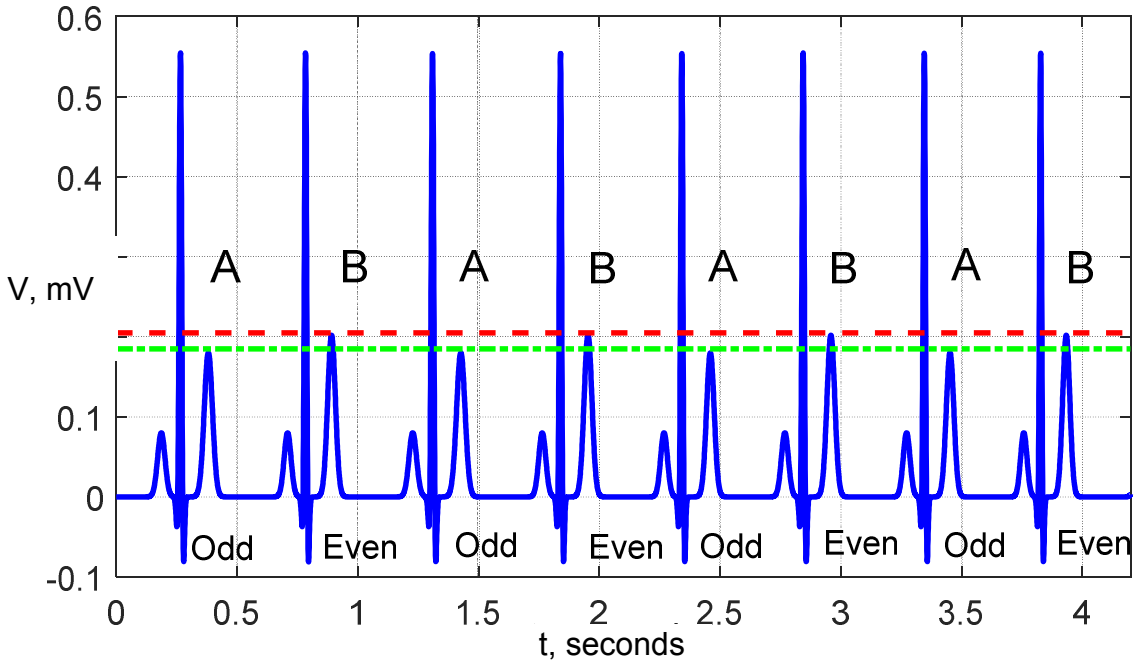

Fig. 3.1. Typical for T wave alternans ABAB pattern

Beat to beat alternation of T wave amplitude, termed T wave alternans, is associated with the dispersion of repolarization and reflects variation that periodically appears in each succeeding cardiocycle. Significant spatial and temporal dispersion of repolarization, variation of the propagation velocity of excitation pulse, fluctuation of the ionic currents, and alternation of duration and shape of the action potentials in cardiac cells lead to arrhythmias. Repolarization alternans at the cellular level, observed in direct recordings of action potentials from the surface of the heart, is several orders of magnitude greater than the manifestation of TWA on the surface ECG. This fact explains why even micro-volt changes on the surface ECG, as TWA manifestation, reflect significant abnormalities of repolarization of cardiomyocytes membrane and have clinical importance.

The peculiarity of the T wave alternans analysis is the need of its assessment within a certain range of heart rate. T wave alternans occurs

at a significant increase in heart rate above a certain threshold. Usually, TWA appears with an increase in heart rate up to 100-110 beats/minute, so it is mainly evaluated during the exercise test, pharmacological stress tests, electrocardiostimulation, or according to the daily ECG monitoring. When heart rate is greater than 110 beats per minute, alternans of repolarization may occur in healthy people. A high heart rate can result in overload and disruption of the cell's ability to maintain calcium homeostasis during myocardial contraction. This leads to an alternation in the calcium circulation process and consequently to alternating action potential duration [1-3].

3.2. Detection and assessment of the level of T wave alternans by the scattergram method

The relevance of using T wave alternans as a noninvasive diagnostic indicator is not in doubt. However, the detection and assessment of the level of T wave alternans from surface ECG data is quite challenging, as the visually implicit changes in T wave amplitude have a level from units to several tens of microvolts, while the amplitude of the T wave is 0.3-0.7 mV. Furthermore, the real ECG signals are usually highly distorted by noise components of biological and nonbiological origin.

The Database used for investigation of TWA is provided by the PhysioNet resource (T Wave Alternans Challenge Database) and contains 100 multichannel ECG records sampled at 500 Hz with 16 bit resolution and approximate duration of two minutes [4-6]. It includes recordings from patients with myocardial infarctions, transient ischemia,

ventricular tachyarrhythmias, and other risk factors for sudden cardiac death, as well as healthy controls and synthetic cases with TWA.

The stage of ECG signal preprocessing is very important for TWA identification and assessment. Even a very weak residual noise can lead to a false-positive result. In the present study preprocessing stage included the elimination of baseline drift and high-frequency noise suppression. The wavelet based multiresolution analysis was applied to remove baseline fluctuations. Wavelet decomposition was performed up to the 12th level of the raw ECG data using Symmetric wavelet of 6th order. The 12th order approximation function and the detail functions from 9 to 12 orders, which reflect slow changes of signal, were not taken into account during signal recovery. To remove high-frequency noises, the spectrum of the previously detrended data was limited up to 30 Hz using FIR Window Lowpass filter.

PQRST-complexes of ECG were selected for QRS detection using original method, based on threshold algorithm applied to the specialy formed reference signal that was obtained by nonlinear conversion of the signal and its first derivative. The algorithm is based on ECG QRS Pan Tompkins algorithm, but has several significant improvements for reliable and accurate QRS detection in noisy signal with artifacts. The detection point of QRS complexes was selected as the peak points of R waves. The peak points of R-waves are located at the local maximum peaks of ECG signal. The beats were synchronized with respect to the peak of R wave; beats, which cross-correlation coefficient with the common beat pattern was below the fixed threshold, were rejected.

After receiving the ensemble of realizations of PQRST complexes the local extremes detection algorithm was applied and the results were used as input for clustering of these “special points” of ECG signal.

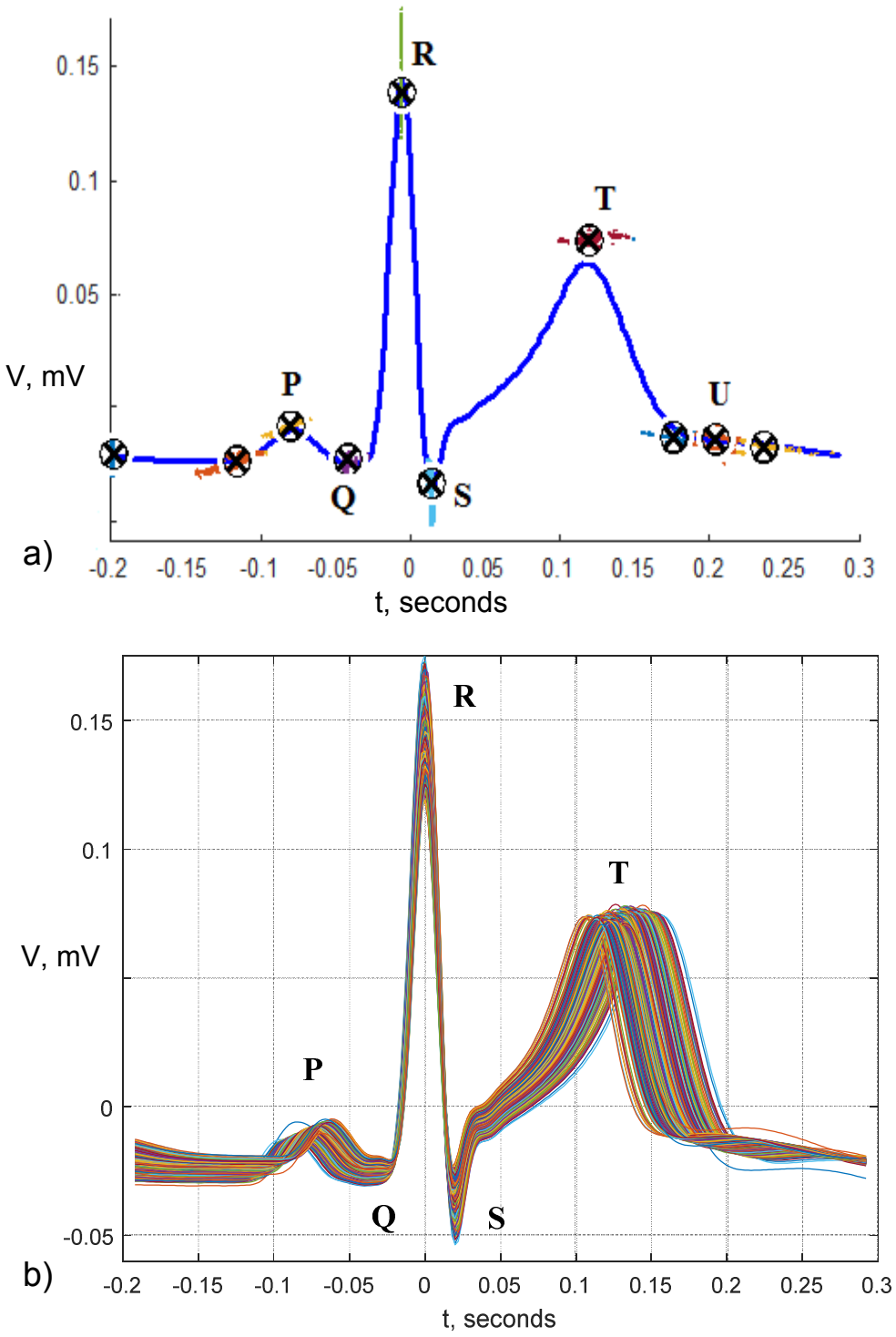

Fig. 3.2. a) ECG characteristic points; b) synchronization of all cardiocycles on R-wave to observe the changes in T wave apex time-location

The results of clustering are shown in Fig. 3.2. After clustering the coordinates of special (characteristic) points as a function of the “big-time” (beat-to-beat series) were obtained. These data were used for future investigation of T wave alternans.

T wave detection was achieved by finding the highest special point after R wave peak special point in a single beat. It was taken into account that the investigation of such aspect of TWA as beat-to-beat alternation in T wave timing requires the synchronization of all cardiocycles on R wave. In this case we can observe the changes in T wave apex time-location (Fig. 3.3, b).

Investigation of T wave alternans with a change in its amplitude and/or morphology involves the alignment of ensemble of T waves on their maximums (Fig. 3.3, a). In case of absence of repolarization alternans, amplitudes of the T waves in ECG signal represent a realization of one random variable (Fig. 3.4, a), which varies with certain dispersion with respect to the average value of the amplitude of T wave. In case of presence of repolarization alternans, amplitudes of the T waves in ECG signal are the realizations of two random variables that vary with given variances with respect to their mathematical expectations on the condition of alternation of these characteristics in consecutive cardiac cycles (Fig. 3.4, b). Here the dependence of the amplitude of the T wave from the number of the cardiac cycle has a sawtooth character (Fig. 3.3, b)

The scatter-plot method of TWA analysis involves graphical representation of the T wave amplitude (or another feature, for instance, the area under the curve of T wave) of each beat against its successor in coordinate plane. Area of the points obtained in this way is called scattergram (scatter-plot, Poincare or Lorenz plot).

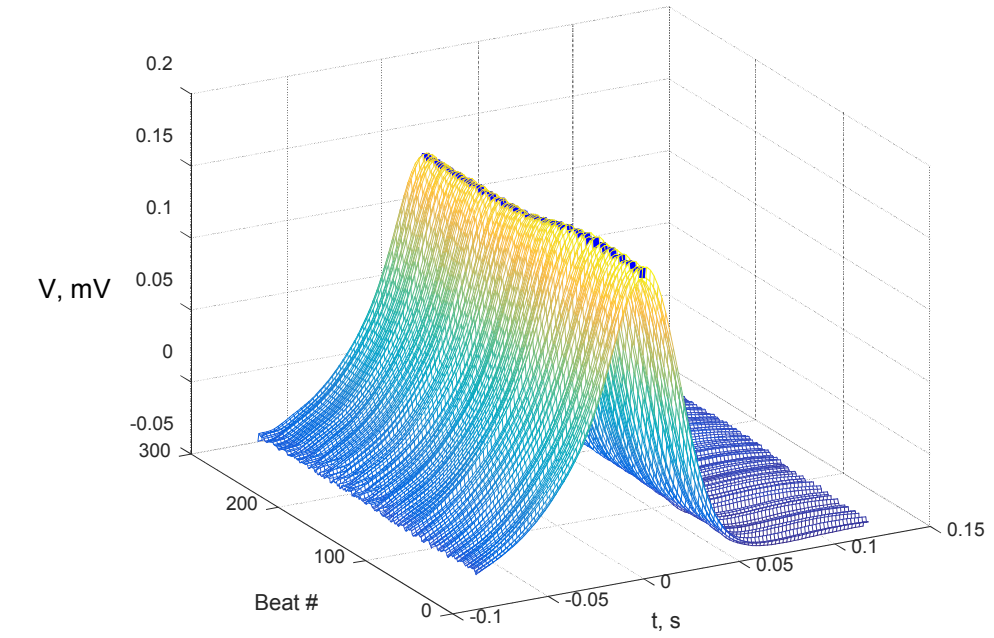

a)

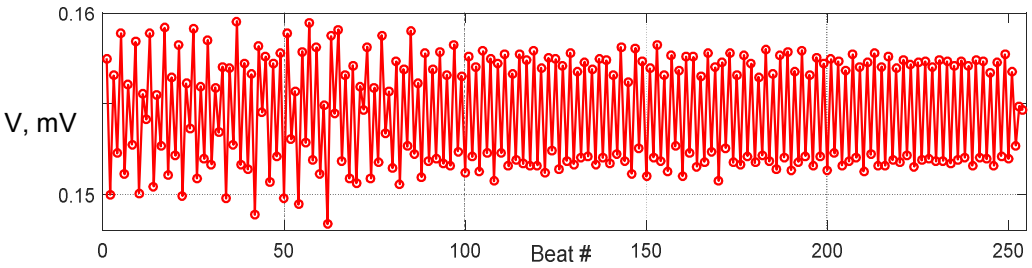

b)

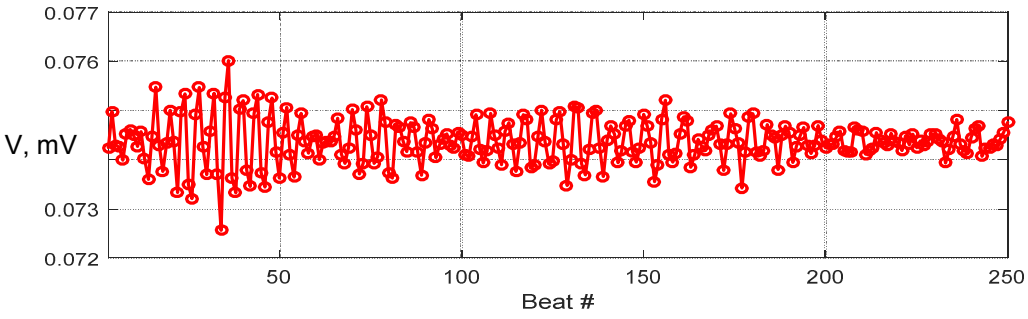

c)

Fig. 3.3: Synchronization of the ensemble of T waves according to their maximums (a); dependence of the amplitude of the T wave from the number of the cardiac cycle: presence of repolarization alternans (b) and absence of repolarization alternans (c)

Cluster analysis of scattergram can be used as for ABABAB pattern of alternans as for ABCABC pattern. Scattergram represents a set of points, the center of which is located on the bisector. The deviation of the point from the bisector to the left indicates, how much more is the T wave amplitude of *N*+1 beat comparing to the T wave amplitude for the previous beat (*N*); deviation of the point from the bisector to the right demonstrates, how much less is the T wave amplitude of *N*+1 beat comparing to the T wave amplitude of the previous beat (*N*).

Comparing scattergrams obtained for the cases of TWA presence and TWA absence, we can observe one cluster of points in case of TWA absence (Fig. 3.5, a) and the apparent separation of the set of points into two clusters corresponding to the amplitudes of T waves from even and odd ECG cardiocycles in the case of TWA presence of ABAB pattern (Fig. 3.5, b). Three clusters are observed in scattergram in case of alternans of ABCABC type.

The amplitude of T wave alternans is estimated by measuring the distance between the centers of two clusters, which were obtained in scattergram for even and odd cardiocycles. The cluster analysis of scattergram involves assessment of intercluster distance S_e, which is calculated between the centers of two clusters (Fig.3.5, b), and the average sum of squares of intracluster distances S_i, which were found for each of the clusters. The squared Euclidean distance measure is usually used for this purpose.

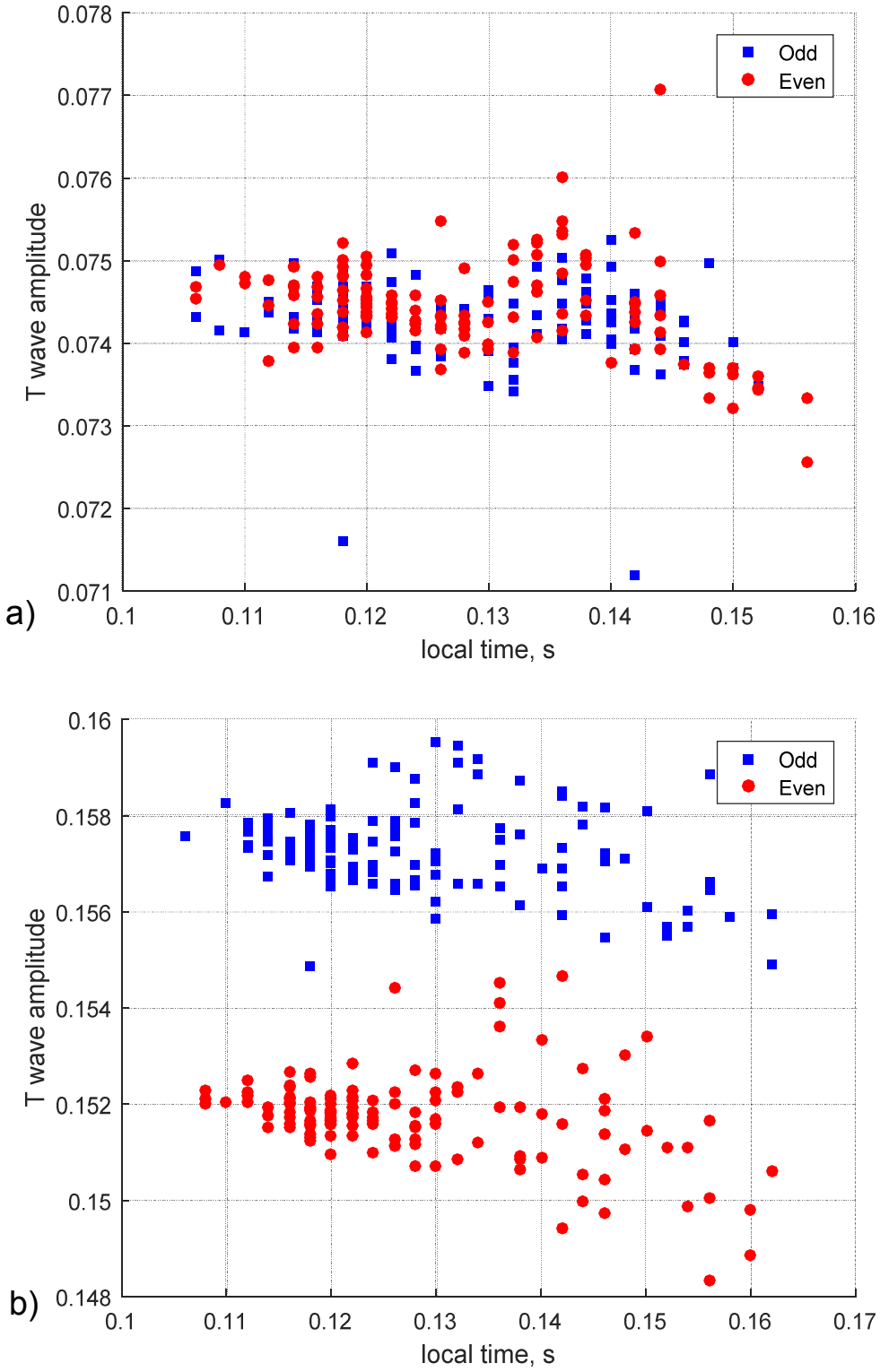

Fig. 3.4. Dependence of T wave amplitude on local time in case of synchronization of all cardiocycles on R wave: a) absence of repolarization alternans; b) presence of repolarization alternans

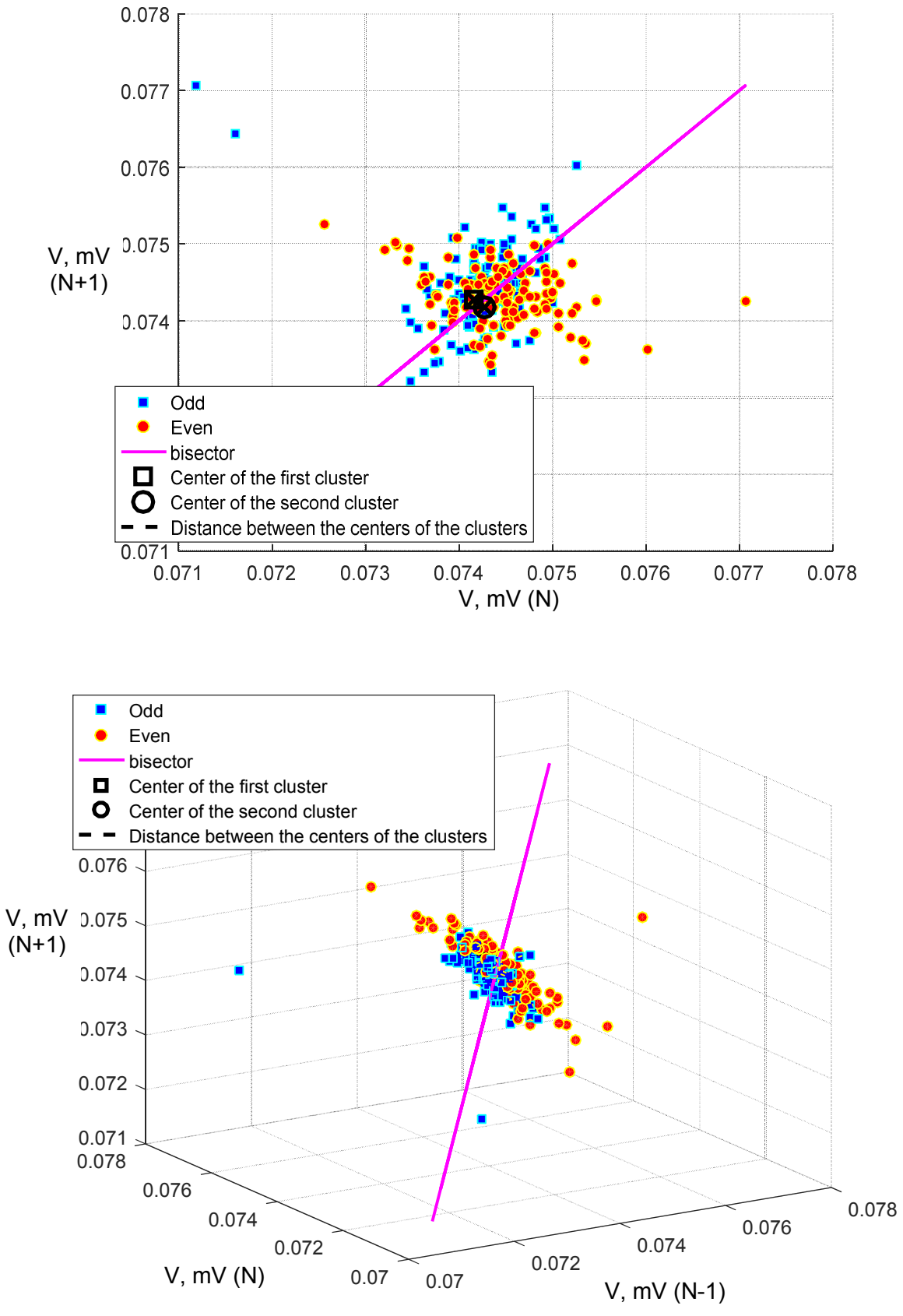
0.078
0.077
0.076
0.075
0.074
0.071
V, mV (N+1)
Odd
Even
bisector
Center of the first cluster
Center of the second cluster
Distance between the centers of the clusters
0.071
0.072
0.073
0.074
0.075
0.076
0.077
0.078
V, mV (N)
V, mV (N+1)
V, mV (N)
V, mV (N-1)
0.07

a)

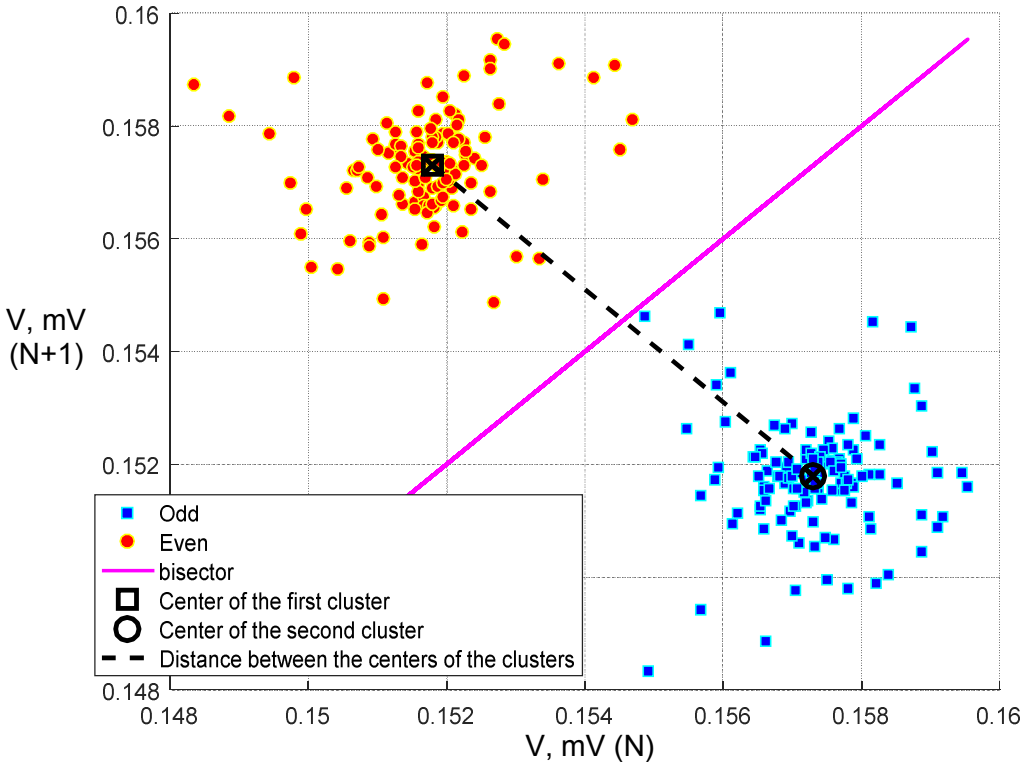

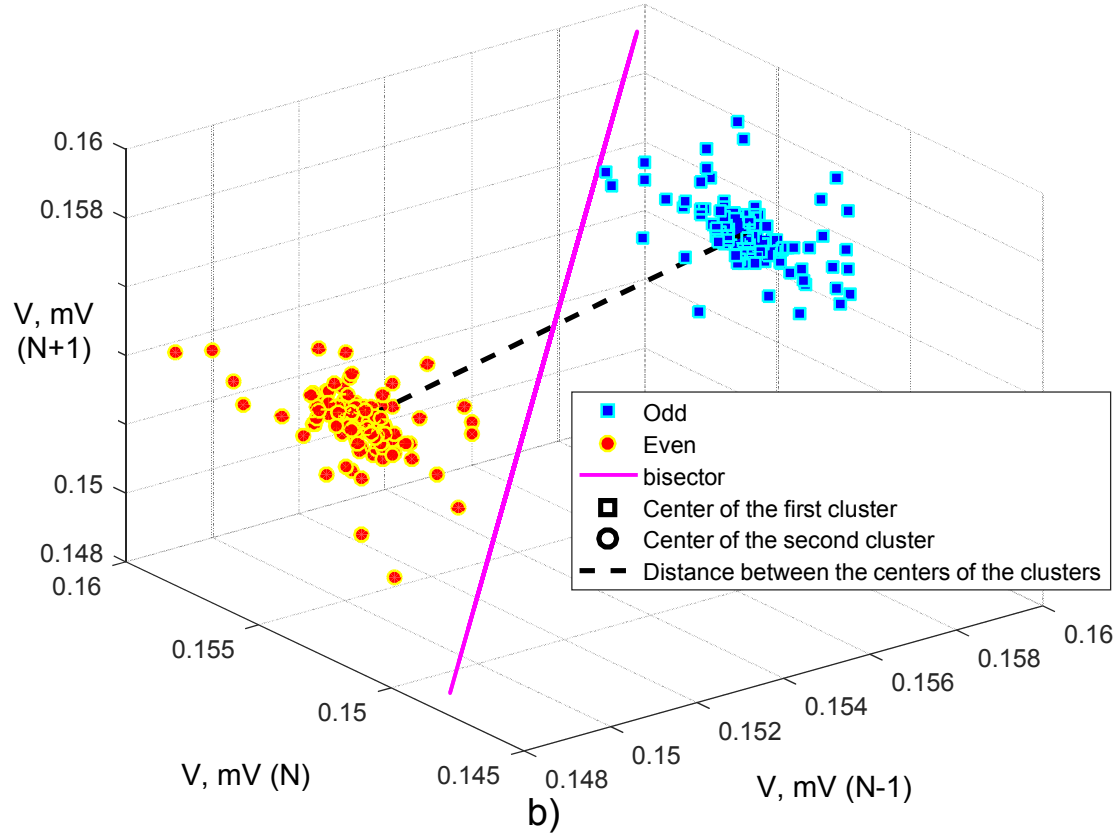

b)

Fig. 3.5. The cluster analysis of 2D and 3D scattergrams:

a) absence of repolarization alternans; b) presence of repolarization alternans

3.3. Detection of T wave alternans using spectral analysis

In order to detect TWA, the spectral analysis is also used, during which the average energy spectrum is calculated based on the averaging of the spectra obtained for the fluctuations of the values of all points of the T wave. The alternation of the T wave is detected on the power spectrum as a peak at the frequency of 0.5 cycle/beat, which is the frequency of the alternation (Fig. 3.6). TWA is characterized by two quantitative parameters: the amplitude of alternation and the coefficient of alternation *K*. Amplitude of alternation is defined as the square root of the difference between the meanings of power spectrum corresponding to the normalized frequency equal to 0.5 cycle/beat (that is the last value of the spectrum) and the mean value of the spectral noise. The coefficient *K* is defined as the ratio of the aforementioned difference to the mean standard deviation of the noise. It shows whether a peak of alternation is statistically significant at the noise level. For the calculation of mean standard deviation the area of spectral noise in the interval of 0.44-0.48 cycle/beat is taken. If $K>3$, the TWA test is considered to be positive.

The algorithm for detection of T wave alternans by means of Fourier transform yields acceptable results only when the amplitude of the T wave varies from beat to beat according to the sinusoidal law. Consequently, the algorithm based on spectral analysis, does not allow us to detect the alternation of the T wave at other frequencies than 0.5 cycle/beat, and also to detect TWA with possible changes in the phase of alternation of the T wave. This significantly reduces the area of practical application of the method. In addition, in order to ensure the robust operation of the algorithm, the signal must have a low noise level,

because spectral components may exceed the characteristic peak of alternation.

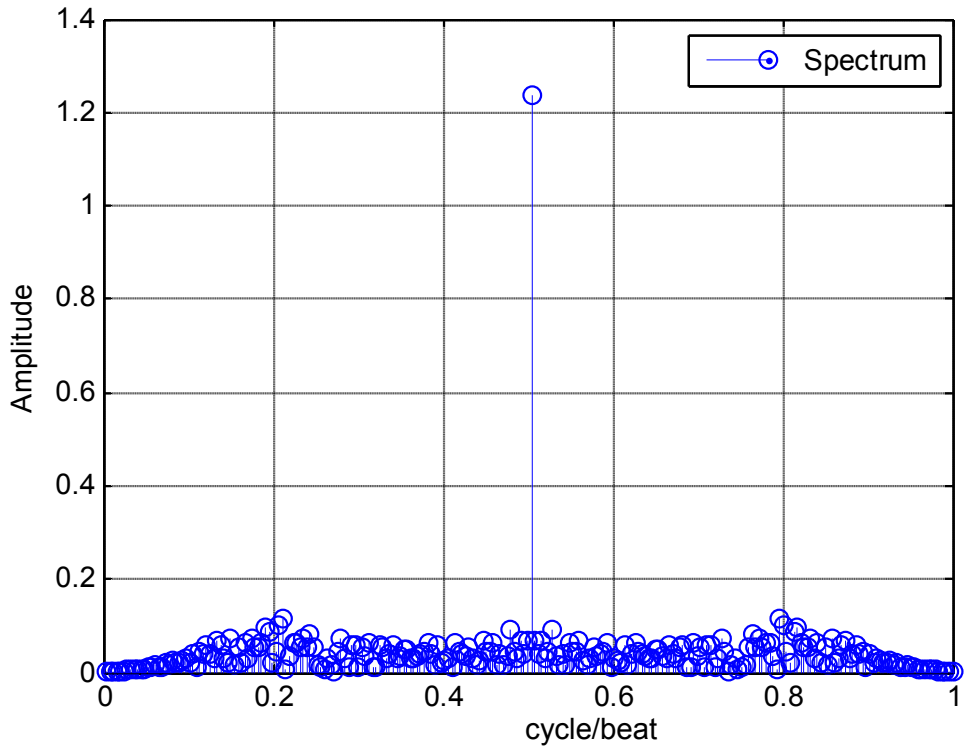

Fig. 3.6. Presence of TWA on the power spectrum

3.3. Identification and evaluation of T wave alternans using principal component analysis

The method of principal components analysis implies decorrelation of the ensemble of T waves through the data projection on the orthogonal axes of eigenvectors of the covariance matrix [7-11]. Error of T wave reconstruction in coordinate basis of principal eigenvectors depends on the number of eigenvectors, which are discarded during reconstruction. It is enough to take into account from 3 to 5 major eigenvectors and their eigenvalues for the analysis of T wave alternans.

The decomposition of the ensemble of T waves consists of calculating b_{ij} coefficients, which are the projections of the signal on the

eigenvectors (Fig. 3.7). Analysis of b_{ij} coefficients allows assessment of beat-to-beat changes in the amplitude and shape of T wave. Depending on the complexity of violations of repolarization in myocardial cells, beat-to-beat changes in the morphology of T wave may comprise as subtle variations of shape, as apparent modifications, including even change of T wave polarity. ABAB pattern of alternans corresponds to one form of T wave in even of cardiac cycles and to another form in odd cardiac cycles. In case of alternans, manifested as beat-to-beat changes in T wave morphology, the values of the coefficients b_{ij} form distinct clusters corresponding to even and odd cardiac cycles.

To reduce dimensionality of this representation we can preserve S main eigenvectors $V_1, V_2, \ldots, V_S$ (S‹‹N) corresponding to the most significant eigenvalues $\lambda_1, \lambda_2, \ldots, \lambda_S$. In general, the sufficient number of eigenvectors must be remained to reproduce T waves with a given accuracy; however, our experiments have shown that using of 3-5 eigenvectors is quite effective to restore original T waves (Fig. 3.8) [10-11].

For ECG signals with the absence of T wave alternans the presence of one cluster of points formed by the values of the coefficients b_1-b_3 of eigenvectors $\mathbf{V}_1$-$\mathbf{V}_3$ is observed (Fig. 3.9, a). For ECG signals with T wave alternans the presence of two clusters in the space of features can be seen (Fig. 3.9, b). These clusters of points correspond to odd and even cardiac cycles. That means that there are two main (base) shapes, around which the shape of T waves fluctuates in odd and even cardiac cycles. These basic shapes of T wave for even and odd cardiocycles are calculated using the coefficient values of the respective centers of the clusters (Fig. 3.10) by obtaining a linear combination of the vectors $\mathbf{V}_1$-$\mathbf{V}_3$ multiplied by the coefficients b_1-b_3.

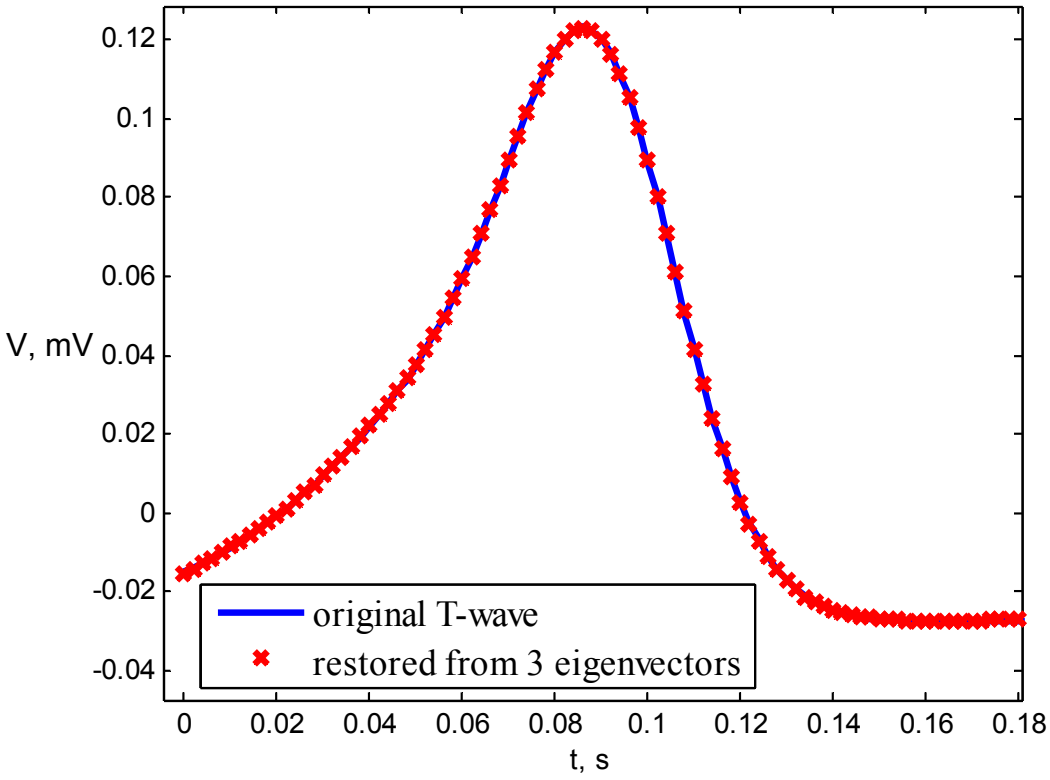

Fig. 3.7. Original T wave and restored from the first 3 eigenvectors.

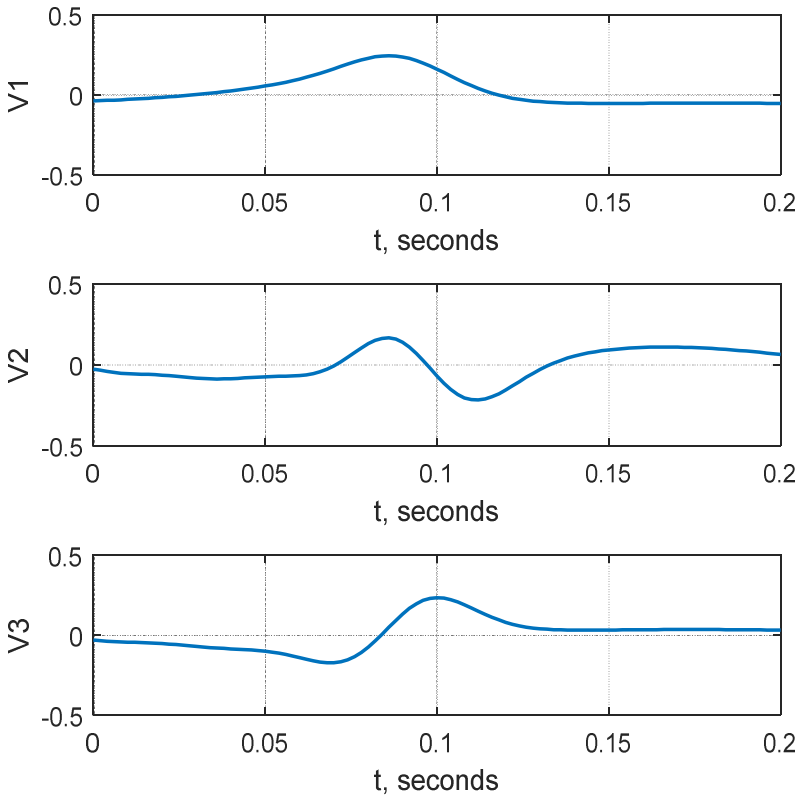

a)

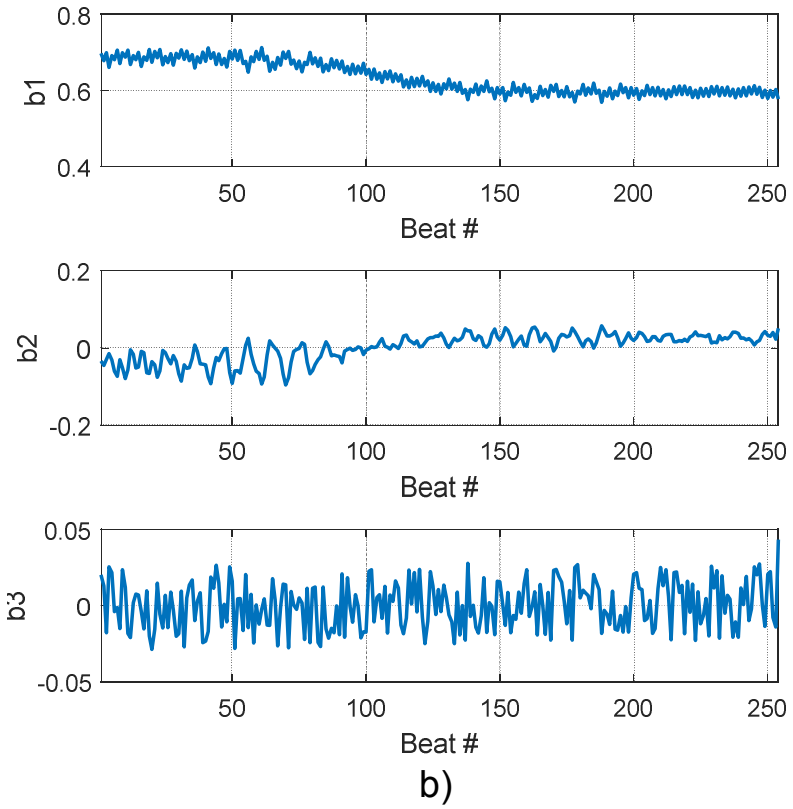

Fig. 3.8. The first 3 eigenvectors $\mathbf{V}_1$-$\mathbf{V}_3$ (a) and their coefficients b_1-b_3 (b) for ensemble of T waves

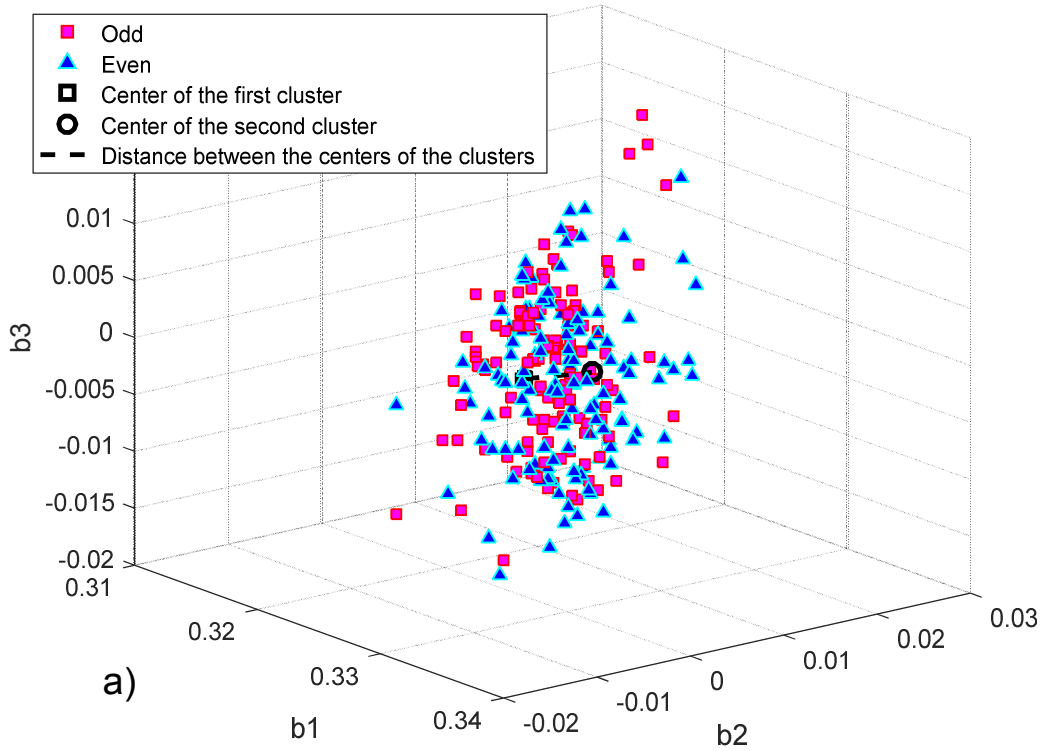

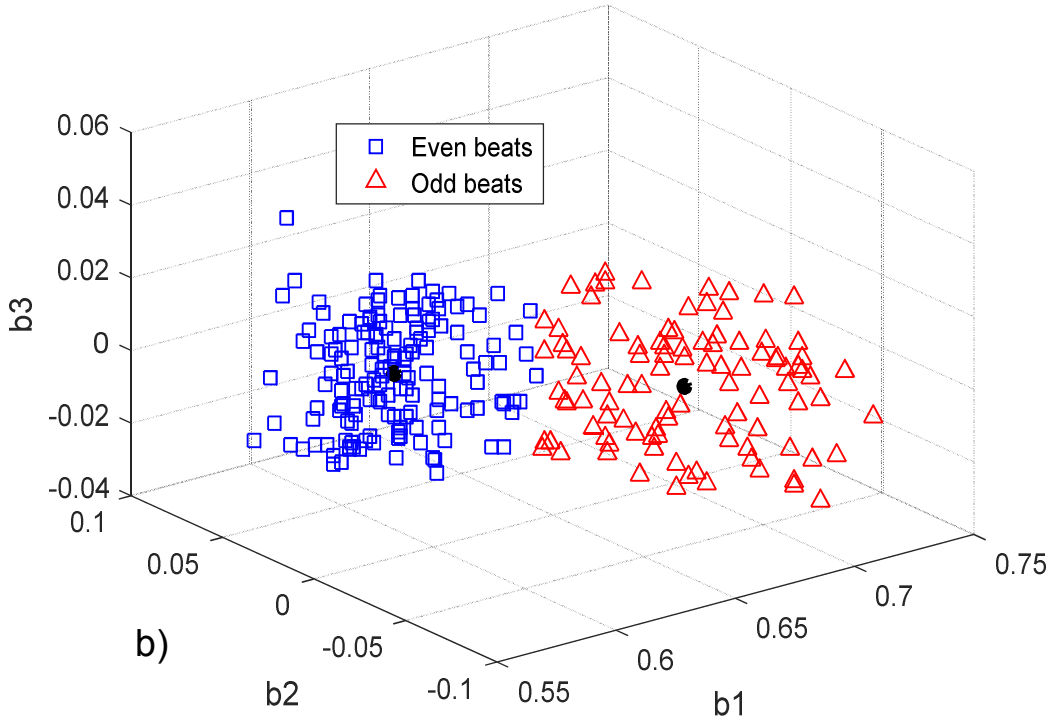

Fig. 3.9. Coefficients b_1-b_3 for odd and even cardiocycles: a) absence of T wave alternans; b) presence of T wave alternans

As a quantitative characteristic for ALP presence identification, the sum of the squares of b_{ij} coefficients, which correspond to the centers of the clusters for even and odd cardiocycles, is proposed to use. Suppose that $C_{odd}(b_{odd1}, b_{odd\ 2},...,b_{oddS})$ and $C_{even}(b_{even\ 1}, b_{even\ 2},...,b_{evenS})$ are the centers of the clusters for even and odd cardiocycles, then

$$H_{odd} = \sum_{i=1}^{S}(b_{odd})_i^2, \quad H_{even} = \sum_{i=1}^{S}(b_{even})_i^2,$$

where S is the selected number coefficients b_i, which correspond to the principal eigenvectors $\mathbf{V}_i$. Significant differences between the values of the parameters, obtained by decomposition in the basis of eigenvectors for T waves from even and odd cardiocycles, indicate the presence of TWA.

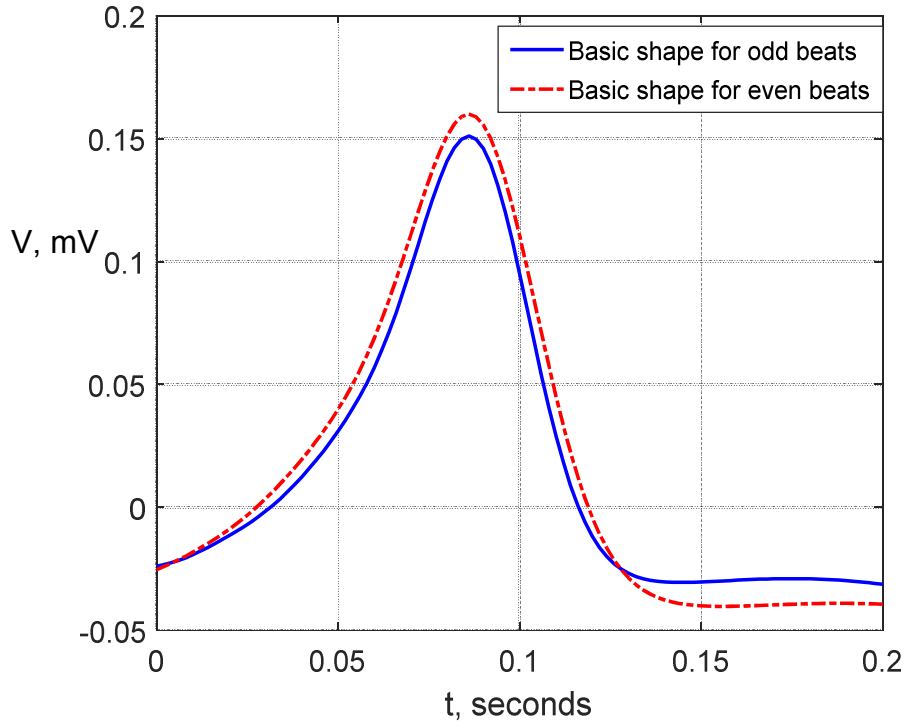

Fig. 3.10. The basic shapes of T wave in even and odd cardiac cycles in the presence of micro-TWA

Analyzing the features of T wave alternans identification by analysis in time domain, cluster analysis of the Lorentz scattergrams and principal component analysis, it should be noted that, since the phenomenon of TWA may relate to changes in the amplitude, shape, and time, it is reasonable to use several different approaches for a comprehensive study of this process. For example, the analysis of TWA in the time domain or by using Lorentz scattergrams reveals the alternans of T wave amplitude, but does not provide information about changing of its morphology. Investigations have shown that the PCA method in addition to the identification of alternans in the amplitude of T wave, can also reveal beat-to-beat variability of its shape.

CONCLUSIONS

The combined methods for the analysis of low-amplitude components of electrocardiogram, based on the creation of eigensubspaces of signals and noise by decomposition in the basis of eigenvectors, principal component analysis, and wavelet analysis, are developed. The proposed techniques allow extraction of low amplitude components, which are markers of cardiac electrical instability, from the noisy ECG.

Identification of markers of cardiac electrical instability may be based on the use of a broad class of algorithms - from the conventional analysis in time and frequency domains to the complex procedures of pattern recognition. However, at this stage wide application of many approaches to the analysis of markers of cardiac electrical instability is limited in clinical practice, due to the ambiguity of medical interpretation, and demands additional clinical studies. Thus, the directions for further research are improvement of theory-based methods and algorithms for detection of low-amplitude components of ECG for early prediction of potentially dangerous arrhythmias and arrangement of wide clinical tests.

CONTROL QUESTIONS AND TASKS

1. Explain the reasons of T wave alternans phenomenon.
2. Explain, how to assess the level of T wave alternans by the scattergram method.
3. What is the idea of using spectral analysis for T wave alternans estimation?
4. How T wave alternans can be evaluated by using principal component analysis?

REFERENCES

[1] Narayan S. M. T-Wave Alternans and the Susceptibility to Ventricular Arrhythmias. Journal of the American College of Cardiology, vol. 47, No. 2, 2006.

[2] Mariah L. Walker, David S. Rosenbaum. Repolarization alternans: implications for the mechanism and prevention of sudden cardiac death. Cardiovascular Research, vol. 57, pp.599–614, 2003.

[3] M. Walker, "Repolarization alternans: Implications for the mechanism and prevention of sudden cardiac death," Cardiovascular Research, vol. 57, no. 3, pp. 599–614, Mar. 2003.

[4] PhysioNet. T-Wave Alternans Challenge Database. http://physionet.org/pn3/twadb

[5] A. L. Goldberger et al., "PhysioBank, PhysioToolkit, and PhysioNet: Components of a new research resource for complex physiologic signals," Circulation, vol. 101, no. 23, pp. 215–220, Jun. 2000.

[6] Moody G.B., "The PhysioNet / Computers in Cardiology Challenge 2008: T Wave Alternans," Computers in Cardiology, 2008, vol. 35, pp. 505–508.

[7] Xue J.Q., Rowlandson G.I. Effect of noise on frequency and time domain methods of T wave alternans. Computers in Cardiology, pp. 449 – 452, 2004.

[8] Simoliuniene R., Krisciukaitis A., Macas A., et al. Principal Component Analysis Based Method for Detection and Evaluation of ECG T-Wave Alternans. Computers in Cardiology, vol.35, pp.521-524, 2008.

[9] Bortolan G., Christov I. T-wave alternans detection by a combined method of principal component analysis and T-wave amplitude. Physiological Measurement, vol.33 , pp.333–343, 2012.

[10] Karplyuk Y., Ivanko K., Ivanushkina N., "Peculiarities of T Wave Alternans Detection and Evaluation". Proceedings of 2015 IEEE 35th International Scientific Conference on ELECTRONICS AND NANOTECHNOLOGY (ELNANO) (Kyiv, Ukraine), April 21-24, 2015, pp. 356-361, 2015.

[11] Ivanko K. O. Identification and assessment of electrocardiographic markers of cardiac electrical instability / K. O. Ivanko, N. G. Ivanushkina, Y. S. Karplyuk // Science news of National Technical University of Ukraine "Kyiv Polytechnic Institute". - 2017. - № 1. - P. 37-47. - http://nbuv.gov.ua/UJRN/NVKPI_2017_1_6

SECTION 4

ATRIAL ELECTRICAL ACTIVITY EXTRACTION FOR ATRIAL FIBRILLATION ASSESSMENT

Development of computerized diagnostic systems in cardiology makes it possible to analyze electrocardiographic signals on qualitatively higher level for non-invasive diagnosis of cardiac pathologies. Actuality of the design of algorithms for atrial electrical activity extraction from ECG and its evaluation in isolation from ventricular component is determined by considerable distribution of cardiac arrhythmias, especially atrial fibrillation (AF). Atrial fibrillation is the most common heart rhythm disturbance, which is characterized by uncoordinated atrial electrical activity. Atrial fibrillation manifests itself on the electrocardiogram (ECG) as an absence of P waves, and the presence of numerous chaotic f waves, which vary in amplitude, frequency, shape and timing (Fig. 4.1). QRS complexes in AF often have no morphological changes, but the ventricular response in AF is usually irregular, consequently the duration of RR intervals varies greatly.

The relevance of the study of atrial fibrillation is conditioned by the wide range of its negative consequences which related not only to a significant deterioration in the quality of life, but also a significant increase in the frequency of serious complications and death.

Extraction and analysis of atrial electrical activity is important in the diagnosis of atrial fibrillation. It is not difficult for an experienced cardiologist to determine the presence of atrial fibrillation on the ECG. However, without advanced computerized analysis of the digital ECG the frequency of atrial activity can not be estimated. The separation of atrial and ventricular activity is quite complicated due to the considerable

difference in amplitudes of the signals. On the surface ECG manifestation of ventricular electrical activity is several times higher in amplitude compared to the atrial activity. Furthermore, low-amplitude atrial electrical activity is distorted by noise and interferences occurring in ECG signals: muscular activity, power line interference, noise of electrodes, motion artifacts, baseline drift caused by breathing, noise of electronic equipment. Atrial and ventricular signals separation by means of frequency filtering is not possible because their spectral ranges overlap.

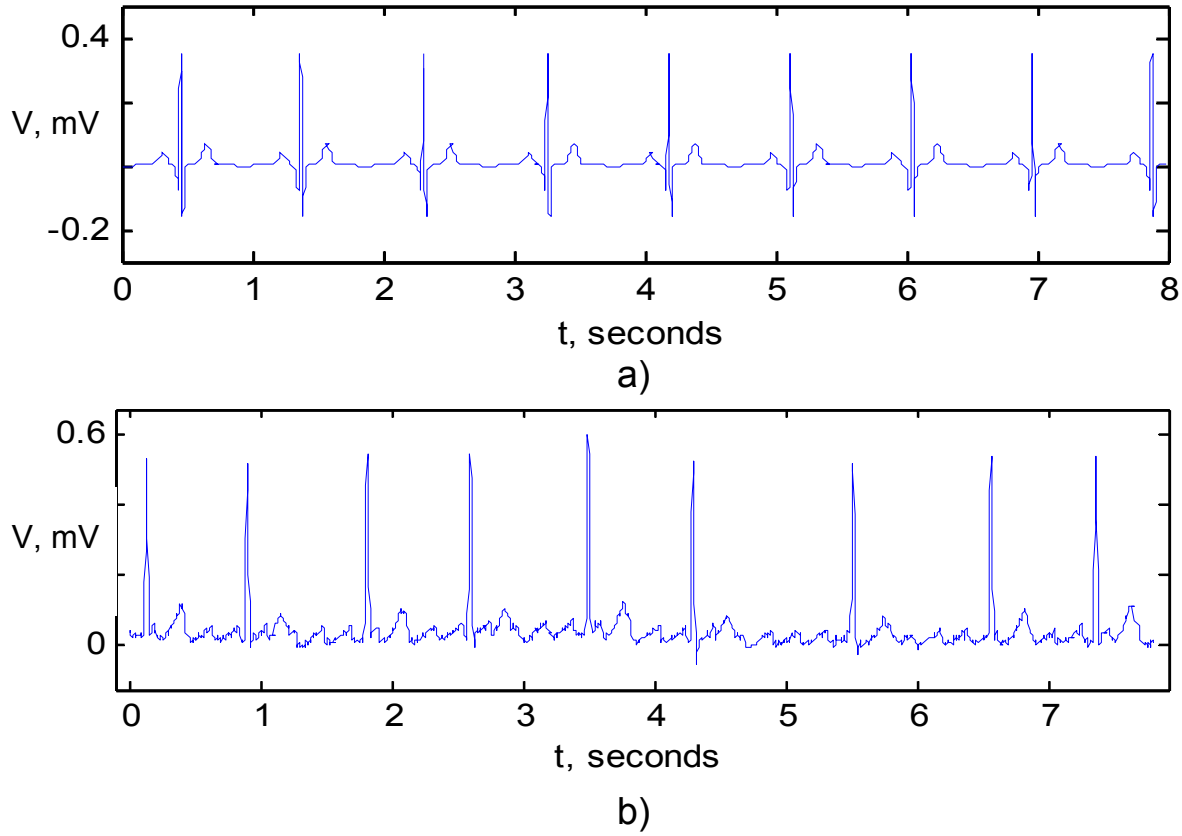

Fig. 4.1. Normal sinus rhythm (a) and atrial fibrillation (b)

4.1. Method of Blind Source Separation for Atrial Activity Extraction

To solve the problem of separation of atrial and ventricular electrical activities in surface ECG signal the method of blind source separation (BSS) was applied. BSS is the algebraic division of the signals from multiple sources that occur as a mixture of signals. The process is called "blind" because very little is known about the nature of the sources to be divided, the properties of the signals and conditions of their mixing. Minimum available information usually consists of the assumptions of statistical independence of the source signals and consistency of coefficients of the mixing matrix in the interval of observation. Independent components analysis (ICA) is a method that implements the idea of blind source separation [1-7].

ICA separation process is based on the assumption of the difference between the statistical characteristics of source signals which have non-Gaussian distribution law and their statistical independence. Separating atrial and ventricular activity by blind source separation we assume that: 1) atrial and ventricular activities are the products of independent sources of bioelectric activity; 2) signals of atrial and ventricular activities have non-Gaussian distribution laws.

For any moment of time vector of ECG's sources can be defined as $s(t) = [s_1(t), s_2(t), ..., s_q(t)]$, where $s_i(t)$, $i = 1, 2, ..., q$ are the ECG sources. Monitoring of ECG signals is conducted by measuring the potential difference between pairs of electrodes placed on the surface of the body. For such *p* couples (*p* ECG leads) a vector of observations can be defined as $x(t) = [x_1(t), x_2(t), ..., x_p(t)]$. For low-frequency ECG signals the body is completely linear and conducting medium with almost infinite

speed of electrical signals propagation. As a result, fluctuations observed in each point of the body surface can be represented as a linear combination of signals from the different sources and additive noise:

$$\begin{aligned} x_1(t) &= m_{11}s_1(t) + m_{12}s_2(t) + ... + m_{1q}s_q(t) + n_1(t); \\ x_2(t) &= m_{21}s_1(t) + m_{22}s_2(t) + ... + m_{2q}s_q(t) + n_2(t); \\ &\vdots \\ x_p(t) &= m_{p1}s_1(t) + m_{p2}s_2(t) + ... + m_{pq}s_q(t) + n_p(t) \end{aligned}$$

or in the matrix form:

$$X(t) = MS(t) + N(t),$$

where $X(t)$ is the vector of observations; M is the mixing matrix that contains the coefficients m_{ij}, which determine including of each source to the vector of observations; $N(t)$ represents the noise components.

The coefficients of the mixing matrix are not determined beforehand as a model of signal propagation from the sources to the receivers is unknown. Shapes of the signals from separately taken sources $s_i(t)$ are also unknown, because they can not be observed directly and are available to us only as a mixture. Assume that the signals from the sources are statistically independent owing to physical independence of bioelectric phenomena that determine them. For the same considerations the noise components $n_j(t)$ can also be regarded as statistically independent in different channels and independent from the source. The separation of individual signals $s_i(t)$ from a mix of the signals from different sources consists in determining the separation matrix W with of the coefficients w_{ij}:

$$
\begin{aligned}
s_1(t) &= w_{11}x_1(t) + w_{12}x_2(t) + \ldots + w_{1p}x_p(t);\\
s_2(t) &= w_{21}x_1(t) + w_{22}x_2(t) + \ldots + w_{2p}x_p(t);\\
&\vdots\\
s_q(t) &= w_{q1}x_1(t) + w_{q2}x_2(t) + \ldots + w_{qp}x_p(t).
\end{aligned}
$$

The separation matrix *W* is the inverse matrix to the mixing matrix *M*. Thus, the problem of atrial and ventricular activities separation is formulated as follows: for registered multichannel ECG measurements it is necessary to determine the mixing matrix and the signals from the different sources [1-7].

Processing of the multichannel ECG signal by means of ICA approach aims of using the information about atrial electrical activity presented in all recorded ECG leads. In general, the number of independent components obtained by ICA is equal to the amount of registered ECG leads. If the estimated number of sources $s_i(t)$ is less than the number of observations $x(t)$, then we receive "extra" components. Otherwise, if the number of sources is larger than the number of observations, then obtained independent components contain the signals from several sources, which makes it difficult to interpret the results. BSS allows us to reconstruct atrial contribution to the ECG signal in various leads regardless of high-amplitude ventricular activity.

The assumption that the signals of atrial and ventricular activities have non-Gaussian distribution law, can be used for their separation through the use of statistical indicators of higher orders than the second. For identification of the atrial electrical activity source among all the sources obtained by ICA the coefficients of skewness and kurtosis as well as spectral analysis were applied.

The central moment of the third order is used to measure the asymmetry of distribution. Dimensionless characteristic of asymmetry

degree of distribution curve concerning of mathematical expectation E(*X*) is coefficient of skewness:

$$Sk(X) = \sum_{j=1}^{n} p_j \left(\frac{x_j - \mathrm{E}(X)}{\sigma(X)} \right)^3 .$$

If *Sk*(X) = 0, then probability density function for the random variable *X* is symmetric regarding to mathematical expectation E(*X*). If the probability distribution is asymmetric and its long part ("tail") is located on the right of mode of a random variable Mo(*X*) (a right-bevel), then the weighted sum of the cubes of positive deviations from E(*X*) is greater than the sum of the cubes of negative deviations and *Sk*(X)>0. Similarly, *Sk*(X)<0 when the density function has left-sided bevel and long "tail" of distribution appears on the left.

The fourth central moment determines how acute the top of curve distribution is. This property is characterized by a dimensionless quantity ─ kurtosis coefficient:

$$Kurt(X) = \sum_{j=1}^{n} p_j \left(\frac{x_j - \mathrm{E}(X)}{\sigma(X)} \right)^4 - 3 .$$

Kurtosis characterizes the slope or in other words the rapidity of increasing of distribution curve compared to the normal curve. The higher the kurtosis, the more acute is the top of probability density function for a random variable. This property of kurtosis coefficient indicates a higher concentration of random variable values in the vicinity of its mathematical expectation. The lower value of the kurtosis corresponds to the more smoothed (less acute) peak of probability density function of random variable.

ECG signals are predominantly non-Gaussian due to the high values of amplitude in the area of QRS complex and the low values in other parts of cardiac cycle. Atrial fibrillation appears on the ECG as the replacement of coordinated P waves by rapid fluctuations which vary in size and shape. For independent component, which corresponds to the separated atrial electrical activity, skewness and kurtosis coefficients are much lower comparing to the independent components that include ventricular activity. This is explained by the presence of more random components in the atrial signal in AF. Thus, in AF atrial independent component has distribution law which is more similar to the normal distribution.

Fig. 5.3 shows an example of the separation of atrial activity from the real 12-lead ECG recording (Fig. 5.2) provided by The PhysioNet resource (St.-Petersburg Institute of Cardiological Technics 12-lead Arrhythmia Database [8-9]). The recording was acquired with 257 Hz sampling rate. Dimension reduction is carried out by Principal component analysis (PCA) prior to ICA and 8 independent components were obtained in result of ICA separation process (Fig. 5.3, a). The 6th independent component contains the isolated atrial activity in AF. For this source of chaotic atrial activity skewness and kurtosis coefficients are the lowest comparing to the other sources (Fig. 5.3, b).

It should be noted that for AA identification it is not enough just to reorder the sources from lower to higher kurtosis and skewness. Spectral analysis should be applied additionally to determine AA source. Atrial fibrillation manifests itself in the frequency spectrum as a well-defined single peak in a frequency range of 3-15 Hz. This maximum peak of the power spectrum of the atrial signal is the dominant fibrillation frequency, which reflects the average refractory period of the atria. For instance,

frequency of the power spectral density peak of the separated atrial source from Fig. 5.3 a, a is 4,67 Hz. In addition, in visual inspection the extracted atrial signal resembles the fibrillatory waves, which are visible in some of the initial ECG leads.

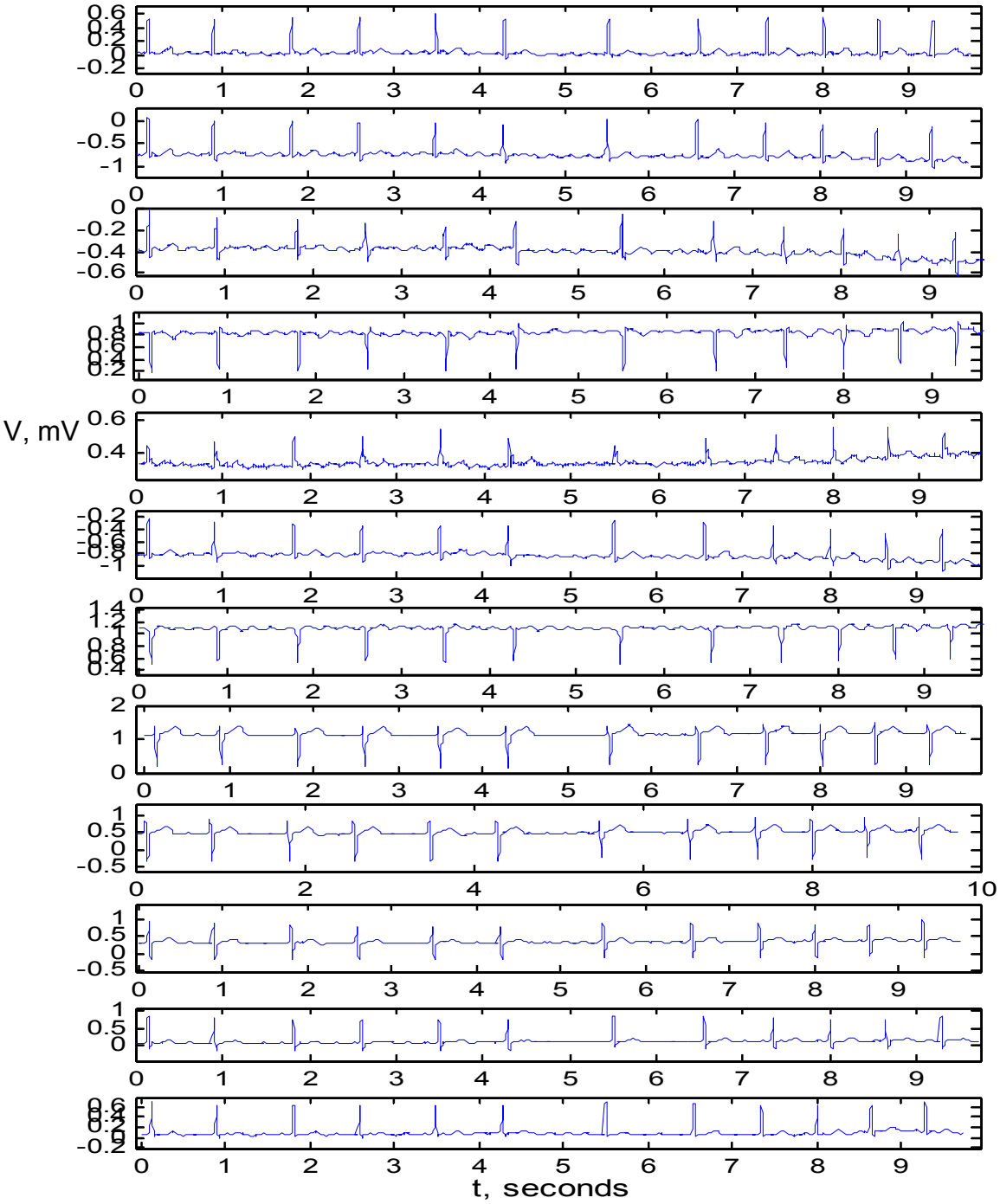

Fig. 5.2. 12-lead ECG with signs of atrial fibrillation, used as input for ICA

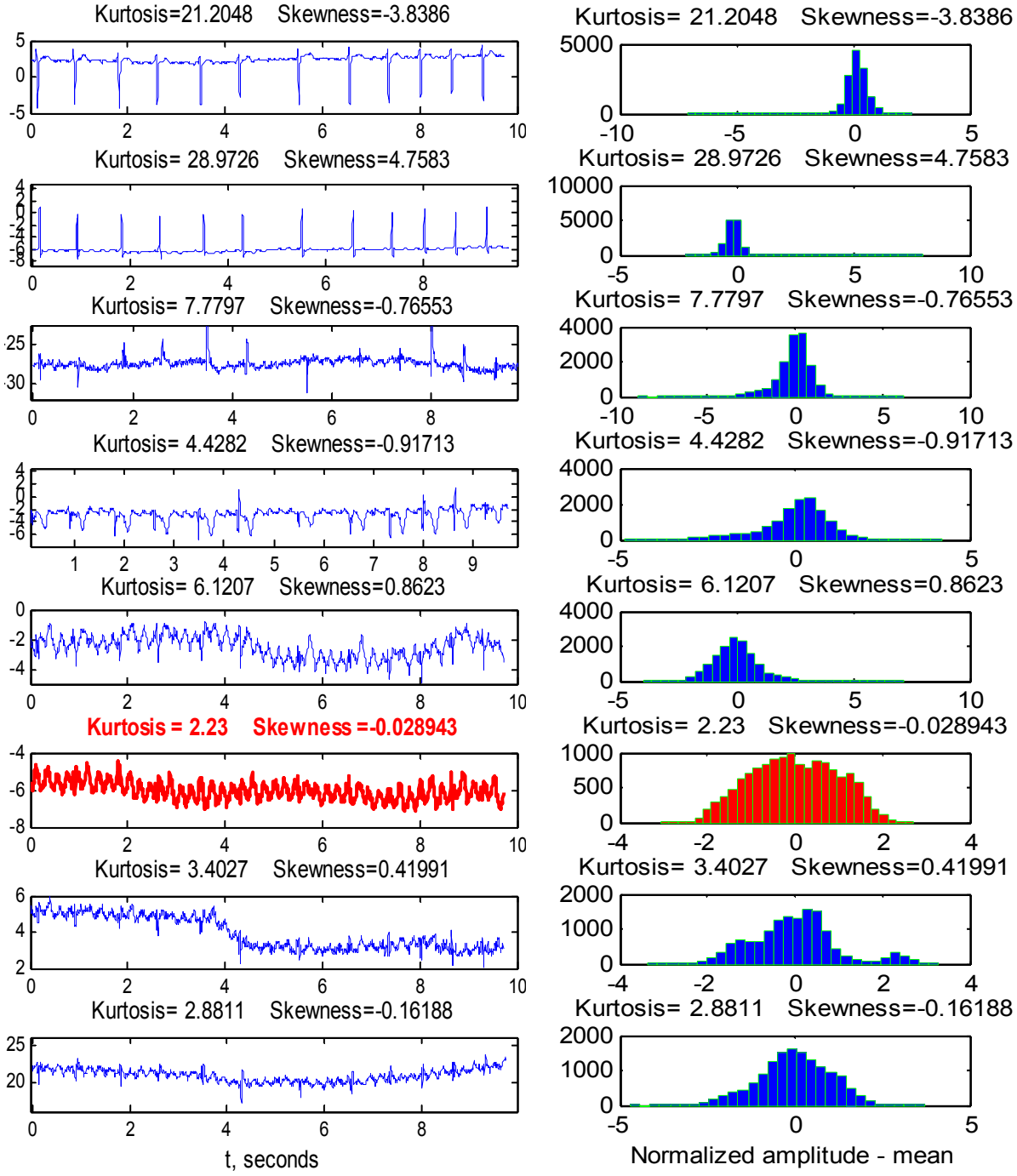

a) b)

Fig. 5.3. (a) 8 estimated sources obtained by means of ICA. Separated atrial electrical activity corresponds to the source #6. (b) Histograms of the separated sources.

Algorithm of atrial electrical activity revealing for the analysis and prediction of AF episodes termination is presented in Fig. 5.4.

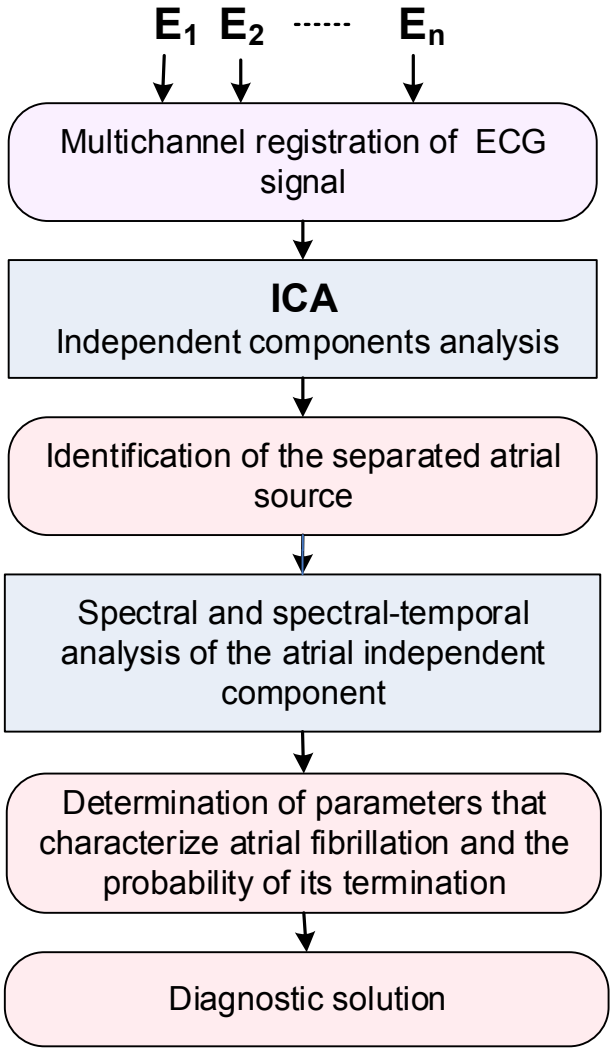

Fig. 5.4. Algorithm of atrial electrical activity extraction for the analysis and prediction of the termination of AF episodes

4.2. Average Beat Subtraction Approach

In the study conducted on the variety of signals ICA applied to AF analysis has shown good performance. As it was mentioned above, sources of atrial and ventricular electrical activities can be separated by

means of BSS algorithms (PCA or ICA) only for multilead ECG recordings. But there are many cases when registration of a multichannel ECG is not possible. ECG recordings with a limited number of channels are usually acquired by medical devices, which are intended for use in intensive care units, surgical wards, in the provision of emergency care in a hospital or during transport of patients. In ECG recordings registered by wearable devices as Holter monitor also only few leads are available, which is not enough for BSS algorithms employment because their performance deteriorates significantly for a small amount of leads. Another type of methods, used for atrial activity extraction, is Average Beat Subtraction (ABS) methods. The approach relies on detection of QRST complexes, their classification and the subtraction from the investigated ECG signal of the average beat of the class to which the current beat belongs. This technique provides a signal of atrial electrical activity for each separately taken ECG lead.

ECG signal preprocessing stage contains baseline drift removal and high-frequency noise suppression. Elimination of baseline fluctuations was based on multiresolution wavelet decomposition of the raw ECG recordings up to the 12^{th} level using symmetric wavelet of the 5^{th} order. The 12^{th} level approximation and the details of 9-12 decomposition levels were removed from the raw ECG as they reflect slow variations of the signal. To suppress high-frequency noises, the spectrum of the detrended data was limited up to 40 Hz using FIR Window Lowpass filter. QRST detection is the fundamental step in ABS approach. QRST detection was performed in the time domain with derivative-based threshold algorithm applied to the specially formed reference signal which was obtained by nonlinear conversion of the ECG signal with its first derivative. The selected algorithm is reliable and accurate for QRST

detection in noisy ECGs with artifacts. The detection point of each QRST complex is the peak of its R wave. The peaks of R waves are located at the local maximums of ECG signal. Before classification the beats were synchronized with respect to R wave peak. QRST morphology clustering was performed for each single lead by minimizing the sum, over all clusters, of the within-cluster sums of point-to-cluster-centroid distances. As a measure of the distance the sum of absolute differences, i.e., the *L*1 distance was used. From each QRST complex the appropriate template (estimated centroid of the corresponding class) was subtracted after alignment. Fig. 5.5 shows QRST templates obtained for VI and aVF leads of the signal depicted in Fig. 5.2.

It should be noted that the number of classes and templates for morphological clustering of QRST complexes is unknown beforehand and selected empirically depending on the signal. If necessary, the number of classes and templates should be redefined. After ventricular activity cancellation the residual signal containing the atrial activity was obtained. It is necessary to note the following disadvantages of the method we have encountered in its implementation. In presence of ectopic beats or artifacts of electrodes motion, the considerable amount of residual QRST complexes remains in the atrial signal. Moreover, if the class consists of only a single representative (for example, unusual for QRST complex splash caused by motion artifact), then after subtraction from this cardiac cycle of a template of the class, an area with zero amplitude occurs in residual atrial signal.

In Fig. 5.6 (a) segment of the ECG signal acquired from the I lead (a), the atrial activity source extracted from 12-lead ECG by means of ICA (b) and the atrial signal obtained by QRST cancellation in average beat subtraction method (c), are compared. Even in visual analysis it is

obvious that atrial activity extracted by ICA method resembles greatly atrial f waves from initial ECG lead. Atrial signal obtained by average beat subtraction method demonstrates the presence of some distortions and residual artifacts which arise from QRST cancellation. The apparent differences in the shape of the atrial signals (b) and (c) can be explained by different approaches to their receiving. While the average beat subtraction method extracts the atrial activity from a single ECG lead, ICA method recovers a global atrial signal with contributions from all leads.

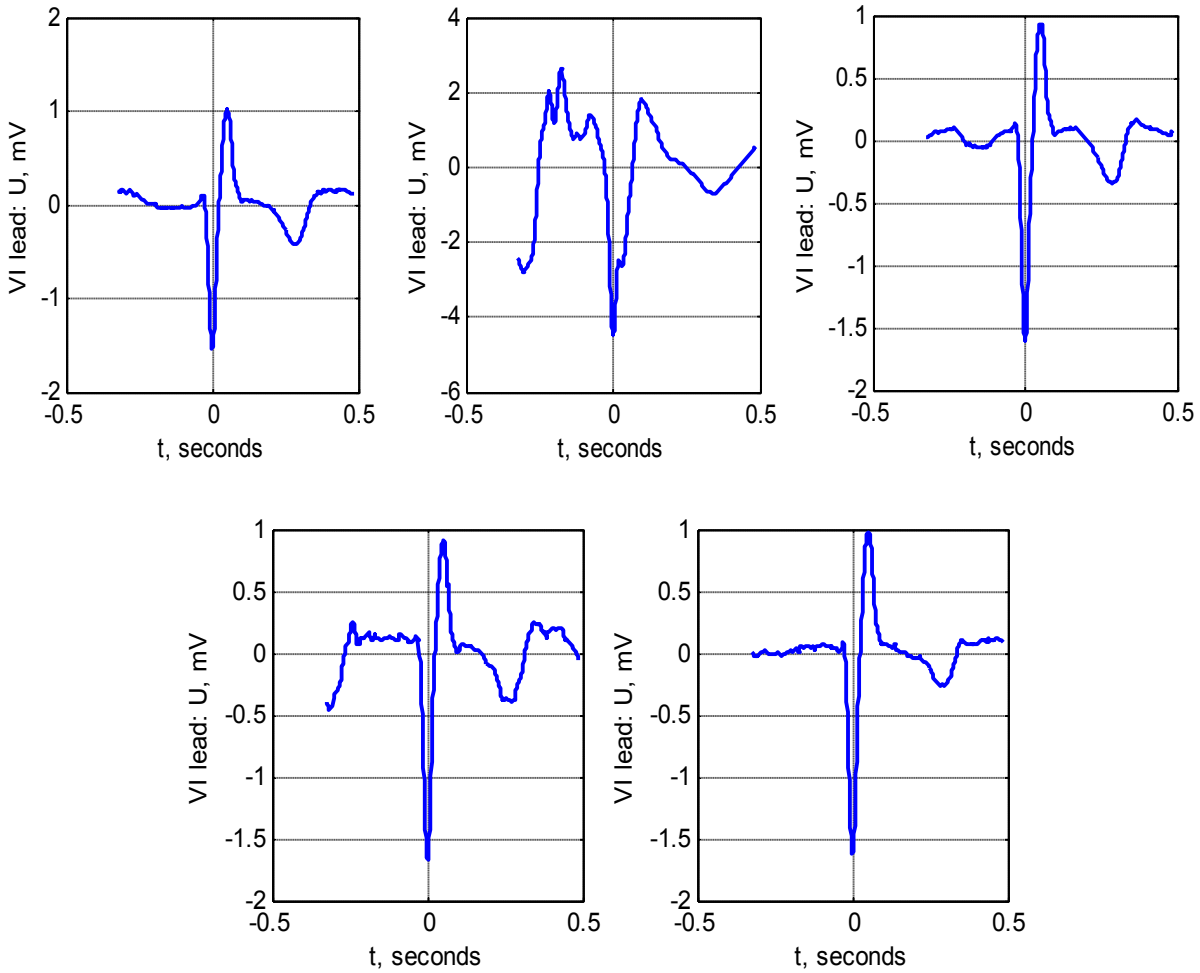

a)

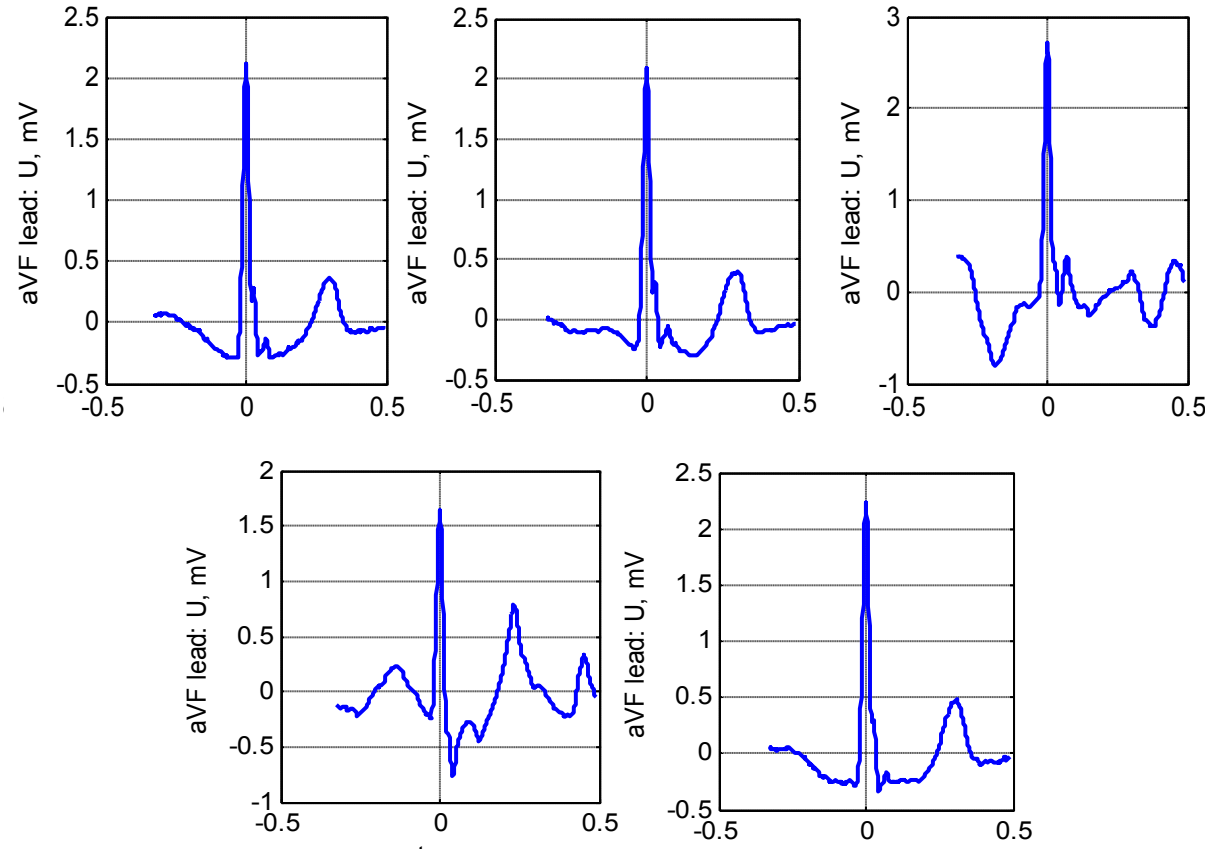

b)

Fig. 5.5. Representative beats for QRST morphology clustering: (a) estimated class centroids for VI lead; (b) estimated class centroids for aVF lead

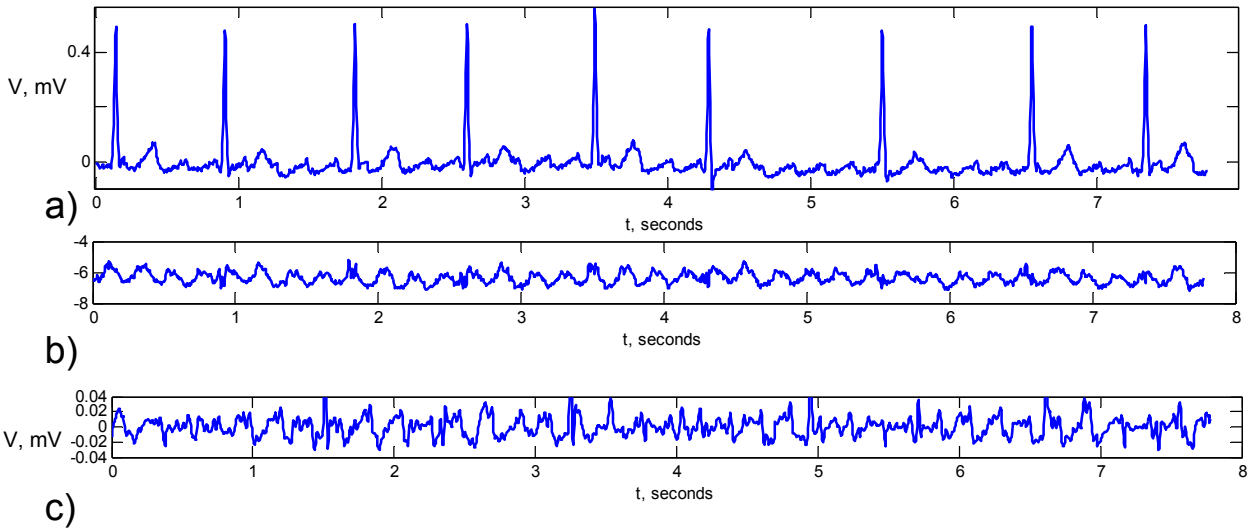

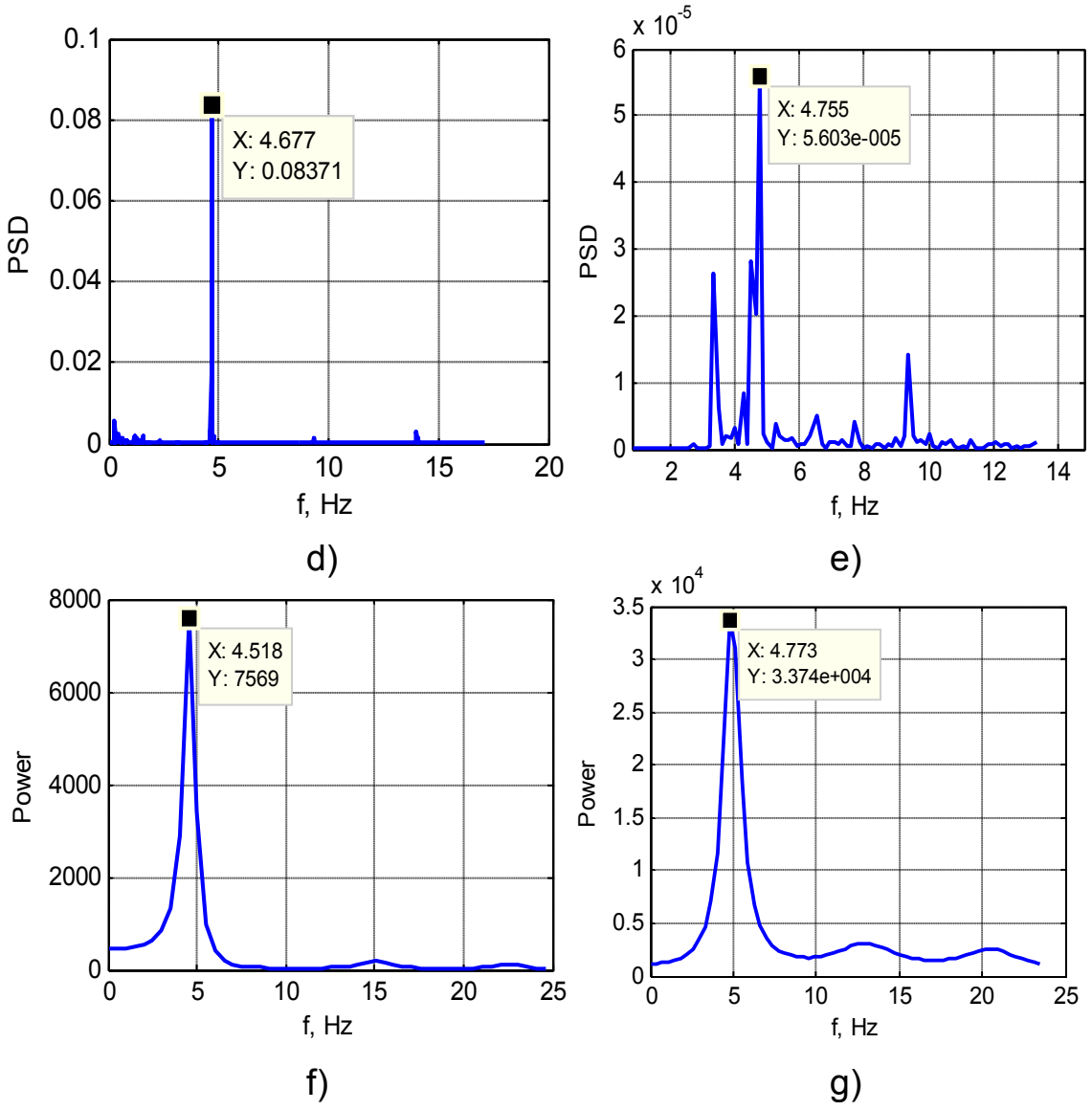

Fig. 5.6. (a) Original ECG signal (I lead) . The atrial activity source extracted from 12-lead ECG by means of ICA (b) and the atrial signal obtained by QRST cancellation in average beat subtraction method (c). Dominant AF frequency estimation via FFT analysis of atrial activity separated by ICA (d) and by ABC method (e). Dominant AF frequency estimation via Multiple Signal Classification (MUSIC) method of atrial activity separated by ICA (f) and by ABC method (g)

4.3. Fibrillatory frequency tracking

The emergence and maintenance of atrial fibrillation can be explained by the continuous propagation of multiple wavelets (re-entries) wandering throughout the atrial tissue. Before AF termination the number of re-entries decreases and atrial activity gradually changes its chaotic pattern to a more organized type, chaotic f waves convert into P waves. This process reflects in the changes (reduction) of the dominant atrial frequency in the spectrogram. There are obvious correlation between AF dominant frequency and the likelihood of spontaneous AF termination [10]. A low fibrillation frequency perceived in the interval 4-5 Hz has proved to be a predictor of spontaneous AF termination. The risk of non-terminating AF is higher for patients with higher AF frequency. Frequencies between 6-15 Hz are considered to be dangerous for patient.

Fast Fourier Transform (FFT) and Multiple Signal Classification (MUSIC) methods were used to obtain the frequency spectrum of the signals. Figure 5.6 shows dominant AF frequency estimation via FFT analysis of atrial activity separated by ICA (d) and by ABC method (e). For (d) maximum peak of the power spectrum, which characterizes the dominant fibrillation frequency, corresponds to 4,67 Hz. For (e) the main peak is located on 4,75 Hz with a difference of 0.078 Hz (1,67%) in comparison to (d). However, since atrial signal obtained by ABS method contains evident distortions after QRST cancellation, its spectrum (e) has additional peaks of the smaller amplitudes [11].

To reduce the effect of these distortions on the assessment of the dominant frequency of atrial fibrillation it is suggested to use MUSIC method of frequency analysis. MUSIC is an eigen-based subspace decomposition method. Eigen-analysis splits up the eigenvectors and the

eigenvalues of the autocorrelation matrix of a noisy signal into 2 subspaces: signal subspace and noise subspace. To estimate dominant AF and reduce the influence of distortions on the spectrum, S ($S<<N$) main eigenvectors V_1, V_2…, V_S which correspond to the largest eigenvalues λ_1, λ_2 ..., λ_S is used. Other $N-S$ eigenvectors correspond to the smallest eigenvalues and characterize the noise subspace.

For (f) the main peak corresponds to 4,518 Hz with a difference of 0.159 Hz (3,39%) in comparison to (d). For (g) the main peak corresponds to 4,773 Hz with a difference of 0.018 Hz (0,37%) in comparison to (e). But there are no additional peaks in Fig. 5.6, e.

Time-frequency analysis of isolated atrial electrical activity was also performed to identify the dominant frequency of atrial fibrillation and to supervise its time variation. Assessment of temporal behavior of atrial electrical activity gives prognostic information in the prediction of spontaneous termination of paroxysmal atrial fibrillation, success of electrical cardioversion or drug treatment of persistent AF.

To investigate the time-varying properties of AF the basic approach to time-frequency analysis was applied to the real 12-channel ECG records from the PhysioNet resource (Fig. 5.7, 5.8) [8-9]. The isolated atrial signal was segmented and the Fourier spectrum was calculated for each segment with Hamming window function of length equal to $3*f_s$, where f_s is the sampling frequency. The segments were considerably overlapping. The choice of segment size was driven by the compromise between time and frequency resolution: a larger value of segment size gives better frequency resolution, but poorer time resolution.

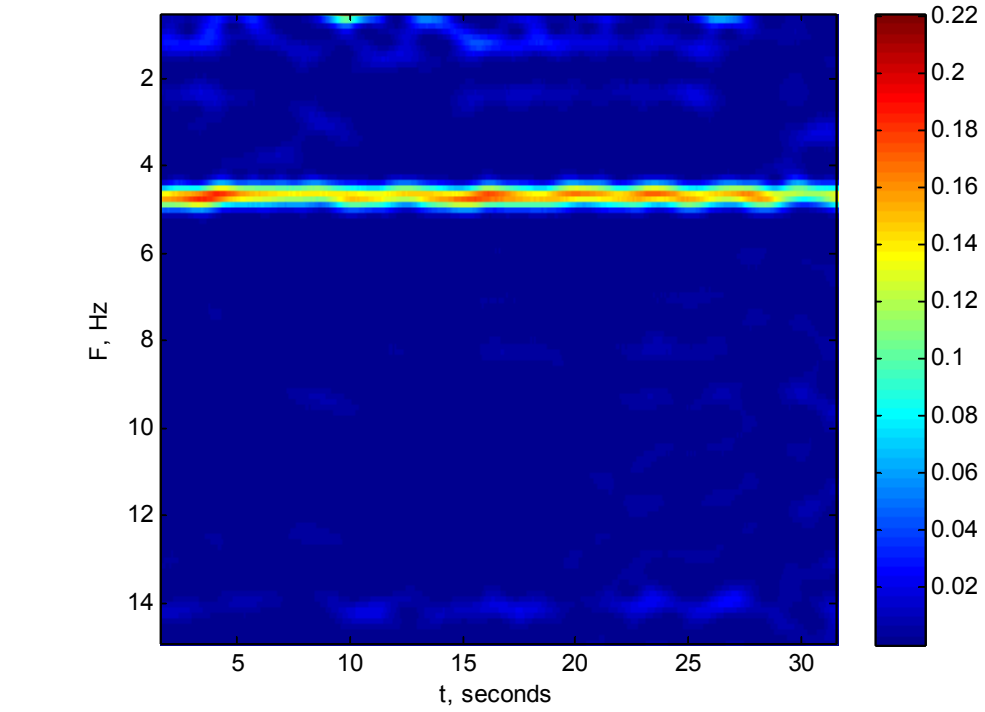

a)

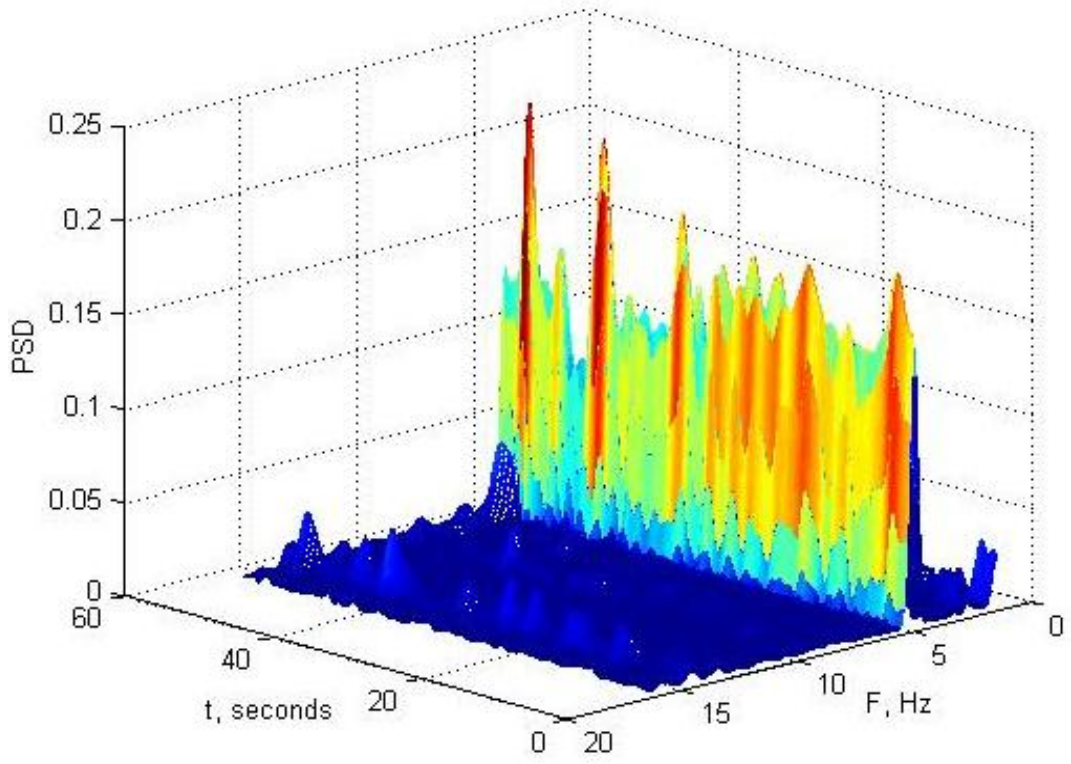

b)

Fig. 5.7. Time-frequency distribution for atrial source obtained by ICA: two-dimensional (a) and three-dimensional spectrograms (b)

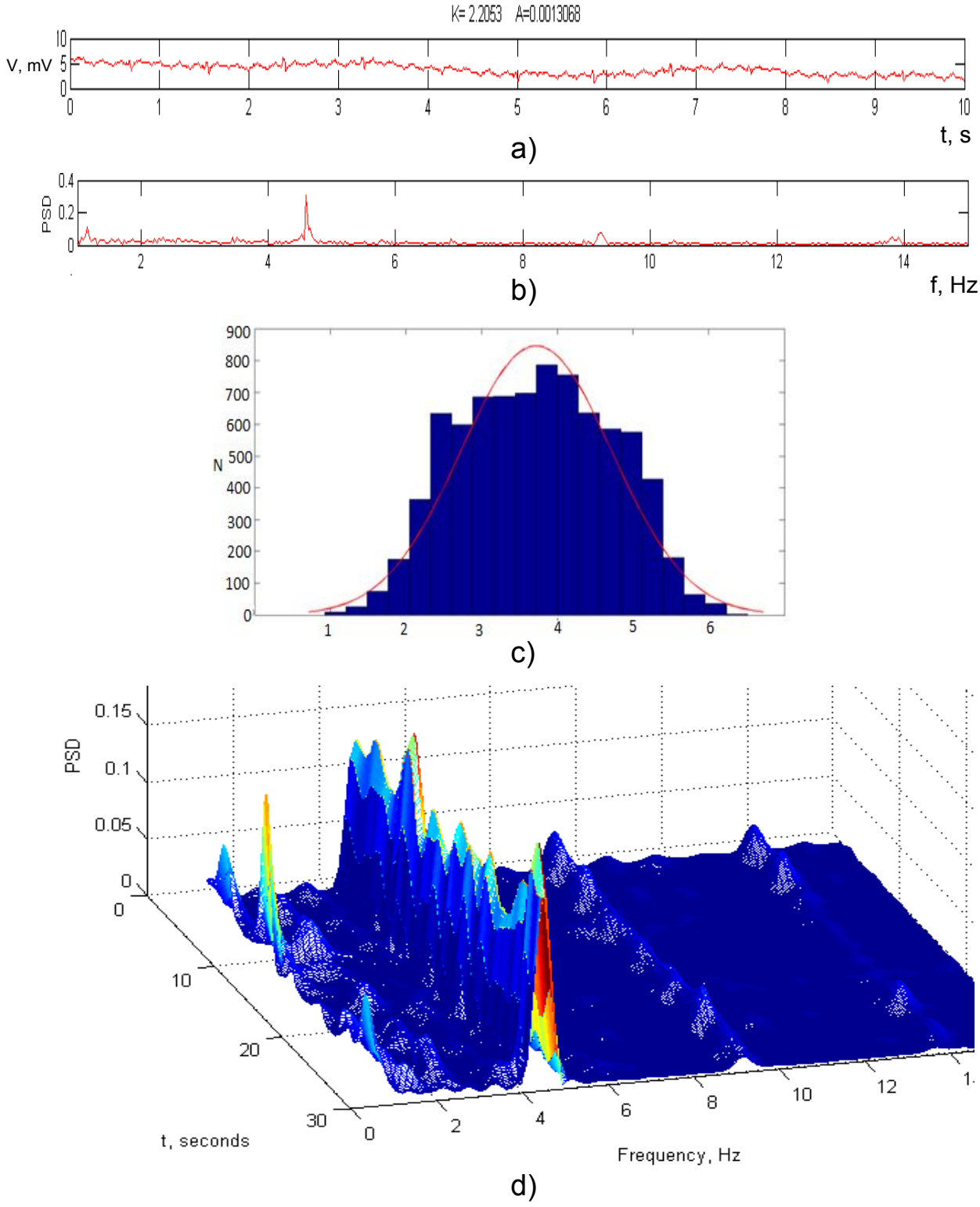

Fig. 5.8. Analysis of another 12-channel ECG record with signs of AF: identified atrial independent component (a), its spectral analysis (b), histogram (c) and spectral-time analysis (d)

CONCLUSIONS

Comparison of ICA and ABS methods in study of the surface ECGs in atrial fibrillation has shown that in the presence of a multichannel ECG recording it is more preferably to use ICA method for atrial electrical activity extraction. However, due to the computational complexity, ICA should be applied to the moderately long segments of ECG (1-2 minutes long at a sampling frequency f_s=257 Hz). ABS method is recommended to use for atrial electrical activity extraction, if only a few leads of ECG are available. In comparison with ICA, ABS method produces the atrial signal with some distortions, but it works well with long ECG segments.

CONTROL QUESTIONS AND TASKS

1. Explain why extraction and analysis of atrial electrical activity is important in the diagnosis of atrial fibrillation.
2. Explain the application of method of blind source separation to the task of atrial activity extraction.
3. Explain the application of average beat subtraction approach to the task of atrial activity extraction.
4. Explain the idea of fibrillatory frequency tracking by time-frequency analysis.

REFERENCES

[1] “Comparison of Atrial Signal Extraction Algorithms in 12-Lead ECGs with Atrial Fibrillation”, IEEE Trans. Biomed. Eng. ─ 2006. ─ vol. 53, no. 2, pp. 343–346.

[2] F. Castells “Atrial fibrillation análisis based on ICA including statistical and temporal source information”/ J. Igual, J. J. Rieta, C.

Sánchez, and J. Millet// in Proc ICASSP, Hong Kong, 2003. — pp.94-96.

[3] F. Castells “An integral atrial wave identification based on spatiotemporal source separation: Clinical validation,”/ J. Igual, J. J. Rieta, C. Sánchez, and J. Millet// Comput. Cardiol., pp. 717–720, 2003.

[4] J. J. Rieta, F. Castells, C. Sánchez, and V. Zarzoso, “Atrial activity extraction for atrial fibrillation analysis using blind source separation,” IEEE Trans. Biomed. Eng., vol. 51, no. 7, pp. 1176–1186.

[5] Choi S. Blind source separation and independent component analysis: A review/ S. Choi, A. Cichocki, H.M. Park, S.Y. Lee// Neural Information Processing. — 2005. — Vol. 6 (1). — P. 1— 57.

[6] R. Llinares and J. Igual “Exploiting periodicity to extract the atrial activity in atrial arrhythmias”, EURASIP Journal on Advances in Signal Processing 2011, 2011:134.

[7] F. Castells, J. J. Rieta, J. Millet, and V. Zarzoso. Spatiotemporal blind source separation approach to atrial activity estimation in atrial tachyarrhythmias. IEEE Transactions on Biomedical Engineering, 52(2):258–267, 2005.

[8] St.-Petersburg Institute of Cardiological Technics 12-lead Arrhythmia Database: doi:10.13026/C2V88N, http://www.physionet.org/physiobank/database/incartdb/

[9] Goldberger AL, Amaral LAN, Glass L, Hausdorff JM, Ivanov PCh, Mark RG, Mietus JE, Moody GB, Peng C-K, Stanley HE. PhysioBank, PhysioToolkit, and PhysioNet: Components of a New Research Resource for Complex Physiologic Signals. Circulation

101(23):e215-e220 [Circulation Electronic Pages; http://circ.ahajournals.org/cgi/content/full/101/23/e215]; 2000.

[10] F. Chiarugi “New Developments in the Automatic Analysis of the Surface ECG: The Case of Atrial Fibrillation”, Hellenic J Cardiol 2008, no. 49, pp. 207-221.

[11] Atrial Electrical Activity Extraction for Atrial Fibrillation Assessment/ Ivanko K., Ivanushkina N., Karplyuk Y.// Proceedings of 2016 IEEE 36th International Scientific Conference on Electronics and Nanotechnology (ELNANO). – 2016. – pp.192-197.

SECTION 5

FETAL ELECTROCARDIOGRAM EXTRACTION FROM MATERNAL ABDOMINAL SIGNALS

5.1. Peculiarities of manifestation of fetal cardiac electrical activity

Despite the difference in fetal and maternal cardiocirculatory systems, the standard fetal electrocardiogram (FECG) contains the same waves and complexes as the maternal electrocardiogram (MECG). At early stages of embryo-fetal development (6-8 weeks) practically all elements of ECG (P, Q, R, S, and T waves) can be differentiated. However, in clinical conditions fetal electrocardiogram can be recorded only beginning from the 10-16th week of pregnancy. Waves on the fetal electrocardiogram have a different degree of intensity and to a great extent are determined by both the technical registration conditions and the term of fetus development: the amplitude of waves of ECG signal increases beginning from the 32nd week of intrauterine growth and up to the delivery.

The heart rate is determined by the degree of fetus development, its bond with the maternal organism, and also changes depending on the period of the day and the term of pregnancy. It is believed that by the end of intrauterine period the heart rate is reduced from 160-170 beats per minute at the 12-week of pregnancy to 130 beats at the end of pregnancy [1-3].

Non-invasive techniques of fetal ECG registration and processing are based on the separation of fetal electrocardiogram from the mixture of abdominal electrocardiosignals registered at different points of the

surface of mother's body (Fig. 5.1). The problem lies in the fact that the signals registered in this case represent a mixture of maternal EGG (100-1500 μV), fetal ECG with much lower amplitude (1-50 μV), and numerous disturbances (Fig. 5.1 b, where markers indicate QRS-complexes of fetal ECG).

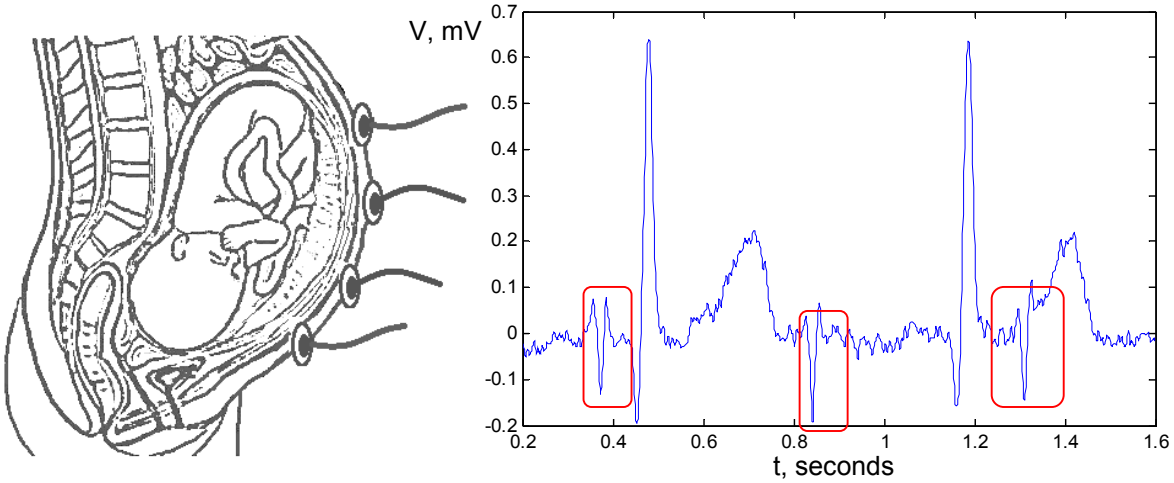

a) b)

Fig. 5.1. a) the principle of registration of abdominal ECG;
b) abdominal ECG with fetal cardiocycles

The enhancement of electrocardiographic fetal diagnostics involves the need of using the high resolution technologies in electrocardiography. Then the early diagnostics of cardiac electrical activity can become a criterion for estimation of the general condition of fetus and detection of hypoxia.

One of the most common abnormalities of the fetal evolution is oxygen starvation, hypoxia, which endangers the health and life of a fetus. STAN (ST analysis) is a computerized analysis of the ST segment of the fetal electrocardiogram [4-10]. Normal form of ST segment indicates a sufficient supply of fetal oxygen, an aerobic metabolism of the myocardium, and a positive energy balance. ST segment and T wave on

fetal ECG correspond to the processes of ventricular repolarization of myocardial cells and preparation to the next heart contraction. These processes require energy. During fetal hypoxia, the energy balance is disturbed, and its recovery is accompanied by the release of potassium ions into the cells. This leads to increase of the membrane potential of myocardial cells, and, consequently, to change of the ST segment, which manifests itself as increase in T wave amplitude. The inability to restore energy balance by widening blood vessels or anaerobic metabolism causes endocardium ischemia, which leads to disruption of ventricular repolarization. Depression of the ST segment with inversion of the T wave or without it can be detected on the fetal ECG. ECG changes in fetal hypoxia in animals are depicted in Fig. 5.2 [4].

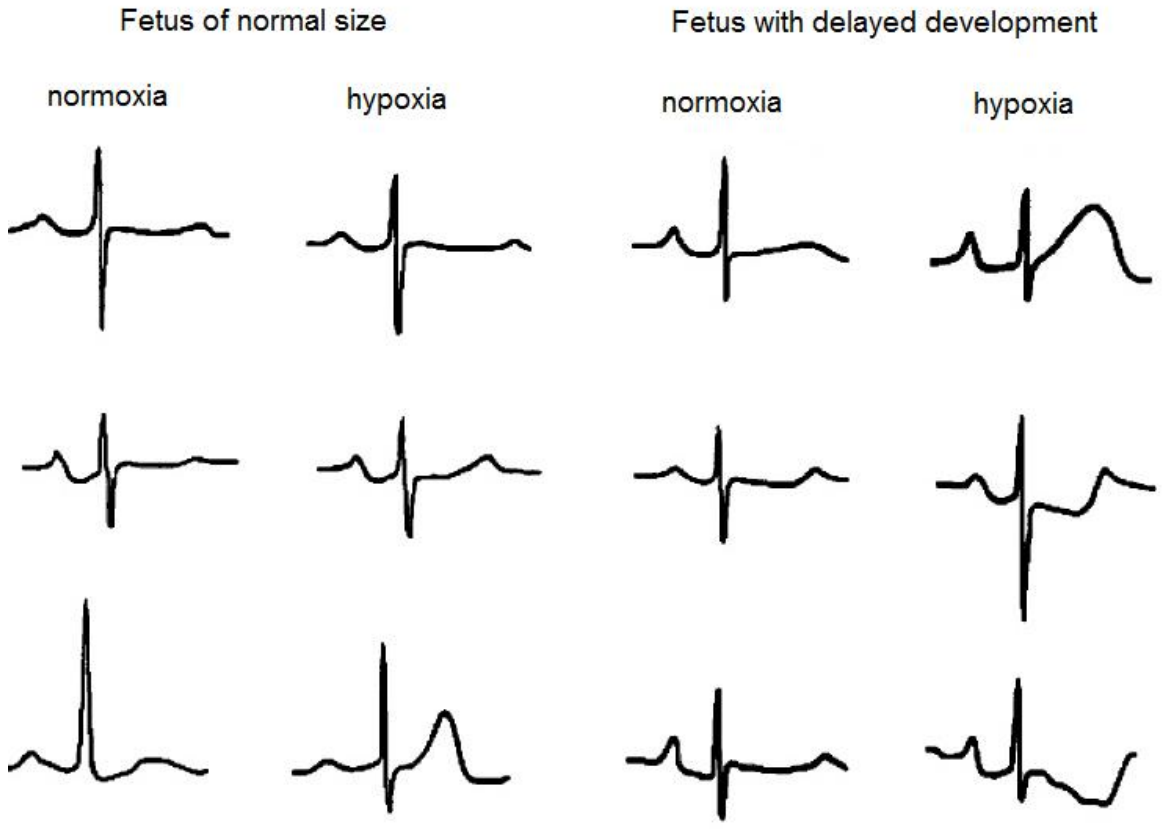

Fig. 5.2. ECG changes in fetal hypoxia in animals [4]

Early development of hypoxia can reflect itself on the fetal ECG in the form of two-phase ST segment or omission of ST segment relative to the baseline. The ST segment leans down and becomes negative, which is accompanied by a gradual decrease in the amplitude of T wave. However, not only hypoxia leads to such changes of fetal ECG. The changes can also be caused by infections, fever, excited state of the mother, as well as myocardial dystrophy or heart failure.

Early detection of hypoxia and its prompt correction can contribute to the birth of a healthy child. Evaluation of cardiac activity is one of the most important components of fetal monitoring because it enables diagnosis of fetal distress. Monitoring of the fetal heart can be carried out using the ultrasound method involving the analysis of the mechanical work of the heart and electrocardiography, which provides the clinician with a measure of the electrical activity of fetal heart. Ultrasound method based on Doppler effect is the most common instrument for detection of fetal hypoxia symptoms. However, it assesses only the mean heart rates.

Registration of the bioelectrical activity of fetal heart makes it possible to analyze morphology and time intervals of the fetal electrocardiogram, which are the reliable parameters for fetal condition determining [1-3]. It can be carried out by invasive and noninvasive methods. Invasive electrocardiography is based on the electrodes placement directly on the fetus head. This restricts the use of the method, because it can be applied only during the labor. Noninvasive method of fetal electrocardiogram acquisition uses electrodes, which are placed on the maternal abdomen, and enables registration of fetal ECG in a wide range of gestation terms. The noninvasive technique performs registration of the abdominal electrocardiosignal, which is the sum of maternal and fetal electrocardiograms. Fetal ECG could be extracted from this mixture using digital signal processing techniques.

There are various ways of locating the electrodes to register the fetal ECG. According to one of the methods, the electrodes are located on the edges of the abdomen of a pregnant woman similar to the way the electrodes are arranged on the limbs for the normal recording of the electrocardiogram in an adult. The electrodes, which are usually fixed on the hands of the adult, are placed in the upper abdomen, and those, which are fixed on the legs, are located in the lower abdomen of the pregnant woman.

With the other approach to registration, all 6 breast electrodes are located in the lower segment of the abdomen, trying to reach the upper part of the fetal body as much as possible, and 4 limb electrodes are located along the abdominal edges. In case of pelvic position of the fetus, the electrodes are placed in the middle upper part of the abdomen.

Normal amplitude of QRS complex ranges from 1 to 50 μV and from 100 to 1000 μV for fetal and maternal ECG respectively. Heart rate varies from 120 to 160 beats per minute and from 60 to 90 beats per minute for fetus and mother respectively. Fetal heart rate variability can be assessed more precisely by the analysis of fetal ECG comparing to the ultrasound method, because in the former case RR intervals are defined directly from the fetal ECG. Morphological analysis of the fetal ECG includes estimation of amplitudes of ECG waves and time intervals between the waves. One of the important parameters is the ratio of T wave amplitude to QRS complex amplitude, which progressively increases with increasing degree of hypoxia [4-10].

Due to the significant difference between amplitudes of fetal and maternal ECG signals as well as noise presence, achieving a high quality fetal ECG extraction from the abdominal ECG signal still remains a difficult task [1-3]. Noise and interferences occurring in the abdominal signal have the different nature and include: maternal ECG, muscular

activity of maternal abdominal muscles and uterus, power line interference, noise of electrodes, fetal motion artifacts, baseline drift caused by maternal breathing, noise of electronic equipment. Signals separation by simple frequency filtering is not possible because frequency spectrums of maternal and fetal ECG overlap. It is also necessary to take into account that a place, from which the fetal ECG could be recorded most clearly, can vary. It is explained by the fetal movement activity during pregnancy.

Among the promising approaches for maternal and fetal ECG signals separation is using of blind source separation methods (BSS) in conjunction with wavelet transform. Standard methods of signals separation from the mixture are based on the difference between their temporary and spectral characteristics. In case when the mixed signals overlap in time and frequency domain, the method of blind source separation is used. BSS is the separation of a set of signals from a set of mixed signals with unknown mixing process. The process is called "blind" because of the minimum of priori information about the nature of separated sources. The minimum a priori information, used in solving the problem, consists of an assumption of the statistical independence of signal sources, difference between statistical characteristics, constancy of the coefficients of mixing matrix on the interval of observation, and the fact that the probability densities of the source amplitude distributions are described by the non-Gaussian law. The method of independent components analysis (ICA) is the most common method to implement BSS.

However, as it can be seen from the problem statement, the rigorous solution is only possible on assumption of the absence of observation noises. In practice, noises are always present during the ECG recording. This results in emergence of additional components in

the separated signal in case of constant number of initial sources.

To overcome the limitations of "blind" nature of separated fetal and maternal sources, a vector model of heart electrical activity with a dipole structure was selected. It is assumed that a heart vector has a fixed spatial position and changes over time in amplitude and direction. Maternal ECG signal (MECG), which is recorded from the abdomen of a pregnant woman, can be represented as a linear superposition of three orthogonal signals – subspace of MECG sources. Similarly, a subspace of fetal ECG (FECG) sources can be imagined. The independence of bioelectrical fetal and maternal cardiac phenomena makes it possible to assume that the signals of sources are statistically independent. Due to the fact that the sources of noise have different physical nature as compared to sources of electrocardiosignals, they can be also considered as statistically independent with respect to sources of signals. Therefore, it is necessary to separate signals of individual sources from the mixture of surface noisy electrocardiosignals, namely fetal electrocardiosignals against the background of maternal electrocardiosignals and noise components.

Numerous investigations of BSS application achieved fetal ECG detection from abdominal maternal ECG. However, the studies were often limited to determination of fetal heart rate variability based on R waves detection and did not use additional information, included in morphological changes of fetal cardiocycles.

5.2. Fetal cardiocycle modeling

Testing of digital signal processing techniques for fetal ECG extraction requires signals with various morphologies. Generation of artificial electrocardiographic signals (Fig. 5.3) based on the real ECG

signals waveforms and modification of the model parameters allows us to create the database of simulated signals, which reflect the states of normal and pathologic fetal conditions [11-14].

According to the biophysical theory, electrical activity of the heart can be expressed as a cumulative effect of the dipoles, the intensity of which is described by Gaussian distribution. Therefore, a model of a cardiac cycle as a sum of Gaussian functions corresponds to maternal and fetal ECG signals. In general, the model must contain a sufficient number of Gaussian functions to reproduce ECG with a given accuracy; however, using of five functions is quite effective. For the task of fetal cardiac cycles modeling in normal condition and in cases of fetal hypoxia, the modified model was used, where each wave (P, Q, R, S) was reproduced by one Gaussian function and ST segment containing T wave was reproduced by two Gaussian functions:

$$\frac{\mathrm{d}V}{\mathrm{d}t} = -\sum_{i=1}^{6} \frac{a_i \omega}{(b_i)^2} \Delta\theta_i \exp\left(-\frac{(\Delta\theta_i)^2}{2(b_i)^2} \right), \qquad (5.1)$$

where V is voltage in the lead, mV; t is time, s; α_i is amplitude of the i-th Gaussian function, mV; $\omega = 2\pi f$, f is heart rate, Hz; b_i is width of the i-th Gaussian function, rad; θ_i is phase of the i-th Gaussian function, rad; $\Delta\theta_i = (\theta - \theta_i) \bmod (2\pi)$, rad; θ is phase of ECG quasiperiod, rad.

Using the equation (5.1) the following mathematical model was obtained for fetal cardiocycle simulation:

$$V = \sum_{i=1}^{6} a_i \exp\left(-\frac{(\theta - \theta_i)^2}{2(b_i)^2} \right). \qquad (5.2)$$

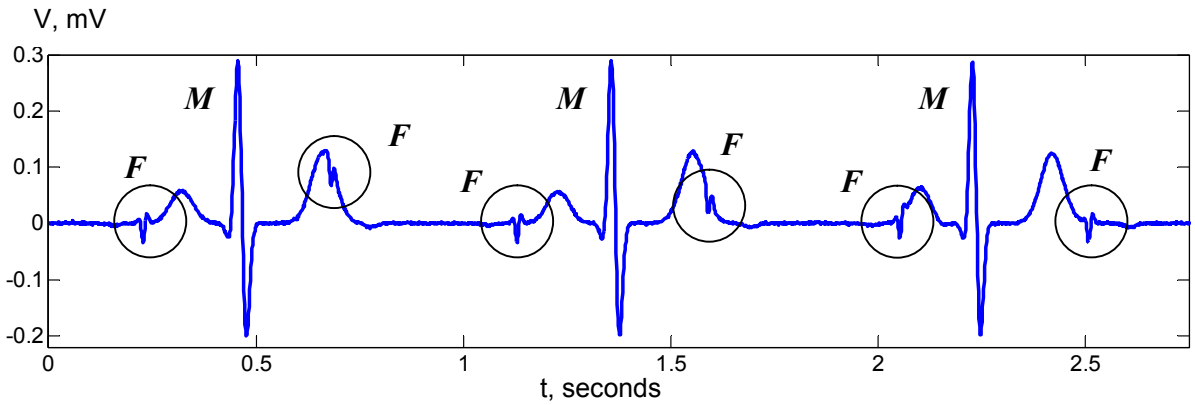

Fig. 5.3. Simulated abdominal ECG:
M **-** maternal cardiocycles, ***F*** ─ fetal cardiocycles

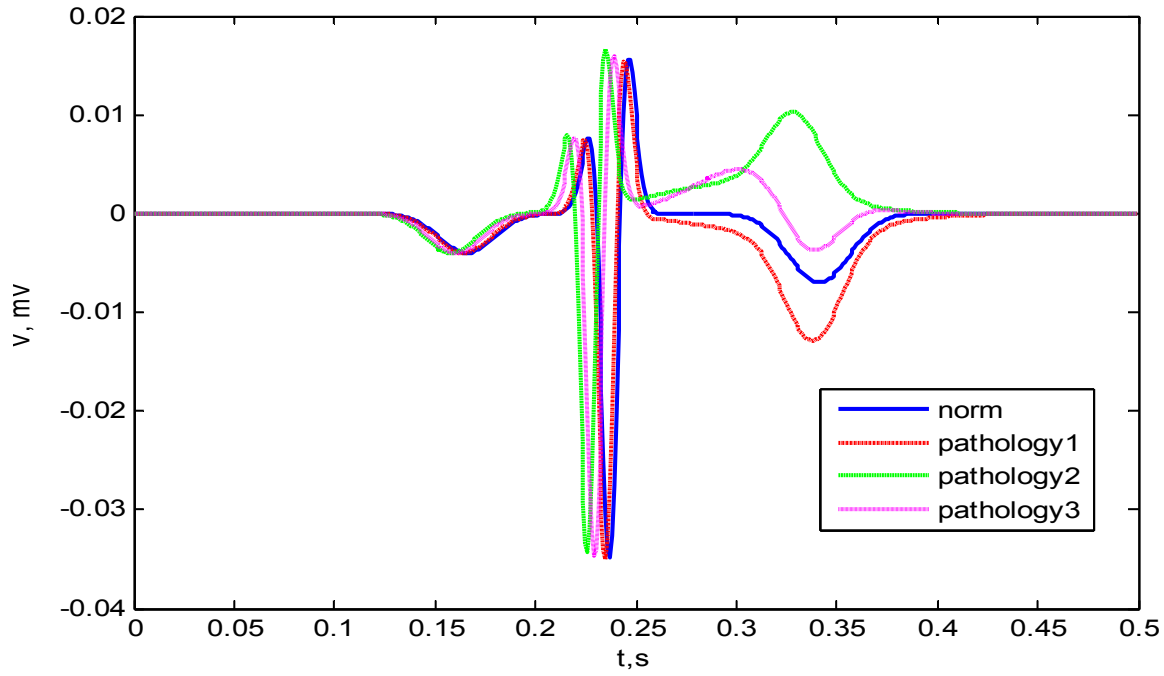

Fig. 5.4. Simulated fetal cardiac cycles corresponding to normal fetal condition and to different manifestations of fetal hypoxia:
increased T wave amplitude (1),
T wave inversion relative to the baseline (2)
and biphasic ST segment (3)

Alterations in amplitudes and durations of ECG waves are the features that signalize about fetal distress. The shape of the ST waveform can change with hypoxia [4-10]. Artificial FECG signals (Fig. 5.4) with the signs of fetal hypoxia state were developed considering three typical cases of hypoxia manifestation on ST segment: increase in T wave amplitude, T wave inversion relative to the baseline, biphasic ST segment.

To investigate the possibility of application of wavelet transform and independent components analysis to the problem of fetal ECG extraction from maternal abdominal ECG signal a model experiment was carried out [14]. Artificial fetal ECG signal and noise components in the form of additive Gaussian white noise were added to artificial maternal abdominal ECG signal (Fig. 5.5). Sampling frequency of the simulated ECG signals was assumed equal to 1 kHz, that corresponds to the sampling frequency of signals recorded by high resolution electrocardiography systems. The average amplitude of fetal QRS complex was approximately 35 μV, which is about 10 times less than the average amplitude of maternal QRS complex. The model also takes into account fetal and maternal heart rate variability (variation in the time interval between heartbeats) and variation in the amplitudes of particular ECG waves. Variation ranges of RR interval duration were ± 10% and ±15% from the mean value for maternal and fetal heart rhythm respectively, which corresponds to the physiology of the adult and the fetal hearts. Durations of RR intervals were set using a pseudorandom numbers generator for normal distribution.

The orientation of the fetal PQRST complexes is the opposite to the maternal PQRST according to the normal fetus position in the uterus. Similarly to the simulated ECG signals in one lead, the models of

multichannel abdominal ECG recordings were received for normal fetal condition and for the presence of hypoxia signs.

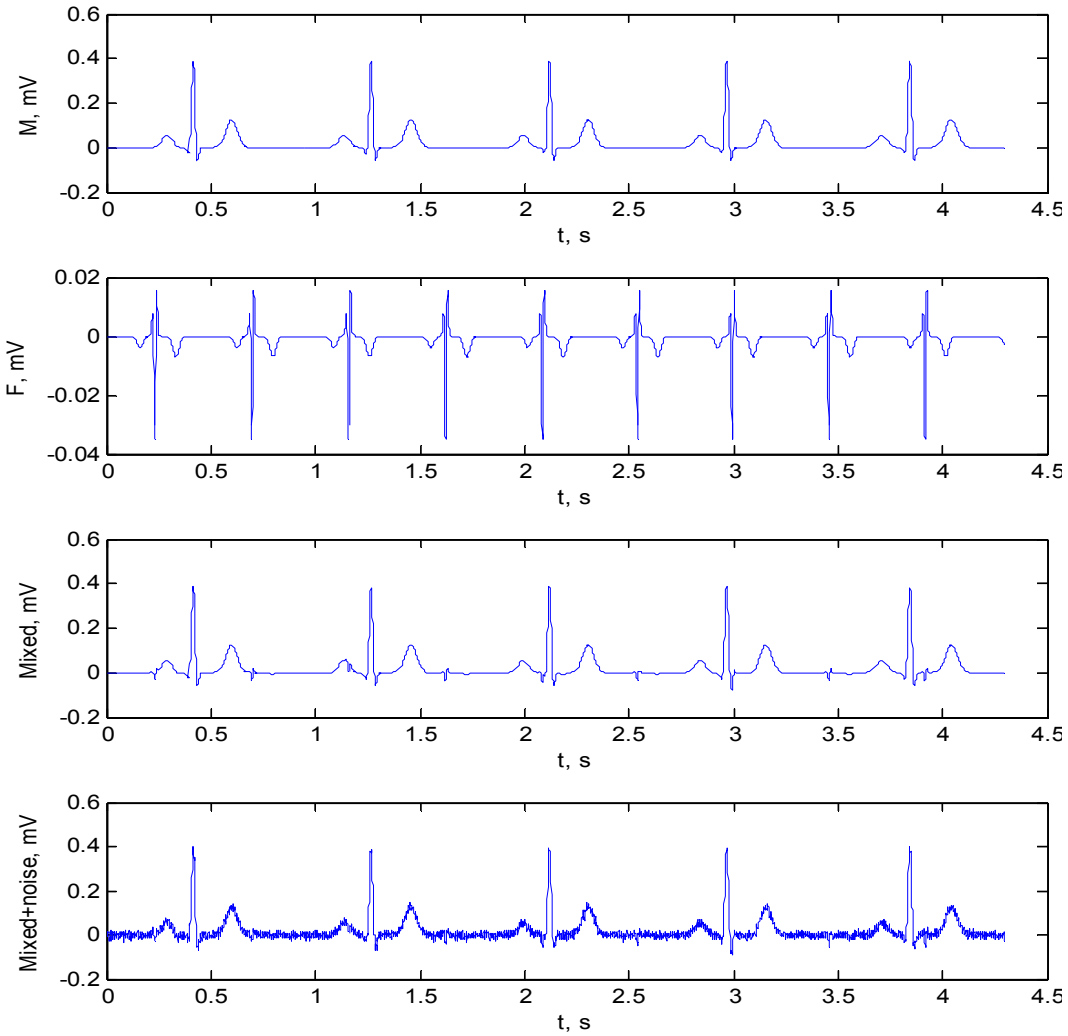

Fig. 5.5. Artificial maternal (a) and fetal (b) ECG signals and a sum of these signals (c); simulated abdominal signal affected by noise (d)

5.3. Fetal ECG detection and analysis based on combined use of ICA and WT methods

Analysis of abdominal ECG by means of wavelet transform includes signal preprocessing to eliminate noise components and fetal ECG extraction to define diagnostic parameters [15-18]. Wavelet decomposition allows us to eliminate noise and suppress the main high-

amplitude interference that dominates in abdominal signal – maternal ECG.

Wavelet transform requires only one abdominal lead for fetal QRS extraction. Abdominal ECG signal can be represented by multiresolution wavelet analysis as a sum of an approximation component a_m and the detail components d_j: $S(t) = a_m(t) + \sum_{j=1}^{m} d_j(t)$, where m is number of wavelet decomposition levels. The approximation coefficients correspond to the low-frequency components of ECG signal and the detail coefficients correspond to high frequency components of short duration. This property of wavelet decomposition allows us to remove noise from the abdominal signals and to separate maternal and fetal ECG. Noise appears at the detail levels of wavelet transform, therefore the task of noise suppression consists in detail coefficients processing. Coefficient values not exceeding a selected threshold level are replaced by zero. Appropriate threshold limit and threshold method (hard or soft) can be different at each level of wavelet decomposition.

The baseline wander and power-line interferences were eliminated from the abdominal signal using wavelet decomposition. As a wavelet function, which was used to eliminate the baseline wander, a symmetric wavelet of 6th order was used (Fig. 5.6). Wavelet decomposition was performed up to the 9th level (Fig. 5.7). The baseline wander is the low-frequency noise, so in order to eliminate it, it is necessary to restore the signal with zero coefficients of the approximating component, which reflects the slow fluctuations of the signal.

To suppress high frequency noise, the simulated abdominal ECG signals were decomposed up to the 5th level with a "symmetric" wavelet of 6th order (Fig. 5.8). The presence of the noise manifested itself at the detail levels d_1, d_2, d_3. Taking into account the noise pattern at these

levels, it was reasonable to replace by zero all wavelet coefficients at the detail levels d_1, d_2 and apply soft thresholding method to wavelet coefficients at the detail level d_3, as this level apart from the noise contained the signs of fetal ECG. Then, using the thresholded coefficients in the inverse wavelet transformation, the abdominal ECG signals without noise were reconstructed.

On the next stage after the noise suppression, the fetal ECG must be extracted from the abdominal signal. Fig. 5.9 shows the wavelet decomposition up to the 5^{th} level performed for the preliminarily denoised abdominal ECG signal.

It is evident that the detail components d_1, d_2, d_3, d_4 contain the signs of the fetal QRS complexes. At the detail level d_5 and at the approximation level a_5 the signs of fetal QRS complexes do not appear. Therefore, to separate the fetal ECG from the abdominal signal it is necessary to consider only the coefficients of the detail levels d_1, d_2, d_3, d_4 and replace by zero the coefficients at d_5 and a_5 levels.

Investigation of WT possibilities in fetal ECG detection with using of different wavelet functions and different number of wavelet decomposition levels showed, that localization of fetal QRS complexes and RR intervals durations for heart rate variability analysis can be accurately determined, but morphology of the fetal cardiocycles can not be analyzed properly (Fig. 5.10).

In the signal obtained after reconstruction the areas containing the features of the maternal QRS complexes must be excluded since maternal QRS complexes occur at all levels of the wavelet decomposition of the abdominal ECG signal (Fig. 5.11).

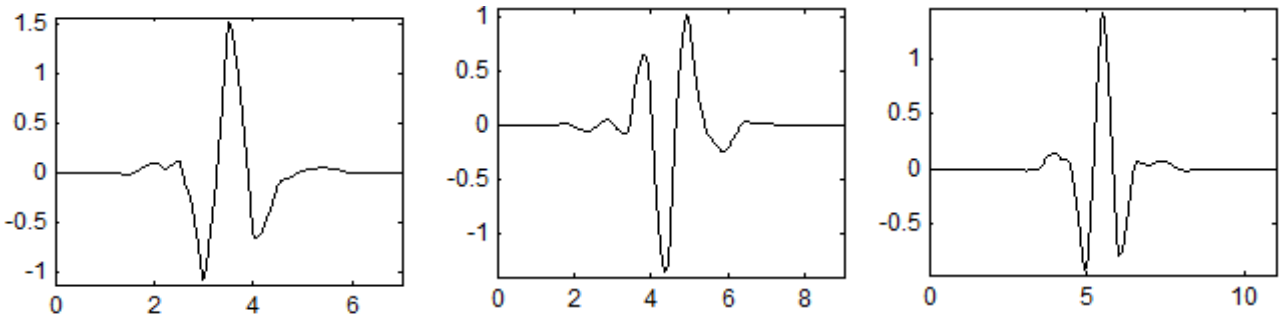

Fig. 5.6. "Symmetric" wavelet functions of the 4th, 5th and 6th orders

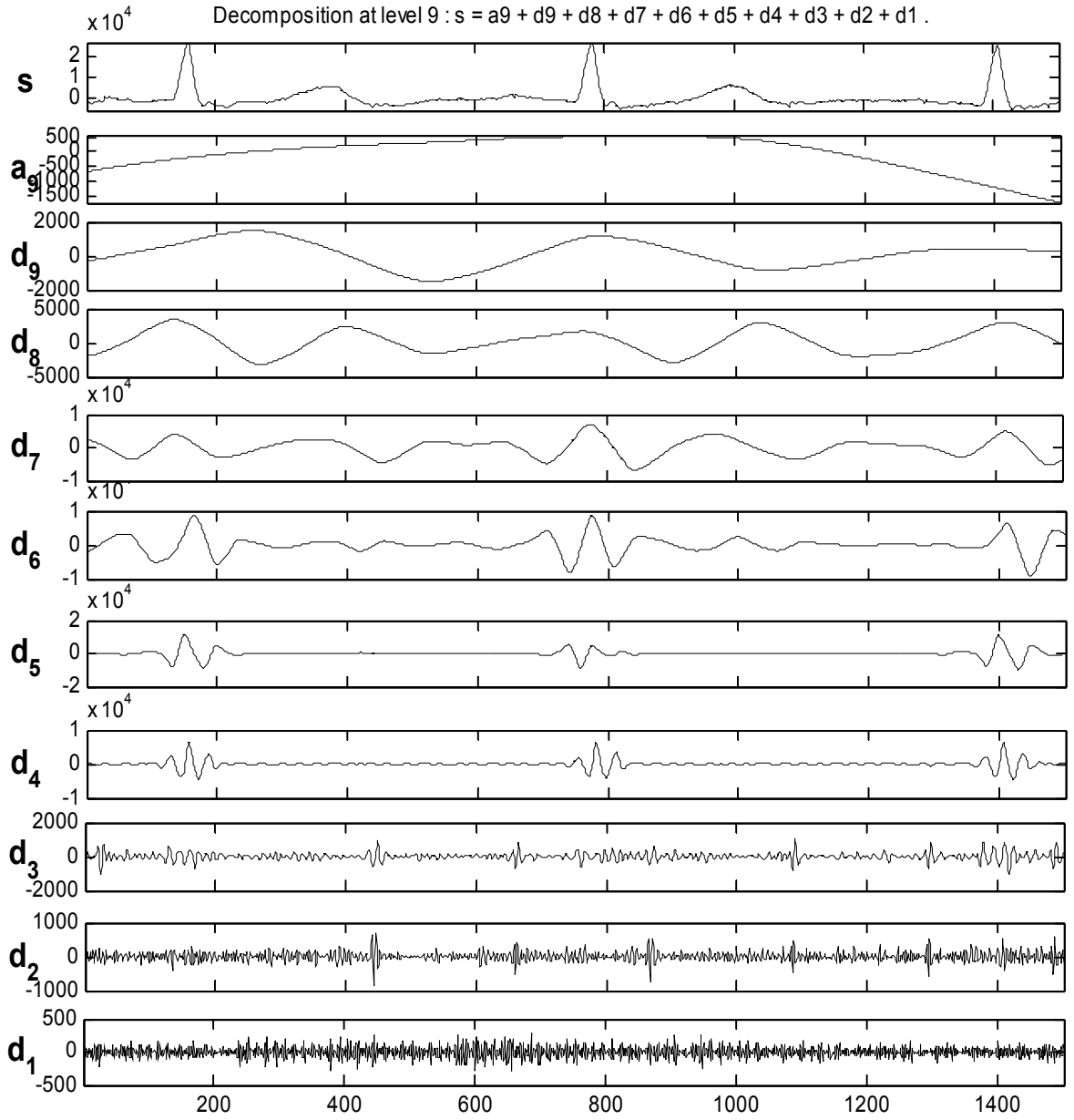

Fig. 5.7. Wavelet-decomposition of the abdominal ECG signal using a "symmetric" wavelet of the 2nd order up to the 9th level

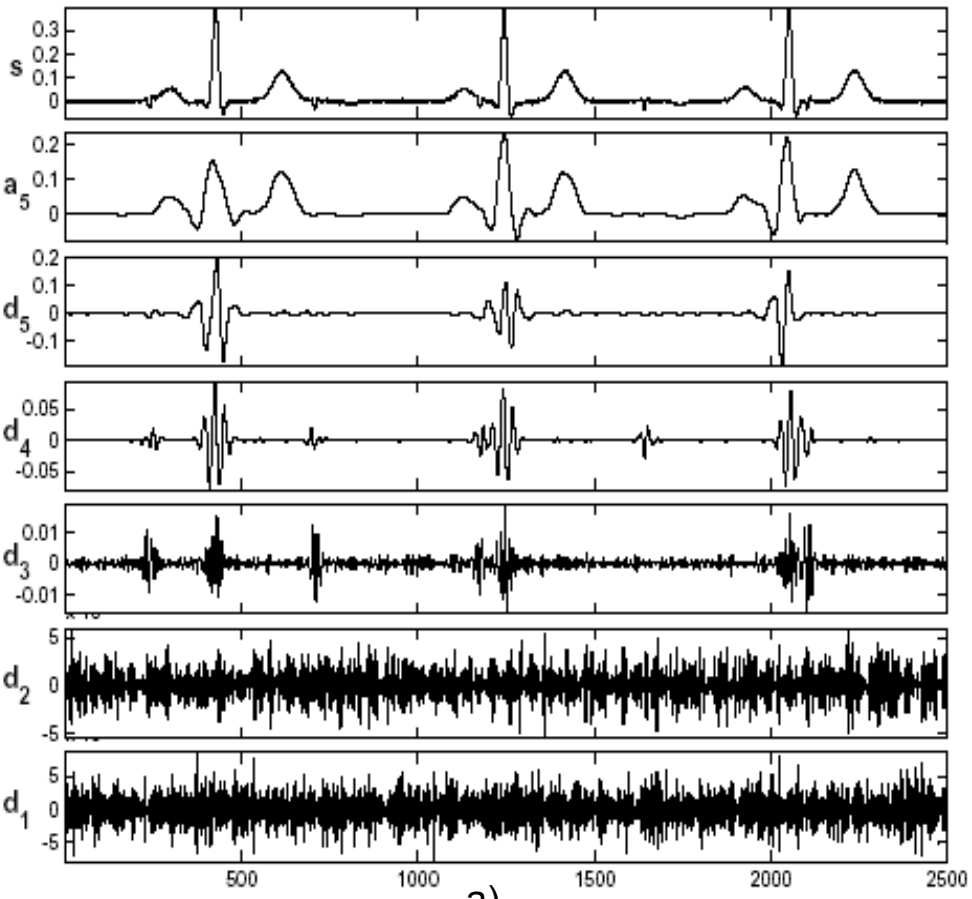

a)

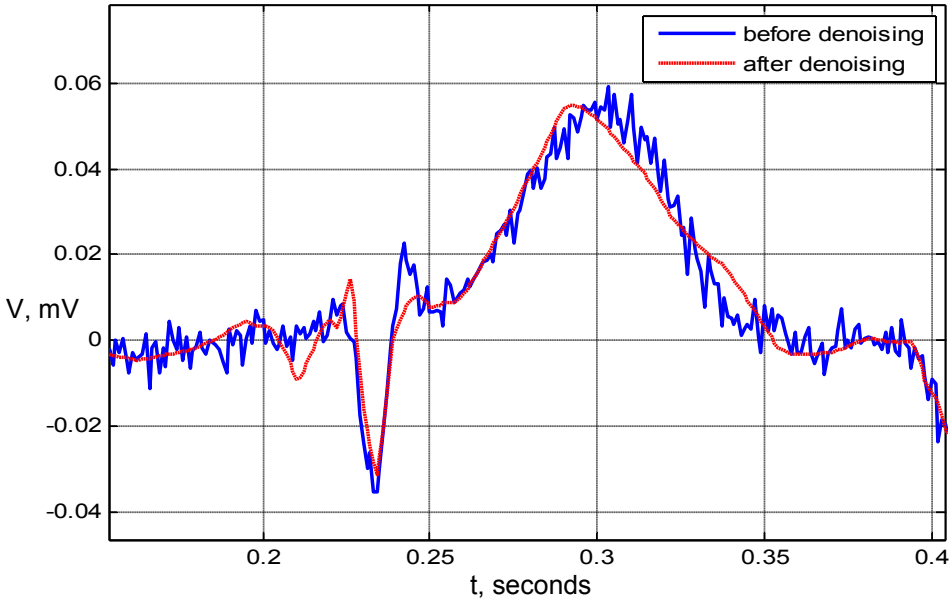

b)

Fig. 5.8. ECG denoising by means of wavelet transform: a) wavelet decomposition of the simulated abdominal ECG signal; b) fragment of the simulated abdominal ECG containing fetal cardiocycle before and after denoising

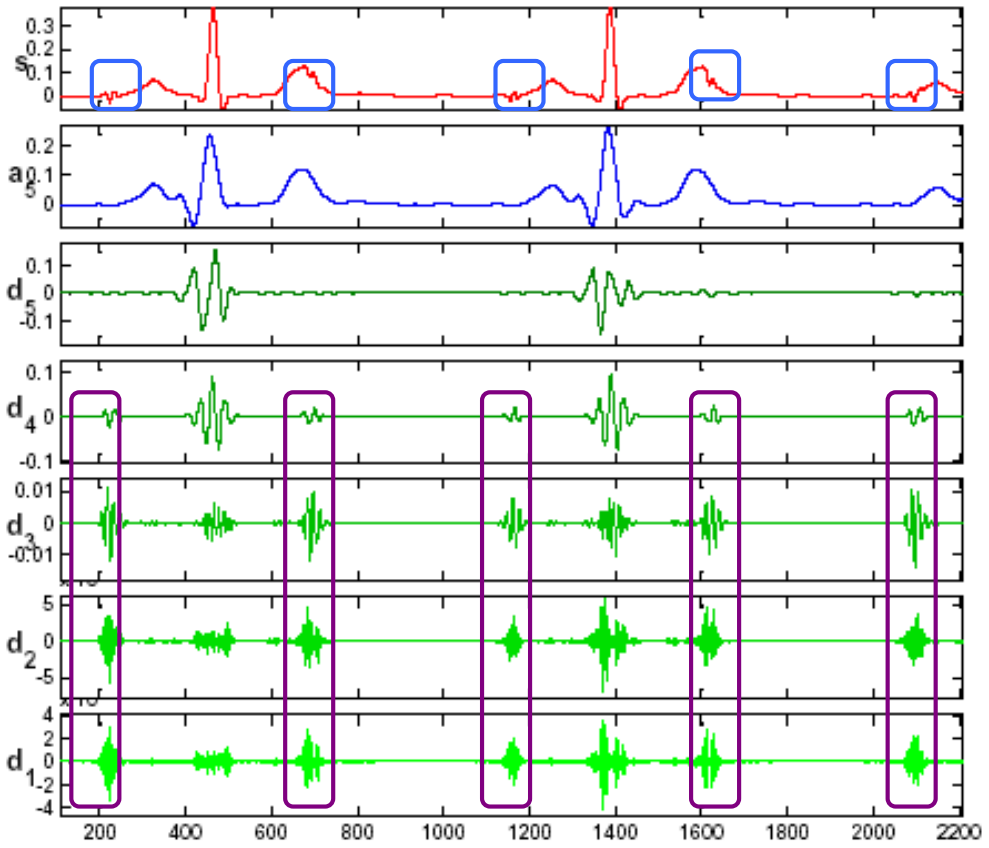

Fig. 5.9. Wavelet decomposition up to the 5th level (with a "symmetric" wavelet of 6th order) perfomed for the simulated abdominal ECG signal that was preliminarily denoised

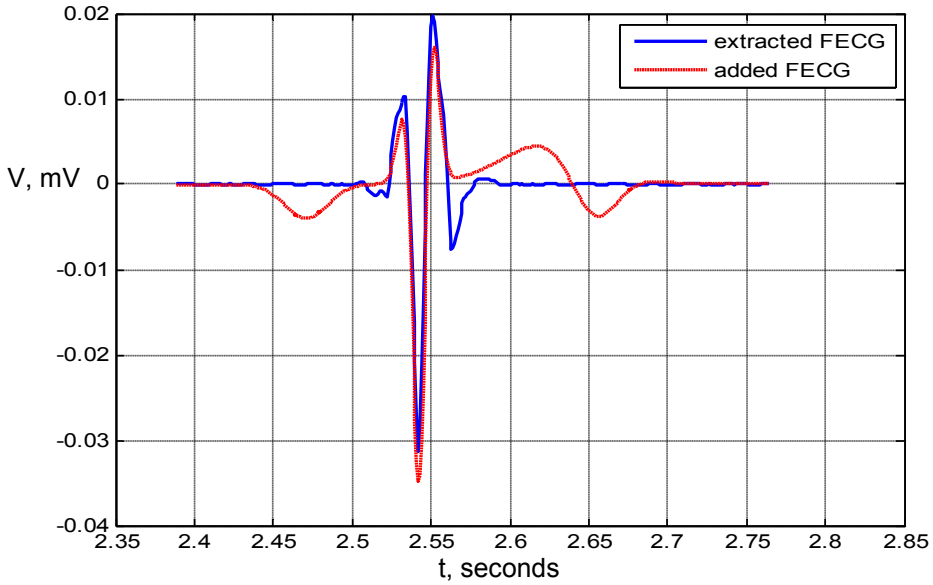

Fig. 5.10. The simulated fetal cardiocycle with the manifestation of fetal hypoxia as biphasic ST segment: added to the abdominal signal and extracted from it using WT. P and T waves were not revealed

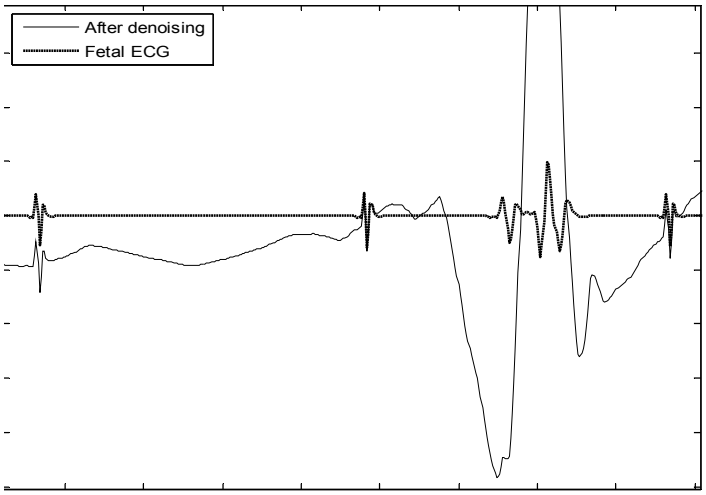

Fig. 5.11. Fragment of the real abdominal ECG after elimination of noise components and sum of the detail components d_1, d_2, d_3, d_4

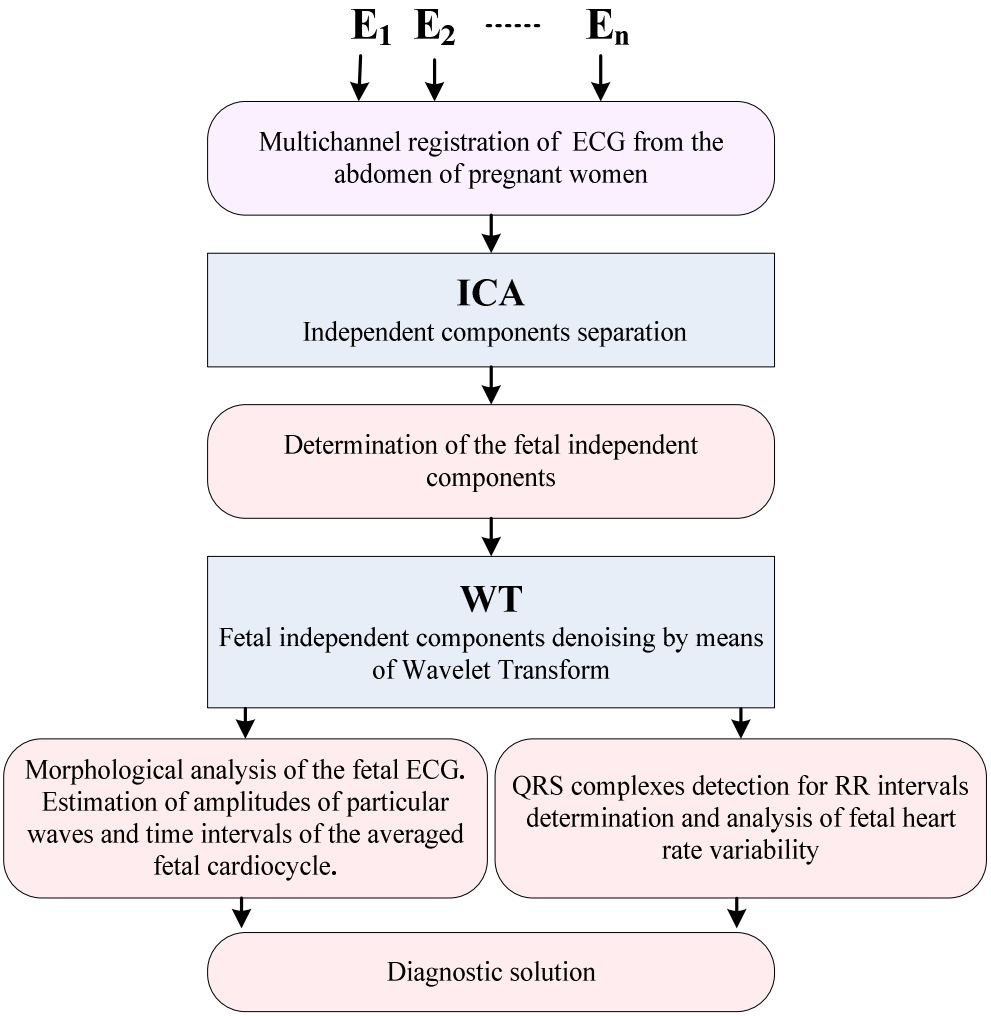

Fig. 5.12. Algorithm of fetal ECG detection and analysis based on combined use of ICA and WT methods

The shapes of the extracted fetal QRS complexes were close to the shapes of QRS complexes from the simulated fetal cardiocycles, which were added to the maternal ECG signal, but there were obvious distortions in low-frequency P and T waves and their diagnostically important information was lost (Fig. 5.11).

A comparative analysis of the results received by simulated signals processing showed, that for fetal ECG extraction with the aim of morphology estimation wavelet transform should be applied as a tool for noise suppression and used in combination with ICA method (Fig. 5.12) [19-23]. Conducted experiments revealed that it is better to apply WT not before ICA, but after independent components separation in order to purify the fetal independent components from the noise. In the case of using WT before ICA method, the slight distortions, which arise in the reconstructed signal due to the specifics of WT, may occur in the fetal independent components as the significant distortions that have the same order of magnitude as the fetal ECG waves.

Fig. 5.13 shows 4 independent components obtained for the simulated 6-channel abdominal ECG. Noise was suppressed by WT (Fig. 5.13, b). Due to the fact, that fetal heart rate exceeds maternal about twice, fetal independent components can be easily identified among maternal independent components. It should be noted that the fetal cardiac cycles extracted from the denoised fetal independent components are very similar in shape to the simulated cardiac cycles added to the abdominal signals.

Values of correlation coefficient for cardiac cycles, shown in Fig. 5.14 a-d, are 0.972, 0.981, 0.977 and 0.974 respectively. Despite the slight distortion, the diagnostically important information about the low-frequency P and T waves as well as about the biphasic ST-segment was not lost after processing and can be estimated

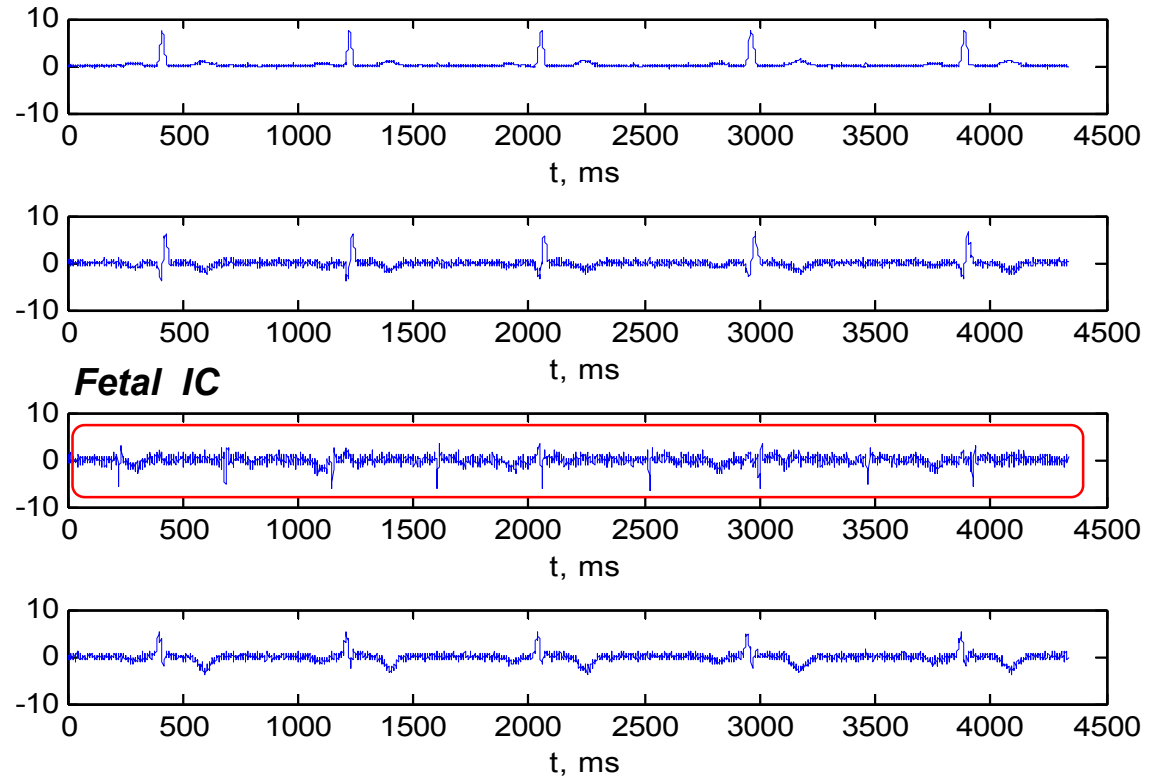

a)

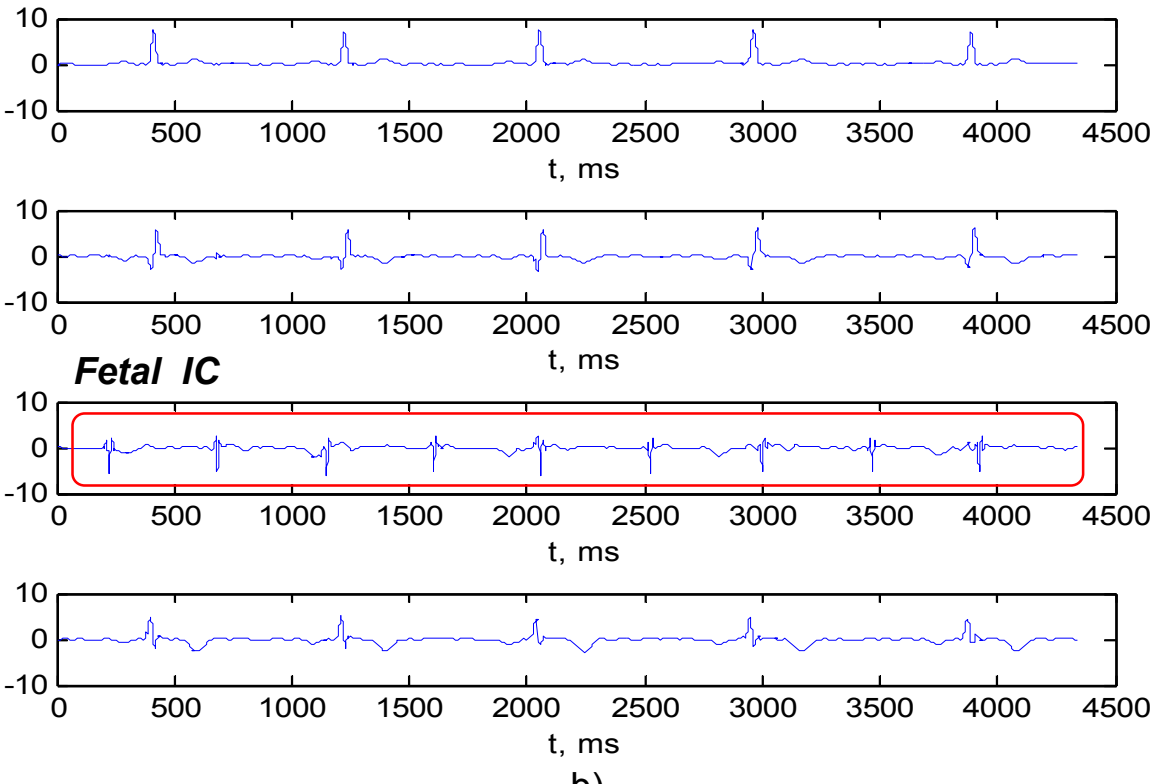

b)

Fig. 5.13. Independent components obtained for the simulated 6-channel abdominal ECG recording: a) before denoising; b) after denoising by means of WT

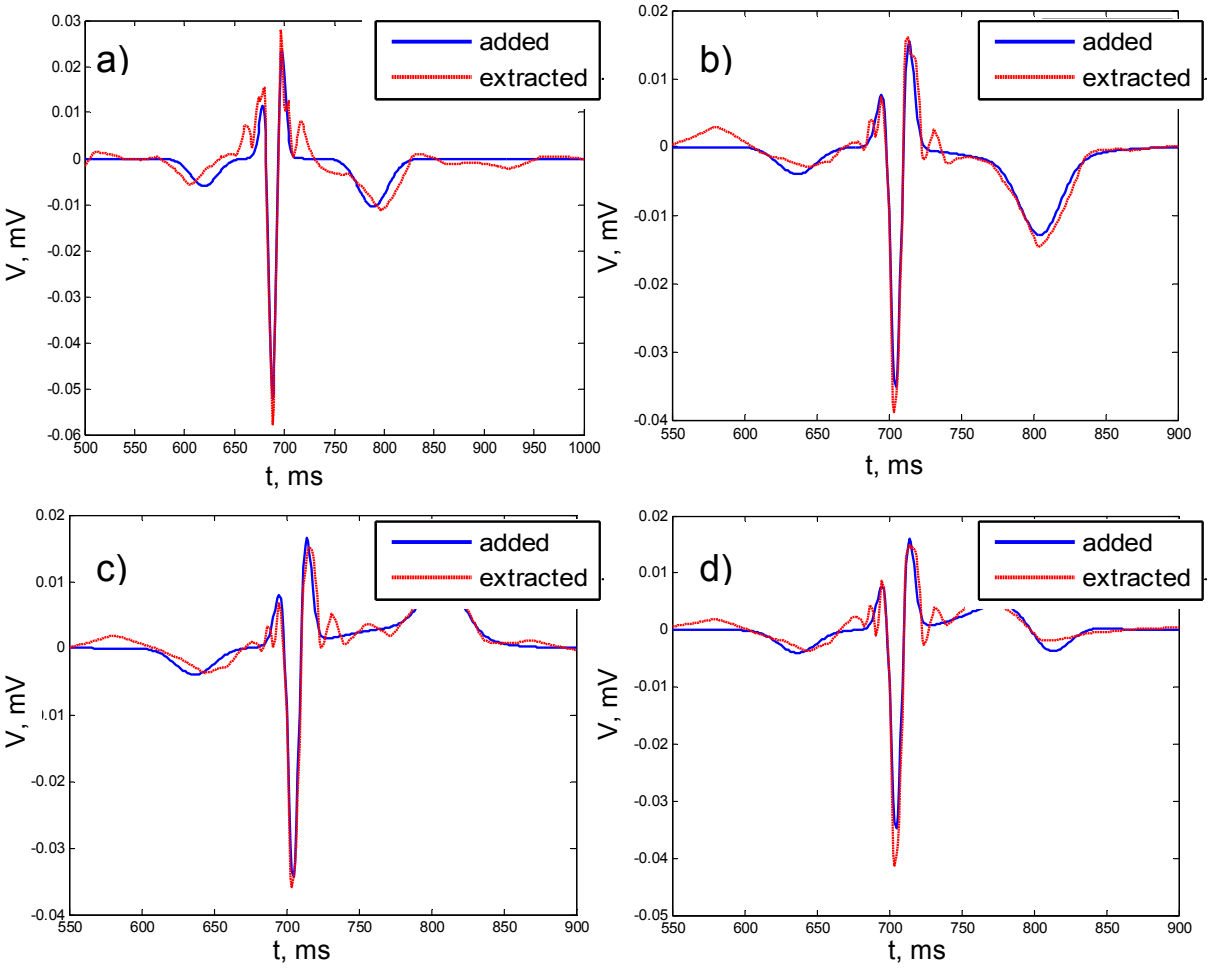

Fig. 5.14. Simulated fetal cardiac cycles added to the mixture of maternal abdominal ECG signal and noise and then extracted from it by combined use of ICA and WT methods. In the extracted signals the information about the subtle structure of the fetal cardiac cycles is saved: a) norm; b) increased T wave amplitude; c) T wave inversion relative to the baseline; d) biphasic ST segment

The value of the coefficient of correlation *r* between the separately taken simulated fetal cardiocycle and the cardiocycle, detected from the total abdominal signal, was found as:

$$r = \frac{\sum_{i=1}^{N}(s_i - \bar{s})(s_i^* - \overline{s^*})}{\sqrt{\sum_{i=1}^{N}(s_i - \bar{s})^2 (s_i^* - \overline{s^*})^2}},$$

where N is the number of samples in the separately taken simulated fetal cardiocycle S and in the cardiocycle S^*, which is detected from the total abdominal signal;

$\bar{s}$ і $\overline{s^*}$ are average values of the separately taken simulated fetal cardiocycle and the detected one.

The proposed approach for fetal ECG extraction, based on the joint application of ICA and WT methods, was then applied to real data from PhysioNet resource [24-27]. Abdominal and Direct Fetal Electrocardiogram Database [24] contains multichannel fetal electrocardiogram recordings obtained from 5 different women in labor, between 38 and 41 weeks of gestation. Each recording comprises four differential signals acquired from maternal abdomen and the reference direct fetal electrocardiogram registered from the fetal head (Fig. 5.15).

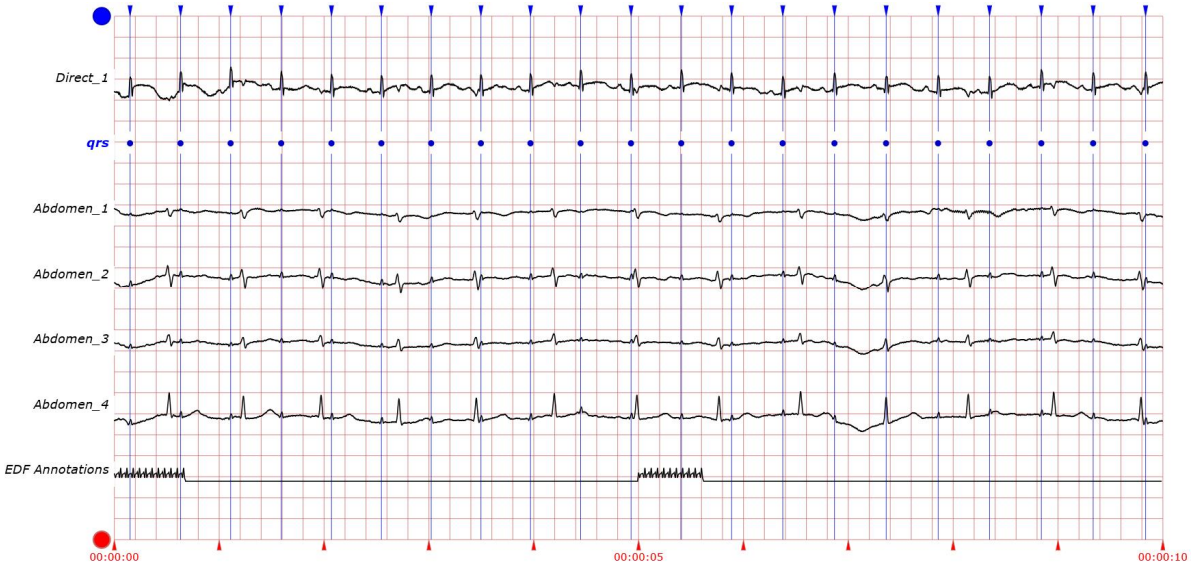

Fig. 5.15. Fragment of the recording from the Abdominal and Direct Fetal Electrocardiogram Database

Non-Invasive Fetal Electrocardiogram Database [27] contains a series of 55 multichannel abdominal non-invasive fetal electrocardiogram recordings, which were taken weekly from a single subject between 21 to 40 weeks of pregnancy. The recordings contain 2 thoracic signals and 3 or 4 abdominal signals (Fig. 5.16).

Fig. 5.16. Fragment of the recording from the Non-Invasive Fetal Electrocardiogram Database

Fig. 5.17 depicts a fragment of 4-channel abdominal electrocardiogram recording obtained from the woman in labor on 39 week of gestation. The recording was acquired with 1 kHz sampling rate and 16 bits resolution. Fetal and maternal independent components, obtained for this recording and denoised by WT, are presented in Fig. 5.18. The fetal cardiocycle extracted from the maternal abdominal ECG resembles the cardiocycle from the direct fetal electrocardiogram registered simultaneously from the fetal head (Fig. 5.18). The differences in the shape of the cardiocycles are explained by placement of electrodes.

The simulation of ECG signals allows us to generate a variety of fetal and maternal ECG signals of different shapes, which correspond to

the states of norm, pre-pathology and pathology. In the simulated fetal signals changes in amplitudes and durations of ECG waves, which indicate the state of fetal hypoxia, are taken into account. Also various types and levels of interferences, that affect abdominal ECG signal, may be set in the model. Creating a database of synthetic ECG, that includes the models with pathological alterations in morphology of fetal ECG, is a promising direction for further investigation and improvement of methods and algorithms for diagnosis of the fetal status throughout pregnancy and recognition of early symptoms of fetal distress.

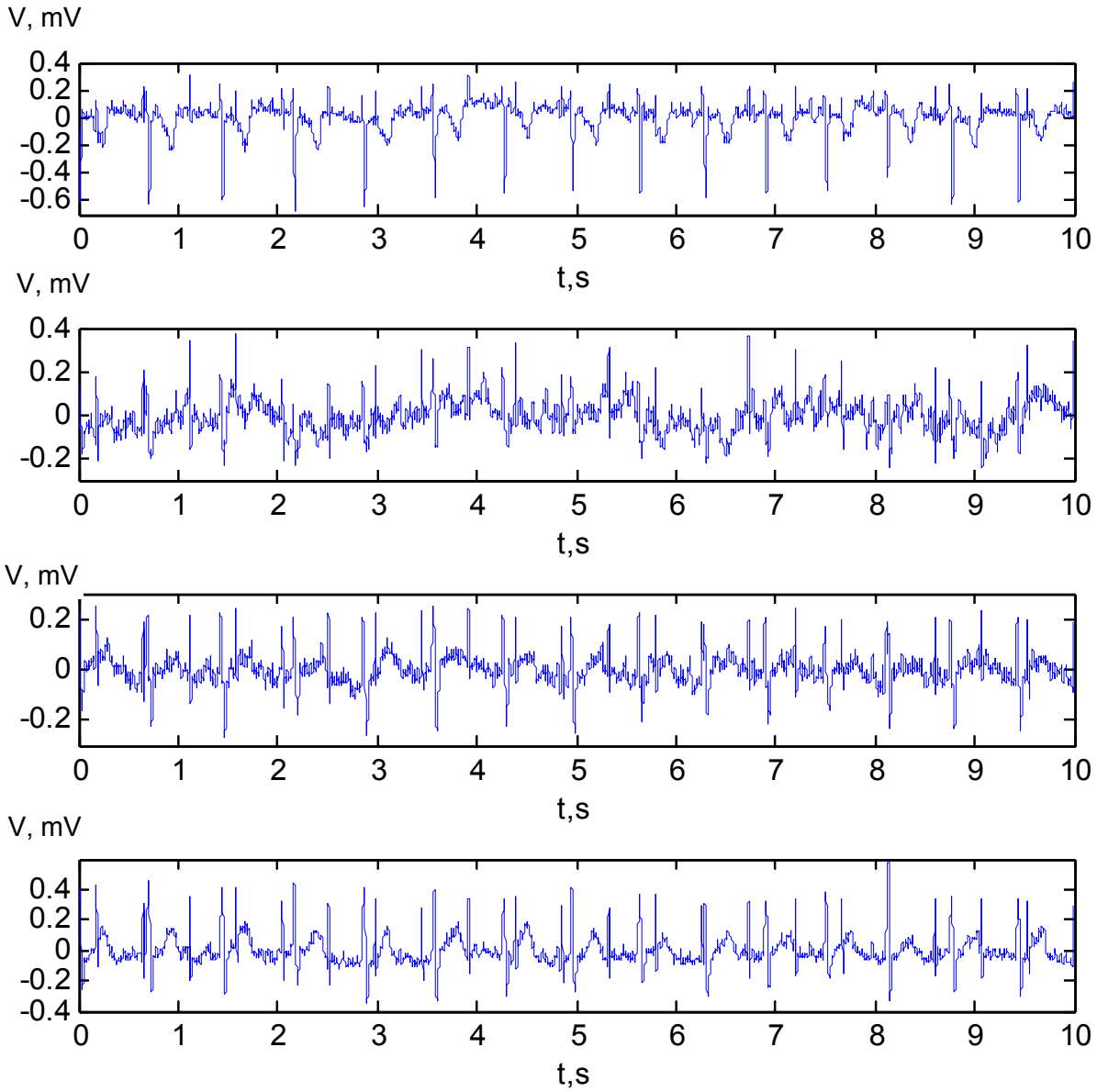

Fig. 5.17. Fragment of the real 4-channel abdominal ECG recording

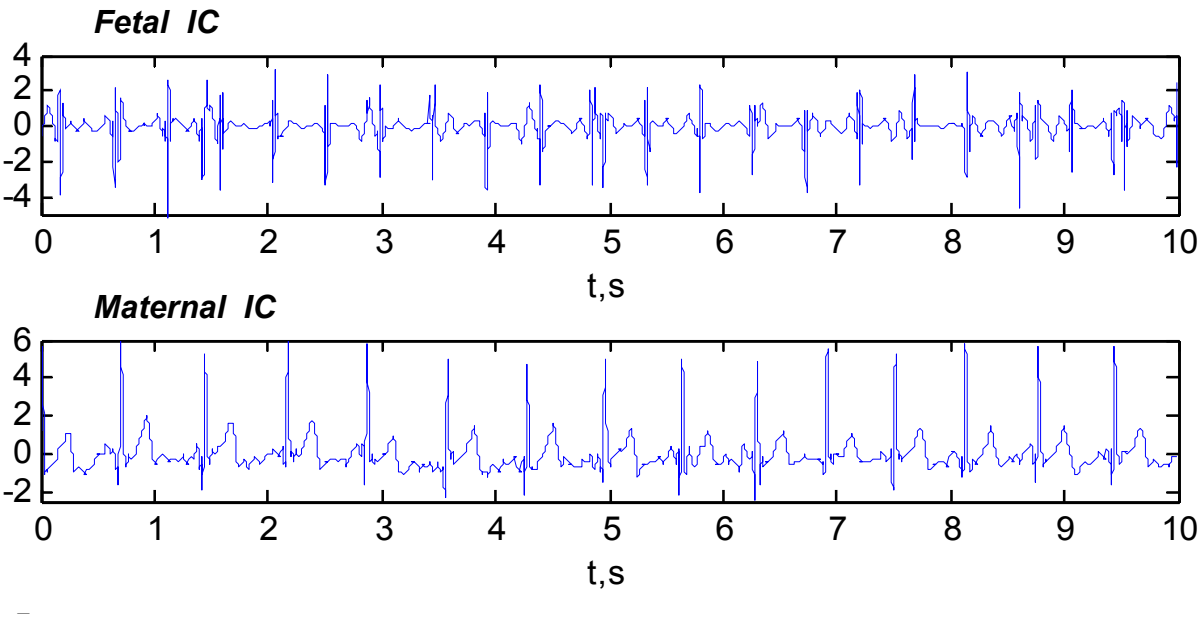

Fig. 5.18. Fetal and maternal independent components after denoising by WT

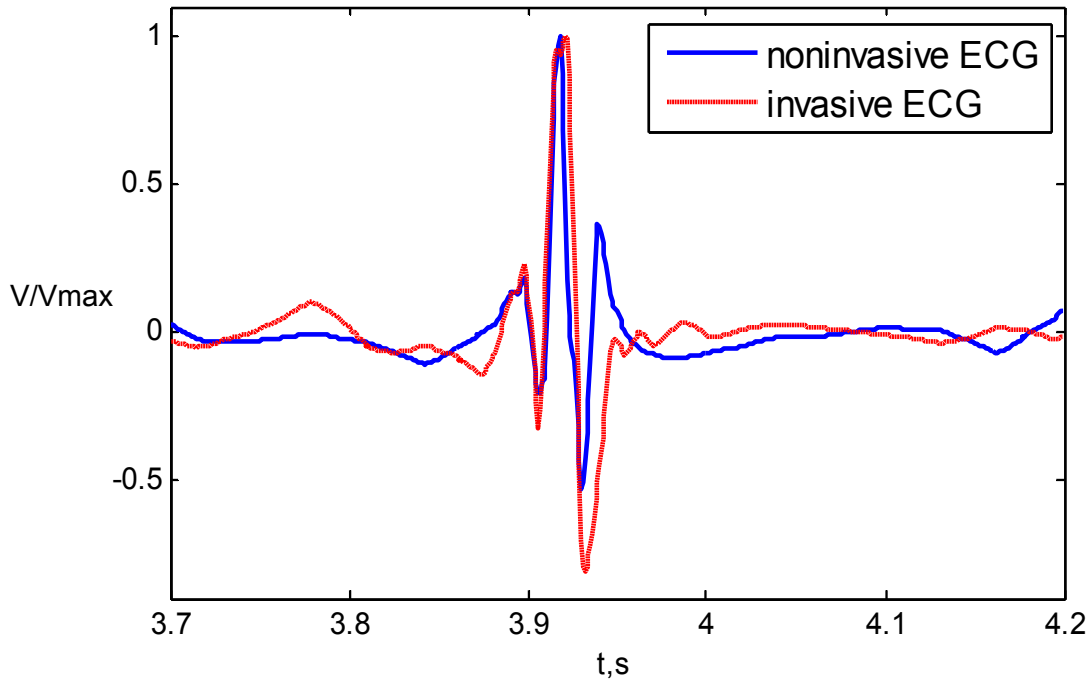

Fig. 5.19. The fetal cardiocycle extracted from the noninvasive maternal abdominal ECG and the cardiocycle from the direct fetal ECG registered simultaneously from the fetal head

Fig. 5.20 shows another example of the application of the proposed complex method to the analysis of real multichannel abdominal ECG signals. 5 independent components were obtained for a real 5-channel abdominal ECG record from the database [28]. One of the independent components is fetal.

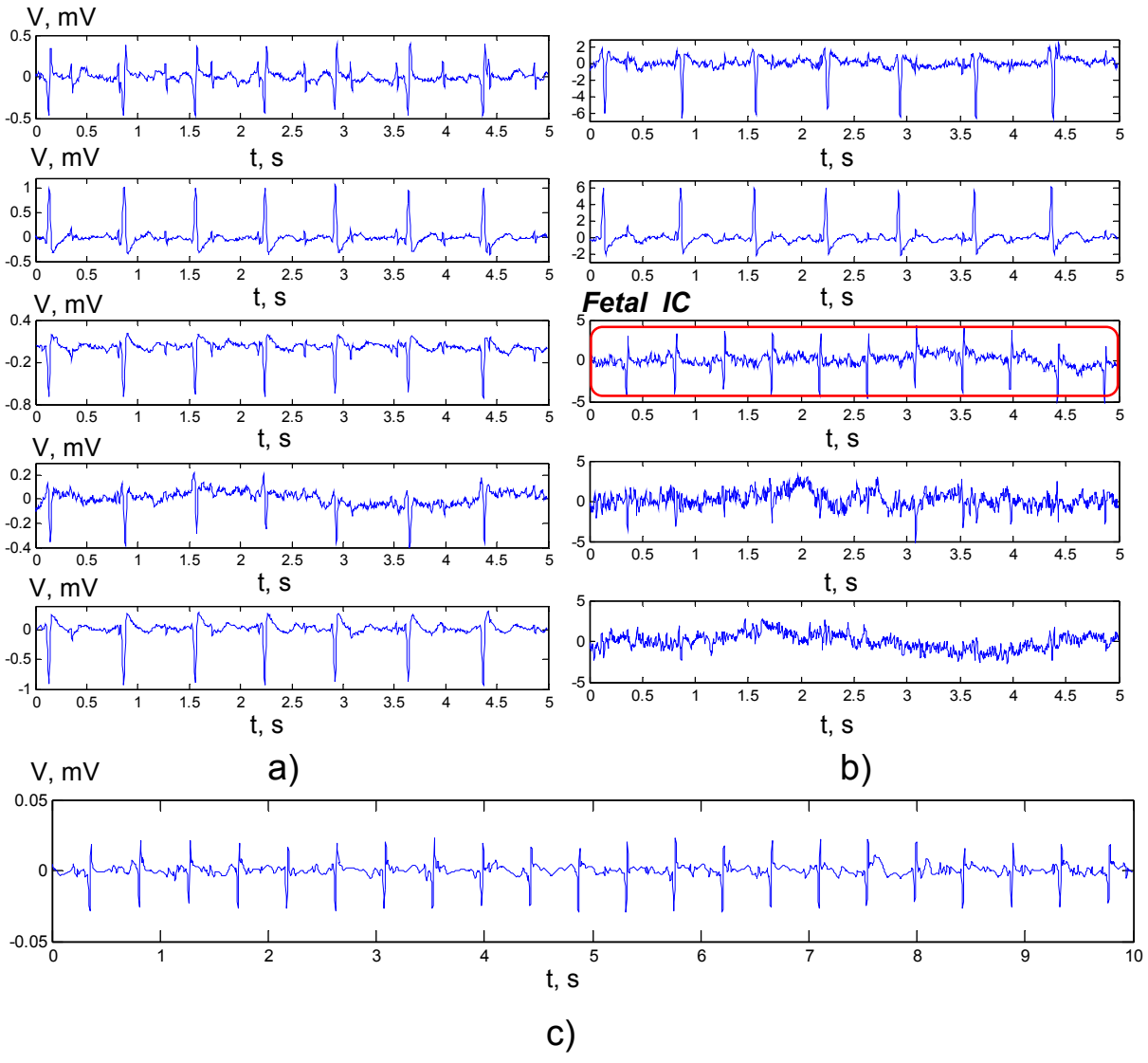

Fig. 5.20. a) abdominal 5-channel ECG record; b) independent components of the abdominal ECG record; c) fetal independent component after removal of baseline wander and high-frequency noise by means of wavelet analysis

The purified fetal independent component can be used to find the RR intervals of the fetal ECG, and also to obtain an average fetal cardiocycle. Averaging of the fetal ECG signal in Fig. 5.21 was performed with the accumulation of fetal cardiocycles with synchronization on the R wave.

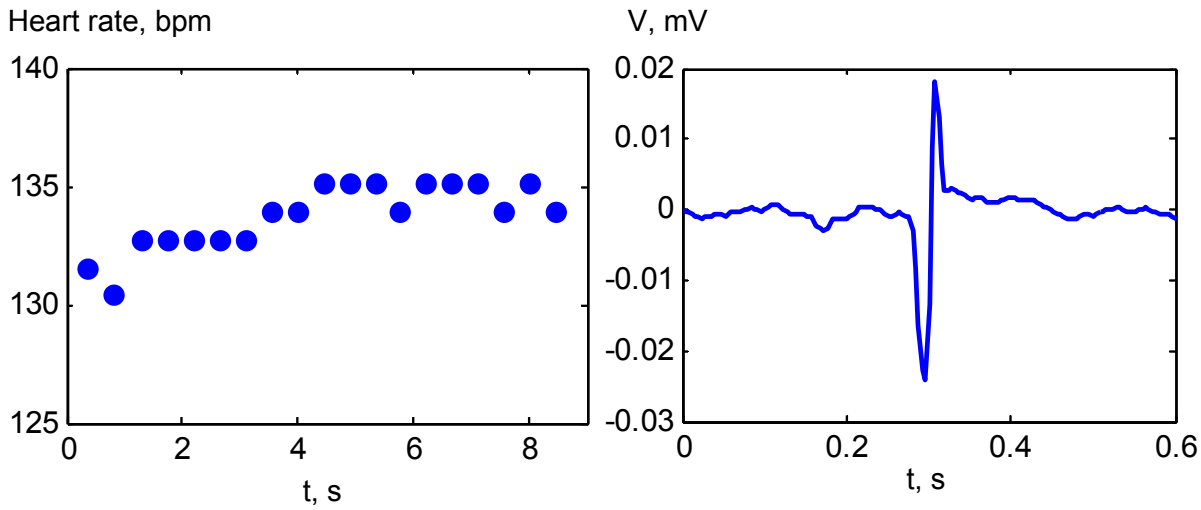

a) b)

Fig. 5.21. a) evaluation of fetal heart rate;
b) determination of the average fetal cardiocycle

Numerical experiments have shown that the considered method makes it possible to perform the evaluation of fetal heart rate, as well as to reveal changes in the morphology of fetal cardiocycles [29].

CONCLUSIONS

The integrated approach of abdominal ECG signals processing for fetal ECG detection, which based on combined use of ICA and WT, was considered. The main stages of the algorithm of fetal ECG extraction from the maternal abdominal signal are the fetal and maternal independent components separation by ICA and noise reduction in these

components by WT. The results obtained for the simulated and real signals have shown, that the presented approach enables us to extract fetal ECG signal with quality that sufficient not only for fetal heart rate variability measurement, but also for assessment of morphological and temporal parameters of fetal cardiac cycles. For the real signals the sufficient number of fetal ECG beats must be registered to enable the signal averaging technique appliance. The averaging of consecutive ECG complexes, obtained from the denoised fetal independent component and synchronized on their R waves, is advisable for accurate assessment of the morphological parameters of fetal ECG.

CONTROL QUESTIONS AND TASKS

1. Explain technique of non-invasive registration of fetal ECG.
2. Explain the peculiarities of manifestation of fetal cardiac electrical activity on maternal abdominal ECG.
3. How can development of hypoxia reflect itself on the fetal ECG?
4. Explain approaches for fetal ECG extraction.
5. Explain, how can be simulated the abdominal ECG signal of a pregnant woman?

REFERENCES

[1] Nandhini P. Literature Review of Fetal ECG Extraction / P. Nandhini, T. Meeradevi // Bonfring International Journal of Advances in Image Processing. — 2012. — Vol. 2. — P. 55 — 62.

[2] Sameni R. A Review of Fetal ECG Signal Processing: Issues and Promising Directions/ R. Sameni, G. Clliford// The Open Pacing, Electrophysiology and Therapy Journal.—2010.— Vol. 3.— P. 4–20.

[3] Vullings R. Non-invasive fetal electrocardiogram: analysis and interpretation/ R.Vullings // Eindhoven: Technische Universteit Eindhoven. — 2010. — 225 p.

[4] Amer-Wahlin. Foetal ECG and STAN technology – a review / Amer-Wahlin, B.Yli, S. Alurkumaran // Eur. Clin. Obstet. Gynaecol. — 2005. — P. 61 — 73.

[5] Amer-Wahlin. Fetal electrocardiogram: ST waveform analysis in intrapartum surveillance / Amer Wahlin, S. Arulkumaran, H. Hagberg, K. Maršál, and G.H. Visser// BJOG. — 2007. — Vol. 114(10). — P. 1191 — 1193.

[6] Kazmi T. ST Analysis of the Fetal ECG, as an Adjunct to Fetal Heart Rate Monitoring in Labour: A Review/T. Kazmi, F. Radfer, and S. Khan// Oman Med J. — 2012. —Vol. 27(5). — P. 415 — 417.

[7] STAN: http://www.okbmedical.com/fetal/

[8] Hokegard K.H. Myocardial metabolism in relation to electrocardiographic changes and cardiac function during graded hypoxia in the fetal lam/K.H. Hokegard, B.O. Eriksson, I. Kjellmer, et. all //Act. Physiol. Scand. — 1981. — Vol. 113(1). — P.1—7.

[9] Wohlfart B. A simple model for demonstration of STT changes in ECG// Eur Heart. — 1987. — Vol. 8 (4). — P. 409 — 416.

[10] Greene K.R. Changes in the ST waveform of the fetal lamb electrocardiogram with hypoxemia/ K.R. Greene, G.S. Dawes, H. Lilja, K.G. Rosen// Am J Obstet Gynecol. —1982. — Vol. 144. — P. 950 — 957.

[11] McSharry P. E. A Dynamic Model for Generating Synthetic Electrocardiogram Signals / P. E. McSharry, G. D. Clifford, L. Tarassenko, L. A. Smith // IEEE Trans. Biomed. Eng., — vol. 50. — 2003. — P. 289 — 294.

[12] Matonia A. Modelling of Non-invasively Recorded Maternal and Fetal Electrocardiographic Signals/ A. Matonia, J. Jezewski, T. Kupka, J. Wrobel [et al.]// Biocybernetics and Biomedical Engineering. — 2005. — Vol. 25. — P. 27 — 39.

[13] Sameni R., Clifford G. D., Jutten C., Shamsollahi M. B. Multi-Channel ECG and Noise Modeling: Application to Maternal and Fetal ECG Signals/ EURASIP Journal on Advances in Signal Processing. — Vol. 2007, 14 pages, 2007.

[14] Ivanushkina N. Fetal Electrocardiogram Extraction from Maternal Abdominal Signals/ Ivanushkina N., Ivanko K., Lysenko E., Borovskyi I., Panasiuk O.// Proceedings of the International Conference “Electronics and Nanotechnology” — Kyiv, 2014. — P.334 — 338.

[15] Mochimaru F. Detecting the Fetal Electrocardiogram by Wavelet Theory-Based Methods/ F. Mochimaru, Y. Fujimoto, Y. Ishikawa // Progress in Biomedical Research. — 2002. — Vol. 7. — No. 3. — P. 185 — 193.

[16] Almagro S. A New Mother Wavelet for Fetal Electrocardiography to Achieve Optimal Denoising and Compressing Results / S. Almagro, M. M. Elena, M. J. Bastiaans, J. M. Quero // Computers in Cardiology. — 2006. — Vol. 33. — P. 157 — 160.

[17] Karvounis E. C. Fetal Heart Rate Extraction from Composite Maternal ECG Using Complex Continuous Wavelet Transform/ E. C. Karvounis, C. Papaloukas, D. I. Fotiadis, L. K. Michalis// Computers in Cardiology.—2004.—Vol. 31.—P. 737- 740.

[18] Singh B. N. Optimal selection of wavelet basis function applied to ECG signal denoising/ B. N. Singh, A. K. Tiwari// Digital Signal Processing. — 2006. — Vol. 16. — P. 275 — 287.

[19] B. Azzerboni. A New Approach Based On Wavelet-ICA Algorithms For Fetal Electrocardiogram Extraction/ B. Azzerboni, F. La Foresta, N. Mammone, F. C. Morabito // In proceeding of: European Symposium on Artificial Neural Networks. — 2005. — P. 193 — 198.

[20] M. Shayesteh, J. Fallahian. Using Wavelet Transformation in Blind Sources Separation of the Fetal Electrocardiogram/ Majlesi Journal of Electrical Engineering. — 2002. —Vol. 7.— No. 3. — P. 185-193.

[21] Seungjin Choi. Blind Source Separation and Independent Component Analysis: A Review/ Andrzej Cichocki, Hyung-Min Park,Soo-Young Lee//Neural Information Processing. — 2005. — Vol.6. — No.1, 57 pages.

[22] Vrins F. Improving Independent Component Analysis Performance by Variable Selection/ Vrins F., Lee J.A., Verleysen M., Vigneron V., Jutten C. // Neural Network for Signal Processing. — Toulouse, 2003. — P. 359 — 368.

[23] Vrins F. Sensor Array and Electrode Selection for Non-invasive Fetal Electrocardiogram Extraction by Independent Component Analysis// F.Vrins, C. Jutten, M. Verleysen// Independent Component Analysis and Blind Signal Separation. Lecture Notes in Computer Science. — 2004. — Vol. 3195. — P. 1017 — 1024.

[24] Goldberger AL, Amaral LAN, Glass L, Hausdorff JM, Ivanov PCh, Mark RG, Mietus JE, Moody GB, Peng C-K, Stanley HE. PhysioBank, PhysioToolkit, and PhysioNet: Components of a New Research Resource for Complex Physiologic Signals. Circulation 101(23):e215-e220 [Circulation Electronic Pages; http://circ.ahajournals.org/content/101/23/e215.full]; 2000.

[25] PhysioNet. Abdominal and Direct Fetal Electrocardiogram Database: http://www.physionet.org/physiobank/database/adfecg

[26] Jezewski J, Matonia A, Kupka T, Roj D, Czabanski R. Determination of the fetal heart rate from abdominal signals: evaluation of beat-to-beat accuracy in relation to the direct fetal electrocardiogram. Biomedical Engineering/Biomedizinische Technik 2012 Jul; 57(5):383-394. doi:10.1515/bmt-2011-0130

[27] PhysioNet. Non-Invasive Fetal Electrocardiogram Database: https://physionet.org/physiobank/database/nifecgdb

[28] Database for the Identification of Systems (DaISy): http://homes.esat.kuleuven.be/~smc/daisy

[29] Analysis of low-amplitude signals of cardiac electrical activity/ N.G. Ivanushkina, K.O. Ivanko, V.I. Timofeyev//Radioelectronics and Communications Systems (distributed by Springer) – 2014. – Vol.57. – №10 – p.465-473.

CONCLUSIONS

Development of methods for detection of early signs of heart disorders can not only predict the disease, but by early treatment can help prevent the pathological process flow. Mathematical methods of ECG analysis are realized in the development of new generation of diagnostic ECG systems, using complex transformations for parameter's estimation of myocardial electrical potential, based on biophysics and electrophysiology of the heart.

Technology of high resolution electrocardiography is perspective direction for digital processing of low-amplitude components of electrocardiosignal. These combined technologies include methods, based on creating eigen subspaces of signals and noise by decomposition in the basis of eigenvectors, principal component analysis, independent component analysis and wavelet analysis.

Research directions of atrial and ventricular late potentials detection and T wave alternans evaluation are both linked by a common idea: detection of markers of cardiac electrical instability in the surface ECG. Application of the combined methods gives the opportunity not only to decide on the presence or absence of late potentials or T wave alternans in the electrocardiosignal, but also to evaluate changes in the pattern of low-amplitude ECG components after antiarrhythmic therapies or surgical procedures in order to judge the effectiveness of the treatment of arrhythmias and to perform early diagnosis of diseases of the cardiovascular system.

Atrial electrical activity and ventricular activity can be separated from real multichannel recordings in atrial fibrillation by means of independent component analysis. To identify the source that corresponds to atrial electrical activity, the frequency spectrums and

coefficients of skewness and kurtosis are determined. Also atrial activity separation is performed by average beat subtraction method.

Non-invasive combined methods of detection of fetal ECG from mother abdominal electrocardiosignals can determine heart rate variability and morphological parameters of fetus cardiac cycles that allows assessing the functional status of the fetus during pregnancy.

Досягнення в області цифрової обробки низькоамплітудних компонент електрокардіосигналів: навчальний посібник/ К.Іванько, Н.Іванушкіна. ─ Київ, 2017 р. ─ 198 стор.

ISBN_____

Навчальний посібник присвячено розробці методів та засобів для неінвазивного виявлення та дослідження тонких проявів електричної активності серця. Особлива увага приділяється вдосконаленню інформаційного та алгоритмічного забезпечення систем електрокардіографії високого розрізнення для ранньої діагностики електричної нестабільності міокарда, а також для оцінки функціонального стану плоду під час вагітності.

Теоретичні основи супроводжуються прикладами реалізації алгоритмів за допомогою системи MATLAB. Навчальний посібник призначений для студентів, аспірантів, а також фахівців у галузі біомедичної електроніки та медичних працівників.

УДК 621.391:004.93:616.12-073.97(075.8)621.38:61(0.75.8)

ISBN _____

Advances in Digital Processing of Low-Amplitude Components of Electrocardiosignals: Teaching book/K.Ivanko, N.Ivanushkina.─ Kyiv, 2017.─198 p.

EDUCATIONAL EDITION

Advances in Digital Processing of Low-Amplitude Components of Electrocardiosignals

K.Ivanko
N.Ivanushkina

Reviewers:
O.Kovalenko, Doctor of Medical Sciences,
Professor of International Research and Training Center for Information Technologies and Systems of NASU

O.Sharpan, Doctor of Technical Sciences,
Professor of Igor Sikorsky Kyiv Polytechnic Institute

Responsible Editor:
V. Timofeev, Doctor of Technical Sciences,
Professor of Igor Sikorsky Kyiv Polytechnic Institute

За редакцією укладачів

Надруковано з оригінал-макета замовника

Підписано до друку __.__.2017. Формат 60x84/16.
Тираж 300 экз.
Видавництво "АВЕРС", 03056, м.Київ, вул. Польова, 21.
Свідоцтво про реєстрацію № 5933 від 24.07.1998 р.